

# **Diffusion in Liquids**

**Equilibrium Molecular Simulations and  
Predictive Engineering Models**

**Xin Liu**



# **Diffusion in Liquids**

Equilibrium Molecular Simulations and Predictive Engineering  
Models

## **PROEFSCHRIFT**

ter verkrijging van de graad van doctor  
aan de Technische Universiteit Delft,  
op gezag van de Rector Magnificus Prof.ir.K.C.A.M. Luyben  
voorzitter van het College voor Promoties,  
in het openbaar te verdedigen op 21 January 2013 om 12.30 uur

door

**Xin Liu**

Master of Science in Biochemical Engineering, Delft University of Technology  
geboren te Daqing, China.

Dit proefschrift is goedgekeurd door de promotoren:

Prof.Dr.Ir. T.J.H. Vlugt

Prof.Dr.-Ing. A. Bardow

Samenstelling promotiecommissie:

Rector Magnificus	voorzitter
Prof.Dr.Ir. T.J.H. Vlugt	Technische Universiteit Delft, Promotor
Prof.Dr.-Ing. A. Bardow	RWTH Aachen University, Promotor
Prof.Dr.-Ing. J. Vrabec	University of Paderborn
Prof.Dr. P. Bolhuis	University of Amsterdam
Prof.Dr. P.L.J. Zitha	Technische Universiteit Delft
Prof.Dr. H.W. Zandbergen	Technische Universiteit Delft
Ir. G. Krooshof	DSM

This thesis was performed as part of the Cluster of Excellence “Tailor-Made Fuels from Biomass”, which is funded by the Excellence Initiative by the German federal and state governments. This thesis was also sponsored by the Stichting Nationale Computerfaciliteiten (National Computing Facilities Foundation, NCF) for the use of supercomputing facilities, with financial support from the Nederlandse Organisatie voor Wetenschappelijk onderzoek (Netherlands Organization for Scientific Research, NWO).



Copyright © 2012 by X. Liu

ISBN 978-94-6186-091-0

Printed by Ipskamp Drukkers

All rights reserved. No part of the material protected by this copyright notice may be reproduced or utilized in any form or by any means, electronic or mechanical, including photocopying, recording or by any information storage and retrieval system, without the prior permission of the author.

# Contents

<b>1</b>	<b>Introduction</b>	<b>1</b>
1.1	Diffusion	2
1.2	Molecular Dynamics simulation	6
1.3	Scope of this thesis	8
<b>2</b>	<b>Maxwell-Stefan Diffusivities in Liquid Mixtures: Using Molecular Dynamics for Testing Model Predictions</b>	<b>11</b>
2.1	Introduction	12
2.2	Prediction of diffusion coefficients	13
2.2.1	Determination of MS diffusivities from Fick diffusivities	13
2.2.2	Predicting MS diffusivities using the Darken equation	14
2.2.3	Predicting MS diffusivity using the Vignes equation	15
2.3	Equilibrium Molecular Dynamics simulation	17
2.4	Evaluation approaches for diffusion models	20
2.4.1	Model validation	20
2.4.2	Indirect comparison	20
2.4.3	Validation of the generalized Vignes equation	23
2.4.4	Direct comparison	24
2.5	Results and discussion	24
2.5.1	Model validation	24
2.5.2	Indirect comparison	26
2.5.3	Validation of the generalized Vignes equation	26
2.5.4	Direct comparison	27
2.6	Conclusions	29

<b>3</b>	<b>Multicomponent Maxwell-Stefan Diffusivities at Infinite Dilution</b>	<b>31</b>
3.1	Introduction	32
3.2	Obtaining Maxwell-Stefan Diffusivities from MD simulations	33
3.2.1	Deriving an expression for $\mathcal{D}_{ij}^{x_k \rightarrow 1}$	34
3.2.2	Obtaining a physically-based model for $\mathcal{D}_{ij}^{x_k \rightarrow 1}$	36
3.3	Details of Molecular Dynamics simulations	37
3.3.1	WCA system	37
3.3.2	n-hexane - cyclohexane - toluene	37
3.3.3	Ethanol - methanol - water	38
3.4	Results and discussion	38
3.4.1	WCA system	38
3.4.2	n-hexane - cyclohexane - toluene	40
3.4.3	Ethanol - methanol - water	41
3.5	Conclusions	41
<b>4</b>	<b>A Predictive Darken Equation for Maxwell-Stefan Diffusivities in Multicomponent Mixtures</b>	<b>49</b>
4.1	Introduction	50
4.2	The predictive Darken-LBV equation	53
4.3	Molecular Dynamics simulation	55
4.3.1	WCA system	55
4.3.2	n-hexane - cyclohexane - toluene	56
4.4	Results and discussion	56
4.4.1	Ternary WCA systems	56
4.4.2	Quaternary WCA systems	62
4.4.3	n-hexane - cyclohexane - toluene	62
4.5	Conclusions	65
<b>5</b>	<b>Maxwell-Stefan Diffusivities in Binary Mixtures of Ionic Liquids with DMSO and H<sub>2</sub>O</b>	<b>67</b>
5.1	Introduction	68
5.2	Molecular Dynamics simulation	70
5.2.1	Obtaining diffusivities from MD simulation	70
5.2.2	Details of equilibrium MD simulation	70

5.3	Predictive models for diffusion coefficients	71
5.3.1	Maxwell-Stefan diffusivities	71
5.3.2	Maxwell-Stefan diffusivities at infinite dilution	74
5.3.3	Salt diffusivity	75
5.4	Results and Discussion	75
5.4.1	Model validation via self-diffusivities	75
5.4.2	Maxwell-Stefan diffusivities and radial distribution functions	81
5.4.3	Diffusivity of IL molecules	84
5.5	Conclusions	85
<b>6</b>	<b>Fick Diffusion Coefficients of Liquid Mixtures Directly Obtained from Equilibrium Molecular Dynamics</b>	<b>93</b>
6.1	Introduction	94
6.2	Diffusion coefficients and the thermodynamic factor	98
6.2.1	Obtaining diffusion coefficients from MD simulations	98
6.2.2	Predictive models for diffusion	98
6.2.3	Obtaining the thermodynamic factor from MD simulations	100
6.3	Simulation details	101
6.4	Results and discussion	103
6.4.1	Model validation for pure component systems	103
6.4.2	Diffusion in acetone - methanol	104
6.4.3	Diffusion in acetone - tetrachloromethane	109
6.5	Conclusions	114
<b>7</b>	<b>Fick Diffusion Coefficients in Ternary Liquid Systems from Equilibrium Molecular Dynamics Simulation</b>	<b>115</b>
7.1	Introduction	116
7.2	Computation of diffusion coefficients and thermodynamic factors	116
7.2.1	Obtaining diffusion coefficients from MD simulations	116
7.2.2	Obtaining thermodynamic factors from MD simulations	117
7.2.3	Obtaining thermodynamic factors from COSMO-SAC	119
7.3	Simulations details	119
7.4	Results and discussion	121
7.4.1	Chloroform - acetone	122

7.4.2	Chloroform - methanol	123
7.4.3	Chloroform - acetone - methanol	126
7.5	Conclusions	136
<b>A</b>	<b>Obtaining Maxwell-Stefan Diffusivities from Molecular Dynamics Trajectories</b>	<b>137</b>
A.1	Binary systems	138
A.2	Ternary systems	138
A.3	Quaternary systems	140
<b>B</b>	<b>Obtaining a Darken Equation for Multicomponent Systems</b>	<b>143</b>
B.1	Binary systems	144
B.2	Ternary systems	145
B.3	Quaternary systems	147
<b>C</b>	<b>Additional Data for Chapter 3</b>	<b>149</b>
<b>D</b>	<b>Additional Data for Chapter 4</b>	<b>157</b>
<b>E</b>	<b>Additional Data for Chapter 5</b>	<b>175</b>
<b>F</b>	<b>Kirkwood-Buff Coefficients from Sampling Fluctuations in Subvolumes</b>	<b>181</b>
	<b>Summary</b>	<b>203</b>
	<b>Samenvatting</b>	<b>207</b>
	<b>Curriculum Vitae</b>	<b>211</b>
	<b>Published Work</b>	<b>212</b>
	<b>Acknowledgments</b>	<b>214</b>



# 1

---

## Introduction

---

## 1.1 Diffusion

If a bulb is filled with hydrogen and connected to another bulb filled with nitrogen at the same pressure and temperature via a capillary tube, hydrogen and nitrogen will spread through the capillary. After some time, the concentration of hydrogen and nitrogen in the two bulbs will become identical. The process responsible for this is called diffusion. Diffusion is the transport of mass that occurs due to a gradient in chemical potential of a component in the system. Equivalently, the gradient in concentration can also be used as driving force. Diffusion can be a slow process. In gases, diffusion coefficients are typically around  $10^{-5} \text{ m}^2 \cdot \text{s}^{-1}$ . In liquids, diffusion coefficients are about  $10^{-9} \text{ m}^2 \cdot \text{s}^{-1}$ . In solids, diffusion is usually even slower<sup>1-3</sup>. In many processes, diffusion occurs simultaneously with other phenomena, such as chemical reactions. When diffusion is the slowest phenomena, it limits the overall rate of the process<sup>4-6</sup>. Accurate models for mass transport are therefore a prerequisite for the design of many industrial processes and the interpretation of diffusion experiments.

It is important to distinguish self-diffusion and transport (mutual) diffusion. Self-diffusion describes the motion of individual molecules. Mutual diffusion can be related to collective motion of one component and is responsible for mass transport. Therefore, mutual diffusion is the relevant phenomena in practice. Diffusion coefficients are a function of concentration, temperature and pressure<sup>7-11</sup>. They do not depend on the magnitude of the concentration gradient or chemical potential gradient<sup>12</sup>. The concentration dependence of diffusivities in liquids is often overlooked in chemical engineering applications<sup>13-15</sup>. To investigate the concentration dependence of diffusion coefficients, the required experimental effort is large<sup>3;16</sup>. As experiments on multicomponent diffusion are difficult and time consuming<sup>3;16</sup>, a detailed understanding of the concentration dependence of diffusion is currently lacking, especially for multicomponent systems. Therefore, it is worthwhile to explore the route of theory and simulation. Molecular Dynamics (MD)<sup>17-20</sup> simulations are a useful method in this respect as one can directly study the effect of molecular interactions on diffusion coefficients.

There are two theories commonly used for the description of diffusion, *i.e.* generalized Fick's law and Maxwell-Stefan (MS) theory. Both can be derived from the theory of irreversible thermodynamics<sup>1;12;21;22</sup>. Their connection is illustrated in Fig-

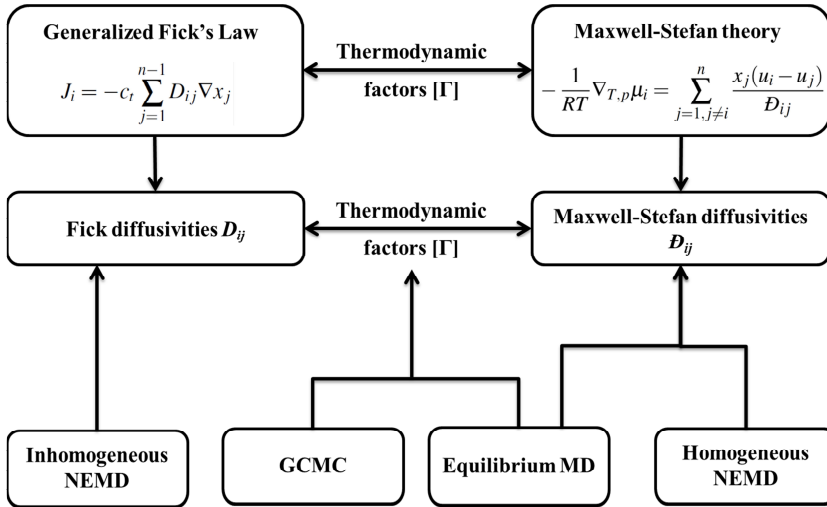


**Figure 1.1:** Schematic overview of computational schemes for diffusion coefficients. Fick's law and the Maxwell-Stefan (MS) theory are often used to describe mass transport by diffusion. The two formalisms are related via the matrix of thermodynamic factors  $[\Gamma]$ . Fick diffusivities can be obtained from inhomogeneous nonequilibrium Molecular Dynamics (NEMD) simulations. MS diffusivities can be obtained from equilibrium MD and homogeneous NEMD simulations. The matrix of thermodynamic factors can be predicted using grand-canonical Monte Carlo (GCMC) simulations. Our recent study shows that it is possible to obtain the thermodynamic factors from equilibrium MD simulations (chapters 6 and 7 of this thesis).

ure 1.1. Generalized Fick's law uses the concentration gradient as the driving force for diffusion while the MS theory uses a gradient in chemical potential as driving force. As two theories describe the same physical process, Fick and MS diffusion diffusivities can be related via the so-called matrix of thermodynamic factors<sup>1;2;21;23-29</sup>. In Figure 1.1, we present an overview of several computational methods for computing the diffusivities and thermodynamic factors. Diffusion coefficients can be obtained from both nonequilibrium Molecular Dynamics (NEMD) simulations<sup>30-32</sup> and equilibrium Molecular Dynamics (MD) simulations<sup>17;33-35</sup> (more details of MD simulations are addressed in section 1.2)<sup>17</sup>:

- In NEMD simulations, a driving force for mass transport is added to a system. The system will be responding to this driving force. By measuring the response of the system, diffusion coefficients can be calculated.
- In equilibrium MD simulations, concentration gradients and other perturbations do not appear in the system. Systems are thus at equilibrium. Diffusion coefficients follow from the motion of the molecules at equilibrium.

NEMD algorithms can be categorized according to the used method of perturbation: inhomogeneous NEMD<sup>18;36;37</sup> and homogeneous NEMD<sup>38–40</sup>. A concentration gradient is established for inhomogeneous NEMD. By monitoring the relaxation of the concentration as a function of time, Fick diffusivities can be obtained by application of Fick's second law. The difficulty of this method is that significant simulation efforts are required for generating many initial concentration gradients<sup>30</sup>. This is essential for determining the linear regime where Fick's law is applicable. In homogeneous NEMD simulation, an external field is applied to the system. The field exerts a force on the molecules while keeping the total external force on the system equal to zero. The external field is coupled to particle properties and usually independent of the positions of the particles. Therefore, concentration gradients do not appear in the system<sup>31;32;38;39</sup>. It is important to note that homogeneous NEMD provides MS diffusivities. Some disadvantages have been observed in NEMD simulations: (1) algorithms for computing diffusion coefficients are inefficient<sup>30</sup>; (2) many simulations are needed to obtain the diffusion coefficients corresponding to equilibrium conditions at a single concentration as one has to extrapolate to a zero driving force. To explore the concentration dependence of diffusion coefficients, this effort is multiplied<sup>38</sup>; (3) very low driving force are needed to avoid so-called "traffic lanes" in the system<sup>38</sup>.

In equilibrium MD simulations, MS diffusivities follow directly from molecular trajectories<sup>17;21;25;27–29;41–46</sup>. The computed MS diffusivities are of high accuracy, even though the simulations are usually computationally expensive (due to the long time scales involved in the collective motions of molecules)<sup>33–35</sup>. To relate experimentally measurable Fick diffusivities to MS diffusivities, the matrix of thermodynamic factors is needed, as shown in Figure 1.1. The matrix of thermodynamic factors can be computed from grand-canonical Monte Carlo (GCMC) simulations<sup>31;32</sup>. However, presently used simulation techniques to determine the matrix of thermo-

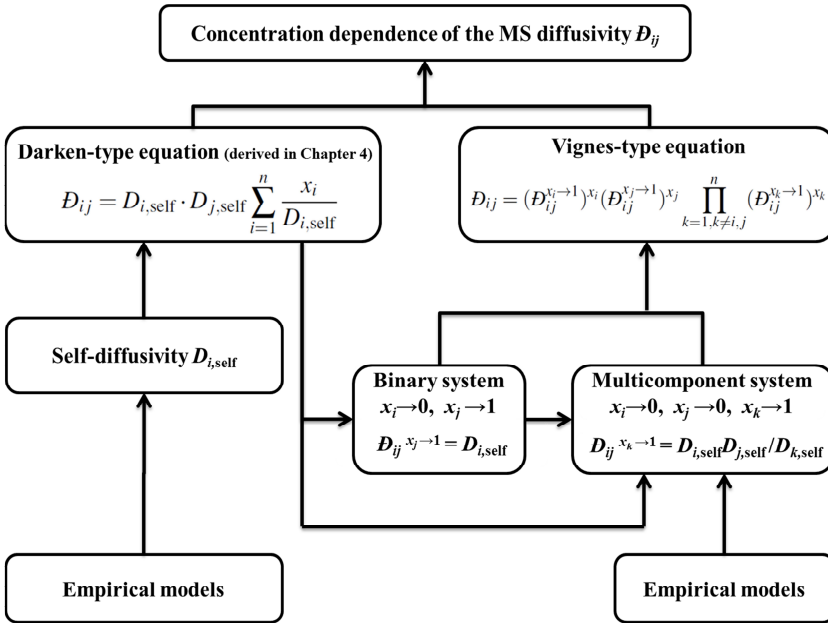


**Figure 1.2:** Schematic overview of predictive models for diffusion coefficients. The Darken-type and the Vignes-type equations are often used to describe the concentration dependence of MS diffusivities  $\mathcal{D}_{ij}$ . The Darken equation requires self-diffusivities, *i.e.*  $D_{i,\text{self}}$  while Vignes-type equation requires the MS diffusivities at dilution, *i.e.*  $\mathcal{D}_{ij}^{x_j \rightarrow 1}$  and  $\mathcal{D}_{ij}^{x_k \rightarrow 1}$ . As in the limit of infinite dilution, self-diffusivities are identical to the MS diffusivities, *i.e.*  $\mathcal{D}_{ij}^{x_j \rightarrow 1} = D_{i,\text{self}}$ , the Darken-type equation can be used to parametrize the Vignes equation.

dynamic factors in dense systems are quite inefficient<sup>47;48</sup>. A recent study shows that it is possible to access the grand-canonical ensemble in MD simulations<sup>49</sup>. This method is accurate and more efficient compared to the GCMC simulations. The thermodynamic factor can also be calculated from experimental vapor-liquid equilibrium data, but this introduces other difficulties, see chapters 6 and 7 of this thesis.

Many efforts have been carried out in developing predictive models for diffusion<sup>2;23;50–53</sup>. The Darken-type and generalized Vignes-type equations are prevalent to describe the relation between diffusion coefficients and mixture composition<sup>1;23;52</sup>, see Figure 1.2. In binary systems, the Darken equation uses concentration dependent self-diffusivities to predict MS diffusivities. However, the Darken equation is only for binary systems, as presented in the original publication<sup>54</sup>. For multicomponent

systems, the Darken-type model is not available. In this thesis, we derive a multicomponent Darken equation for the description of MS diffusivities. Details are discussed in chapter 4. The concentration dependence of self-diffusivities can be obtained via an empirical diffusion model and experiments<sup>7;23</sup>. The Vignes equation is an empirical approach for the prediction of MS diffusivities<sup>1;2;47;55</sup>. Unlike the Darken equation, the Vignes equation requires binary MS diffusivities at infinite dilution. In binary mixtures, MS diffusivities at infinite dilution are easily obtained as they are identical to the self-diffusivity of the component that is infinitely diluted<sup>1;7</sup>. However, in systems containing more than two components, the Vignes equation requires MS diffusivities representing two infinitely diluted components in a third one (solvent). This quantity is nearly impossible to directly obtain in experiments. Over the past 20 years, several models have been proposed in the literature for the estimation of these ternary MS diffusivities in the limit of dilution<sup>23;24;50;51</sup>. Unfortunately, these models are empirical and lack a solid theoretical background which introduce difficulties in identifying the physical cause of their success or failure in describing diffusion<sup>23;50-52</sup>. In chapter 3 of this thesis, we provide a physically motivated alternative.

The questions and challenges in the field of diffusion in liquids can be summarized as follows:

1. Can measurable Fick diffusivities be predicted more efficiently using a consistent methodology?
2. Can multicomponent diffusion be predicted based upon the corresponding binary systems?
3. What microscopic information is important for predicting multicomponent diffusion?

## 1.2 Molecular Dynamics simulation

Molecular Dynamics (MD) simulation is a computational technique which uses atomic interactions to compute the equilibrium and transport properties of a many-body system. Usually, these interactions can be described by a classical force field, although

they can also be obtained from ab-initio techniques.<sup>56</sup> A classical force field describes the interaction between particles (atoms or molecules), *i.e.* bonded and non-bonded potentials. Usually, the force field parameters appearing in the force field function are derived from experiments and/or quantum mechanical calculations. In this thesis, bonded interactions typically consist of bond stretching, bond bending and torsion interactions while non-bonded interactions consist of Lennard-Jones (LJ) and Coulombic interactions. In MD simulations, the equations of motion (Newton's second law) are integrated numerically<sup>17-19</sup>. Newton's second law states that the acceleration of a particle is proportional to the net force and inversely proportional to the mass (second derivative of position with respect to the time),

$$a_i = \frac{F_i}{m_i} = \frac{d^2 r_i}{d t^2}, \quad (1.1)$$

in which  $a_i$  is the acceleration of particle  $i$ ,  $F_i$  is the net force acting on particle  $i$ ,  $m_i$  is the mass of particle  $i$ ,  $r_i$  is the position of particle  $i$  and  $t$  is the time. To integrate the equations of motion, several algorithms are available. For example, the time-reversible velocity Verlet algorithm is often used<sup>17;18</sup>.

$$r_i(t + \Delta t) = r_i(t) + v_i(t)\Delta t + \frac{F_i(t)}{2m_i}\Delta t^2, \quad (1.2)$$

$$v_i(t + \Delta t) = v_i(t) + \frac{F_i(t + \Delta t) + F_i(t)}{2m_i}\Delta t, \quad (1.3)$$

in which  $r_i(t)$  and  $v_i(t)$  are the position and velocity of particle  $i$  at time  $t$ , respectively. The velocities of particles are related to the temperature<sup>17</sup>.  $\Delta t$  is the time step for integration and the typical value for  $\Delta t$  is  $10^{-15}$  s<sup>17</sup>.  $F_i(t)$  is the net force acting on particle  $i$  at time  $t$  and can be calculated using a classical force field. Typically, we use hundred to a few thousand molecules in MD simulation. Periodic boundary conditions are usually applied<sup>17-19</sup>. By integrating the equation of motion, the typical trajectories of interacting particles are obtained from MD simulation. From these trajectories, thermodynamic and transport properties can be computed. The time scale of MD simulation depends on the properties of interest ranging from a few to hundred nanoseconds. For studying diffusion, simulations using quantum mechanical interactions are not feasible due to the required time scale (*i.e.*  $\geq 100$  ns). For more details on MD simulations, the reader is referred to some excellent standard textbooks<sup>17-20</sup>.

### 1.3 Scope of this thesis

The objectives of this thesis are three-fold:

1. Developing a consistent methodology for the prediction of multicomponent diffusion coefficients.
2. Developing predictive engineering models for diffusion coefficients.
3. Improving predictive models for diffusivities.

In chapter 2, diffusion in the ternary systems n-hexane - cyclohexane - toluene is investigated using equilibrium MD simulations. In this system, components are not highly associated and the electrostatic interactions are excluded. We tested the quality of often used predictive engineering models for ternary diffusion in the limit of infinite dilution. Even though these models sometimes predict reasonable diffusion coefficients, they may fail in other systems due to the lack of a sound theoretical basis. To solve this problem, *i.e.* the LBV model, (taken from the initials of the authors: Liu, Bardow and Vlugt) was derived in chapter 3 for diffusion in ternary systems at infinite dilution based on the Onsager relations. We investigated the LBV model for ternary systems with different complexities, *i.e.* a ternary Weeks-Chandler-Andersen (WCA) fluid, the ternary system n-hexane - cyclohexane - toluene and the ternary system methanol - ethanol - water. We show that the LBV model is superior compared to other existing models for describing diffusion at infinite dilution. In chapter 4, we study diffusion for the full concentration range. A consistent multicomponent Darken equation is developed for describing the concentration dependence of MS diffusivities. In addition, a predictive model for the required self-diffusivities is proposed. The quality of these novel models has been evaluated in ternary and quaternary WCA systems and the ternary system n-hexane - cyclohexane - toluene. To explore the limitations of predictive models, we investigated a more complex ionic liquid (IL) system (IL with water and DMSO) in which electrostatic interactions are important (chapter 5). We found that for these systems, MS diffusivities vary by a factor of 10 within the concentration range which is still significantly smaller than the variation of the self-diffusivities. As explained earlier, Fick diffusivities can be measured in experiments while molecular simulations provide MS diffusivities. These two quantities can be related by the so-called matrix of thermodynamic factors which



---

is usually only known with large uncertainty, thereby leaving a gap between experiments and molecular simulations. To connect experiments and theories, we developed an approach to obtain the measurable Fick diffusivities using only equilibrium MD simulations. This approach allows for a consistent way for the description of diffusion. The validation of this method in binary systems acetone - methanol and acetone - tetrachloromethane is discussed in chapter 6. In chapter 7, this method is validated and extended to the ternary system chloroform - acetone - methanol. Compared to the available experimental diffusion data, MD results show good agreement with experiments.



# 2

---

## **Maxwell-Stefan Diffusivities in Liquid Mixtures: Using Molecular Dynamics for Testing Model Predictions**

---

This chapter is for a large part based on:

X. Liu, T.J.H. Vlugt, A. Bardow, *Maxwell-Stefan diffusivities in liquid mixtures: using molecular dynamics for testing model predictions*, *Fluid Phase Equilibria*, **2011**, 301, 110-117.

## 2.1 Introduction

The study of MS diffusivities in multicomponent systems is of great practical and theoretical interest as the MS theory accounts for chemical potential gradients as driving forces for transport diffusion<sup>21;27;57</sup>. In experiments, it is impossible to directly measure MS diffusivities. Instead, MS diffusivities are obtained from measurable Fick diffusivities and the matrix of thermodynamic factors<sup>2</sup>. As this procedure may introduce errors, predictive models for MS diffusivities based on easily measurable quantities are desirable<sup>7;8;10;11;58</sup>. In binary systems, several predictive models are available for estimating MS diffusivities and their dependence on temperature, mixture density and composition<sup>1;59;60</sup>. However, models for estimating MS diffusivities in mixtures containing three or more components are less established due to a lack of accurate experimental and simulation data. Several studies report that in multicomponent systems, MS diffusivities strongly depend on the overall density and composition, which seriously complicates the development of predictive models<sup>23;25;61</sup>.

The objectives of this chapter are threefold. First, we use an approach based on optimal computational design for efficiently evaluating predictive models for MS diffusivities in ternary systems. This approach enables us to evaluate different predictive models using a limited number of simulations. Second, we present two different ways to evaluate these predictive models: an indirect comparison using self-diffusivities at infinite dilution and a direct comparison using MS diffusivities. Third, we directly test the predictive capability of the well-known Vignes equation without using any additional assumptions. For this, we performed equilibrium Molecular Dynamics (MD) simulations to compute the self- and MS diffusivities of liquid mixtures of n-hexane, cyclohexane and toluene. This system was chosen because the MS diffusivities obtained by predictive models show significant differences compared to other mixtures for which experimental reference data is available<sup>7</sup>.

This chapter is organized as follows. In section 2.2 we briefly review the various approaches for estimating self- and MS diffusivities. The simulation method used for computing these diffusivities is described in section 2.3. In section 2.4 we construct the framework for evaluating the predictive models. Three different comparisons are presented. The efficiency of each comparison is discussed in section 2.5. Our findings are summarized in section 2.6.

## 2.2 Prediction of diffusion coefficients

### 2.2.1 Determination of MS diffusivities from Fick diffusivities

Generalized Fick's law relates the molar flux  $J_i$  of component  $i$  to the Fick diffusivity  $D_{ij}$  and its driving force  $\nabla x_j$

$$J_i = -c_t \sum_{j=1}^{n-1} D_{ij} \nabla x_j. \quad (2.1)$$

Here,  $c_t$  is the total molar concentration and  $x_j$  is the mole fraction of component  $j$ . There are  $(n-1)$  independent fluxes and  $(n-1)$  independent driving forces in an  $n$ -component system as the net flux of the system is zero in the molar reference frame, *i.e.*  $\sum_{i=1}^n J_i = 0$ . From Eq. (2.1) it follows directly that the elements of the matrix of Fick diffusivities  $[D]$  depend on the labeling of the components. The MS formulation uses chemical potential gradients as driving forces for mass transport. For liquid mixtures at constant temperature and pressure, the MS equation equals<sup>62</sup>

$$\sum_{j=1}^{n-1} \Gamma_{ij} \nabla x_j = \sum_{\substack{j=1 \\ j \neq i}}^n \frac{x_i J_j - x_j J_i}{c_t \mathcal{D}_{ij}}, \quad (2.2)$$

where  $\mathcal{D}_{ij}$  is the MS diffusivity which describes the interaction or friction between components  $i$  and  $j$  due to the difference in their velocities.  $\Gamma_{ij}$  is the thermodynamic factor which is defined as

$$\Gamma_{ij} = \delta_{ij} + x_i \left( \frac{\partial \ln \gamma_i}{\partial x_j} \right)_{T,p,\Sigma}, \quad (2.3)$$

in which  $\delta_{ij}$  is the Kronecker delta, and  $\gamma_i$  is the activity coefficient of component  $i$  in the mixture. The symbol  $\Sigma$  indicates that the partial differentiation of  $\ln \gamma_i$  with respect to mole fraction  $x_j$  is carried out at constant mole fraction of all other components except the  $n$ -th one, so that  $\sum_{i=1}^n x_i = 1$  during the differentiation. Since generalized Fick's law and the MS approach describe the same process, the MS formulation can be related to the Fick formulation by<sup>1;21;23</sup>

$$[D] = [B]^{-1} [\Gamma]. \quad (2.4)$$

in which  $[D]$  is the matrix of Fick diffusivities in a molar reference frame and  $[\Gamma]$  is the matrix of thermodynamic factors. The elements of matrix  $[B]$  are defined as:

$$B_{ii} = \frac{x_i}{D_{in}} + \sum_{\substack{j=1 \\ j \neq i}}^n \frac{x_j}{D_{ij}}, \quad \text{with } i = 1, 2, \dots, (n-1), \quad (2.5)$$

$$B_{ij} = -x_i \left( \frac{1}{D_{ij}} - \frac{1}{D_{in}} \right), \quad \text{with } i, j = 1, 2, \dots, (n-1) \text{ and } i \neq j. \quad (2.6)$$

In practice, the large uncertainty in the thermodynamic factor  $[\Gamma]$  makes it difficult to obtain MS diffusivities from the measurable Fick diffusivities<sup>62</sup>.

## 2.2.2 Predicting MS diffusivities using the Darken equation

Krishna and van Baten<sup>23</sup> proposed a generalized Darken equation to predict MS diffusivities in multicomponent system using self-diffusivities at the same mixture composition:

$$D_{ij} = \frac{x_i}{x_i + x_j} D_{j,\text{self}} + \frac{x_j}{x_i + x_j} D_{i,\text{self}}. \quad (2.7)$$

For binary systems, Eq. (2.7) reduces to the well-known Darken equation<sup>25</sup>.

$$D_{ij} = x_i D_{j,\text{self}} + x_j D_{i,\text{self}}. \quad (2.8)$$

In the limit of  $x_i \rightarrow 1$  or  $x_j \rightarrow 1$ , the Darken equation (Eq. (2.8)) is exact. The following empirical models have been proposed<sup>23</sup> for relating the self-diffusivity  $D_{i,\text{self}}$  at any mixture composition to the self-diffusivity in a diluted solution  $D_{i,\text{self}}^{x_j \rightarrow 1}$ :

$$D_{i,\text{self}} = \sum_{j=1}^n x_j D_{i,\text{self}}^{x_j \rightarrow 1}, \quad (2.9)$$

$$D_{i,\text{self}} = \sum_{j=1}^n w_j D_{i,\text{self}}^{x_j \rightarrow 1}, \quad (2.10)$$

$$D_{i,\text{self}} = \sum_{j=1}^n v_j D_{i,\text{self}}^{x_j \rightarrow 1}. \quad (2.11)$$

In these equations,  $w_j$  is the mass fraction,  $v_j$  is the volume fraction, and  $D_{i,\text{self}}^{x_j \rightarrow 1}$  is the self-diffusivity of component  $i$  in an  $i$ - $j$  mixture when the mole fraction of component  $j$  is approaching 1. Krishna and van Baten<sup>23</sup> showed that the generalized Darken relation (Eq. (2.7)) can accurately predict MS diffusivities in liquid mixtures of linear alkanes. However, Eq. (2.7) suffers from an inconsistency, that is, it leads to two different limits if both  $x_i$  and  $x_j$  are vanishing for a system containing three or more components. This will be discussed further in chapters 3 and 4.

### 2.2.3 Predicting MS diffusivity using the Vignes equation

A geometrically consistent generalization of the Vignes equation for ternary mixtures was proposed by Wesselingh and Krishna<sup>24</sup>:

$$D_{ij} = (D_{ij}^{x_i \rightarrow 1})^{x_i} (D_{ij}^{x_j \rightarrow 1})^{x_j} (D_{ij}^{x_k \rightarrow 1})^{x_k}. \quad (2.12)$$

The terms  $D_{ij}^{x_i \rightarrow 1}$  and  $D_{ij}^{x_j \rightarrow 1}$  describe the interaction between components  $i$  and  $j$  if one component is infinitely diluted in the other one. These binary diffusion coefficients are easily obtained from both simulations and empirical equations<sup>25;47;63–66</sup>. The term  $D_{ij}^{x_k \rightarrow 1}$  describes the interaction between components  $i$  and  $j$  while both  $i$  and  $j$  are infinitely diluted in a third component  $k$ . This diffusion coefficient  $D_{ij}^{x_k \rightarrow 1}$  is not directly accessible in experiments. Several predictive models have been proposed for  $D_{ij}^{x_k \rightarrow 1}$ : (1) the WK model proposed by Wesselingh and Krishna<sup>24</sup>; (2) the KT model proposed by Kooijman and Taylor<sup>50</sup>; (3) the VKB model; (4) the DKB model, both the Vignes-type VKB and the Darken-type DKB model were proposed by Krishna and van Baten<sup>23</sup>; (5) the RS model proposed by Rehfeldt and Stichlmair<sup>51</sup>:

○ WK (Wesselingh and Krishna<sup>24</sup>):

$$D_{ij}^{x_k \rightarrow 1} = \sqrt{D_{ij}^{x_j \rightarrow 1} D_{ij}^{x_i \rightarrow 1}}, \quad (2.13)$$

○ KT (Kooijman and Taylor<sup>50</sup>):

$$D_{ij}^{x_k \rightarrow 1} = \sqrt{D_{ik}^{x_k \rightarrow 1} D_{jk}^{x_k \rightarrow 1}}, \quad (2.14)$$

- VKB (Krishna and van Baten<sup>23</sup>):

$$\mathcal{D}_{ij}^{x_k \rightarrow 1} = \left( \mathcal{D}_{ik}^{x_k \rightarrow 1} \right)^{\frac{x_i}{x_i + x_j}} \left( \mathcal{D}_{jk}^{x_k \rightarrow 1} \right)^{\frac{x_j}{x_i + x_j}}, \quad (2.15)$$

- DKB (Krishna and van Baten<sup>23</sup>):

$$\mathcal{D}_{ij}^{x_k \rightarrow 1} = \frac{x_j}{x_i + x_j} \mathcal{D}_{ik}^{x_k \rightarrow 1} + \frac{x_i}{x_i + x_j} \mathcal{D}_{jk}^{x_k \rightarrow 1}, \quad (2.16)$$

- RS (Rehfeldt and Stichlmair<sup>51;67</sup>):

$$\mathcal{D}_{ij}^{x_k \rightarrow 1} = \left( \mathcal{D}_{ik}^{x_k \rightarrow 1} \mathcal{D}_{jk}^{x_k \rightarrow 1} \mathcal{D}_{ij}^{x_j \rightarrow 1} \mathcal{D}_{ij}^{x_i \rightarrow 1} \right)^{1/4}. \quad (2.17)$$

All these predictive models suggest to estimate the MS diffusivity  $\mathcal{D}_{ij}^{x_k \rightarrow 1}$  based on easily measurable binary diffusion coefficients. The WK model relates the MS diffusivity  $\mathcal{D}_{ij}^{x_k \rightarrow 1}$  to the diffusion coefficients in binary mixtures of components  $i$  and  $j$ , *i.e.*  $\mathcal{D}_{ij}^{x_i \rightarrow 1}$  and  $\mathcal{D}_{ij}^{x_j \rightarrow 1}$ . The KT model suggests to estimate  $\mathcal{D}_{ij}^{x_k \rightarrow 1}$  using diffusion coefficients obtained from  $i$ - $k$  and  $j$ - $k$  mixtures, *i.e.*  $\mathcal{D}_{ik}^{x_k \rightarrow 1}$  and  $\mathcal{D}_{jk}^{x_k \rightarrow 1}$ . The VKB and DKB models are also based on binary diffusion coefficients  $\mathcal{D}_{ik}^{x_k \rightarrow 1}$  and  $\mathcal{D}_{jk}^{x_k \rightarrow 1}$ , but different weights are assigned to these coefficients. In chapter 3, we will show that in the limit  $x_k \rightarrow 1$ , the MS diffusivity  $\mathcal{D}_{ij}$  should not depend on the ratio  $x_i/x_j$ . The RS model is a combination of WK and KT approaches. However, all these models are empirical in nature and lack a solid theoretical foundation. A thorough experimental validation of these models has been prohibited by the lack of experimental data and the uncertainty introduced by the thermodynamic factor. It is important to note that it is extremely difficult to obtain  $\mathcal{D}_{ij}^{x_k \rightarrow 1}$  from experiments. In the limit where components  $i$  and  $j$  are infinitely diluted in component  $k$ , it is also extremely difficult to obtain good statistics for  $\mathcal{D}_{ij}^{x_k \rightarrow 1}$  in equilibrium MD simulations. The CPU requirements for calculating  $\mathcal{D}_{ij}^{x_k \rightarrow 1}$  are far beyond the simulations for binary systems. To the best of our knowledge, due to this difficulty, MS diffusivities  $\mathcal{D}_{ij}^{x_k \rightarrow 1}$  have not been analyzed in simulations previously.



## 2.3 Equilibrium Molecular Dynamics simulation

Equilibrium MD simulations are used to determine the self- and MS diffusivities in the mixtures of n-hexane, cyclohexane and toluene. In the equilibrium MD simulations, we use the united-atom approach and consider the  $\text{CH}_x$  groups as single uncharged interaction centers with their own effective interaction potentials. All bond lengths are kept fixed using the SHAKE algorithm<sup>17;18</sup>. For n-hexane and cyclohexane, a harmonic bond bending potential controls the bond-bending between three consecutive beads. The interaction between four consecutive atoms in a molecule is described by a torsion potential taken from Ref.<sup>68</sup>. Toluene is treated as a rigid body. LJ interactions are used to describe the non-bonded interactions. Wick *et al.* reported a force field for linear and branched alkanes as well as alkylbenzenes, using a potential truncated at 14 Å and analytical tail corrections<sup>68</sup>. Dubbeldam *et al.* reported LJ potentials for alkanes using a potential truncated and shifted in these models at 12 Å<sup>69</sup>. We slightly adjusted these LJ energy parameters for the following reasons (keeping the LJ size parameters fixed): (1) the LJ parameters were fitted at higher temperatures (above 400 K) while standard conditions (298.15 K, 1 atm) are of interest in the present work. As diffusivities strongly depend on the density, we feel that it is important to accurately reproduce the experimental liquid density; (2) different cutoff radii were used in Refs.<sup>68;69</sup>. In this work, we use a LJ potential that is truncated and shifted at 12 Å without using analytical tail corrections. The LJ energy parameters are therefore rescaled to match the experimental densities at standard conditions and are listed in Table 2.1. The LJ parameters for the interactions of unlike atoms are calculated using the standard Lorentz-Berthelot mixing rules<sup>18</sup>. Using these parameters the experimental liquid density at standard conditions is correctly reproduced as shown in Table 2.2.

To simulate one component infinitely diluted in another one, a binary mixture consisting of 1 molecule of component  $i$  and 599 molecules of component  $j$  is used. A system consisting of 1 molecule of component  $i$ , 1 molecule of component  $j$  and 598 molecules of component  $k$  is used to represent a system of components  $i$  and  $j$  infinite diluted in the third component  $k$ . A ternary mixture of 1 molecule of component  $i$ , 300 molecules of components  $j$  and  $k$  respectively is used to represent a system in which component  $i$  infinite diluted in  $j$ - $k$  mixture with equimolar composition. Thus, binary and ternary mixtures containing 600 or 601 molecules in total are used

**Table 2.1:** Comparison of the LJ parameters of various united-atom models. The interactions between unlike pseudo-atoms are calculated using Lorentz-Berthelot mixing rules<sup>18</sup>. Here, the LJ potentials are truncated and shifted at 12 Å.

pseudo-atom	this work		Wick <i>et al.</i> <sup>68</sup>		Dubbeldam <i>et al.</i> <sup>69</sup>	
	$\sigma$ [Å]	$\epsilon/k_B$ [K]	$\sigma$ [Å]	$\epsilon/k_B$ [K]	$\sigma$ [Å]	$\epsilon/k_B$ [K]
CH <sub>3</sub> -CH <sub>3</sub> (in n-hexane)	3.760	92.61	3.750	98.0	3.760	108.0
CH <sub>3</sub> -CH <sub>3</sub> (in toluene)	3.760	100.83	3.750	98.0	3.760	108.0
CH <sub>2</sub> -CH <sub>2</sub> (in n-hexane)	3.960	48.02	3.950	46.0	3.960	56.0
CH <sub>2</sub> -CH <sub>2</sub> (in cyclohexane)	3.960	57.12	3.950	46.0	3.960	56.0
CH-CH (in toluene)	3.965	51.96	3.965	50.5	-	-
C-C (in toluene)	3.880	21.66	3.880	21.0	-	-

**Table 2.2:** Density of pure components  $\rho_i$  (g · ml<sup>-1</sup>) at 298.15 K, 1 atm. Here, “1” represents n-hexane, “2” represents cyclohexane and “3” represents toluene. The values obtained in this work are obtained from equilibrium MD simulations in the  $NpT$  ensemble.

$i$	this work	Experimental Results	
1	0.6574	0.6548 (Ref. <sup>70</sup> )	0.6551 (Ref. <sup>71</sup> )
2	0.7757	0.7739 (Ref. <sup>70</sup> )	0.7739 (Ref. <sup>72</sup> )
3	0.8636	0.8619 (Ref. <sup>73</sup> )	0.8685 (Ref. <sup>74</sup> )

in all simulations. Such a system is generated as follows. Starting from an initial configuration, the system is equilibrated using equilibrium MD in the  $NpT$  ensemble at 298.15 K, and 1 atm using the Nosé-Hoover thermostat with a time constant of 1 ps. Periodic boundary conditions are used. The integration time step is 2 fs for which the pseudo-Hamiltonian is well conserved. When the average density of the systems does not change with time, we use the equilibrated system at this average density for computing the self- and MS diffusivities in the microcanonical ( $NVE$ ) ensemble.

The self-diffusivity describes the motion of individual molecules. The Einstein equation connects the self-diffusivity  $D_{i,\text{self}}$  to the average molecular displacements<sup>17</sup>

$$D_{i,\text{self}} = \frac{1}{6N_i} \lim_{m \rightarrow \infty} \frac{1}{m \cdot \Delta t} \left\langle \sum_{l=1}^{N_i} (r_{l,i}(t + m \cdot \Delta t) - r_{l,i}(t))^2 \right\rangle. \quad (2.18)$$

An alternative but equivalent expression is

$$D_{i,\text{self}} = \frac{1}{3N_i} \int_0^\infty dt' \left\langle \sum_{l=1}^{N_i} (v_{l,i}(t) \cdot v_{l,i}(t+t')) \right\rangle. \quad (2.19)$$

In these equations,  $D_{i,\text{self}}$  is the self-diffusivity of component  $i$ ,  $N_i$  is the total number molecules of component  $i$ ,  $r_{l,i}(t)$  is the position of  $l^{\text{th}}$  molecule of component  $i$  at time  $t$  and  $v_{l,i}(t)$  is its velocity. The MS diffusivities follow directly from the Onsager coefficients, which are obtained from equilibrium MD simulations using<sup>23</sup>

$$\Lambda_{ij} = \frac{1}{6} \lim_{m \rightarrow \infty} \frac{1}{N} \frac{1}{m \cdot \Delta t} \times \left\langle \left( \sum_{l=1}^{N_i} (r_{l,i}(t+m \cdot \Delta t) - r_{l,i}(t)) \right) \left( \sum_{k=1}^{N_j} (r_{k,j}(t+m \cdot \Delta t) - r_{k,j}(t)) \right) \right\rangle. \quad (2.20)$$

The Green-Kubo form for obtaining  $\Lambda_{ij}$  is

$$\Lambda_{ij} = \frac{1}{3N} \int_0^\infty dt' \left\langle \sum_{l=1}^{N_i} v_{l,i}(t) \cdot \sum_{k=1}^{N_j} v_{k,j}(t+t') \right\rangle. \quad (2.21)$$

In these equations,  $N$  is the total number of molecules in the simulation, and  $i, j$  are the molecule types. Note that the matrix  $[\Lambda]$  is symmetric, *i.e.*  $\Lambda_{ij} = \Lambda_{ji}$  and that the Onsager coefficients are constraint by  $\sum_i M_i \Lambda_{ij} = 0$  in which  $M_i$  is the molar mass of component  $i$ <sup>23</sup>. In all cases, mean squared displacement is updated with different frequencies according to the order- $n$  algorithm described in Refs.<sup>17;75</sup>. By plotting the mean squared displacements as a function of time on a log-log scale, we determined the regime for diffusion and extracted the diffusivities<sup>76</sup>. For more information on how to extract MS diffusivities from equilibrium MD simulations, we refer the reader to appendix A. The self- and MS diffusivities for a certain mixture are averaged over 30 independent simulations of 40 ns each. The initial configurations of these simulations were generated such that they were independent. The statistical errors in the computed self- and MS diffusivities are below 1% and 4% for both binary and ternary mixtures, respectively.

## 2.4 Evaluation approaches for diffusion models

### 2.4.1 Model validation

The excess molar volume  $V^E$  is one possible way to study the interaction between different components. It is defined as

$$V^E = \sum_{i=1}^n \frac{x_i M_i}{\rho} - \sum_{i=1}^n \frac{x_i M_i}{\rho_i}, \quad (2.22)$$

where  $M_i$  is the molar mass of component  $i$ ,  $\rho_i$  is the density of pure component  $i$ ,  $\rho$  is the density of the mixture, and  $n$  is the number of components. The excess molar volume of a binary mixture can be used to validate the simulation model. The Redlich-Kister equation can be used to correlate the composition dependence of the excess molar volume. In a binary mixture, this equation equals<sup>77</sup>

$$V^E = x_1(1 - x_1) \sum_{i=0}^p a_i (2x_1 - 1)^i, \quad (2.23)$$

in which  $x_1$  is the mole fraction of the first component, and  $p$  is the total number of parameters used in Eq. (2.23). The coefficients  $a_i$  can be calculated using a least squares fit.

### 2.4.2 Indirect comparison

Recently, it was shown that predictive models for MS diffusivities can be accessed in experiments directly via self-diffusivities at infinite dilution<sup>7</sup>. The same approach can be used in simulations. In experiments, the MS diffusivities are determined from the measurable Fick diffusion coefficients using Eq. (2.4) while in the simulations they can be computed directly, see section 2.3. As discussed in the previous section, the presence of the thermodynamic factors  $[\Gamma]$  in Eq. (2.4) introduces large uncertainties in determining MS diffusivities from experiments<sup>62</sup>. To avoid difficulties associated with the thermodynamic factors  $[\Gamma]$ , we consider simulations in the region of infinite dilution for which  $[\Gamma]$  for any system reduces to

$$\Gamma_{ii}^{x_i \rightarrow 0} = 1, \quad (2.24)$$

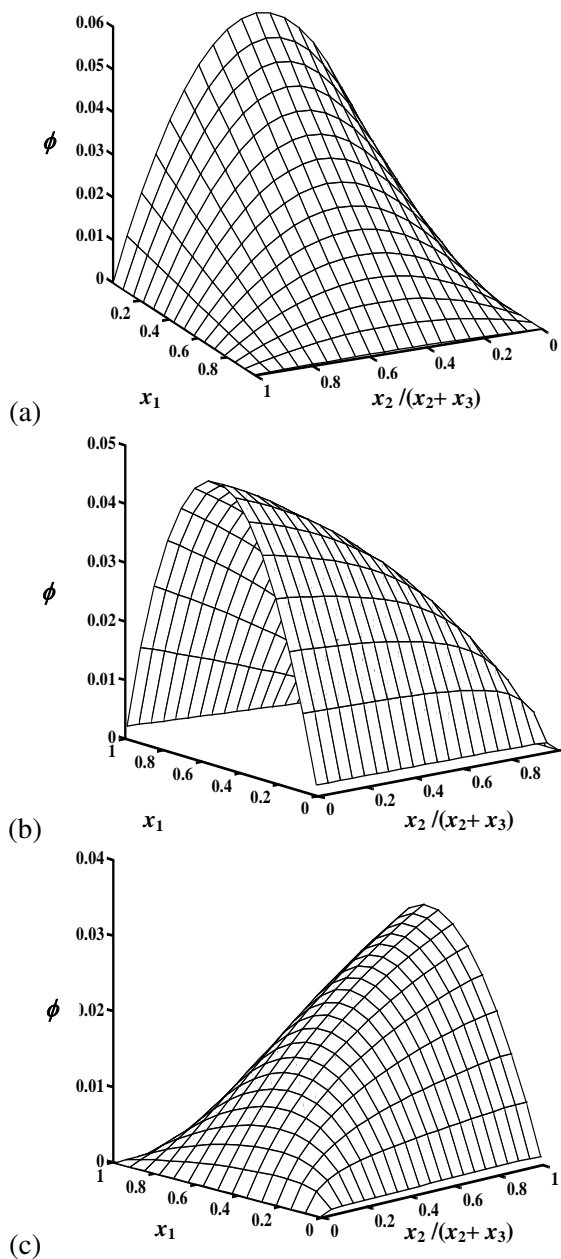


**Figure 2.1:** Objective functions  $\phi$  (Eq. (2.29)) for screening the differences between predictive models: Eq. (2.28) + Eq. (2.12) + Eqs. (2.13) to (2.17). The parameters for the predictive models were taken from the simulations in Table 2.4. (a)  $D_{1,\text{self}}$  (b)  $D_{2,\text{self}}$ , (c)  $D_{3,\text{self}}$ . Here, “1” represents n-hexane, “2” represents cyclohexane and “3” represents toluene.

$$\Gamma_{ij, i \neq j}^{x_i \rightarrow 0} = 0. \quad (2.25)$$

Furthermore, at these conditions ( $x_i \rightarrow 0$ ), the off-diagonal elements of the Fick matrix vanish

$$D_{ij}^{x_i \rightarrow 0} = 0, \quad (2.26)$$

and the diagonal elements become identical to the self-diffusivities

$$D_{ii}^{x_i \rightarrow 0} = D_{i,\text{self}}^{x_i \rightarrow 0}. \quad (2.27)$$

In this limit, the self-diffusivity of component  $i$  is related to the MS diffusivities by<sup>62</sup>

$$\frac{1}{D_{i,\text{self}}^{x_i \rightarrow 0}} = \sum_{j=1, j \neq i}^n \frac{x_j}{\mathcal{D}_{ij}}. \quad (2.28)$$

It is important to note that Eqs. (2.24) to (2.28) hold for any  $n$ -component system, and that Eq. (2.28) is exact. To relate the self-diffusivity in ternary mixtures to the binary diffusion coefficients, the following procedure can be used. The MS diffusivities in Eq. (2.28) are estimated using the generalized Vignes equation (Eq. (2.12)). The binary diffusion coefficients ( $\mathcal{D}_{ij}^{x_i \rightarrow 1}$  and  $\mathcal{D}_{ij}^{x_j \rightarrow 1}$ ) that appear in the generalized Vignes equation can be obtained from experiments or simulations. The value of  $\mathcal{D}_{ij}^{x_k \rightarrow 1}$  can be obtained from any of the five predictive models (Eqs. (2.13) to (2.17)), requiring binary diffusion data only. This results in five predictions for  $D_{i,\text{self}}^{x_i \rightarrow 0}$ , here denoted by  $D_{il,\text{self}}^{\text{prediction}}$  with  $l = 1, 2, \dots, 5$ . In the following sections, we refer to these predictions as “Eq. (2.28) + Eq. (2.12) + Eqs. (2.13) to (2.17)”. To minimize the amount of simulations required to discriminate between these models, an objective function  $\phi_i$  is constructed to analyze the differences between the five predictive models:

$$\phi_i = \frac{\sum_{l=1}^M |D_{il,\text{self}}^{\text{prediction}} - D_{i,\text{self}}^{\text{average}}|}{M \cdot D_{i,\text{self}}^{\text{average}}}, \quad (2.29)$$

in which  $M$  is the number of predictive models (here:  $M = 5$ ). The term  $D_{i,\text{self}}^{\text{average}}$  is the average of  $D_{il,\text{self}}^{\text{prediction}}$ . Figure 2.1 shows the objective function  $\phi_i$  as a function of the mixture composition using binary diffusion data from equilibrium MD simulations. Here, the system consists of n-hexane, cyclohexane and toluene. The value of  $\phi_i$  is large when  $x_i \approx 0$  and  $x_j \approx x_k$  ( $i \neq j \neq k$ ). This is the case for all 3 components.

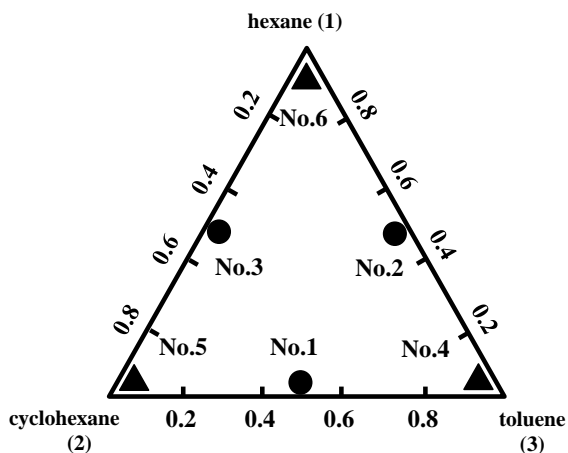


**Figure 2.2:** Ternary diagram for the system n-hexane (1) - cyclohexane (2) - toluene (3). The various labeled compositions (No. 1, 2, 3, 4, 5, 6) are referred to in the main text.

The results are consistent with the conclusion of a previous study in which a different method was applied to analyze the differences<sup>7</sup>. These compositions are referred to as No. 1, 2 and 3 in Figure 2.2. Simulations at these conditions contain the maximum information regarding the discrimination between the considered models based on diffusion coefficients.

### 2.4.3 Validation of the generalized Vignes equation

The indirect comparison described in the previous subsection critically relies on the generalized Vignes equation (Eq. (2.12)). However, it is unknown whether or not the generalized Vignes equation provides an accurate estimate for  $\bar{D}_{ij}$  at any concentration in multicomponent mixtures. To test the quality of the predictions of the generalized Vignes equation, we parametrize the generalized Vignes equation using binary MS diffusivities obtained from equilibrium MD simulations. The predictions of the generalized Vignes equation are compared directly to ternary MS diffusivities obtained from equilibrium MD simulations.

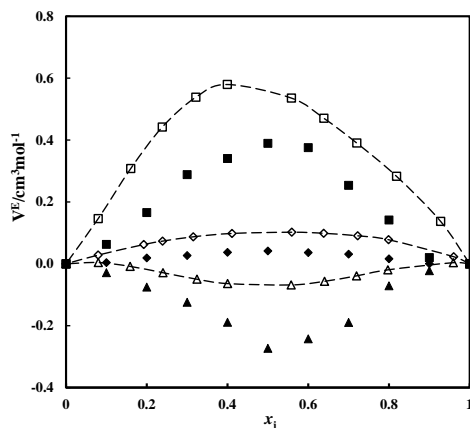


**Figure 2.3:** Excess molar volumes of binary systems as a function of the composition at 298.15 K, 1 atm. The filled symbols are simulation results and the dash lines plus open symbols are experimental data from Ref.<sup>77</sup>. Diamonds: “1-2” mixture, triangles: “1-3” mixture, Squares: “2-3” mixture.  $x_i$  refers to the mole fraction of  $i$  in an  $i$ - $j$  mixture. Here, “1” represents n-hexane, “2” represents cyclohexane and “3” represents toluene.

## 2.4.4 Direct comparison

Several models (Eqs. (2.13) to (2.17)) are available to predict  $(\mathcal{D}_{ij}^{x_k \rightarrow 1})$  using binary MS diffusivities. As mentioned earlier, these models are empirical in nature and lack a solid theoretical foundation. Therefore, we performed equilibrium MD simulations in the corners of the ternary diagram corresponding to the limiting conditions  $x_i, x_j \rightarrow 0, x_k \rightarrow 1$ , defined by No. 4, 5 and 6 in Figure 2.2.

## 2.5 Results and discussion

### 2.5.1 Model validation

The excess molar volumes of binary mixtures are calculated to validate the simulation models. The dependency of excess molar volume on the mixture composition is well described using the Redlich-Kister equation using three coefficients  $a_i$ . In Figure 2.3, we compare the computed excess molar volume to the experimental data. We observe that (1) the computed excess molar volume has the same sign as in the corresponding experiment; the agreement is thus reasonable; (2) both simulation and experimental results show a maximum or minimum of the excess molar volume around the equimo-



**Table 2.3:** Self-diffusivity of pure components  $D_{i,\text{self}}/(10^{-9} \text{ m}^2 \cdot \text{s}^{-1})$  at 298.15 K, 1 atm. The statistical errors in equilibrium MD simulations are below 1%. Here, “1” represents n-hexane, “2” represents cyclohexane and “3” represents toluene.

$i$	MD	Experiment
1	5.50	4.25 (Ref. <sup>78</sup> )
2	2.05	1.37 (Ref. <sup>78</sup> )
3	2.89	2.25 (Ref. <sup>78</sup> )

lar composition. In summary, our model is considered to be adequately detailed for the present study.

The self-diffusivities of the pure components at 298.15 K, 1 atm are calculated from equilibrium MD simulations, see Table 2.3. Compared to the experimental data, the computed diffusivities are systematically somewhat larger. The MS diffusivities in binary mixtures are shown in Table 2.4. The MS diffusivities at infinite dilution  $\mathcal{D}_{ij}^{x_j \rightarrow 1}$  calculated from equilibrium MD simulations are also larger than the experimental results. The degree to which the simulation results agree with the experimental data is governed by three elements: (1) how accurately the model (force field) matches reality. In this work, a united-atom model was used. The LJ parameters were rescaled to reproduce the density of pure components at 298.15 K, 1 atm. However, the force field was not optimized for describing transport properties. Even with this simple interaction model, we still obtain the correct order of magnitude and qualitative trends for the MS diffusivities; (2) the statistical error in the computed MS diffusivities. As mentioned earlier, this error is below 4%; (3) the accuracy of the experimental data. It is important to note that in the experiments, the self-diffusivity of component  $i$  is obtained as a function of its mole fraction  $x_i$ . The function  $D_{i,\text{self}}(x_i)$  is extrapolated to  $x_i \rightarrow 0^7$ , and by definition in this limit  $\mathcal{D}_{ij} = D_{i,\text{self}}$ . These extrapolated values are listed in Table 2.4. In summary, we feel that the agreement between experiments and simulations is quite good and that our model for the ternary system n-hexane - cyclohexane - toluene is a suitable test system to investigate models for MS diffusivities.

**Table 2.4:** Comparison between MS diffusivities  $\mathcal{D}_{ij}^{x_j \rightarrow 1} / (10^{-9} \text{m}^2 \cdot \text{s}^{-1})$  in binary mixtures obtained both from experiments and equilibrium MD simulations. The statistical errors in equilibrium MD simulations are less than 1%. Here, “1” represents n-hexane, “2” represents cyclohexane and “3” represents toluene. The limit  $x_j \rightarrow 1$  is approached by considering a system of 1 molecule of type  $i$  and 599 molecules of type  $j$ .

$i - j$	MD	Experiment
1 - 2	2.63	1.69 (Ref. <sup>79</sup> )
2 - 1	4.30	3.88 (Ref. <sup>79</sup> )
1 - 3	2.98	2.39 (Ref. <sup>78</sup> )
3 - 1	4.84	4.35 (Ref. <sup>78</sup> )
2 - 3	2.73	2.23 (Ref. <sup>78</sup> )
3 - 2	2.10	1.13 (Ref. <sup>78</sup> )

## 2.5.2 Indirect comparison

As explained earlier, the self-diffusivities at infinite dilution are predicted using Eqs. (2.12), (2.28) and Eqs. (2.13) to (2.17), requiring only MS binary diffusion data at infinite dilution which were obtained from equilibrium MD simulations, see Table 2.4. This analysis corresponds to the experimental test carried out in Ref.<sup>7</sup>. Table 2.5 shows a comparison between these predictions and the self-diffusivities computed directly from equilibrium MD simulations. The predicted self-diffusivities of n-hexane and cyclohexane are all systematically larger than the directly computed self-diffusivities. The differences are of the order of 10-40%. For toluene, the predictions are all systematically lower than the directly computed self-diffusivities but the differences are much smaller than for n-hexane and cyclohexane. From Table 2.5 it is however clear that none of the predictions is significantly better than the others. Given this result, it is important to investigate the origin of the observed differences with the computed self-diffusivity individually, *i.e.* the quality of the generalized Vignes equation (Eq. (2.12)) and the quality of the predictive models for  $\mathcal{D}_{ij}^{x_k \rightarrow 1}$ .

## 2.5.3 Validation of the generalized Vignes equation

To directly assess the quality of the generalized Vignes equation (Eq. (2.12)), we parametrize the generalized Vignes equation using MS diffusivities from equilibrium

**Table 2.5:** Predictions for self-diffusivities  $D_{i,\text{self}}/(10^{-9} \text{ m}^2 \cdot \text{s}^{-1})$  in ternary mixtures (composition corresponding to No.1, 2 and 3 in Figure 2.2 using Eq. (2.28). The binary diffusion coefficients in Table 2.4 are used as input. The procedure is explained in the main text. The statistical errors in the equilibrium ns are below 1%. RelDiff is the relative difference between simulation results and predictions. Here, “1” represents n-hexane, “2” represents cyclohexane and “3” represents toluene.

	$D_{1,\text{self}}$	RelDiff	$D_{2,\text{self}}$	RelDiff	$D_{3,\text{self}}$	RelDiff	Averaged RelDiff
Eqs. (2.28)+(2.12)+WK	3.16	46%	3.00	6%	2.95	12%	21%
Eqs. (2.28)+(2.12)+KT	2.70	25%	3.42	22%	3.23	4%	17%
Eqs. (2.28)+(2.12)+VKB	2.60	20%	3.41	25%	3.27	2%	16%
Eqs. (2.28)+(2.12)+DKB	2.81	30%	3.43	19%	3.19	5%	18%
Eqs. (2.28)+(2.12)+RS	2.92	35%	3.23	15%	3.12	7%	19%
MD	2.16	–	2.88	–	3.35	–	–

MD simulations (Tables 2.4 and 2.7). Table 2.6 shows the MS diffusivities estimated using the generalized Vignes equation (composition corresponding to Figure 2.2, No. 1, 2 and 3). For our test mixture, the generalized Vignes equation provides reasonable predictions of the MS diffusivities with relative differences less than 17%. However, these differences are certainly significant and it suggests that a large part of the differences observed in Table 2.5 are due to the fact that the generalized Vignes equation is not exact. This result also serves as an estimate of the best accuracy that can be expected from any Vignes-based model.

### 2.5.4 Direct comparison

Table 2.7 shows the predicted MS diffusivities at infinite dilution ( $\mathcal{D}_{ij}^{x_k \rightarrow 1}$ ) using five different models Eqs. (2.13)-(2.17). These models are parametrized using MS diffusivities of binary mixtures as shown in Table 2.4. The accuracy of the predictive models depends on both the accuracy of the binary MS diffusivities and the quality of predictive models. As the MS diffusivities in binary mixtures are computed with the high accuracy, the errors are less than 4%, we are able to address the quality of predictive models. For predicting  $\mathcal{D}_{12}^{x_3 \rightarrow 1}$  (composition corresponding to Figure 2.2, No. 4), the KT, VKB, DKB and RS models are accurate. The WK model is clearly the worst. For predicting  $\mathcal{D}_{13}^{x_2 \rightarrow 1}$  (composition corresponding to Figure 2.2, No. 5),

**Table 2.6:** Predictions for MS diffusivities  $\mathcal{D}_{ij}/(10^{-9} \text{ m}^2 \cdot \text{s}^{-1})$  in ternary mixtures (composition corresponding to No. 1, 2 and 3 in Figure 2.2) using the generalized Vignes equation (Eq. (2.12)). The binary diffusion coefficients  $\mathcal{D}_{ij}^{x_i \rightarrow 1}$ ,  $\mathcal{D}_{ij}^{x_j \rightarrow 1}$  and ternary diffusion data  $\mathcal{D}_{ij}^{x_k \rightarrow 1}$  obtained from equilibrium MD simulations are shown in Tables 2.4 and 2.7. The statistical errors in equilibrium MD simulations are below 4%. RelDiff is the relative difference between simulations and predictions. Here, “1” represents n-hexane, “2” represents cyclohexane and “3” represents toluene.

		MD	Vignes	RelDiff
Fig. 2.2 No.1	$\mathcal{D}_{12}$	2.48	2.78	12%
	$\mathcal{D}_{13}$	2.74	2.56	7%
	$\mathcal{D}_{23}$	2.28	2.40	5%
Fig. 2.2 No.2	$\mathcal{D}_{12}$	3.19	3.55	11%
	$\mathcal{D}_{13}$	4.10	3.79	7%
	$\mathcal{D}_{23}$	2.85	3.33	17%
Fig. 2.2 No.3	$\mathcal{D}_{12}$	3.68	3.36	9%
	$\mathcal{D}_{13}$	3.86	3.26	16%
	$\mathcal{D}_{23}$	3.41	2.92	14%

**Table 2.7:** Predictions for the MS diffusivities  $\mathcal{D}_{ij}^{x_k \rightarrow 1}/(10^{-9} \text{ m}^2 \cdot \text{s}^{-1})$  in ternary mixtures (composition corresponding to No. 4, 5 and 6 in Figure 2.2) compared with direct equilibrium MD simulations. These predictive models are parametrized using the binary diffusivities shown in Table 2.4. The statistical errors in equilibrium MD simulations are below 4%. Here, RelDiff is the relative difference between simulation results and predictions. “1” represents n-hexane, “2” represents cyclohexane and “3” represents toluene. In the MD simulations,  $\mathcal{D}_{ij}^{x_k \rightarrow 1}$  is approached by considering a system of 1 molecule of type  $i$ , 1 molecule of type  $j$ , and 598 molecules of type  $k$ .

	$\mathcal{D}_{12}^{x_3 \rightarrow 1}$	RelDiff	$\mathcal{D}_{13}^{x_2 \rightarrow 1}$	RelDiff	$\mathcal{D}_{23}^{x_1 \rightarrow 1}$	RelDiff	Averaged RelDiff
WK	3.36	14%	3.80	74%	2.39	41%	43%
KT	2.85	3%	2.35	7%	4.56	12%	8%
VKB	2.85	3%	2.35	7%	4.56	12%	8%
DKB	2.86	3%	2.37	8%	4.57	13%	8%
RS	3.10	5%	2.99	37%	3.31	18%	20%
MD	2.94	–	2.19	–	4.06	–	–

the KT, VKB and DKB models still provide reasonable predictions while the WK and RS models give large errors. For predicting  $D_{23}^{x_1 \rightarrow 1}$  (composition corresponding to Figure 2.2, No. 6), the performance of the five models is similar to the second case. Considering their average performance, the WK model predicts MS diffusivities with deviations more than 40%, and the KT, VKB and DKB models yield the best predictions. Here, we would stress that both VKB and DKB models suffer from inconsistencies when  $x_i$  and  $x_j$  are approaching zero simultaneously. Therefore, we would prefer the KT model over the VKB and DKB models. The RS model behaves worse than KT, VKB and DKB models. This suggests that in a ternary mixture, the interaction between two diluted components (expressed by  $D_{ij}^{x_k \rightarrow 1}$ ) strongly depends on how each solute interacts with the solvent in the corresponding binary mixture (expressed by  $D_{ik}^{x_k \rightarrow 1}$  and  $D_{jk}^{x_k \rightarrow 1}$ ). Therefore, it is natural to consider the following generalized model for  $D_{ij}^{x_k \rightarrow 1}$

$$D_{ij}^{x_k \rightarrow 1} = (D_{ij}^{x_i \rightarrow 1} D_{ij}^{x_j \rightarrow 1})^{\frac{\alpha}{2}} (D_{ik}^{x_k \rightarrow 1} D_{jk}^{x_k \rightarrow 1})^{(\frac{1}{2} - \frac{\alpha}{2})}. \quad (2.30)$$

For  $\alpha = 0$ , this equation reduces to the KT model,  $\alpha = 0.5$  corresponds to the RS model, and  $\alpha = 1$  corresponds to the WK model. We fitted the computed diffusivities at the three compositions (Figure 2.2, No. 4, 5, 6) simultaneously using a least-squares method. The optimal value of  $\alpha$  equals 0.18, resulting in an average relative difference of 6%. This cannot be considered as a major improvement over the existing models for the tested systems.

## 2.6 Conclusions

The MS theory is the most natural method for describing mass transport, as it uses the chemical potential gradient as driving force. MS diffusivities often do not depend strongly on the concentration, *i.e.* the concentration dependence is often quite smooth, in sharp contrast to multicomponent Fick diffusivities. As MS diffusivities cannot be measured directly in experiments and molecular simulations are often time consuming, there is a clear need for predictive models based on easily measurable quantities. For diffusion in binary mixtures, several predictive models are able to estimate MS diffusion coefficients with a reasonable accuracy. Some recent studies on binary mixtures show that the binary predictive models may fail in mixtures including

water and alcohols<sup>28;29</sup>. The situation in multicomponent systems is certainly more complicated. The applicability of predictive models in multicomponent systems is much less investigated. This hampers the progress of investigations of multicomponent diffusion processes.

In this chapter, we have demonstrated an efficient method for evaluating predictive models for estimating MS diffusivities. This method allows for a critical assessment of different predictive models with minimal simulation effort. We analyzed two different ways for evaluating these predictive models: (1) a direct comparison of MS diffusivities is the most straightforward way and it can be conducted using simulations; (2) an indirect comparison using self-diffusivities at infinite dilution, as proposed by the experimental study of Ref.<sup>7</sup>. We found that for predicting the MS diffusivity  $\mathcal{D}_{ij}^{x_k \rightarrow 1}$  in ternary mixtures of n-hexane - cyclohexane - toluene, the Kooijman-Taylor model is favored. The same finding is also observed in the indirect comparison, both in experiments<sup>7</sup> and in our simulations. However, the differences between predictive models are significantly reduced in the indirect comparison which indicates that the self-diffusivity is not very sensitive to the used predictive model. Therefore, evaluating self-diffusivities is not the best choice for evaluating the predictive models. Also, we directly tested the applicability of the generalized Vignes equation in ternary mixtures. Our results show that the generalized Vignes equation is a reasonable engineering model for the prediction of MS diffusivities in the investigated ternary mixture but it still introduces a significant error of more than 10%. Our results also show that the MS diffusivities in  $i$ - $k$  and  $j$ - $k$  mixtures should be included in predicting the MS diffusivities  $\mathcal{D}_{ij}^{x_k \rightarrow 1}$  in n-hexane - cyclohexane - toluene mixtures. In these mixtures, the interaction between solutes and solvent is important for studying diffusion even at infinite dilution. The observation that in the system n-hexane - cyclohexane - toluene none of the approaches is able to accurately predict MS diffusivities from binary data suggests that new models and/or approaches are needed. From recent results on binary mixtures<sup>28;29</sup>, it can be expected that these situations are even more critical for mixtures including water and alcohols. The approach developed in this work shows that molecular simulations can be used as a tool to develop better models for predicting transport diffusivities in ternary mixtures.

# 3

---

## Multicomponent Maxwell-Stefan Diffusivities at Infinite Dilution

---

This chapter is for a large part based on:

X. Liu, A. Bardow, T.J.H. Vlugt, *Multicomponent Maxwell-Stefan diffusivities at infinite dilution*, *Industrial & Engineering Chemistry Research*, **2011**, 50, 4776-4782.

### 3.1 Introduction

Diffusion plays an important role in (bio)chemical processes. The MS theory provides a sound theoretical basis and is therefore preferred for modeling of diffusion in liquids<sup>1;2;21</sup>. Unfortunately, it is difficult to obtain MS diffusivities from experiments while obtaining MS diffusivities from MD simulations is time consuming. In experiments, Fick diffusivities are measured<sup>8;58</sup> which have to be converted to MS diffusivities via a thermodynamic factor. This introduces large uncertainties<sup>7;80</sup>. Extracting MS diffusivities from simulations may lead to extensive CPU-time requirements<sup>28;29</sup>. Therefore, predictive models for the concentration dependence of MS diffusivities based on easily measurable quantities are highly desired. The Vignes equation is often recommended to predict the concentration dependence of MS diffusivities<sup>1;2</sup>. In ternary mixtures, the generalized Vignes equation equals<sup>24</sup>

$$\mathcal{D}_{ij} = (\mathcal{D}_{ij}^{x_i \rightarrow 1})^{x_i} (\mathcal{D}_{ij}^{x_j \rightarrow 1})^{x_j} (\mathcal{D}_{ij}^{x_k \rightarrow 1})^{x_k}, \quad (3.1)$$

in which  $\mathcal{D}_{ij}$  is the MS diffusivity describing the friction between components  $i$  and  $j$ , and  $x_i$  is the mole fraction of component  $i$ . The terms  $\mathcal{D}_{ij}^{x_i \rightarrow 1}$  and  $\mathcal{D}_{ij}^{x_j \rightarrow 1}$  describe the friction between a diluted component and the solvent and therefore these are equal to their value in a binary mixture of  $i$  and  $j$  only. The generalized Vignes equation requires the value of  $\mathcal{D}_{ij}^{x_k \rightarrow 1}$ , which describes the friction between components  $i$  and  $j$  when both are infinitely diluted in a third component  $k$ . This quantity is not easily accessible in experiments since no direct measurement is possible<sup>7</sup>. In the past decades, several empirical models were proposed for estimating  $\mathcal{D}_{ij}^{x_k \rightarrow 1}$  from binary diffusion data, as presented in chapter 2, Eqs. (2.13) to (2.17)<sup>23;24;50;51;67</sup>. These empirical models can be classified into three categories: (1) the friction between the two diluted components is taken into account and the friction between the diluted components and the solvent is neglected, *i.e.* the WK model; (2) the friction between the diluted components and the solvent is taken into account and the friction between the diluted components themselves is neglected, *i.e.* the KT, VKB, DKB models; (3) a combination of the first two categories, *i.e.* the RS model. Since there is no physical basis for any of these models, it is unclear which one to use for a specific system. It is important to note that errors introduced by modeling the concentration dependence of MS diffusivities using the generalized Vignes equation (Eq. (3.1)) may be either



be reduced or enhanced by a particular choice for a model for  $\mathcal{D}_{ij}^{x_k \rightarrow 1}$ <sup>33</sup>. In the remainder of this chapter, we will not consider this issue further and focus instead on how  $\mathcal{D}_{ij}^{x_k \rightarrow 1}$  can be predicted.

In this chapter, we show that  $\mathcal{D}_{ij}^{x_k \rightarrow 1}$  is a well-defined quantity that is independent of the ratio  $x_i/x_j$ . Based on linear response theory and the Onsager relations, we propose a new model for estimating  $\mathcal{D}_{ij}^{x_k \rightarrow 1}$  from easily measurable self-diffusivities. Unlike the WK, KT, VKB, DKB, and RS models, our model has a sound theoretical basis. The key assumption is that velocity cross-correlations between particles are negligible. We perform MD simulations to assess the quality of our new model. It turns out that the model works very well for systems consisting of non-associating molecules. For the highly associating system water - methanol - ethanol, the earlier mentioned cross-correlations between particle velocities cannot be neglected due to the collective motion of molecules, originating from networks of hydrogen bonds.

This chapter is organized as follows. In section 3.2, we explain how MS diffusivities can be obtained from MD simulations. We show that  $\mathcal{D}_{ij}^{x_k \rightarrow 1}$  does not depend on the molar ratio  $x_i/x_j$  and we derive a model for estimating  $\mathcal{D}_{ij}^{x_k \rightarrow 1}$  using easily measurable pure-component and binary self-diffusivities. Details about the MD simulations are addressed in section 3.3. In section 3.4, we test our model for the following ternary systems: (1) a system without attractions, *i.e.* particles interact with a WCA potential<sup>81</sup>; (2) the n-hexane - cyclohexane - toluene system, in which molecules interact with LJ interactions; (3) the ethanol - methanol - water system in which electrostatic interactions play an important role. We compare the predictions of  $\mathcal{D}_{ij}^{x_k \rightarrow 1}$  with the results from MD simulations. Our conclusions are summarized in section 3.5.

## 3.2 Obtaining Maxwell-Stefan Diffusivities from MD simulations

MD simulations can be used to directly compute the MS diffusivities  $\mathcal{D}_{ij}$  from local fluctuations. The Onsager coefficients  $\Lambda_{ij}$  can be obtained directly from the motion of the molecules in MD simulations<sup>23</sup>, see section 2.3 and appendix A.

### 3.2.1 Deriving an expression for $\mathcal{D}_{ij}^{x_k \rightarrow 1}$

In appendix A, we show the exact expression of  $\mathcal{D}_{ij}$  as a function of  $x_i, x_j, x_k$  for ternary systems, and all elements of the matrix  $[\Lambda]$  (Eq. (A.11)).

$$\mathcal{D}_{ij} = f(x_i, x_j, x_k, [\Lambda]). \quad (3.2)$$

Using these expressions, we consider the situation in which components  $i$  and  $j$  are infinitely diluted in component  $k$ . It is possible to find a convenient expression for the term  $\Lambda_{ii}$  using the Green-Kubo formulation of the Onsager coefficients (Eq. (2.21)). As component  $i$  is infinitely diluted in component  $k$ , we can neglect correlations in the velocities between two distinct molecules of component  $i$ . Therefore,

$$\begin{aligned} \Lambda_{ii} &= \frac{1}{3N} \int_0^\infty dt' \left\langle \sum_{l=1}^{N_i} v_{l,i}(t) \cdot \sum_{g=1}^{N_i} v_{g,i}(t+t') \right\rangle \\ &= \frac{1}{3N} \int_0^\infty dt' \left\langle \sum_{l=1}^{N_i} v_{l,i}(t) \cdot v_{l,i}(t+t') \right\rangle + \quad (3.3) \\ &\quad \frac{1}{3N} \int_0^\infty dt' \left\langle \sum_{l=1}^{N_i} \sum_{g=1, g \neq l}^{N_i} v_{l,i}(t) \cdot v_{g,i}(t+t') \right\rangle \\ &\approx \frac{1}{3N} \int_0^\infty dt' \left\langle \sum_{l=1}^{N_i} v_{l,i}(t) \cdot v_{l,i}(t+t') \right\rangle \\ &= \frac{N_i}{3N} \int_0^\infty dt' \langle v_{i,1}(t) \cdot v_{i,1}(t+t') \rangle \\ &= x_i C_{ii}, \quad (3.4) \end{aligned}$$

in which  $C_{ii}$  is a constant which does not depend on the total number of molecules. Similarly, we can write for the other component  $j$  that is diluted in component  $k$ ,

$$\Lambda_{jj} \approx x_j C_{jj}. \quad (3.5)$$

In the limit of infinite dilution (which requires the thermodynamic limit), Eqs. (3.3) and (3.5) will be exact. For the solvent  $k$ , the expression for  $\Lambda_{kk}$  is

$$\begin{aligned}\Lambda_{kk} &= \frac{1}{3N} \int_0^\infty dt' \left\langle \sum_{l=1}^{N_k} v_{l,k}(t) \cdot \sum_{g=1}^{N_k} v_{g,k}(t+t') \right\rangle \\ &= \frac{1}{3N} \int_0^\infty dt' \left\langle \sum_{l=1}^{N_k} v_{l,k}(t) \cdot v_{l,k}(t+t') \right\rangle +\end{aligned}\quad (3.6)$$

$$\begin{aligned}& \frac{1}{3N} \int_0^\infty dt' \left\langle \sum_{l=1}^{N_k} \sum_{g=1, g \neq l}^{N_k} v_{l,k}(t) \cdot v_{g,k}(t+t') \right\rangle \\ & \approx x_k C_{kk} + x_k^2 N C_{kk}^*,\end{aligned}\quad (3.7)$$

in which  $C_{kk}$  and  $C_{kk}^*$  account for self- and cross-correlations of the velocities of molecules of type  $k$ , respectively. The value of  $C_{kk}$  is independent of the total number of molecules. For  $\Lambda_{ij}$  with  $i \neq j$ , *i.e.* correlations between unlike molecules, we can write

$$\begin{aligned}\Lambda_{ij} &= \frac{1}{3N} \int_0^\infty dt' \left\langle \sum_{l=1}^{N_i} v_{l,i}(t) \cdot \sum_{k=1}^{N_j} v_{k,j}(t+t') \right\rangle \\ &\approx \frac{N_i N_j}{3N} \int_0^\infty dt' \langle v_{1,i}(t) \cdot v_{1,j}(t+t') \rangle \\ &= N x_i x_j C_{ij}.\end{aligned}\quad (3.8)$$

By inserting Eqs. (3.3) to (3.8) into Eq. (A.11) and setting  $x_j = a x_i$  ( $a$  being a positive constant), we take the limit  $x_i \rightarrow 0$ . The resulting expression is:

$$\mathcal{D}_{ij}^{x_k \rightarrow 1} = \frac{C_{ii} C_{jj}}{C_{kk} + C_x}, \quad (3.9)$$

with

$$C_x = N (C_{ij} - C_{ik} - C_{jk} + C_{kk}^*). \quad (3.10)$$

Eq. (3.9) clearly shows that  $\mathcal{D}_{ij}^{x_k \rightarrow 1}$  is independent of the ratio  $a = x_j/x_i$ . This was already suggested in the study by Kooijman and Taylor 20 years ago<sup>50</sup>, however in that study no formal proof was provided. The fact that  $\mathcal{D}_{ij}^{x_k \rightarrow 1}$  should be independent of  $x_i/x_j$  suggests that Eqs. (2.15) and (2.16) violate Onsager's reciprocal relations

at infinite dilution. Note that all terms in Eq. (3.10) originate from velocity cross-correlations, *i.e.* correlations of the velocities of different molecules. As the Onsager coefficients  $\Lambda_{ij}$  are intensive properties, the terms  $NC_{kk}^*$ ,  $NC_{ij}$ ,  $NC_{ik}$ , and  $NC_{jk}$  will approach finite values when  $N \rightarrow \infty$ . A numerical confirmation of this is provided in Ref.<sup>82</sup>. Therefore, the term  $C_x$  converges to a finite value when  $N \rightarrow \infty$ . Weingärtner<sup>83</sup> used a similar method to study the diffusivities in binary systems. More discussion on the self- and cross-correlations (so-called distinct diffusion coefficients) in binary systems can be found in Ref.<sup>83</sup>.

### 3.2.2 Obtaining a physically-based model for $\mathcal{D}_{ij}^{x_k \rightarrow 1}$

In general, the self-diffusivity of component  $i$  in a medium can be computed from Eq. (2.19)<sup>17</sup>. From Eqs. (3.3) and (2.19), it follows that

$$C_{ii} = D_{i,\text{self}}. \quad (3.11)$$

Therefore, Eq. (3.9) can be written as

$$\mathcal{D}_{ij}^{x_k \rightarrow 1} = \frac{D_{i,\text{self}}^{x_k \rightarrow 1} \cdot D_{j,\text{self}}^{x_k \rightarrow 1}}{D_{k,\text{self}}^{x_k \rightarrow 1} + C_x}, \quad (3.12)$$

in which the self-diffusivities  $D_{i,\text{self}}^{x_k \rightarrow 1}$ ,  $D_{j,\text{self}}^{x_k \rightarrow 1}$  and  $D_{k,\text{self}}^{x_k \rightarrow 1}$  are taken from a system in which  $x_k \rightarrow 1$ . It is natural to assume that integrals of velocity auto-correlations are much larger than integrals of velocity cross-correlations, suggesting that  $C_x$  is small compared to  $D_{k,\text{self}}$ . Using this assumption, Eq. (3.12) then becomes

$$\mathcal{D}_{ij}^{x_k \rightarrow 1} = \frac{D_{i,\text{self}}^{x_k \rightarrow 1} \cdot D_{j,\text{self}}^{x_k \rightarrow 1}}{D_{k,\text{self}}^{x_k \rightarrow 1}}. \quad (3.13)$$

This equation allows us to predict the ternary diffusivity  $\mathcal{D}_{ij}^{x_k \rightarrow 1}$  based on binary diffusion coefficients  $\mathcal{D}_{ik}^{x_k \rightarrow 1}$ ,  $\mathcal{D}_{jk}^{x_k \rightarrow 1}$  and the pure component self-diffusivity  $D_{k,\text{self}}$ . In the remainder of this chapter, we will verify the predictions of Eqs. (3.12) and (3.13) using MD simulations. It is worthwhile to note that Eq. (3.13) reduces to the KT model (Eq. (2.14)) in the case that  $D_{k,\text{self}} = \sqrt{\mathcal{D}_{ik}^{x_k \rightarrow 1} \mathcal{D}_{jk}^{x_k \rightarrow 1}}$ .

### 3.3 Details of Molecular Dynamics simulations

The predictions of Eqs. (3.12) and (3.13) are tested for the following ternary systems: (1) a simple system in which only repulsive interactions are considered; here particles interact with a WCA potential<sup>81</sup>. The three components only differ in their molar mass; (2) the system n-hexane - cyclohexane - toluene in which particles interact with LJ potentials; (3) the system ethanol - methanol - water in which both LJ and electrostatic interactions are considered. For all systems, diffusivities were obtained from MD simulations in the *NVE* ensemble (constant number of particles, constant total energy and constant volume). Self- and MS diffusivities are computed using Eqs. (2.21) and (2.19). The details of extracting correlation functions and mean-squared displacements from the MD trajectories are described in Refs.<sup>17;33;75</sup>. Errors of the computed diffusivities are calculated by performing at least 5 independent MD simulations for each system (*i.e.* simulations using different initial positions of the molecules) and analyzing their differences.

#### 3.3.1 WCA system

Simulations were carried out in a system containing 400 particles that interact with a WCA potential<sup>81</sup>. The WCA potential is constructed by truncating and shifting the LJ potential at  $2^{1/6}\sigma$ . A linked-cell algorithm is applied to improve the efficiency<sup>17</sup>. For convenience, we express all quantities in reduced units<sup>17</sup> by setting the LJ parameters  $\sigma$  and  $\varepsilon$  as units for length and energy. The mass of the lightest component is set as unit of mass, *i.e.*  $M_1 = 1$ . We investigate the influence of the mass of the solvent molecules (here:  $M_3$ ) and the total number density  $\rho$ .

#### 3.3.2 n-hexane - cyclohexane - toluene

The united-atom model is used in which  $\text{CH}_x$  groups are considered as single interaction sites. For n-hexane and cyclohexane, the SHAKE algorithm is used to constrain the distance between two neighboring atoms<sup>84</sup>. Bond bending and torsion potentials describe the interaction between three and four consecutive atoms, respectively. Toluene is treated as a rigid molecule. The non-bonded interactions are described by LJ potentials. The Lorentz-Berthelot mixing rule is applied to obtain the LJ parameters for the interaction of unlike atoms<sup>18</sup>. LJ interactions are truncated and shifted

at 12 Å. The equations of motion are integrated using the velocity Verlet algorithm with a time step of 1 fs. The simulations were performed at a total energy and density corresponding to a pressure of 1 atm and a temperature of 298 K. The force field parameters for this system are listed in Table 2.1.

### 3.3.3 Ethanol - methanol - water

In the ethanol-methanol-water system, intermolecular interactions are described by LJ and electrostatic interactions with parameters listed in Table 3.1. LJ interactions are truncated and shifted at 12 Å. Electrostatic interactions are handled by the Ewald summation using a relative precision<sup>85</sup> of  $10^{-4}$ . Ethanol and methanol are described using TraPPE-UA model<sup>86</sup> in which the  $\text{CH}_x$  groups are considered as united atoms. A flexible simple point-charge (SPC-FW) model is used to describe water<sup>87</sup>. The simulations were performed at a total energy and density corresponding to a pressure of 1 atm. and a temperature of 298 K.

## 3.4 Results and discussion

### 3.4.1 WCA system

In Table 3.2, a comparison is made between the MS diffusivities obtained from MD simulations and the predictions from Eqs. (3.12) and (3.13). Ternary mixtures in which particles interact using a WCA potential are considered. The components only differ in their masses and we consider the case that components 1 and 2 are diluted in component 3. We refer to the latter component as the solvent. Eqs. (3.12) and (3.13) are parametrized using the computed self-diffusivities and velocity cross-correlation functions which are listed in Tables C.1 and C.2 of appendix C. The influence of the total number density ( $\rho$ ), the mass of solvent molecules ( $M_3$ ) and the molar ratio of the diluted components ( $x_1/x_2$ ) on  $\mathcal{D}_{12}$  are studied. All reported quantities are listed in reduced units. The molecular mass of component 1 was used as unit of mass ( $M_1 = 1$ ).

As discussed earlier,  $\mathcal{D}_{ij}^{x_k \rightarrow 1}$  is well defined so it should be independent of the ratio  $x_i/x_j$  in the limit of infinite dilution. The simulation results of Table 3.2 show that indeed  $\mathcal{D}_{ij}^{x_k \rightarrow 1}$  does not depend on  $x_i/x_j$  within the accuracy of the simulations. For all conditions, Eqs. (3.12) and (3.13) result in accurate predictions. This result

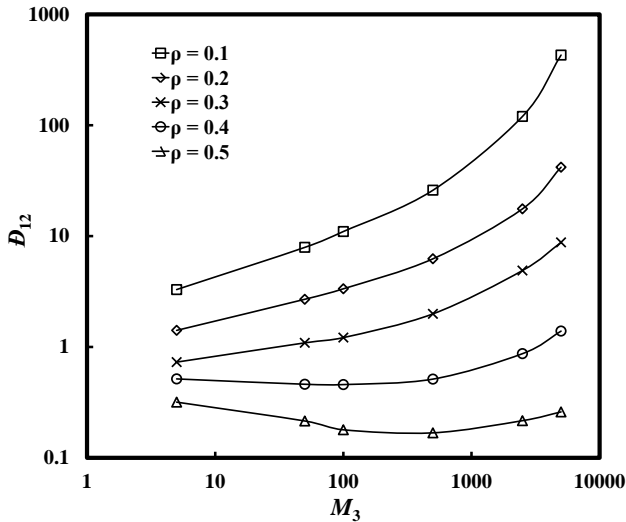


**Figure 3.1:** Computed MS diffusivities for a ternary mixture in which particles interact with a WCA potential. We consider the case that components 1 and 2 are diluted in component 3. The MS diffusivity  $\mathcal{D}_{12}$  is plotted as a function of the mass of component 3 ( $M_3$ ) for different number densities  $\rho$ . All quantities are reported in reduced units. Details of MD simulations: total number of molecules = 400;  $M_1 = 1$ ;  $M_2 = 1.5$ ;  $x_1/x_2 = 1$ ;  $x_3 = 0.95$ ;  $T=2$ . The statistical errors of the computed diffusivities are smaller than the symbol sizes.

implies that velocity cross-correlations play a minor role in a WCA system, which is conformed by the computed values for the coefficients  $C_{ij}$  (see Table C.2 of appendix C).

For densities  $\rho$  ranging from 0.1 to 0.8, as expected, the MS diffusivity  $\mathcal{D}_{12}$  decreases with increasing number density  $\rho$ . At a constant  $\rho$ , Figure 3.1 and Table 3.2 show that for sufficiently low number density  $\rho$  the diffusivity  $\mathcal{D}_{ij}^{x_k \rightarrow 1}$  strongly increases with increasing mass of the solvent ( $M_3$ ). This observation is well captured by Eq. (3.13): increasing the mass of the solvent molecules  $k$  reduces the mobility of molecules of component  $k$  leading to a lower self-diffusivity of the solvent molecules and therefore a larger  $\mathcal{D}_{12}$ . At the same time, at low  $\rho$ , a large free space is available for diffusion and therefore the self-diffusion of components  $i$  and  $j$  is not much affected by the mass of solvent molecules  $k$ . This is clearly shown in Table C.1 of appendix C. According to Eq. (3.13), a strong increase of  $\mathcal{D}_{ij}^{x_k \rightarrow 1}$  is expected with increasing molar mass of component  $k$ . In the limit when the mass of the solvent

molecules becomes infinitely large, the solvent can be considered as an immobile medium. This situation corresponds to the diffusion of guest molecules of type  $i$  and  $j$  in a porous solid (*e.g.* zeolites). For the diffusion of small guest molecules in an immobile zeolite framework, it was observed earlier that the MS diffusivity describing the interactions between two adsorbed components is indeed infinitely large<sup>27;88</sup>. Our results and Eq. (3.13) may provide a clear explanation for this observation from simulations.

In Table 3.3, predictions for  $\mathcal{D}_{12}^{x_3 \rightarrow 1}$  are compared with MD simulations. The WK, KT, VKB, DKB and RS models as well as Eq. (3.13) are parametrized using MS diffusivity of binary mixtures. This binary diffusion data is listed in Table C.3 of appendix C. Eqs. (3.12) and (3.13) always result in excellent predictions at densities  $\rho = 0.2$  and  $\rho = 0.5$ , for any mass of the solvent molecules. In sharp contrast to this, the quality of the predictions of the empirical WK, KT, VKB, DKB and RS models strongly depend on the density and the value of  $M_3$ . For each of these models (WK, KT, VKB, DKB, RS), it is always possible to choose a combination of the density  $\rho$  and the mass of the solvent molecules ( $M_3$ ) such that the model prediction completely fails. As this is not the case for Eq. (3.13), we feel that this model equation should be preferentially used for predictions of  $\mathcal{D}_{ij}^{x_k \rightarrow 1}$ .

### 3.4.2 n-hexane - cyclohexane - toluene

The computed and predicted MS diffusivities using Eqs. (3.12) and (3.13) in the n-hexane - cyclohexane - toluene system are shown in Table 3.4. Self-diffusivities in ternary mixtures are used as input for Eqs. (3.12) and (3.13). Using data from binary systems in these equations lead to identical results for  $\mathcal{D}_{ij}^{x_k \rightarrow 1}$ . Part of the data is taken from Table C.4 of appendix C. We observe that Eq. (3.12) accurately predicts  $\mathcal{D}_{ij}^{x_k \rightarrow 1}$  while Eq. (3.13) provides very reasonable approximations. The reason for this is that in Eq. (3.13) velocity cross-correlations are neglected. Although these velocity cross-correlations (represented by the term  $C_x$ ) are smaller than the velocity auto-correlations, there is still a non-negligible contribution to  $\mathcal{D}_{ij}^{x_k \rightarrow 1}$ . Values for the velocity auto-correlations and velocity cross-correlation functions are provided in Table C.5 of appendix C. As shown in Ref.<sup>33</sup>, the predictions of  $\mathcal{D}_{ij}^{x_k \rightarrow 1}$  using the WK, KT, VKB, DKB and RS models result in average deviations of 8-43% from the computed  $\mathcal{D}_{ij}^{x_k \rightarrow 1}$  for this system. We can therefore conclude that for this system,



Eq. (3.13) is equally accurate as the best empirical model prediction from the set WK, KT, VBK, DKB, RS, while also providing a clear physical interpretation of the observed deviations.

### 3.4.3 Ethanol - methanol - water

Table 3.5 shows the computed MS diffusivities, as well as the predictions using Eqs. (3.12) and (3.13) for the ethanol - methanol - water system. Self-diffusivities as well as velocity cross-correlations as used in Eqs. (3.12) and (3.13) are shown in Tables C.6 and C.7 of appendix C. It is clear that Eq. (3.12) perfectly agrees with the results from MD simulations. This shows that this equation captures the correct physics of the problem and should form the basis for the development of further predictive models.

However, Eq. (3.13) significantly underestimates the MS diffusivity  $\mathcal{D}_{ij}^{x_k \rightarrow 1}$ . Again, the reason for this is that in Eq. (3.13) velocity cross-correlations are neglected. In this system, these cross-correlations are particularly strong as there is a strong collective motion of molecules due to the formation of networks of hydrogen bonds. In Table 3.5, the predictions of  $\mathcal{D}_{ij}^{x_k \rightarrow 1}$  using various predictive models are compared with the results from MD simulations. The WK, KT, VKB, DKB and RS models are parametrized using MS diffusivity in binary mixtures. This binary diffusion data is listed in Table C.8 of appendix C. In the ethanol-methanol-water system, the WK, KT, VKB, DKB and RS models also fail to predict  $\mathcal{D}_{ij}^{x_k \rightarrow 1}$ , leading to similar deviations from MD data as Eq. (3.13). A better model from predicting  $\mathcal{D}_{ij}^{x_k \rightarrow 1}$  could be obtained by using a model for the velocity cross-correlations represented by the term  $C_x$  in Eq. (3.12). Unfortunately, to the best of our knowledge such a model is currently not available.

## 3.5 Conclusions

In this chapter, we investigated the MS diffusivity  $\mathcal{D}_{ij}^{x_k \rightarrow 1}$  which describes the friction of components  $i$  and  $j$  infinitely diluted in component  $k$ . Neither experiments nor simulations are well suited to obtain this quantity due to large uncertainties in experiments and extensive CPU-time requirements in simulations. Several empirical models are available from literature for estimating  $\mathcal{D}_{ij}^{x_k \rightarrow 1}$ . All of these are lacking a

sound theoretical basis. We derived a new model for  $\mathcal{D}_{ij}^{x_k \rightarrow 1}$  requiring easily obtainable self-diffusivities (Eq. (3.13)). In sharp contrast to other models (Eqs. (2.13) to (2.17)), our model does have a sound physical background. The model is tested for the following ternary systems: (1) a simple system in which only repulsive interactions are considered; particles interact using a WCA potential. The three components only differ in their molar mass; (2) the n-hexane - cyclohexane - toluene system in which particles interact using LJ potentials; (3) the ethanol-methanol-water system in which both LJ and electrostatic interactions are considered. Our results show that: (1) in all tested systems, Eq. (3.12) perfectly predicts the MS diffusivity at infinite dilution. It is important to note that Eq. (3.12) requires knowledge on velocity cross-correlations. At present, no analytical or empirical methods are available to estimate these velocity cross-correlations and one has to rely on molecular simulation; (2) for the WCA system, the predictions of Eq. (3.13) are superior to the WK, KT, VBK, DKB and RS models; (3) Eq. (3.13) may provide an explanation for the observation that for diffusion of guest molecules in zeolites, the MS diffusivity  $\mathcal{D}_{ij}$  describing the friction between guest molecules of different type ( $i$  and  $j$ ) is usually infinitely large; (4) for systems with weak attractions, *i.e.* the n-hexane - cyclohexane - toluene system, Eq. (3.13) leads to predictions that are equally accurate as the best model prediction from the set WK, KT, VBK, DKB, RS. This is due to the fact that velocity cross-correlations are relatively small for these systems. (5) in the ethanol-methanol-water system, Eq. (3.13) significantly underestimates the MS diffusivity  $\mathcal{D}_{ij}^{x_k \rightarrow 1}$  as it neglects velocity cross-correlations. The rigorous derivation of Eq. (3.13) allows the identification of the physical cause of its failure which was not possible for the previous empirical models. The other predictive models fail in a similar way. This result suggests that the velocity cross-correlations play a significant role when polar compounds are involved and that it is important to correctly capture the collective motion of molecules. (6) the applicability of the WK, KT, VKB, DKB and RS models is unpredictable and strongly depends on the system under investigation. Large deviations are expected when using these models to estimate  $\mathcal{D}_{ij}^{x_k \rightarrow 1}$ .

**Table 3.1:** LJ parameters and partial charges used for the ethanol-methanol-water system.  $\text{CH}_x$  groups are treated as united atoms. The LJ interactions between unlike united atoms are calculated using the Lorentz-Berthelot mixing rules<sup>18</sup>. The LJ interactions are truncated and shifted at 12 Å. Electrostatics are handled using the Ewald summation<sup>17</sup>. The force field parameters are taken from Refs.<sup>86;87</sup>.

pseudo-atom	$\sigma/[\text{Å}]$	$\varepsilon/k_B$ [K]	$q/e$
$\text{CH}_x\text{-O-H}$	3.02	93	-0.700
<b>O-H</b>	-	-	+0.435
<b>CH<sub>3</sub>-OH</b>	3.75	98	+0.265
<b>CH<sub>3</sub>-CH<sub>x</sub></b>	3.75	108	-
$\text{CH}_x\text{-CH}_2\text{-OH}$	3.95	51	+0.265
<b>O</b> (in $\text{H}_2\text{O}$ )	3.16	78	-0.820
<b>H</b> (in $\text{H}_2\text{O}$ )	-	-	+0.410

**Table 3.2:** Computed MS diffusivities compared to the predictions of Eqs. (3.12) and (3.13) for ternary mixtures in which particles interact with a WCA potential. Eqs. (3.12) and (3.13) are parametrized using self-diffusivities and velocity cross-correlations. Details of the self-diffusivities and velocity cross-correlations are listed in Tables C.1 and C.2 of appendix C. Here, we consider the case that components 1 and 2 are diluted in component 3. In all cases, the total number of molecules is 400. All reported quantities are in reduced units. The statistical errors of the computed diffusivities are less than 3%.

		MS Diffusivity $\mathcal{D}_{12}$				
		MD simulation	Prediction			
			Eq. (3.12)	AD <sup>a</sup>	Eq. (3.13)	AD <sup>a</sup>
Number Density <sup>b</sup>	0.1	3.294	3.212	2%	3.341	1%
	0.2	1.411	1.401	1%	1.441	2%
	0.5	0.318	0.310	2%	0.315	1%
	0.7	0.144	0.145	1%	0.149	3%
	0.8	0.094	0.092	2%	0.097	4%
Mass of Species 3 <sup>c</sup>	5	1.411	1.401	1%	1.441	2%
	50	2.692	2.686	0%	2.560	5%
	100	3.348	3.344	0%	3.288	2%
	500	6.238	6.237	0%	6.619	6%
	2500	17.609	17.609	0%	18.923	7%
	5000	41.794	41.792	0%	44.051	5%
Mass of Species 3 <sup>d</sup>	5	0.318	0.310	2%	0.315	1%
	10	0.270	0.267	1%	0.275	2%
	50	0.218	0.217	0%	0.227	5%
	100	0.172	0.172	0%	0.161	7%
Ratio of $x_1/x_2$ <sup>e</sup> with $x_3 = 0.95$	1/3	0.318	0.312	2%	0.312	2%
	1	0.318	0.310	2%	0.315	1%
	3	0.318	0.312	2%	0.326	2%
Ratio of $x_1/x_2$ <sup>f</sup> with $x_3 = 0.97$	1/3	0.318	0.316	1%	0.320	1%
	1	0.318	0.320	1%	0.325	2%
	3	0.319	0.322	1%	0.321	1%

<sup>a</sup> absolute difference normalized with corresponding value from MD simulations

<sup>b</sup>  $M_1 = 1; M_2 = 1.5; M_3 = 5; x_1/x_2 = 1; x_3 = 0.95; T = 2$

<sup>c</sup>  $\rho = 0.2; M_1 = 1; M_2 = 1.5; x_1/x_2 = 1; x_3 = 0.95; T = 2$

<sup>d</sup>  $\rho = 0.5; M_1 = 1; M_2 = 1.5; x_1/x_2 = 1; x_3 = 0.95; T = 2$

<sup>e</sup>  $\rho = 0.5; M_1 = 1; M_2 = 1.5; M_3 = 5; x_3 = 0.95; T = 2$

<sup>f</sup>  $\rho = 0.5; M_1 = 1; M_2 = 1.5; M_3 = 5; x_3 = 0.97; T = 2$

**Table 3.3:** Computed and predicted MS diffusivities in ternary mixtures in which particles interact with a WCA potential. We consider the case that components 1 and 2 are diluted in component 3. Eqs. (3.12) and (3.13) are parametrized using self-diffusivities and velocity cross-correlations. Details of the self-diffusivities and velocity cross-correlations are listed in Tables C.1 and C.2 of appendix C. The WK, KT, VKB, DKB, RS models are parametrized using binary diffusivities obtained from MD simulations, see Table C.3 of appendix C. All reported quantities are in reduced units. The statistical errors of the computed diffusivities are less than 3%.

	MS diffusivity $D_{12}^{x_3 \rightarrow 1}$						
	Eq. (3.12)	Eq. (3.13)	WK	KT	VKB	DKB	RS
Prediction	1.401	1.441	1.296	0.952	0.952	0.952	1.111
MD <sup>b</sup>	1.411	1.411	1.411	1.411	1.411	1.411	1.411
AD <sup>a</sup>	1%	2%	8%	32%	32%	32%	21%
Prediction	0.310	0.315	0.390	0.248	0.248	0.248	0.311
MD <sup>c</sup>	0.318	0.318	0.318	0.318	0.318	0.318	0.318
AD <sup>a</sup>	2%	1%	23%	22%	22%	22%	2%
Prediction	3.344	3.288	1.296	0.682	0.682	0.683	0.940
MD <sup>d</sup>	3.348	3.348	3.348	3.348	3.348	3.348	3.348
AD <sup>a</sup>	0%	2%	61%	80%	80%	80%	72%
Prediction	0.172	0.161	0.389	0.085	0.085	0.086	0.182
MD <sup>e</sup>	0.172	0.172	0.172	0.172	0.172	0.172	0.172
AD <sup>a</sup>	0%	7%	126%	50%	50%	50%	6%

<sup>a</sup> absolute difference normalized with corresponding value from MD simulations

<sup>b</sup>  $\rho = 0.2; M_1 = 1; M_2 = 1.5; M_3 = 5; x_1/x_2 = 1; x_3 = 0.95; T = 2$

<sup>c</sup>  $\rho = 0.5; M_1 = 1; M_2 = 1.5; M_3 = 5; x_1/x_2 = 1; x_3 = 0.95; T = 2$

<sup>d</sup>  $\rho = 0.2; M_1 = 1; M_2 = 1.5; M_3 = 100; x_1/x_2 = 1; x_3 = 0.95; T = 2$

<sup>e</sup>  $\rho = 0.5; M_1 = 1; M_2 = 1.5; M_3 = 100; x_1/x_2 = 1; x_3 = 0.95; T = 2$

**Table 3.4:** Computed and predicted MS diffusivities in ternary mixtures of n-hexane - cyclohexane - toluene at 298 K, 1 atm. “1”: n-hexane; “2”: cyclohexane; “3”: toluene. Eqs. (3.12) and (3.13) are parametrized using self-diffusivities and velocity cross-correlations. Details of the self-diffusivities and velocity cross-correlations are listed in Tables C.4 and C.5 of appendix C. The statistical errors of the computed diffusivities are less than 5%.

	MS Diffusivity/( $10^{-9} \text{ m}^2\text{s}^{-1}$ )				
	MD simulation	Prediction of $\mathcal{D}_{ij}^{x_k \rightarrow 1}$			
$x_1 \rightarrow 1^b$	$\mathcal{D}_{23}$ 4.07	Eq. (3.12) 4.12	AD <sup>a</sup> 1%	Eq. (3.13) 3.78	AD <sup>a</sup> 7%
$x_2 \rightarrow 1^c$	$\mathcal{D}_{13}$ 2.19	Eq. (3.12) 2.21	AD <sup>a</sup> 1%	Eq. (3.13) 2.69	AD <sup>a</sup> 23%
$x_3 \rightarrow 1^d$	$\mathcal{D}_{12}$ 2.99	Eq. (3.12) 2.93	AD <sup>a</sup> 2%	Eq. (3.13) 2.82	AD <sup>a</sup> 6%

<sup>a</sup> absolute difference normalized with corresponding value from MD simulations

<sup>b</sup> 598 n-hexane molecules; 1 cyclohexane molecule; 1 toluene molecule

<sup>c</sup> 1 n-hexane molecule; 598 cyclohexane molecules; 1 toluene molecule

<sup>d</sup> 1 n-hexane molecule; 1 cyclohexane molecule; 598 toluene molecules

**Table 3.5:** MD simulation results and predictions of MS diffusivities  $\mathcal{D}_{ij}^{x_k \rightarrow 1}$  in ethanol-methanol-water mixtures at 298K, 1 atm. 1: ethanol; 2: methanol; 3: water. Eqs. (3.12) and (3.13) are parametrized using self-diffusivities and velocity cross-correlations. Details of the self-diffusivities and velocity cross-correlations are listed in Tables C.6 and C.7 of appendix C. The WK, KT, VKB, DKB, RS models are parametrized using binary simulation results shown in Table C.8 of appendix C. The statistical errors of the computed diffusivities are less than 5%.

	$\mathcal{D}_{ij}^{x_k \rightarrow 1}/(10^{-9} \text{ m}^2\text{s}^{-1})$						
	Eq. (3.12)	Eq. (3.13)	WK	KT	VKB	DKB	RS
Prediction of $\mathcal{D}_{23}$	2.68	1.57	2.07	1.25	1.25	1.32	1.61
MD <sup>b</sup>	2.68	2.68	2.68	2.68	2.68	2.68	2.68
AD <sup>a</sup>	0%	41%	23%	53%	53%	51%	40%
Prediction of $\mathcal{D}_{13}$	3.17	2.07	1.20	2.04	2.04	2.06	1.56
MD <sup>c</sup>	3.24	3.24	3.24	3.24	3.24	3.24	3.24
AD <sup>a</sup>	2%	36%	63%	37%	37%	37%	52%
Prediction of $\mathcal{D}_{12}$	5.01	1.06	1.78	1.72	1.72	1.73	1.75
MD <sup>d</sup>	4.76	4.76	4.76	4.76	4.76	4.76	4.76
AD <sup>a</sup>	5%	78%	63%	64%	64%	64%	63%

<sup>a</sup> absolute difference normalized with corresponding result from MD simulations

<sup>b</sup> 168 ethanol molecules; 1 methanol molecule; 1 water molecule

<sup>c</sup> 1 ethanol molecule; 248 methanol molecules; 1 water molecule

<sup>d</sup> 1 ethanol molecule; 1 methanol molecule; 598 water molecules





# 4

---

## A Predictive Darken Equation for Maxwell-Stefan Diffusivities in Multicomponent Mixtures

---

This chapter is for a large part based on:

X. Liu, T.J.H. Vlugt, A. Bardow, *Predictive Darken equation for Maxwell-Stefan diffusivities in multicomponent mixtures*, *Industrial & Engineering Chemistry Research*, **2011**, 50, 10350-10358.

## 4.1 Introduction

For the description of multicomponent mass transport in gases and liquids, the MS theory is commonly used in chemical engineering as it provides a convenient description of diffusion in  $n$ -component systems<sup>1</sup>. The key point of this approach is that the driving force for diffusion of component  $i$  (*i.e.* the gradient in chemical potential  $\nabla\mu_i$ ) is balanced by a frictional force, resulting in the following transport equation

$$-\frac{1}{RT}\nabla\mu_i = \sum_{j=1, j \neq i}^n \frac{x_j(u_i - u_j)}{\mathcal{D}_{ij}}. \quad (4.1)$$

The frictional force between components  $i$  and  $j$  is proportional to the velocity difference  $(u_i - u_j)$ .  $R$  and  $T$  represent the gas constant and absolute temperature respectively.  $x_j$  is the mole fraction of component  $j$ . The MS diffusivity  $\mathcal{D}_{ij}$  acts as an inverse friction coefficient describing the magnitude of the friction between components  $i$  and  $j$ . It is not possible to directly obtain the MS diffusivities  $\mathcal{D}_{ij}$  from experiments<sup>7;8;80</sup>, and obtaining the MS diffusivities from MD simulations requires extensive large amounts of CPU time<sup>33</sup>. Predictive models for MS diffusivities based on easily measurable quantities are therefore highly desired. The prediction of MS diffusivities usually follows a two-step approach: (1) prediction of MS diffusivities  $\mathcal{D}_{ij}^{x_i \rightarrow 0}$  in binary systems at infinite dilution; and (2) estimation of MS diffusion coefficients  $\mathcal{D}_{ij}$  in concentrated mixtures using mixing rules. For the first step, a large number of models are available with the Wilke-Chang equation<sup>89</sup> still being the most popular (for a critical review we refer the reader to Ref.<sup>2</sup>). In this work, we focus on the second step.

For the estimation of MS diffusion coefficients of concentrated mixtures, empirical models are typically employed interpolating the diffusion coefficients at infinite dilution  $\mathcal{D}_{ij}^{x_i \rightarrow 0}$ . The logarithmic interpolation suggested by Vignes<sup>52</sup> is typically recommended<sup>1;2</sup>. The Vignes equation has been generalized to multicomponent mixtures as follows<sup>24</sup>

$$\mathcal{D}_{ij} = (\mathcal{D}_{ij}^{x_i \rightarrow 1})^{x_i} (\mathcal{D}_{ij}^{x_j \rightarrow 1})^{x_j} \prod_{k=1, k \neq i, j}^n (\mathcal{D}_{ij}^{x_k \rightarrow 1})^{x_k}. \quad (4.2)$$

The generalized Vignes equation requires  $\mathcal{D}_{ij}^{x_k \rightarrow 1}$  which describes the friction between

components  $i$  and  $j$  when both are diluted in component  $k$  as explained earlier in chapters 2 and 3. This quantity is not directly accessible in experiments<sup>7</sup>. Several predictive models have been proposed to estimate  $\mathcal{D}_{ij}^{x_k \rightarrow 1}$  from binary diffusion data<sup>23;24;50;51;67</sup>. However, all of these models are empirical and lack a sound theoretical basis. In chapter 3, we derived a physically-based model for estimating this quantity using the self-diffusivities obtained from pure- and binary mixtures at infinite dilution<sup>34</sup>

$$\mathcal{D}_{ij}^{x_k \rightarrow 1} = \frac{D_{i,\text{self}}^{x_k \rightarrow 1} D_{j,\text{self}}^{x_k \rightarrow 1}}{D_{k,\text{self}}^{x_k \rightarrow 1}} = \frac{\mathcal{D}_{ik}^{x_k \rightarrow 1} \mathcal{D}_{jk}^{x_k \rightarrow 1}}{D_{k,\text{self}}^{x_k \rightarrow 1}}. \quad (4.3)$$

In the remainder of this chapter, we will refer to this as the LBV equation (taken from the author's names). At infinite dilution, the self-diffusion coefficient  $D_{i,\text{self}}^{x_k \rightarrow 1}$  is equal to the MS diffusivity  $\mathcal{D}_{ik}^{x_k \rightarrow 1}$ <sup>2</sup>. The central assumption in Eq. (4.3) is that velocity correlations between different molecules are neglected. Eq. (4.3) leads to superior and more robust predictions compared to the previous empirical models<sup>34</sup>. By inserting Eq. (4.3) into Eq. (4.2), we obtain the so-called Vignes-LBV equation

$$\mathcal{D}_{ij} = (D_{j,\text{self}}^{x_i \rightarrow 1})^{x_i} (D_{i,\text{self}}^{x_j \rightarrow 1})^{x_j} \prod_{k=1, k \neq i, j}^n \left( \frac{D_{i,\text{self}}^{x_k \rightarrow 1} D_{j,\text{self}}^{x_k \rightarrow 1}}{D_{k,\text{self}}^{x_k \rightarrow 1}} \right)^{x_k}. \quad (4.4)$$

This physically-based multicomponent form of the Vignes equation requires the pure component self-diffusivities  $D_{k,\text{self}}^{x_k \rightarrow 1}$  as additional information. For this property, there are also predictive models available<sup>2;23</sup>. The Vignes-LBV equation thus allows the prediction of multicomponent MS diffusion coefficients based on pure component data and binary mixture data at infinite dilution.

The popularity of the generalized Vignes equation (Eq. (4.2)) has, however, recently been challenged by a number of groups working on diffusion using molecular simulation<sup>23;25;43;45–47;90</sup>. Their simulation results show that the Darken equation<sup>54</sup> is superior to the Vignes equation. In the Darken equation, the MS diffusion coefficient  $\mathcal{D}_{ij}$  is estimated from the self-diffusion coefficients of the two components  $D_{i,\text{self}}$  and  $D_{j,\text{self}}$  in the binary mixture<sup>54</sup>

$$\mathcal{D}_{ij} = x_i D_{j,\text{self}} + x_j D_{i,\text{self}}. \quad (4.5)$$

While often regarded as an empirical mixing rule, the Darken equation can be

rigorously derived as limiting case from statistical-mechanical theory<sup>91;92</sup>, see appendix B for an alternative derivation. Despite this theoretical advantage and the support from simulations, the Darken equation is generally seen as “of little practical use due to the fact that it relies on the self-diffusion coefficients in the mixture, which are rarely available.”<sup>46</sup> In addition, the Darken equation had been only formulated for binary mixtures.

To overcome these limitations, Krishna and van Baten<sup>23</sup> recently proposed a generalized Darken equation for describing the concentration dependence of MS diffusivities in multicomponent mixtures based on molecular simulations of liquid mixtures of linear alkanes,

$$D_{ij} = \frac{x_i}{x_i + x_j} D_{j,\text{self}} + \frac{x_j}{x_i + x_j} D_{i,\text{self}}. \quad (4.6)$$

The authors suggested to estimate the self-diffusivities  $D_{i,\text{self}}$  and  $D_{j,\text{self}}$  in Eq. (4.6) as mass-weighted averages of the values at infinite dilution

$$D_{i,\text{self}} = \sum_{j=1}^n w_j D_{i,\text{self}}^{w_j \rightarrow 1}. \quad (4.7)$$

Here,  $w_j$  is mass fraction of component  $j$ . The *generalized Darken equation* (Eqs. (4.6) and (4.7)) thus allows to predict MS diffusivities using the same information as for the Vignes-LBV equation: the diffusion coefficient in the binary mixtures at infinite dilution and the pure component self-diffusivities. Note that in the limit of infinite dilution, both are equal, *i.e.*  $D_{ij}^{x_i \rightarrow 1} = D_{j,\text{self}}^{x_i \rightarrow 1}$ .

While retaining the Darken equation (Eq. (4.5)) as binary limit, both the generalization of the Darken equation (Eq. (4.6)) and the model for the self-diffusivity (Eq. (4.7)) are empirical in nature. In particular, it is important to note that in systems with three or more components, the limit where both  $x_i \rightarrow 0$  and  $x_j \rightarrow 0$  is not well-defined by Eq. (4.6)<sup>7</sup>, see also chapter 3. Furthermore, Eq. (4.6) suggests that the MS diffusivities of an infinitely-diluted component in a mixture should all become equal, *i.e.*,  $D_{ij}^{x_i \rightarrow 0} = D_{ik}^{x_i \rightarrow 0}$  for all  $j, k \neq i$ . This assumption seems unphysical and is in fact not supported by the authors’ own data for linear alkanes<sup>23</sup>.

In this chapter, we derive a sound extension of the Darken equation to multicomponent mixtures. In addition, a physically-motivated model for the estimation of the required self-diffusivities is provided. The resulting predictive Darken-LBV equation

for multicomponent mixtures is validated using molecular simulations in ternary and quaternary mixtures. The remainder of this chapter is organized as follows. In section 4.2, the predictive Darken-LBV equation is derived based on linear response theory and the Onsager relations. In section 4.3, we introduce the details concerning the MD simulations. In section 4.4, we test our model for ternary and quaternary systems in which purely repulsive pair interactions are used, *i.e.* particles interact using a WCA potential<sup>81</sup>. We also test our model for the ternary system n-hexane - cyclohexane - toluene. Our conclusions are summarized in section 4.5. It is shown that the predictive Darken-LBV model is clearly superior to the generalized Darken equation and it even outperforms the Vignes-LBV equation for the prediction of multicomponent MS diffusion coefficients.

## 4.2 The predictive Darken-LBV equation

MS diffusivities  $\mathcal{D}_{ij}$  can be obtained from the Onsager coefficients  $\Lambda_{ij}$ , *i.e.* Eq. (2.21), see section 2.3 and appendix A. For the terms  $\Lambda_{ii}$ , we can write<sup>34</sup>

$$\begin{aligned} \Lambda_{ii} &= \frac{1}{3N} \int_0^\infty dt' \left\langle \sum_{l=1}^{N_i} v_{l,i}(t) \cdot \sum_{g=1}^{N_i} v_{g,i}(t+t') \right\rangle \\ &= \frac{1}{3N} \int_0^\infty dt' \left\langle \sum_{l=1}^{N_i} v_{l,i}(t) \cdot v_{l,i}(t+t') \right\rangle + \end{aligned} \quad (4.8)$$

$$\begin{aligned} &\frac{1}{3N} \int_0^\infty dt' \left\langle \sum_{l=1}^{N_i} \sum_{g=1, g \neq l}^{N_i} v_{l,i}(t) \cdot v_{g,i}(t+t') \right\rangle \\ &\approx x_i C_{ii} + x_i^2 N C_{ii}^*, \end{aligned} \quad (4.9)$$

in which  $C_{ii}$  and  $C_{ii}^*$  account for self- and cross-correlations of the velocities of molecules of component  $i$ , respectively. We assumed here that  $N_i^2 - N_i \approx N_i^2$ . In general, the self-diffusivity of component  $i$  in a medium can be computed from a Green-Kubo relation. From Eqs. (4.9) and (2.19), it follows that

$$C_{ii} = D_{i,\text{self}}. \quad (4.10)$$

For  $\Lambda_{ij}$  with  $i \neq j$ , *i.e.* the correlations between unlike molecules, we can write<sup>34</sup>

$$\begin{aligned}\Lambda_{ij} &= \frac{1}{3N} \int_0^\infty dt' \left\langle \sum_{l=1}^{N_i} v_{l,i}(t) \cdot \sum_{k=1}^{N_j} v_{k,j}(t+t') \right\rangle \\ &\approx \frac{N_i N_j}{3N} \int_0^\infty dt' \langle v_{1,i}(t) \cdot v_{1,j}(t+t') \rangle \\ &= N x_i x_j C_{ij}.\end{aligned}\tag{4.11}$$

It has been shown that in systems in which particles are not or weakly associated (*e.g.* the system in which particles are interacting with a WCA potential, or the n-hexane - cyclohexane - toluene system), the terms involving integrals of these velocity cross-correlation functions,  $C_{ij,i \neq j}$  and  $C_{ii}^*$ , are small at infinite dilution compared to the terms involving auto-correlation functions ( $C_{ii}$ ), see chapter 3. For ideal-diffusing mixtures, we assume that this is also the case at finite concentrations. As shown in appendix B, this approach leads to a multicomponent Darken-like equation for an  $n$ -component system:

$$D_{ij} = \frac{D_{i,\text{self}} D_{j,\text{self}}}{D_{\text{mix}}},\tag{4.12}$$

with  $D_{\text{mix}}$  defined as

$$\frac{1}{D_{\text{mix}}} = \sum_{i=1}^n \frac{x_i}{D_{i,\text{self}}}.\tag{4.13}$$

We will refer to Eqs. (4.12) and (4.13) as the multicomponent Darken equation. For binary systems ( $n = 2$ ), the multicomponent Darken equation reduces to the well-known Darken equation (Eq. (4.5))<sup>23;90;93;94</sup>. For ternary systems ( $n = 3$ ), the multicomponent Darken equation reduces to the Cooper model<sup>93;95</sup>. To demonstrate this correspondence, the derivation of the binary Darken equation and the ternary Cooper model is presented using the same approach in appendix B. It is important to note that for a ternary system at infinite dilution, Eqs. (4.12) and (4.13) directly result in Eq. (4.3).

As noted above, the applicability of the Darken equation has been suffering from the fact that it requires the self-diffusivities of all components in the mixtures. Comparing Eqs. (4.3), (4.12) and (4.13) suggests that the quantity  $D_{\text{mix}}$  describes the effective diffusivity of the medium. Its mixing rule (Eq. (4.13)) motivates the following equation to estimate the self-diffusivity of component  $i$  in a multicomponent

system

$$\frac{1}{D_{i,\text{self}}} = \sum_{j=1}^n \frac{x_j}{D_{i,\text{self}}^{x_j \rightarrow 1}}. \quad (4.14)$$

We thus model the self-diffusivity of species  $i$  in the mixture as the inverse mole-fraction weighted sum of its pure component value and its values at infinite dilution. Note that in the limit  $x_i \rightarrow 0$ , Eq. (4.14) reduces to Eq. (2.28). Therefore, in the limit of infinite dilution Eq. (4.14) is exact. We refer to the combined models of the multicomponent Darken equation (Eqs. (4.12) and (4.13)) and the predictive model for the self-diffusivities (Eq. (4.14)) as the *predictive Darken-LBV* equation. MD simulations are used to generate benchmark values. Comparisons are made between our model and existing models.

### 4.3 Molecular Dynamics simulation

The predictive models for  $D_{ij}$  and  $D_{i,\text{self}}$  described in sections 4.1 and 4.2 are tested for two systems: (1) systems in which only repulsive pair interactions are considered *i.e.* particles interact with a WCA potential<sup>81</sup>; (2) the ternary system n-hexane - cyclohexane - toluene in which united atoms interact with LJ potentials. Errors in computed diffusivities are calculated by performing at least 10 independent MD simulations for each system and analyzing their differences. Using 10 simulations with different initial positions of the molecules allows us to provide a better estimate of the error in the average values of the diffusivities.

#### 4.3.1 WCA system

Both ternary and quaternary mixtures are considered. All components only differ in their molar mass. Diffusivities were obtained from MD simulations in the micro-canonical (NVE) ensemble. Self- and MS diffusivities are computed using equations provided in appendix A. An order- $n$  algorithm was used to compute correlation functions<sup>17;75</sup>. All simulations were carried out in a system containing  $N = 400$  particles. The WCA potential is constructed by truncating and shifting the LJ potential at  $2^{1/6}\sigma$ . A linked-cell algorithm is applied to improve the efficiency<sup>17</sup>. For convenience, we express all quantities in reduced units by setting the LJ parameters  $\sigma$  and  $\varepsilon$  as units for length and energy<sup>17</sup>. The mass of the lightest component is set as unit of mass,

*i.e.*  $M_1 = 1$ . The equations of motion were integrated using a time step of  $\Delta t = 0.001$  (in reduced units) and typically  $10^9$  integration steps were needed.

### 4.3.2 n-hexane - cyclohexane - toluene

A united-atom model is used in which  $\text{CH}_x$  groups are considered as single interaction sites. For n-hexane and cyclohexane, the SHAKE algorithm is used to constrain the bond length<sup>84</sup>. Bond bending and torsion potentials describe the interaction between three and four consecutive atoms, respectively. Toluene is modeled as a rigid molecule. The LJ potentials describe the non-bonded interactions which are truncated and shifted at 12 Å. The Lorentz-Berthelot mixing rules are applied to obtain the LJ parameters for the interaction of unlike atoms<sup>18</sup>. The equations of motion were integrated using the velocity Verlet algorithm with a time step of 2 fs. The simulations were performed at a constant total energy and density corresponding to a pressure of 1 atm. and a temperature of 298 K. All force field parameters for this system are shown in Table 2.1. Typical simulations to extract MS diffusivities took at least 50 ns.

## 4.4 Results and discussion

### 4.4.1 Ternary WCA systems

Figures 4.1, 4.2, 4.3 and 4.4 show a comparison between computed and predicted self-diffusivities in ternary WCA systems. Two predictive models are considered: (1) the mass-weighted average of the values at infinite dilution Eq. (4.7); and (2) Eq. (4.14) as presented in this study. In Figures 4.1 and 4.2, the mole fraction of component 1 is kept constant while the ratio  $x_2/x_3$  varies. At  $\rho = 0.2$  (typical density of a dense gas), an excellent agreement between computed self-diffusivities and predictions using Eq. (4.14) was observed. Eq. (4.7) consistently underestimates the self-diffusivities computed by MD. At a higher number density ( $\rho = 0.5$ , corresponding to a typical liquid density), slightly larger deviations between the computed self-diffusivities and predictions are observed as shown in Figure 4.2. Here, both models underestimate the self-diffusivities. However, Eq. (4.14) leads to much better predictions than Eq. (4.7) with an average absolute deviation of 5% instead of 18%.



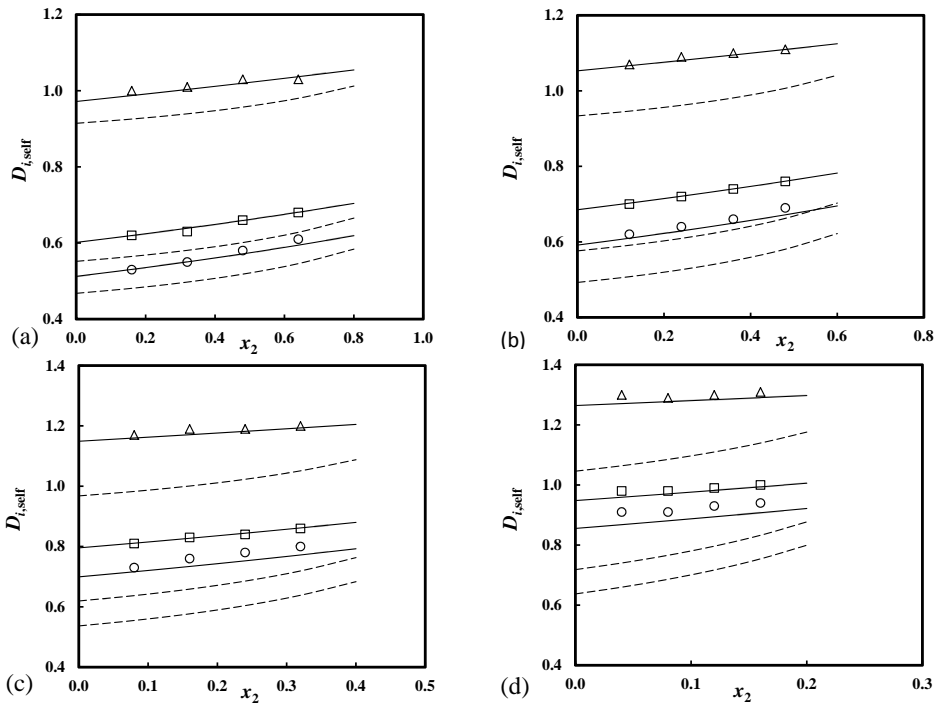


**Figure 4.1:** Computed and predicted self-diffusivities in ternary systems in which particles interact with a WCA potential. Open symbols represent the computed self-diffusivities using MD. Solid lines represent the predictions using Eq. (4.14). Dashed lines represent the predictions using Eq. (4.7). Triangles represent the self-diffusivity of component 1. Squares represent the self-diffusivity of component 2. Circles represent the self-diffusivity of component 3. (a)  $x_1 = 0.2$ ; (b)  $x_1 = 0.4$ ; (c)  $x_1 = 0.6$ ; (d)  $x_1 = 0.8$ . Simulation details:  $\rho = 0.2$ ;  $M_1 = 1$ ;  $M_2 = 5$ ;  $M_3 = 10$ ;  $T = 2$ ;  $N = 400$ .

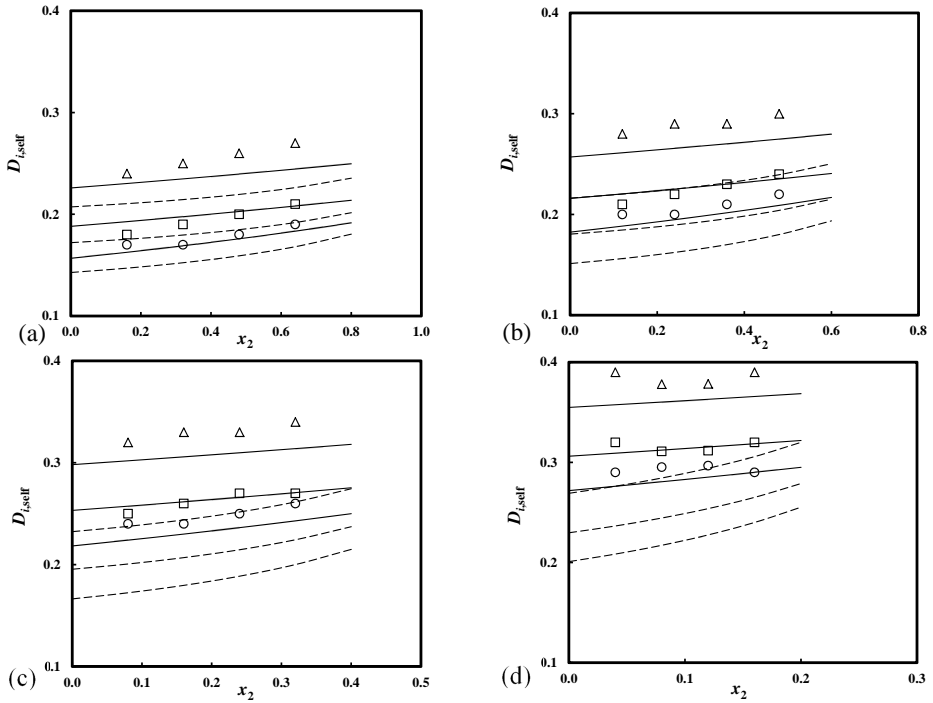


**Figure 4.2:** Computed and predicted self-diffusivities in ternary systems in which particles interact with a WCA potential. Open symbols represent the computed self-diffusivities using MD. Solid lines represent the predictions using Eq. (4.14). Dashed lines represent the predictions using Eq. (4.7). Triangles represent the self-diffusivity of component 1. Squares represent the self-diffusivity of component 2. Circles represent the self-diffusivity of component 3. (a)  $x_1 = 0.2$ ; (b)  $x_1 = 0.4$ ; (c)  $x_1 = 0.6$ ; (d)  $x_1 = 0.8$ . Simulation details:  $\rho = 0.5$ ;  $M_1 = 1$ ;  $M_2 = 5$ ;  $M_3 = 10$ ;  $T = 2$ ;  $N = 400$ .

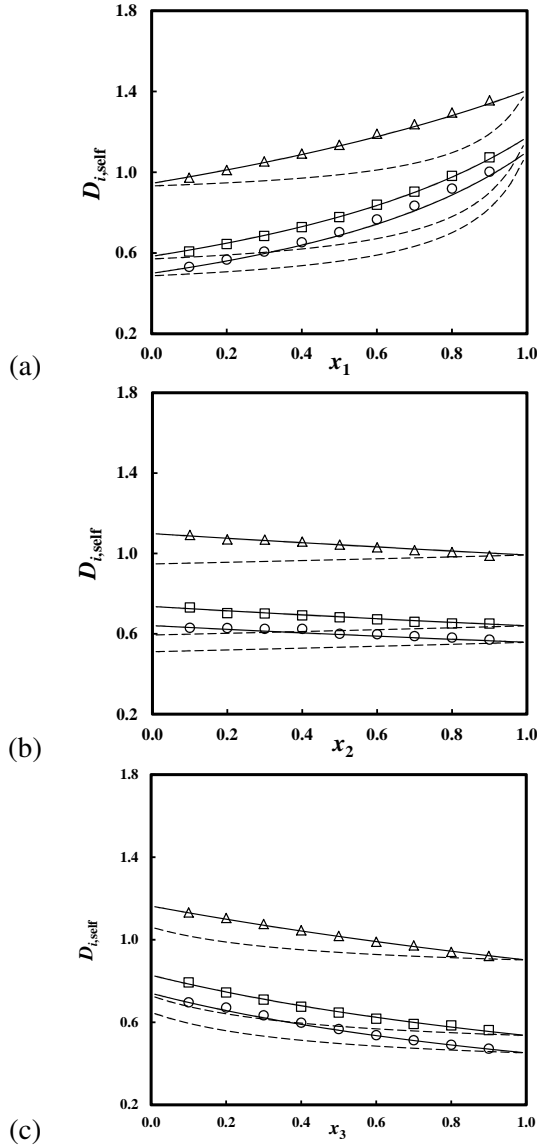


**Figure 4.3:** Computed and predicted self-diffusivities in ternary systems in which particles interact with a WCA potential. Open symbols represent the computed self-diffusivities using MD. Solid lines represent the predictions using Eq. (4.14). Dashed lines represent the predictions using Eq. (4.7). Triangles represent the self-diffusivity of component 1. Squares represent the self-diffusivity of component 2. Circles represent the self-diffusivity of component 3. (a)  $x_1$  varies,  $x_2/x_3=1$ ; (b)  $x_2$  varies,  $x_1/x_3=1$ ; (c)  $x_3$  varies,  $x_1/x_2=1$ . Simulation details:  $\rho = 0.2$ ;  $M_1 = 1$ ;  $M_2 = 5$ ;  $M_3 = 10$ ;  $T = 2$ ;  $N = 400$ .

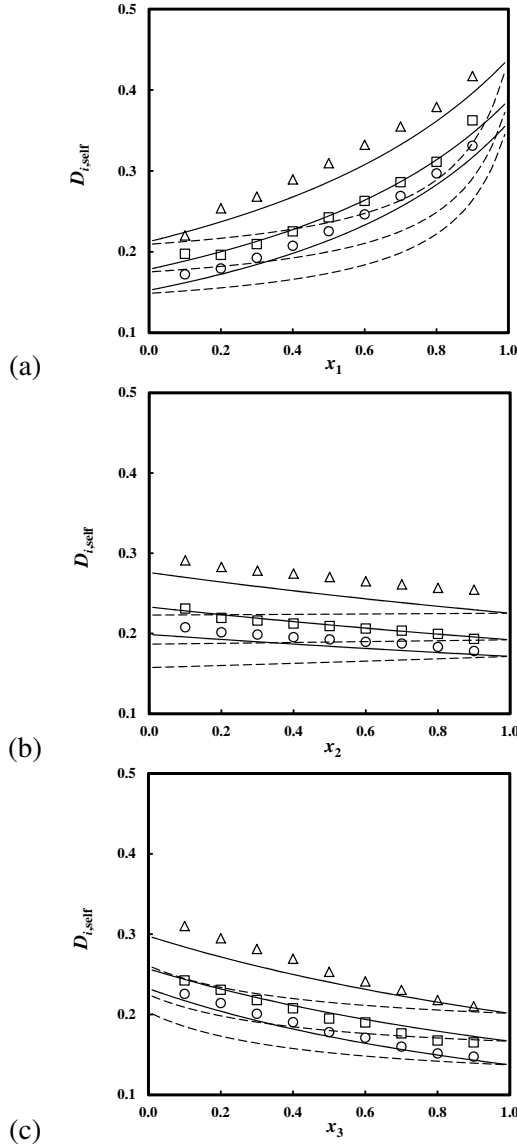


**Figure 4.4:** Computed and predicted self-diffusivities in ternary systems in which particles interact with a WCA potential. Open symbols represent the computed self-diffusivities using MD. Solid lines represent the predictions using Eq. (4.14). Dashed lines represent the predictions using Eq. (4.7). Triangles represent the self-diffusivity of component 1. Squares represent the self-diffusivity of component 2. Circles represent the self-diffusivity of component 3. (a)  $x_1$  varies,  $x_2/x_3=1$ ; (b)  $x_2$  varies,  $x_1/x_3=1$ ; (c)  $x_3$  varies,  $x_1/x_2=1$ . Simulation details:  $\rho = 0.5$ ;  $M_1 = 1$ ;  $M_2 = 5$ ;  $M_3 = 10$ ;  $T = 2$ ;  $N = 400$ .

Exactly the same trends were observed when keeping  $x_i/x_j$  constant and varying  $x_k$ , see Figures 4.3 and 4.4.

Tables D.1 and D.2 compare predicted MS diffusivities to computed MS diffusivities using MD. The multicomponent Darken equation (Eqs. (4.12) and (4.13)) is parametrized using data from MD simulations, while the Darken-LBV (Eqs. (4.12), (4.13) and (4.14)), Vignes-LBV (Eq. (4.4)) and generalized Darken equations (Eqs. (4.6) and (4.7)) are parametrized using pure-component and binary diffusion data which are listed in Tables D.3 to D.4 of appendix D. Absolute differences between the predictive models and the MD simulations are calculated and normalized with the corresponding MD results. The averaged absolute difference is used to qualify the various models.

At lower number densities ( $\rho = 0.2$ ), the predictive Darken-LBV equation performs equally well as the Vignes-LBV equation and leads to lower maximum deviations (Table D.1). This suggests that the Darken-LBV model is more robust. The performance of the generalized Darken equation is worse than the other predictive models with average errors larger by a factor 2. The differences between multicomponent Darken and Darken-LBV are small.

At higher number densities ( $\rho = 0.5$ ), similar observations are found as seen for lower densities, see Table D.2. The maximum deviation from MD data is always obtained for the generalized Darken equation. In Figures 4.5 and 4.6, the comparison is visualized for mixtures in which  $x_1$  varies and  $x_2/x_3 = 1$  (results for mixtures in which  $x_2$  is varied while  $x_1/x_3 = 1$  as well as for mixtures in which  $x_3$  is varied while  $x_1/x_2 = 1$  are shown in Figures D.1, D.2, D.3 and D.4 of appendix D). The results shown in Tables D.1 and D.2 as well as Figures 4.5 and 4.6 can be summarized as follows: (1) Differences between the multicomponent Darken equation and the Darken-LBV equation are small, as Eq. (4.14) accurately predicts self-diffusivities of components in a mixture from pure component data; (2) the Darken-LBV equation performs even slightly better than the Vignes-LBV equation, and much better than the generalized Darken equation. The outperformance of the Vignes-LBV model by the Darken-LBV model becomes especially clear from Figures 4.5 and 4.6, in particular Figures 4.5b and 4.6c which allow for the clearest discrimination. It is important to note that the accuracy of the Vignes-LBV equation (Eq. (4.4)) relies on an accurate estimate of  $\mathcal{D}_{ij}^{x_k \rightarrow 1}$ . It was previously shown that Eq. (4.3) provides the best prediction for  $\mathcal{D}_{ij}^{x_k \rightarrow 1}$ <sup>34</sup>. With this model, the Darken-LBV and the Vignes-LBV models are in

fact identical in the corners of the ternary diagram, where the mole fraction of one of the components approaches unity. Other predictive models for  $\mathcal{D}_{ij}^{x_k \rightarrow 1}$  introduce deviations ranging from 10-80%<sup>33</sup>. Therefore, much larger errors are expected when combining the Vignes equation with other predictive models for  $\mathcal{D}_{ij}^{x_k \rightarrow 1}$ . The reason for the poor performance of the generalized Darken equation can be twofold: (1) the quality of the generalized Darken equation itself; and (2) the quality of the predictive model for self-diffusivities. We also used the computed self-diffusivities from MD at the given compositions to parametrize the generalized Darken equation. In this way, deviations introduced by the predicted self-diffusivities are avoided. Our results show that this results in averaged absolute differences of 14-20% (see Figures 4.5 and 4.6 and Tables D.5 and D.6 of appendix D). These deviations are similar to the deviations when Eq. (4.7) is used for predicting self-diffusivities in a mixture, suggesting that the differences are not due to the choice of model for self-diffusivities but due to the generalized Darken equation itself. As stated above, the model structure of Eq. (4.6) suffers from inconsistencies at infinite dilution.

#### 4.4.2 Quaternary WCA systems

In Table D.7 of appendix D, it is shown that self-diffusivities in quaternary systems are very well predicted using Eq. (4.14), while the predictions using Eq. (4.7) show large deviations from MD results. Tables D.8 and D.9 compare the computed and predicted MS diffusivities in quaternary mixtures. The multicomponent Darken equation (Eq. (4.12)) provides reasonable predictions and again the Darken-LBV equation which requires only binary- and pure-component diffusivities performs equally well. Also here the performance of the Vignes-LBV equation is quite good with the present choice for the terms  $\mathcal{D}_{ij}^{x_k \rightarrow 1}$ . These models retain their prediction quality from the ternary case. The performance of the generalized Darken equation is again significantly worse with average and maximum deviations larger by at least a factor 2.

#### 4.4.3 n-hexane - cyclohexane - toluene

In Table D.10, computed and predicted self-diffusivities in the n-hexane - cyclohexane - toluene system at a pressure of 1 atm and a temperature of 298 K are listed. A detailed comparison between simulations and experiments for this mixture is given

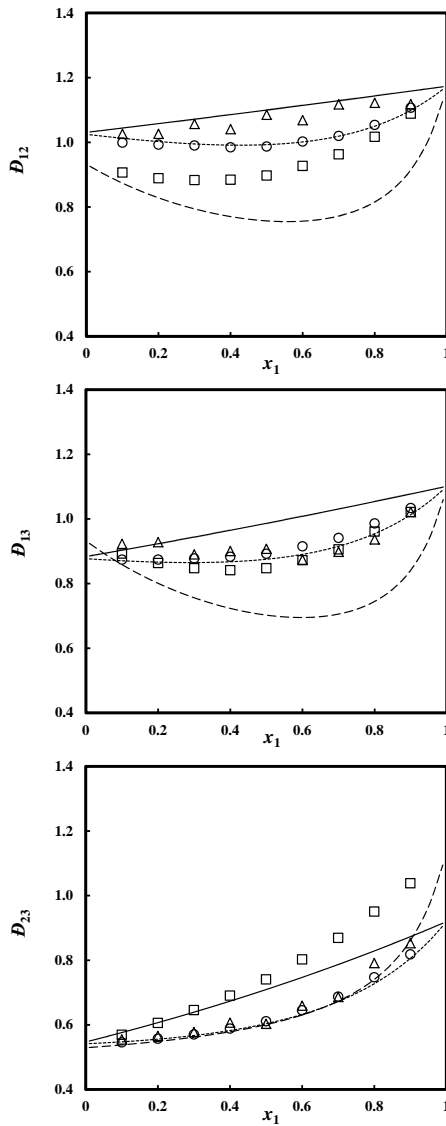


**Figure 4.5:** Computed and predicted MS diffusivities in ternary systems in which particles interact with a WCA potential. Triangles represent computed MS diffusivities using MD. Solid lines represent predictions using the Vignes-LBV equation (Eq. (4.4)). Dashed lines represent predictions using the generalized Darken equation (Eqs. (4.6)+(4.7)). Squares represent predictions using the generalized Darken equation with the self-diffusivities obtained from MD simulation (Eq. (4.6)+MD). Dotted lines represent predictions using the Darken-LBV equation (Eqs. (4.12)+(4.14)). Circles represent predictions using the multicomponent Darken equation with the self-diffusivities obtained from MD simulation (Eq. (4.12)+MD). Simulation details:  $\rho = 0.2$ ;  $M_1 = 1$ ;  $M_2 = 5$ ;  $M_3 = 10$ ;  $T = 2$ ;  $N = 400$ ,  $x_2/x_3 = 1$ .

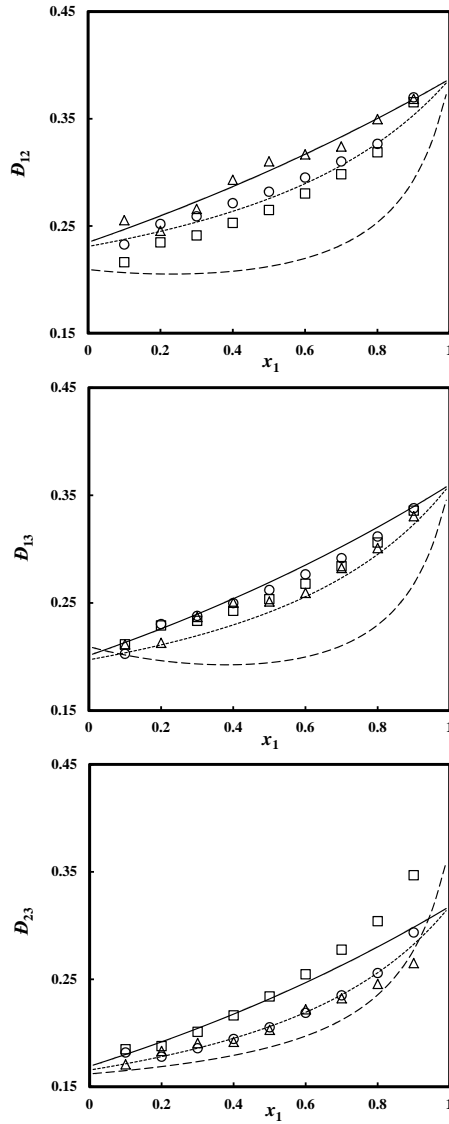


**Figure 4.6:** Computed and predicted MS diffusivities in ternary systems in which particles interact with a WCA potential. Triangles represent computed MS diffusivities using MD. Solid lines represent predictions using the Vignes-LBV equation (Eq. (4.4)). Dashed lines represent predictions using the generalized Darken equation (Eqs. (4.6)+(4.7)). Squares represent predictions using the generalized Darken equation with the self-diffusivities obtained from MD simulation (Eq. (4.6)+MD). Dotted lines represent predictions using the Darken-LBV equation (Eqs. (4.12)+(4.14)). Circles represent predictions using the multicomponent Darken equation with the self-diffusivities obtained from MD simulation (Eq. (4.12)+MD). Simulation details:  $\rho = 0.5$ ;  $M_1 = 1$ ;  $M_2 = 5$ ;  $M_3 = 10$ ;  $T = 2$ ;  $N = 400$ ,  $x_2/x_3 = 1$ .



in chapter 2 showing that the simulations correctly capture the experimental behavior. In this ternary system, the self-diffusivities are again much better predicted by Eq. (4.14) than Eq. (4.7). Table D.11 compares the predicted MS diffusivities to the computed MS diffusivities at same conditions. The pure and binary diffusion coefficients were taken from chapter 2. We observe that using the multicomponent Darken equation results in most accurate predictions of the MS diffusivities (average deviations of 7%), requiring self-diffusivities at a given composition. It is therefore very encouraging that the Darken-LBV performs equally well (average deviations of 9%), while the performance of the Vignes-LBV is similar but slightly worse (average deviations of 11%). The performance of the generalized Darken equation is significantly worse (average deviations of 15%). This is especially reflected by the large maximum deviations.

## 4.5 Conclusions

In this chapter, we derived a predictive Darken-LBV model for MS diffusivities in multicomponent systems (Eqs. (4.12) and (4.13)). MS diffusivities can be expressed as functions of easily obtainable self-diffusivities and the integrals of velocity correlations between different molecules. Neglecting the latter terms results in the multicomponent Darken equation. By combining the multicomponent Darken equation with a new predictive model for self-diffusivities in a mixture (4.14) we obtain the so-called Darken-LBV model (Eqs. (4.12), (4.13) and (4.14)). We compared our Darken-LBV equation to the Vignes-LBV model (Eq. (4.4)) and the generalized Darken model (Eqs. (4.6) and (4.7)) for WCA systems and the ternary n-hexane - cyclohexane - toluene system. Our results show that the Darken-LBV equation provides very good predictions for MS diffusivities and is superior compared to the other models. Since the Darken-LBV model is rigorously derived, it should also provide the preferred framework to extensions for the prediction of diffusion in liquid mixtures.



# 5

---

## Maxwell-Stefan Diffusivities in Binary Mixtures of Ionic Liquids with DMSO and H<sub>2</sub>O

---

This chapter is for a large part based on:

X. Liu, T.J.H. Vlugt, A. Bardow, *Maxwell-Stefan Diffusivities in Binary Mixtures of Ionic Liquids with DMSO and H<sub>2</sub>O*, *Journal of Physical Chemistry B*, **2011**, 115, 8506-8517.

## 5.1 Introduction

Ionic liquids (ILs) are salts which have melting points below 100 °C. An enormous number of different ILs can be prepared by a well-chosen selection of the cation and anion pair<sup>96;97</sup>. They offer an alternative to common organic solvents, for example for CO<sub>2</sub> capture<sup>98–101</sup>. Several properties make ILs popular, like small vapor pressure, thermal stability and the ability to dissolve a wide range of compounds<sup>102;103</sup>. Imidazolium-based ILs as shown in Figure 5.1 are widely studied in both experiments and computer simulations as these ILs are already used in practice and are easy to synthesize<sup>96;97;103–105</sup>.

The study of diffusion in ILs receives increasing interest as diffusion restricts the applicability of ILs in many processes. Self-diffusion of these systems was extensively studied in the past. This quantity can be measured using Pulsed-Field Gradient Nuclear Magnetic Resonance (PFG-NMR) spectroscopy. For instance, Lovell *et al.* studied the dependence of self-diffusivities on concentration in 1-ethyl-3-methylimidazolium acetate and cellulose<sup>106</sup>. Iacob *et al.* measured self-diffusivities of 1-hexyl-3-methylimidazolium hexafluorophosphate in silica membranes<sup>107</sup>. Bara *et al.* studied self-diffusivities of flue gases absorbed in imidazolium-based ILs and provided guidelines for separating CO<sub>2</sub> from flue gases using imidazolium-based ILs<sup>108</sup>. To gain a molecular understanding of diffusion, MD simulations are often used. However, the nature of ILs implies strong electrostatic interactions which significantly increases the computational cost for obtaining adequate sampling<sup>109</sup>. This becomes even more severe for computing collective properties like transport diffusivities<sup>33;110</sup>. While previous studies on diffusion in ILs focused on self-diffusivities<sup>111</sup>, the collective (or mutual) diffusion coefficient is required to describe mass transport in applications. Both experimental and simulation studies of mutual diffusion in ILs have mostly been concentrated on the infinite dilution regime where mutual and self-diffusivities become equal<sup>112–117</sup>. The concentration dependence of mutual diffusivities in systems with ILs has only been studied experimentally by Richter *et al.*<sup>118</sup>. To the best of our knowledge, a molecular understanding of the concentration dependence of MS diffusivities in ILs is still lacking. Mutual diffusion is conveniently described using the MS theory. General interest in MS diffusivities increases as (1) they usually depend less on concentration than Fick diffusivities; (2) the (electro)chemical potential gradient is used as the driving force of diffusion. In a system containing  $n$

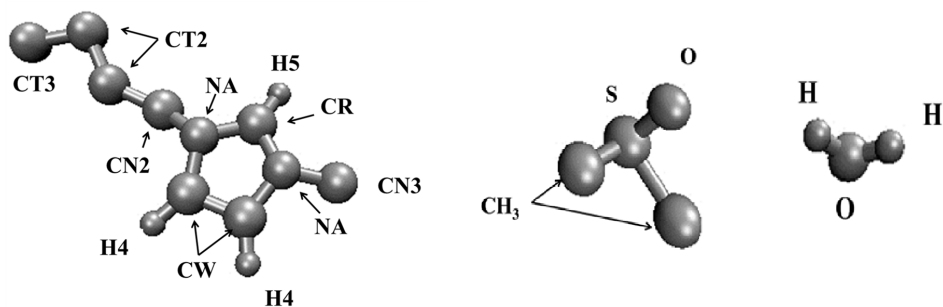


**Figure 5.1:** Schematic representation of the structure of  $C_n\text{mim}^+$  cations (here,  $n = 4$ ), DMSO and water. The atom labeling for the IL is as follows: NA:N, CR:C, CW:C, H4:H, H5:H, CN3:CH<sub>3</sub>, CN2:CH<sub>2</sub>, CT2:CH<sub>2</sub>, CT3:CH<sub>3</sub>.

components,  $n(n-1)/2$  MS diffusivities are sufficient to describe mass transport while  $(n-1)^2$  Fick diffusivities are needed. The  $(n-1)^2$  Fick diffusivities are not independent; (3) In multicomponent systems, MS diffusivities can be predicted using the MS diffusivities obtained from binary mixtures. Multicomponent Fick diffusivities are not related to their binary counterparts, which hinders the development of predictive models for describing multicomponent mass transport. MS diffusion coefficients cannot be directly accessed in experiments but need to be derived from Fick diffusivities. In chapters 2, 3 and 4, we showed that MD simulations are a valuable tool for developing and testing predictive models for MS diffusivities<sup>33;34</sup>.

In this chapter, MD simulations have been performed in binary mixtures with 1-alkyl-3-methylimidazolium chloride ( $C_n\text{mimCl}$ ,  $n = 2,4,8$ ), DMSO (dimethyl sulfoxide) and H<sub>2</sub>O. Our model is validated using experimental self-diffusivities. Self- and MS diffusivities in various binary mixtures are computed. We find that: (1) self- and MS diffusivities strongly decrease with increasing IL concentration; (2) additions of H<sub>2</sub>O or DMSO have a different influence on liquid structure: ILs stay in a form of isolated ions in  $C_n\text{mimCl-H}_2\text{O}$  mixtures, however, ion pairs are preferred in  $C_n\text{mimCl-DMSO}$  systems; (3) velocity cross-correlations cannot be neglected, so the predictions of Eq. (3.13) for  $\mathcal{D}_{ij}^{x_k \rightarrow 1}$  do not work well.

This chapter is organized as follows. In section 5.2, we describe the procedure of obtaining diffusion coefficients from MD simulations as well as the simulation details. In section 5.3, we review several predictive models which are often used for estimating the diffusion coefficients. The computed diffusivities and the quality

of predictive models are analyzed in section 5.4. Our conclusions are addressed in section 5.5.

## 5.2 Molecular Dynamics simulation

### 5.2.1 Obtaining diffusivities from MD simulation

Equilibrium MD simulations are used to determine self- and MS diffusivities. We refer the reader to section 2.3 and appendix A for details on this.

### 5.2.2 Details of equilibrium MD simulation

To describe the interactions between atoms and molecules in the system, we used a classical force field approximation for the total potential energy  $U$ ,

$$\begin{aligned}
 U = & \sum_{\text{bonds}} K_r (r - r_0)^2 + \sum_{\text{angles}} K_\theta (\theta - \theta_0)^2 + \sum_{\text{dihedrals}} K_\chi [1 + \cos(n\chi - \delta)] \\
 & + \sum_{i < j} 4\epsilon_{ij} \left[ \left( \frac{\sigma_{ij}}{r_{ij}} \right)^{12} - \left( \frac{\sigma_{ij}}{r_{ij}} \right)^6 \right] + \sum_{i < j} \frac{1}{4\pi\epsilon_0} \frac{q_i q_j}{r_{ij}}, \quad (5.1)
 \end{aligned}$$

in which  $K_r$ ,  $K_\theta$  and  $K_\chi$  are energy parameters for bond-stretching, bond-bending and dihedrals, respectively;  $\epsilon_{ij}$  and  $\sigma_{ij}$  are the energy and size parameters of the LJ potential, and  $q_i$  is the partial charge of (united) atom  $i$ . We use the united-atom approach for ILs and DMSO.  $\text{CH}_x$  groups are considered as single interaction centers with their own effective interaction potentials. Bead types H4 and H5 (see Figure 5.1) in the imidazolium ring are not treated as united atoms as they are more active and important for describing hydrogen bonding<sup>110</sup>. A flexible SPC model is used to describe water<sup>87</sup>. In this work, the LJ potential is truncated and shifted at 12 Å. The Lorentz-Berthelot mixing rules are applied to calculate the LJ parameters for the interactions of unlike atoms<sup>18</sup>. Electrostatic interactions are handled by Ewald summation using a relative precision<sup>85</sup> of  $10^{-5}$ . Since the force fields for 1-alkyl-3-methylimidazolium, chloride [ $\text{C}_n\text{mim}$ ][Cl], DMSO and  $\text{H}_2\text{O}$  were fitted at different cut-off radii (see Refs.<sup>87;110;119</sup>), we fixed the cut-off radius for LJ interactions at  $r_{\text{cut}} = 12$  Å and slightly adjusted the force field by keeping the size parameter  $\sigma$  constant

and changing the energy parameter  $\varepsilon$ . We fit the force field to the experimental density at lower temperatures (5 K above the melting points) as it is important that the simulations reproduce the experimental density<sup>33;34</sup>. The values of the force field parameters for non-bonded interactions are listed in Tables E.1 and E.2 of appendix E. Pure component data at higher temperatures are well reproduced and comparable with the experimental results as shown in Tables 5.1 and 5.2. Recently, Chen *et al.* used this force field for ILs to compute the viscosity of BmimCl and its mixture with water, acetonitrile and glucose<sup>120</sup>. Their results showed reasonable agreement between simulations and experiments, *i.e.* the computed viscosity of ILs is 20-50% larger than that obtained from experiments. Therefore, we can expect that our computed diffusivities of ILs are lower than in experiments. It is important to note that we are aiming to study the dependence of diffusivities on mixture composition instead of expanding the database of diffusion coefficients of ILs. Therefore, we feel that the force field applied in this work is sufficiently accurate for our purpose.

The simulations were carried out as follows: first, independent initial configurations are generated and equilibrated using equilibrium MD simulations in the  $NpT$  ensemble at the target temperature and pressure. The total number of molecules ranges from 100 (pure ILs) to 600 (pure water). The Nosé-Hoover thermostat and barostat are used with a time constants of 0.2 and 1 ps, respectively. Three dimensional periodic boundary conditions consistent with a cubic box were applied to obtain properties corresponding to bulk systems. A time step of 1 fs is used for integrating the equation of motion. When the average density of the systems does not change with time, we use the equilibrated system at this average density for computing the self- and MS diffusivities in the microcanonical ( $NVE$ ) ensemble. Simulations longer than 100 ns are often needed to obtain accurate diffusivities.

## 5.3 Predictive models for diffusion coefficients

### 5.3.1 Maxwell-Stefan diffusivities

The MS formulation uses (electro)chemical potential gradients as driving forces for mass transport. For liquid mixtures at constant temperature and pressure, in the absence of external electric fields the MS equation equals<sup>21;62</sup>

**Table 5.1:** Comparison of experimental and computed densities and self-diffusivities of DMSO and H<sub>2</sub>O at 1 atm. The statistical errors of computed densities are less than 1% and less than 3% for the computed self-diffusivities.

DMSO				
$T/\text{K}$	$\rho/(\text{g} \cdot \text{cm}^{-3})$		$D_{\text{self}}/(10^{-9} \text{m}^2 \cdot \text{s}^{-1})$	
	this work	experiment	$D_{\text{self}}^{\text{this work}}$	$D_{\text{self}}^{\text{exp}}$
298	1.090	1.096 <sup>121</sup>	0.79	0.80 <sup>122</sup>
303	1.082	1.091 <sup>121</sup>	0.97	n.a. <sup>a</sup>
318	1.068	n.a.	1.30	1.07 <sup>123</sup>
328	1.061	n.a.	1.40	1.26 <sup>123</sup>
368	1.026	n.a.	2.38	n.a.
H <sub>2</sub> O				
$T/\text{K}$	$\rho/(\text{g} \cdot \text{cm}^{-3})$		$D_{\text{self}}/(10^{-9} \text{m}^2 \cdot \text{s}^{-1})$	
	this work	experiment	$D_{\text{self}}^{\text{this work}}$	$D_{\text{self}}^{\text{exp}}$
298	1.003	0.997 <sup>124</sup>	3.00	2.49 <sup>122</sup>
310	0.995	0.993 <sup>125</sup>	3.70	3.07 <sup>126</sup>
323	0.986	0.988 <sup>125</sup>	4.69	3.95 <sup>126</sup>
348	0.972	0.975 <sup>125</sup>	6.12	6.08 <sup>126</sup>
368	0.946	0.960 <sup>125</sup>	8.40	n.a.

<sup>a</sup> not available.



$$\sum_{j=1}^{n-1} \Gamma_{ij} \nabla x_j = \sum_{\substack{k=1 \\ k \neq i}}^n \frac{x_i J_k - x_k J_i}{c_t \mathcal{D}_{ik}}, \quad (5.2)$$

where  $\Gamma_{ij}$  is the thermodynamic factor.  $\mathcal{D}_{ik}$  represent the MS diffusivity describing the friction between components  $i$  and  $k$ . MD simulations can be used to directly compute the MS diffusivities  $\mathcal{D}_{ij}$  from local particle fluctuations as shown in section 5.2. It is important to note that MS diffusivities do depend on the concentration<sup>23</sup>. For ordinary electrolyte solutions, the concentration dependence has usually been studied from infinite dilution to the solubility limit. Convenient prediction models covering the full concentration range are lacking. For mixtures of organic compounds, the Vignes equation is often recommended to predict the concentration dependence of MS diffusivities<sup>1,2</sup>. In a binary electrolyte solution, the generalized Vignes equation becomes

$$\begin{aligned} \mathcal{D}_{+-} &= \left( \mathcal{D}_{+-}^{x_+ \rightarrow 1} \right)^{x_+} \left( \mathcal{D}_{+-}^{x_- \rightarrow 1} \right)^{x_-} \left( \mathcal{D}_{+-}^{x_k \rightarrow 1} \right)^{x_k}, \\ \mathcal{D}_{+k} &= \left( \mathcal{D}_{+k}^{x_+ \rightarrow 1} \right)^{x_+} \left( \mathcal{D}_{+k}^{x_- \rightarrow 1} \right)^{x_-} \left( \mathcal{D}_{+k}^{x_k \rightarrow 1} \right)^{x_k}, \\ \mathcal{D}_{-k} &= \left( \mathcal{D}_{-k}^{x_+ \rightarrow 1} \right)^{x_+} \left( \mathcal{D}_{-k}^{x_- \rightarrow 1} \right)^{x_-} \left( \mathcal{D}_{-k}^{x_k \rightarrow 1} \right)^{x_k}, \end{aligned} \quad (5.3)$$

in which the subscripts  $+$  and  $-$  represent the cation and anion of the IL respectively.  $k$  represents a component carrying no net charge. It is important to note that Eq. (5.3) is a valid mathematical operation even though it is physically impossible as it violates electroneutrality *i.e.*  $\mathcal{D}_{ij}^{x_+ \rightarrow 1}$  and  $\mathcal{D}_{ij}^{x_- \rightarrow 1}$  do not exist. To preserve electroneutrality, we rewrite the Vignes equation as

$$\begin{aligned} \mathcal{D}_{+-} &= \left( \mathcal{D}_{+-}^{x_{\text{IL}} \rightarrow 1} \right)^{x_{\text{IL}}} \left( \mathcal{D}_{+-}^{x_k \rightarrow 1} \right)^{x_k}, \\ \mathcal{D}_{+k} &= \left( \mathcal{D}_{+k}^{x_{\text{IL}} \rightarrow 1} \right)^{x_{\text{IL}}} \left( \mathcal{D}_{+k}^{x_k \rightarrow 1} \right)^{x_k}, \\ \mathcal{D}_{-k} &= \left( \mathcal{D}_{-k}^{x_{\text{IL}} \rightarrow 1} \right)^{x_{\text{IL}}} \left( \mathcal{D}_{-k}^{x_k \rightarrow 1} \right)^{x_k}, \end{aligned} \quad (5.4)$$

in which  $x_{\text{IL}}$  is the number of IL molecules divided by the total number of molecules in the system (IL + solvent). Therefore

$$x_{\text{IL}} + x_k = 1. \quad (5.5)$$

in which  $x_k$  is the mole fraction of the uncharged component  $k$ .

### 5.3.2 Maxwell-Stefan diffusivities at infinite dilution

Eq. (5.4) requires the value of  $\mathcal{D}_{+-}^{x_k \rightarrow 1}$  (or  $\mathcal{D}_{ij}^{x_k \rightarrow 1}$ ) which describes the friction between cation and anion when both are infinitely diluted in solvent  $k$ . This quantity is not easily accessible in experiments as no direct measurement is possible<sup>7</sup>. In the past decades, several empirical models were proposed for estimating the quantity  $\mathcal{D}_{ij}^{x_k \rightarrow 1}$ . However, all of them are lacking a sound theoretical basis<sup>23;24;50;51;67</sup>. In chapter 3, we have showed that  $\mathcal{D}_{ij}^{x_k \rightarrow 1}$  does exist (*i.e.* does not depend on the ratio  $x_i/x_j$ ) and we have developed a new predictive model for  $\mathcal{D}_{ij}^{x_k \rightarrow 1}$  based on the linear response theory and the Onsager relations<sup>34</sup>. We find that  $\mathcal{D}_{ij}^{x_k \rightarrow 1}$  can be expressed in terms of self-diffusivities and integrals over velocity cross-correlation functions<sup>34</sup>

$$\mathcal{D}_{ij}^{x_k \rightarrow 1} = \frac{D_{i,\text{self}}^{x_k \rightarrow 1} \cdot D_{j,\text{self}}^{x_k \rightarrow 1}}{D_{k,\text{self}}^{x_k \rightarrow 1} + C_x}, \quad (5.6)$$

where  $D_{i,\text{self}}$  is the self-diffusivity of component  $i$ . The parameter  $C_x$  is related to integrals over velocity cross-correlation functions, see chapter 3. We assumed that in the limit of infinite dilution (here, we consider a case in which components  $i$  and  $j$  are infinitely diluted in component  $k$ ), the correlation of molecules that are of type  $k$  is much larger than the correlation of unlike molecules, *i.e.*  $C_x/D_{k,\text{self}} \approx 0$ . By neglecting the integrals over velocity cross-correlation functions, we obtain a convenient predictive model for  $\mathcal{D}_{ij}^{x_k \rightarrow 1}$ <sup>34</sup>

$$\mathcal{D}_{ij}^{x_k \rightarrow 1} = \frac{D_{i,\text{self}}^{x_k \rightarrow 1} \cdot D_{j,\text{self}}^{x_k \rightarrow 1}}{D_{k,\text{self}}^{x_k \rightarrow 1}}. \quad (5.7)$$

It was shown in chapter 3 that Eq. (5.7) is superior compared to the existing models in several systems, *i.e.* systems in which particles interacting using WCA potential or ternary mixtures of n-hexane-cyclohexane-toluene. In the ethanol-methanol-water system, Eq. (5.7) deviates from direct calculations of  $\mathcal{D}_{ij}$  revealing that velocity cross-correlation functions should be taken into account as  $C_x$  is of the same order

of magnitude as  $D_{k,\text{self}}^{x_k \rightarrow 1}$ . This deviation is mainly due to the formation of hydrogen bonds. In this work, we also test the ability of Eq. (5.7) in predicting  $D_{ij}^{x_k \rightarrow 1}$  in mixtures with ILs.

### 5.3.3 Salt diffusivity

The electroneutrality condition forces both ions of ILs to diffuse at the same rate in the absence of an electric current. This phenomenon is known as salt diffusion. It is well known that the correct driving force for diffusion is the electrochemical potential gradient. The MS diffusion coefficient of IL molecules based on a thermodynamic driving force is defined as<sup>127</sup>

$$\mathcal{D}_{\text{IL}} = \frac{\mathcal{D}_{+k}\mathcal{D}_{-k}(z_+ - z_-)}{z_+\mathcal{D}_{+k} - z_-\mathcal{D}_{-k}}, \quad (5.8)$$

with  $z$  is the charge number of the ion.  $\mathcal{D}_{+k}$  and  $\mathcal{D}_{-k}$  are defined by Eq. (5.2). The often used salt diffusivity  $D_{\text{IL}}$  which considers the concentration gradient as driving force of diffusion can be related to  $\mathcal{D}_{\text{IL}}$  using<sup>127</sup>

$$D_{\text{IL}} = \mathcal{D}_{\text{IL}} \frac{c_T}{c_0} \left( 1 + \frac{d \ln \gamma_{+-}}{d \ln m} \right), \quad (5.9)$$

where  $\gamma_{+-}$  is the mean molal activity coefficient. In this equation,  $m$  is the molarity (moles of electrolyte per kilogram of solvent),  $c_T$  is the total solution concentration ( $\text{mol}/\text{m}^3$ ), and  $c_0$  is the concentration of the solvent ( $\text{mol}/\text{m}^3$ ). In the limit of infinite dilution, the equation for the salt diffusivity  $D_{\text{IL}}$  can be simplified as<sup>127</sup>

$$D_{\text{IL}} = \frac{D_{+,\text{self}}D_{-,\text{self}}(z_+ - z_-)}{z_+D_{+,\text{self}} - z_-\mathcal{D}_{-,\text{self}}}. \quad (5.10)$$

## 5.4 Results and Discussion

### 5.4.1 Model validation via self-diffusivities

#### Pure ILs

Table 5.2 shows the computed self-diffusivities of  $C_n\text{mimCl}$  at 1 atm. Simulations were carried out above the melting points of  $C_n\text{mimCl}$ . The results shown in Table

**Table 5.2:** Comparison of experimental and computed densities of  $C_n$ mimCl at 1 atm. Computed self-diffusivities of ions are also listed. The statistical errors of computed densities are less than 1% and less than 4% for the computed self-diffusivities.

$C_1$ mimCl <sup>a</sup>				
$T/K$	$\rho/(g \cdot cm^{-3})$		$D/(10^{-9} m^2 \cdot s^{-1})$	
	this work	experiment	$D_{+,self}$	$D_{-,self}$
400	1.119	1.140 <sup>128</sup>	0.190	0.162
425	1.105	1.120 <sup>128</sup>	0.298	0.258
$C_2$ mimCl <sup>b</sup>				
$T/K$	$\rho/(g \cdot cm^{-3})$		$D/(10^{-9} m^2 \cdot s^{-1})$	
	this work	experiment	$D_{+,self}$	$D_{-,self}$
368	1.105	n.a. <sup>c</sup>	0.109	0.074
373	1.098	1.11 <sup>128</sup>	0.119	0.097
400	1.072	1.09 <sup>128</sup>	0.247	0.210
$C_4$ mimCl <sup>d</sup>				
$T/K$	$\rho/(g \cdot cm^{-3})$		$D/(10^{-9} m^2 \cdot s^{-1})$	
	this work	experiment	$D_{+,self}$	$D_{-,self}$
353	1.048	n.a.	0.010	0.009
368	1.042	n.a.	0.027	0.026
373	1.033	n.a.	0.028	0.028
400	1.024	n.a.	0.079	0.070
$C_8$ mimCl <sup>e</sup>				
$T/K$	$\rho/(g \cdot cm^{-3})$		$D/(10^{-9} m^2 \cdot s^{-1})$	
	this work	experiment	$D_{+,self}$	$D_{-,self}$
368	0.989	n.a.	0.007	0.008
400	0.968	n.a.	0.037	0.039

<sup>a</sup> The melting point of  $C_1$ mimCl is 398 ~ 399 K, see Refs. <sup>128;129</sup>.

<sup>b</sup> The melting point of  $C_2$ mimCl is 357 K, see Ref. <sup>128</sup>.

<sup>c</sup> not available.

<sup>d</sup> The melting point of  $C_4$ mimCl is 314 ~ 339 K depending on the type of crystal polymorph, see Ref. <sup>130</sup>.

<sup>e</sup> The melting point of  $C_8$ mimCl is 285 K, see Ref. <sup>131</sup>.

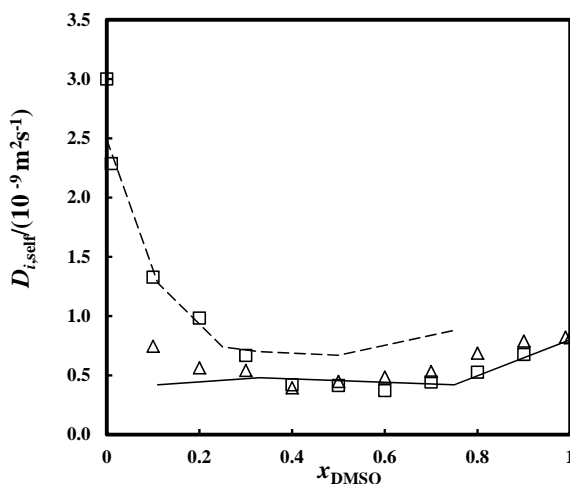


**Figure 5.2:** Computed self-diffusivities of DMSO-H<sub>2</sub>O mixtures at 298 K, 1 atm. Triangles represent the computed self-diffusivity of DMSO and squares represent the computed self-diffusivity of H<sub>2</sub>O. The solid line represents the self-diffusivity of DMSO obtained from experiments and the dashed line represents the experimental self-diffusivity of H<sub>2</sub>O<sup>122</sup>. The error bars of computed diffusivities are smaller than the symbol size.

5.2 can be summarized as follows: (1) as the temperature increases, self-diffusivities of  $C_n\text{mimCl}$  increase as well. This is due to both decreased density and enhanced mobilities of molecules; (2) for  $C_n\text{mimCl}$  with shorter tail, *i.e.*  $n = 1$  and  $2$ , the self-diffusivity of cations is larger than that of anions; (3) as the side chain increases, the self-diffusivities of cation and anion are almost equal. This is in agreement with the observations by Feng *et al.*<sup>132</sup>.

## H<sub>2</sub>O-DMSO

Figure 5.2 compares self-diffusivities in DMSO-H<sub>2</sub>O system obtained from both simulations and experiments<sup>122</sup>. A strongly non-ideal behavior of the mixture was observed due to the strong hydrogen bond between DMSO and H<sub>2</sub>O. The smallest values for self-diffusivities of both components were found between  $x_{\text{DMSO}} = 0.4$ - $0.6$ . Moreover, it is clear that the dynamics of water is more strongly affected than that of DMSO. A similar feature has been observed in both experiments and simulations<sup>133;134</sup>. A general understanding of the structure of water-DMSO mixtures was derived earlier mainly from x-ray, neutron scattering and computer simu-

lations<sup>135–138</sup>. It is well established that the local minimum in Figure 5.2 is due to the formation of 1:DMSO-2:H<sub>2</sub>O or 2:DMSO-1:H<sub>2</sub>O rigid structures which restrict the mobility of molecules yielding lower self-diffusivities<sup>122;133;134</sup>. In the range  $x_{\text{DMSO}} < 0.4$  or  $x_{\text{DMSO}} > 0.6$ , excess water molecules and DMSO molecules are available which are less restricted by these rigid structures. This results in larger self-diffusivities.

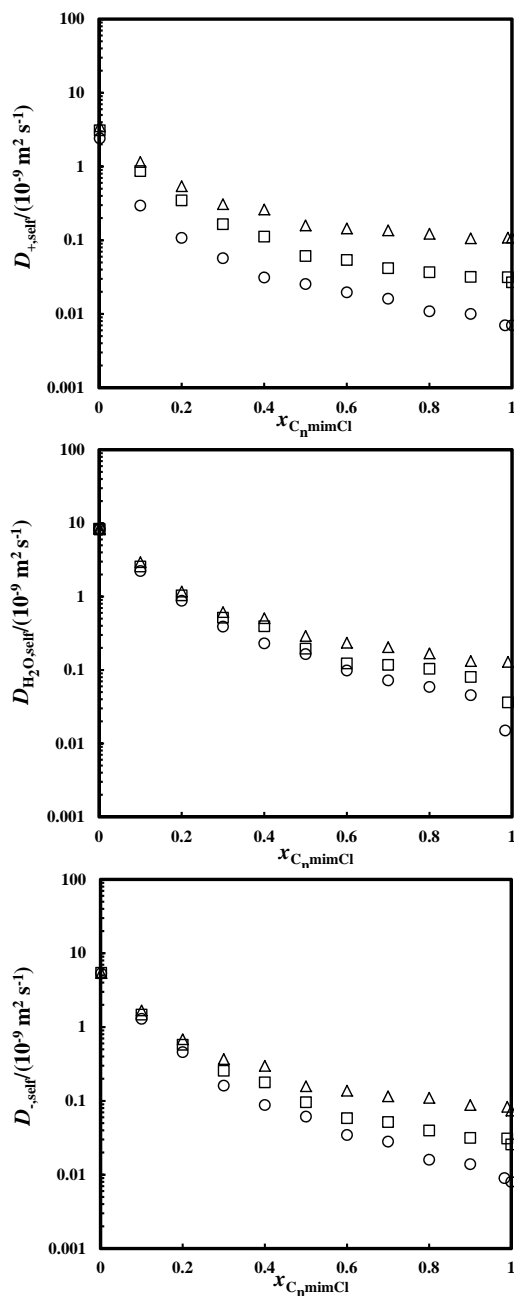
### ILs-H<sub>2</sub>O

Experimental studies have shown that  $C_n\text{mimCl}$  ( $n = 2, 4, 8$ ) is completely miscible with H<sub>2</sub>O at 368 K, 1 atm.<sup>131;139</sup> Figure 5.3 shows computed self-diffusivities of  $C_n\text{mim}^+$ ,  $\text{Cl}^-$  and H<sub>2</sub>O in ILs-H<sub>2</sub>O mixtures. The self-diffusivities of all components strongly decrease with increasing concentration of ILs. For the self-diffusivities of anions and H<sub>2</sub>O, two regimes are formed. At lower ILs concentration, the influence of the size of cation on self-diffusivity is negligible. As the ILs concentration increases, the influence originating from the cation size becomes important. Due to the two regimes, deviations from a single exponential behavior are observed for self-diffusivities in IL-H<sub>2</sub>O mixtures. Strongly decreasing self-diffusivities with increasing IL concentration were observed in several other studies<sup>106;132</sup>. Lovell measured self-diffusivities in 1-ethyl-3-methyl-imidazolium acetate cellulose solutions using <sup>1</sup>H NMR<sup>106</sup>. Feng *et al.* computed the self-diffusivities in  $C_n\text{mimCl}$ -H<sub>2</sub>O and  $C_n\text{mimBF}_4$ -H<sub>2</sub>O mixtures using MD simulations<sup>132</sup>. These authors found that an exponential relation is the best description for the concentration dependence of the self-diffusivities of ions.

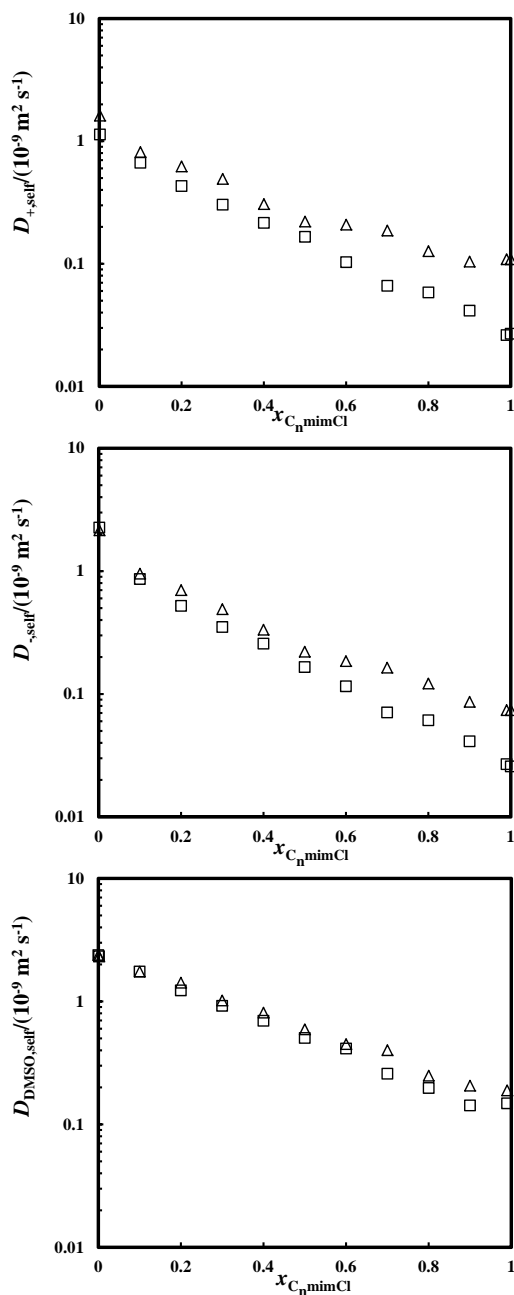
### ILs-DMSO

Figure 5.4 shows the self-diffusivities in  $C_n\text{mimCl}$ -DMSO mixtures. We only studied  $C_n\text{mimCl}$ -DMSO systems with  $n = 2$  and 4. The  $C_8\text{mimCl}$ -DMSO system is not included in this study as the solubility of  $C_8\text{mimCl}$  in DMSO is not known. For  $C_n\text{mimCl}$ -DMSO systems, self-diffusivities exponentially decrease with increasing IL concentration. However, the decrease of self-diffusivities in  $C_n\text{mimCl}$ -DMSO mixtures is less pronounced than that in ILs aqueous solutions.

The observations from Figures 5.3 and 5.4 can be summarized as follows: (1) the self-diffusivities of all components decrease strongly as the ILs concentration in-



**Figure 5.3:** Computed self-diffusivities of  $C_n$ mimCl-H<sub>2</sub>O mixtures at 368 K, 1 atm. Triangles represent the C<sub>2</sub>mimCl-H<sub>2</sub>O mixture. Squares represent the C<sub>4</sub>mimCl-H<sub>2</sub>O mixture. Circles represent the C<sub>8</sub>mimCl-H<sub>2</sub>O mixture. The error bars of computed diffusivities are smaller than the symbol size.



**Figure 5.4:** Computed self-diffusivities of  $C_n$  mimCl-DMSO mixtures at 368 K, 1 atm. Triangles represent the  $C_2$  mimCl- $\text{H}_2\text{O}$  mixture. Squares represent the  $C_4$  mimCl- $\text{H}_2\text{O}$  mixture. The error bars of computed diffusivities are smaller than the symbol size.



creases; (2) larger cations result in smaller self-diffusivities; (3) the side chain length of cations plays a minor role in determining the self-diffusivities in the IL-DMSO systems. The values of the computed diffusivities in these figures are listed in Tables E.3 and E.4 of appendix E.

## 5.4.2 Maxwell-Stefan diffusivities and radial distribution functions

### ILs-H<sub>2</sub>O

Figure 5.5 shows the MS diffusivities  $\mathcal{D}_{+-}$ ,  $\mathcal{D}_{+\text{H}_2\text{O}}$  and  $\mathcal{D}_{-\text{H}_2\text{O}}$  in  $C_n\text{mimCl-H}_2\text{O}$  mixtures. It is clear that (1) both  $\mathcal{D}_{+-}$  and  $\mathcal{D}_{-\text{H}_2\text{O}}$  decrease with increasing IL concentration; (2)  $\mathcal{D}_{+\text{H}_2\text{O}}$  is less sensitive to the concentration compared to  $\mathcal{D}_{+-}$  and  $\mathcal{D}_{-\text{H}_2\text{O}}$ ; (3) at the same water content, the MS diffusivities are smaller in a system containing larger IL molecules. As MS diffusivities can be considered as inverse friction coefficients (see Eq. (5.2)), this implies stronger effective interactions between different components; (4) the Vignes equation (Eq. (5.4)) does not describe the simulation data very well. In all systems, lower diffusivities than predicted by the Vignes equation are observed.

Radial distribution functions (RDFs) characterize the liquid structure and can be used to understand trends in values of the diffusivities. Figures 5.6 (a), (c), (e) show the RDFs of CR-O (CR is the atom located on the ring of the cation and connected with nitrogen, see Figure 5.1; O is the oxygen atom in H<sub>2</sub>O) in a  $C_n\text{mimCl-H}_2\text{O}$  mixture. In IL-rich mixtures, *i.e.*  $x_{\text{H}_2\text{O}} = 0.2$ , the peak of the RDFs first increases with increasing tail length of cations, followed by a decrease. In water-rich mixtures, *i.e.*  $x_{\text{H}_2\text{O}} = 0.8$ , a continuous increasing trend of this peak was observed. Figures 5.6 (b), (d), (f) show the RDFs of Cl-O in  $C_n\text{mimCl-H}_2\text{O}$  mixtures. Much higher peaks were found compared to the RDFs of CR-O indicating a much stronger interaction (also due to less steric hindrance) between anions and water.

### ILs-DMSO

Figure 5.7 presents the MS diffusivities in  $C_n\text{mimCl-DMSO}$  mixtures with  $n = 2$  and 4. We observe that (1)  $\mathcal{D}_{+-}$  is not sensitive to the mixture composition meaning that adding DMSO has a negligible effect on the interaction or friction between cations and anions; (2) both  $\mathcal{D}_{+\text{DMSO}}$  and  $\mathcal{D}_{-\text{DMSO}}$  are larger than  $\mathcal{D}_{+-}$  indicating the cation-

anion interaction is the most strongest; (3)  $D_{+\text{DMSO}}$  and  $D_{-\text{DMSO}}$  are decreasing with increased IL concentration. The Vignes equation gives a better description of the concentration dependence than for IL- $\text{H}_2\text{O}$  system but systematic deviations are still discernible.

Figure 5.8 shows the RDFs of CR-S and Cl-S (CR is the atom located on the ring of the cation and connected with nitrogen; S is the sulfur atom in DMSO). Similar coordination numbers were observed for both CR-S and Cl-S which is different from the RDFs in ILs aqueous solution. This similar trend for CR-S and Cl-S suggests that the interaction between cation and DMSO is comparable with that of the anion and DMSO.

### Ionization of ILs

Figure 5.9 compares the RDFs between cation and anion in  $C_n\text{mimCl-H}_2\text{O}$  and  $C_n\text{mimCl-DMSO}$  mixtures. In the  $C_n\text{mimCl-H}_2\text{O}$  system, the first peak is reduced as the water concentration increases, as shown in Figure 5.9 (a), (c), (e), suggesting that the interaction between cations and anions is reduced. This reduced cation-anion interaction is due to the dilution by water. In other words, water molecules replace anions around the cations. The opposite behavior was observed for  $C_n\text{mimCl-DMSO}$  mixtures; a dramatic increase of the first peak was observed with the increased DMSO concentration, as shown in Figure 5.9 (b), (d). This result suggests that the interaction between cations and anions is strengthened with increasing DMSO concentration.

$C_n\text{mimCl}$  is miscible with both water and DMSO but there are clear differences:  $C_n\text{mimCl}$  dissolves in water in form of isolated ions. The results presented in Figure 5.9 suggest that in the case of DMSO,  $C_n\text{mimCl}$  dissolves in a form of ion pairs. It would be very interesting to investigate the lifetime of these ion pairs in more detail<sup>140</sup>. A similar phenomenon was observed in both MD simulations and NMR measurement for a binary mixture with  $C_4\text{mimCl}$ <sup>139</sup>. This feature has been proposed for explaining a phenomenon observed previously in dissolving bio-polymers using ILs<sup>139</sup>. IL-bio-polymer systems are highly viscous. Therefore, a second solution is often added to reduce the viscosity. Experimental studies show that by adding water, the ability of ILs for dissolving bio-polymers is dramatically reduced<sup>141</sup>. In contrast, adding DMSO has a negligible effect on the dissolution of bio-polymers<sup>139</sup>.

**Table 5.3:** Diffusivities of ILs infinitely diluted in H<sub>2</sub>O or DMSO at 368 K, 1 atm. Comparison between MS diffusivities obtained from MD simulations and the predictive model Eq. (5.7).

$i - j$	$\mathcal{D}_{+-}^{\text{MD}}$	$\mathcal{D}_{+-}^{\text{Prediction}}$	AD <sup>a</sup>
C <sub>2</sub> mimCl-H <sub>2</sub> O	1.08	2.29	112%
C <sub>4</sub> mimCl-H <sub>2</sub> O	0.84	1.65	96%
C <sub>8</sub> mimCl-H <sub>2</sub> O	0.56	1.55	177%
C <sub>2</sub> mimCl-DMSO	0.11	2.46	2140%
C <sub>4</sub> mimCl-DMSO	0.07	1.08	1446%

<sup>a</sup> absolute difference normalized with corresponding result from MD simulations

### MS diffusivities at infinite dilution

In the limit of infinite dilution, MS diffusivity  $\mathcal{D}_{+-}^{k \rightarrow 1}$  can be obtained from both MD simulations and predictive model Eq. (5.7) as shown in Table 5.3. Eq. (5.7) is parametrized using self-diffusivities which are listed in Table E.5 of appendix E. Absolute differences between MD simulations and predictions were calculated to evaluate the quality of Eq. (5.7). We found that: (1) Eq. (5.7) overestimates the MS diffusivity  $\mathcal{D}_{+-}^{k \rightarrow 1}$ ; (2) Eq. (5.7) results in large deviations in ILs-DMSO mixtures. As discussed in chapter 3, in mixtures with none or weakly associated molecules, Eq. (5.7) is accurate and superior to the existing predictive models; in mixtures with highly associated molecules, Eq. (5.7) either overestimates or underestimates the MS diffusivity at infinite dilution. The assumption that the correlation of unlike molecules is negligible does not hold in these systems. Detailed information of velocity cross-correlations should then be taken into account. In this work, we found that the largest deviation occurred in ILs-DMSO mixtures. This is mainly due to the increasing interaction between cation and anion in the presence of DMSO. In the ILs-water mixtures, this interaction between ions is greatly reduced yielding a relatively smaller deviations. The information of velocity cross-correlation function in the studied mixtures is listed in Table E.6 of appendix E.

### 5.4.3 Diffusivity of IL molecules

As mentioned previously, the electroneutrality condition forces both ions of ILs to diffuse at the same rate in the absence of an electric current. This phenomenon is known as salt diffusion. The MS diffusion coefficient of IL molecules  $\mathcal{D}_{\text{IL}}$  based on a thermodynamic driving force are calculated using Eq. (5.8) and presented in Figure 5.10. Not surprisingly, in ILs-H<sub>2</sub>O mixtures, the concentration dependence of  $\mathcal{D}_{\text{IL}}$  is in between the one found for  $\mathcal{D}_{+\text{H}_2\text{O}}$  and  $\mathcal{D}_{-\text{H}_2\text{O}}$ . The IL MS diffusivity in water shows a strong, nontrivial dependence on the IL concentration. The influence of the alkyl chain length on the IL MS diffusion coefficient, however, is minor and for  $x_{\text{IL}} < 0.5$  even negligible.

Sarraute *et al.* measured the Fick diffusivities of C<sub>4</sub>mimCl-H<sub>2</sub>O mixtures at infinite dilution using the Taylor dispersion technique at temperatures ranging from 283 K to 333 K<sup>115</sup>. According to the Arrhenius relation given by these authors, the value of the Fick diffusivity of IL molecules can be extrapolated to 368K resulting in a value  $4.3 \cdot 10^{-9} \text{ m}^2 \text{ s}^{-1}$ . Here, the calculated MS diffusivity of IL molecules is  $4.0 \cdot 10^{-9} \text{ m}^2 \text{ s}^{-1}$  for the same system. At infinite dilution, the thermodynamic factor equals one revealing an excellent agreement between the computed diffusivity and experimental data. Recall that the computed diffusivity of pure H<sub>2</sub>O is larger than the experimental data while the computed diffusivities of ILs are expected to be lower than experimental results. These deviations from experimental data are thus compensated in IL-H<sub>2</sub>O systems yielding a good agreement between computed and measured diffusivities.

In the ILs-DMSO systems, the decrease of  $\mathcal{D}_{\text{IL}}$  is comparable to that of  $\mathcal{D}_{+\text{DMSO}}$  and  $\mathcal{D}_{-\text{DMSO}}$ . Again, the length of the alkyl chain in the IL does not influence the diffusion coefficient in the studied IL-DMSO mixtures. The data in Figure 5.10 are listed in Tables E.3 and E.4 of appendix E.

For obtaining the salt diffusivity  $D_{\text{IL}}$ , it is essential to know the thermodynamic factor. The thermodynamic factor can be measured in experiments *i.e.* Karl Fischer titration<sup>142</sup>. However, difficulties still exist in implementing these methods. For example, the uncertainty in measured activity coefficient is 20% in a BmimCl-H<sub>2</sub>O mixture<sup>142</sup>. Since the thermodynamic factor requires the concentration derivative of the activity coefficient, even larger errors have to be expected. In our view, MD simulations are thus the preferred method to study the behavior of MS diffusivities.

## 5.5 Conclusions

ILs are often considered as green solvents and good candidates for many processes. Their physical and chemical properties can be well tuned through varied combinations of cations and anions. Imidazolium-based ILs are extensively studied in both experiments and computer simulations as they have been employed in practice *i.e.* as gas storage fluids, and as separation media<sup>143;144</sup>.

To the best of our knowledge, MS diffusivities in the mixtures with ILs have not yet been reported. In this study, we computed MS diffusivities using MD simulations in  $C_n\text{mimCl-H}_2\text{O}$  ( $n = 2,4,8$ ) and  $C_n\text{mimCl-DMSO}$  mixtures ( $n = 2,4$ ). The effects of alkyl chain length and mixture composition on the diffusion coefficients are explored. Our results show that: (1) self- and MS diffusivities strongly decrease with the increasing concentration of ILs; (2) the MS diffusivities of the ionic liquid ( $\mathcal{D}_{\text{IL}}$ ) are almost independent of the alkyl chain length. The dependence is much smaller than for the self-diffusivities indicating the necessity for studying mutual diffusion in detail; (3) addition of  $\text{H}_2\text{O}$  and DMSO have a different influence on the liquid structure of ILs. ILs stay in a form of isolated ions in  $C_n\text{mimCl-H}_2\text{O}$  mixtures, however, ion pairs are preferred in  $C_n\text{mimCl-DMSO}$  systems; (4) in the limit of infinite dilution, MS diffusivity  $\mathcal{D}_{ij}^{x_k \rightarrow 1}$  can be predicted by Eq. (5.7) based on easily obtained self-diffusivities. In the studied mixtures with ILs, Eq. (5.7) results in larger deviations in estimating MS diffusivity suggesting that velocity cross-correlations are important.

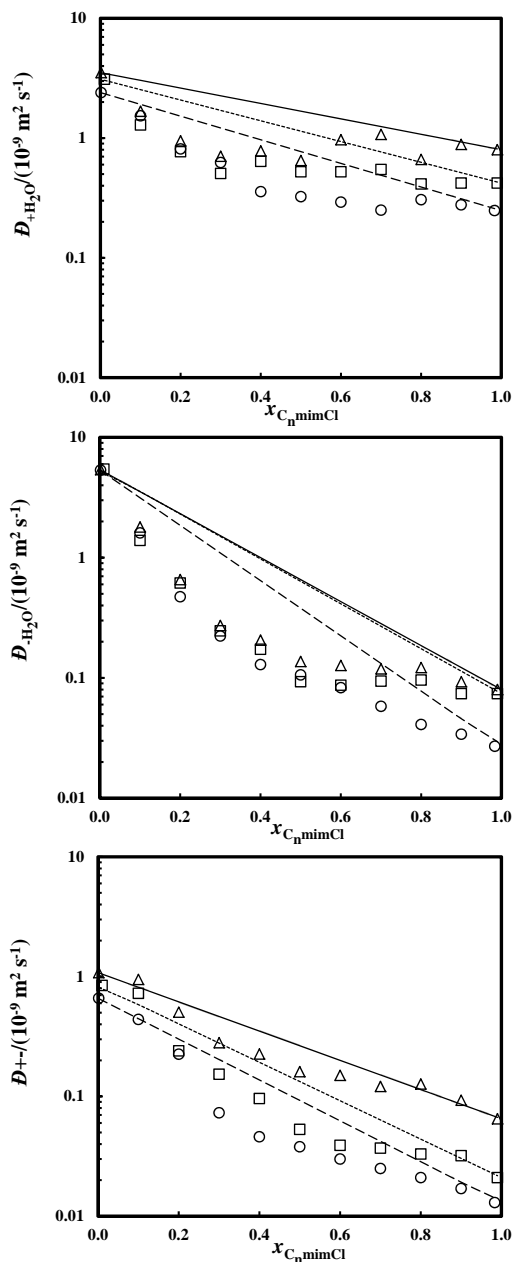


**Figure 5.5:** MS diffusivities of  $C_n$ mimCl- $H_2O$  mixtures at 368 K, 1 atm. Triangles represent the  $C_2$ mimCl- $H_2O$  mixture. Squares represent the  $C_4$ mimCl- $H_2O$  mixture. Circles represent the  $C_8$ mimCl- $H_2O$  mixture. Lines are the predicted MS diffusivities using Eq. (5.4). Solid lines represent the  $C_2$ mimCl- $H_2O$  mixture. Dotted lines represent the  $C_4$ mimCl- $H_2O$  mixture. Dashed lines represent the  $C_8$ mimCl- $H_2O$  mixture.

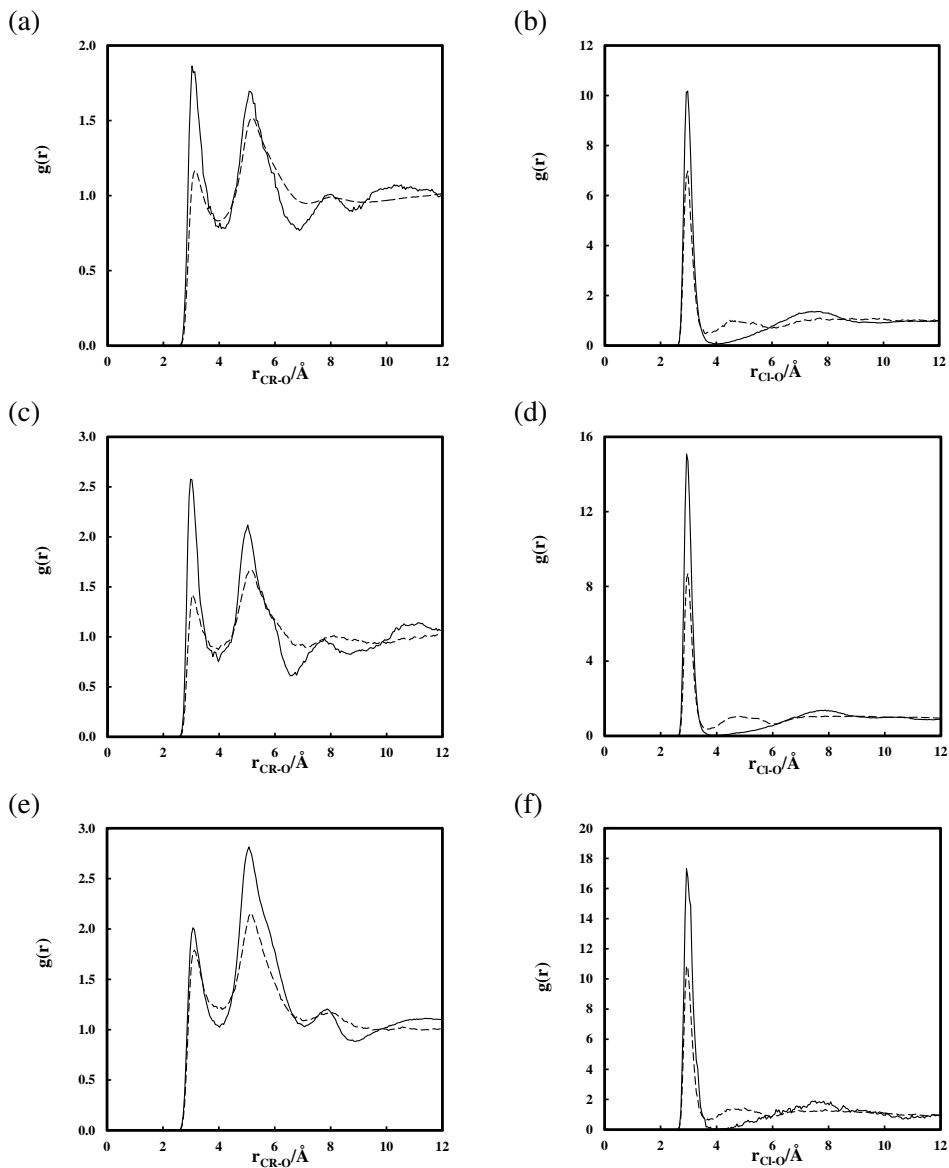


**Figure 5.6:** Radial distribution functions of CR-O and Cl-O atom pairs in water at 368 K, 1 atm. Solid lines represent  $x_{\text{H}_2\text{O}} = 0.2$ . Dashed line represents  $x_{\text{H}_2\text{O}} = 0.8$  (a) CR-O in a  $\text{C}_2\text{mimCl}$ -water mixture. CR is the atom located on the ring of the cation and connected with nitrogen, see Figure 5.1; (b) Cl-O in a  $\text{C}_2\text{mimCl}$ -water mixture; (c) CR-O in a  $\text{C}_4\text{mimCl}$ -water mixture; (d) Cl-O in a  $\text{C}_4\text{mimCl}$ -water mixture; (e) CR-O in a  $\text{C}_8\text{mimCl}$ -water mixture; (f) Cl-O in a  $\text{C}_8\text{mimCl}$ -water mixture.

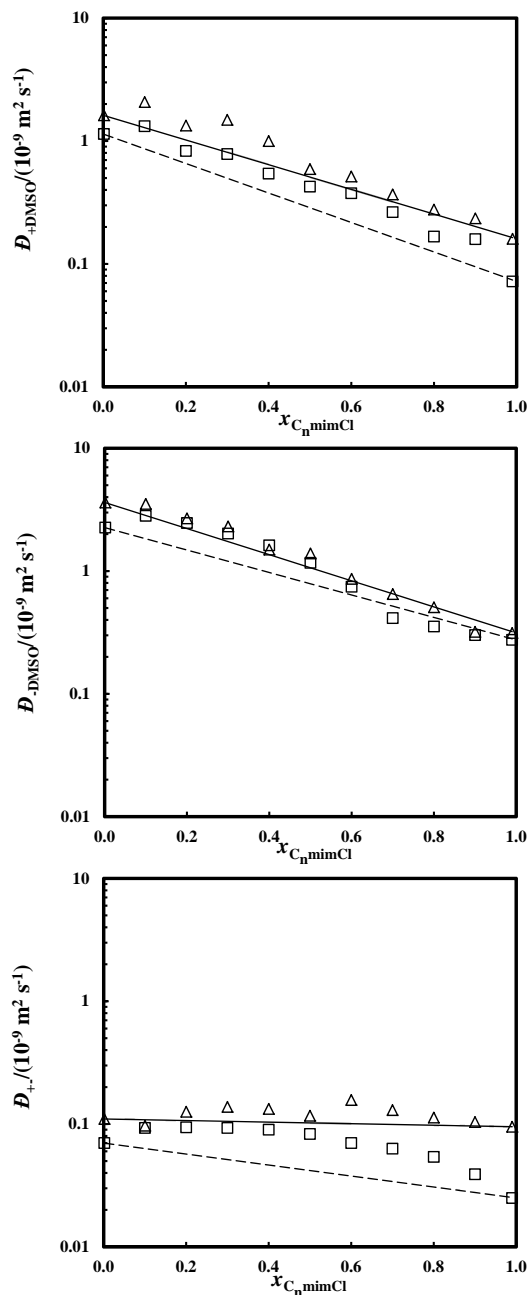


**Figure 5.7:** MS diffusivities in  $C_n$  mimCl-DMSO mixtures at 368 K, 1 atm. Triangles represent the  $C_2$  mimCl-H<sub>2</sub>O mixture. Squares represent the  $C_4$  mimCl-H<sub>2</sub>O mixture. Lines are the predicted MS diffusivities using Eq. (5.4). Solid lines represent the  $C_2$  mimCl-H<sub>2</sub>O mixture. Dotted lines represent the  $C_4$  mimCl-H<sub>2</sub>O mixture.



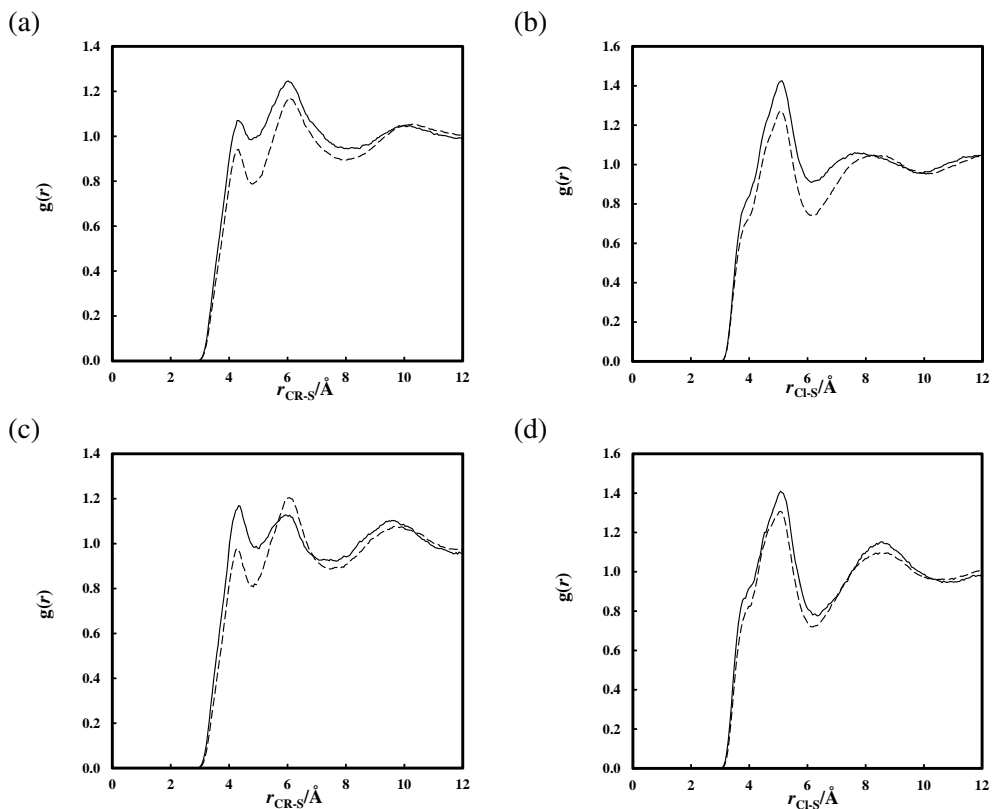


**Figure 5.8:** Radial distribution function of CR-S and Cl-S atom pairs in DMSO at 368 K, 1 atm. Solid lines represent  $x_{\text{H}_2\text{O}} = 0.2$ . Dashed line represents  $x_{\text{H}_2\text{O}} = 0.8$ . (a) CR-S in a  $C_2\text{mimCl}$ -DMSO mixture. CR is the atom located on the ring of the cation and connected with nitrogen, see Figure 5.1; (b) Cl-S in a  $C_2\text{mimCl}$ -DMSO mixture; (c) CR-S in a  $C_4\text{mimCl}$ -DMSO mixture; (d) Cl-S in a  $C_4\text{mimCl}$ -DMSO mixture.

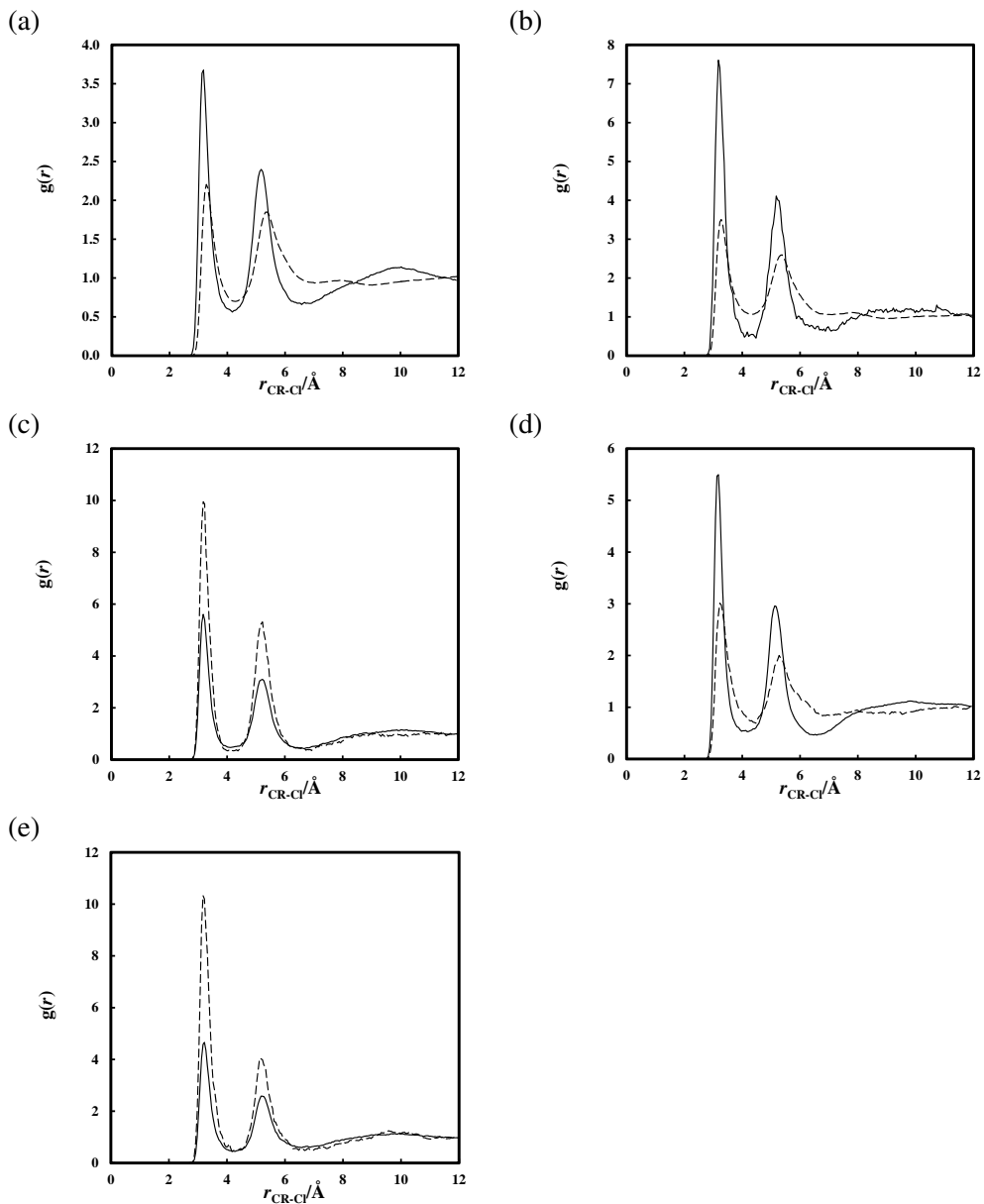


**Figure 5.9:** Radial distribution function of CR-Cl atom pairs in a binary mixture of  $C_n$ mimCl and water / DMSO at 368 K, 1 atm. Solid lines represent  $x_{\text{H}_2\text{O}} = 0.2$ . Dashed lines represent  $x_{\text{H}_2\text{O}} = 0.8$ . (a) CR-Cl in a  $C_2$ mimCl-water mixture; (b) CR-Cl in a  $C_2$ mimCl-DMSO mixture; (c) CR-Cl in a  $C_4$ mimCl-water mixture; (d) CR-Cl in a  $C_4$ mimCl-DMSO mixture. (e) CR-Cl in a  $C_8$ mimCl-water mixture. CR is the atom located on the ring of the cation and connected with nitrogen, see Figure 5.1.

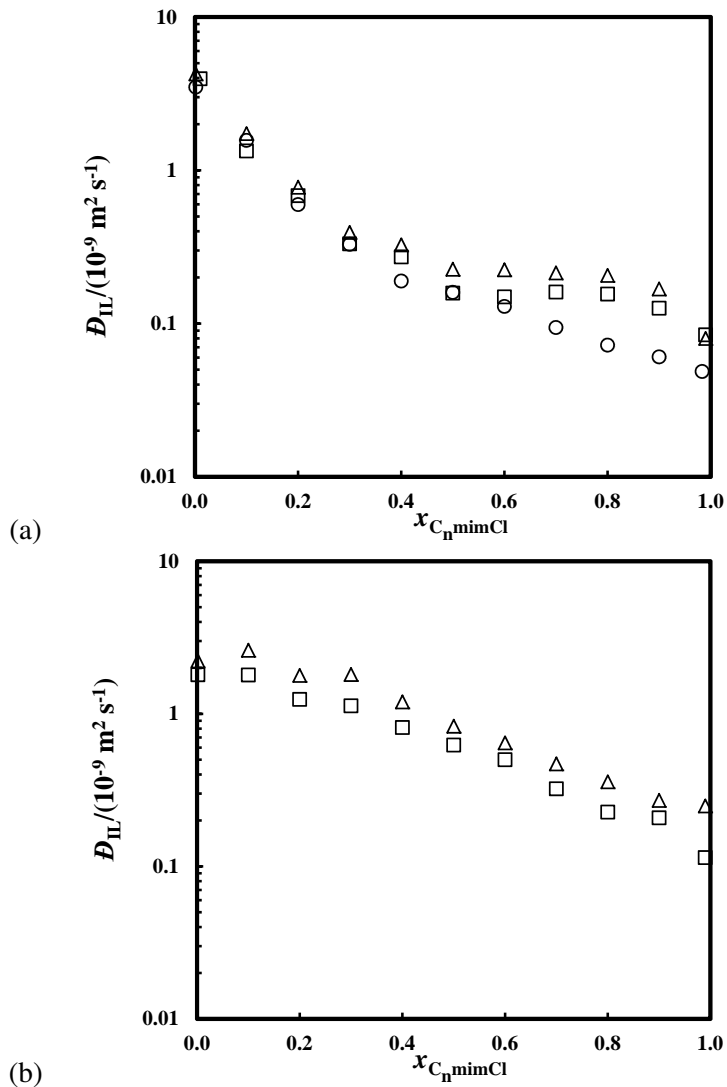


**Figure 5.10:** MS diffusivities of IL molecules in  $C_n \text{ mimCl-H}_2\text{O}$  and  $C_n \text{ mimCl-DMSO}$  mixtures at 368 K, 1 atm. (a)  $\mathcal{D}_{IL}$  in  $C_n \text{ mimCl-H}_2\text{O}$  (b)  $\mathcal{D}_{IL}$  in  $C_n \text{ mimCl-DMSO}$ .



# 6

---

## **Fick Diffusion Coefficients of Liquid Mixtures Directly Obtained from Equilibrium Molecular Dynamics**

---

This chapter is for a large part based on:

X. Liu, S.K. Schnell, J-M, Simon, D. Bedeaux, S. Kjelstrup, A. Bardow and T.J.H. Vlugt, *Fick diffusion coefficients of liquid mixtures directly obtained from equilibrium Molecular Dynamics*, Journal of Physical Chemistry B, **2011**, 115, 12921-12929.

## 6.1 Introduction

Understanding mass transport in liquids by mutual diffusion is an important issue for many applications in chemistry and chemical engineering<sup>21;145</sup>. The reason for this is that diffusion is often the rate limiting step in chemical reactors and separators. To describe mass transport in liquid mixtures, generalized Fick's law and the MS theory are often used. In an  $n$ -component system, generalized Fick's law in a molar reference frame equals<sup>7</sup>

$$J_i = -c_t \sum_{j=1}^{n-1} D_{ij} \nabla x_j, \quad (6.1)$$

in which  $J_i$  is the molar diffusion flux of component  $i$ ,  $c_t$  is the total molar concentration,  $D_{ij}$  are Fick diffusivities, and  $x_j$  is the mole fraction of component  $j$ . The reference frame for the diffusion fluxes is the average molar velocity

$$\sum_{i=1}^n x_i u_i = u_{\text{reference}}, \quad (6.2)$$

in which  $u_i$  is the average velocity of component  $i$ . From this it follows that  $\sum_{i=1}^n J_i = 0$ . Other reference frames, like the barycentric, the mean volume or the solvent frames of reference, are alternatively used depending on their convenience for experimental conditions. We refer to Refs.<sup>1;146</sup> for the transformation rules from one reference frame to the other. For binary mixtures, the resulting Fick diffusion coefficient is the same for all reference frames provided that one uses the gradient of the appropriate concentration in Eq. (6.1)<sup>1</sup>. From Eq. (6.1) it follows directly that the elements of the matrix of Fick diffusivities  $[D]$  depend on the labeling of the components.

Some problems arise when applying generalized Fick's law: (1) Fick diffusivities strongly depend on the concentration, and in multicomponent systems, they can be either positive or negative<sup>21</sup>; (2) multicomponent Fick diffusivities are unrelated to their binary counterparts which seriously hinders their prediction; (3) generalized Fick's laws is difficult to handle in practice due to the large number of concentration dependent coefficients, *i.e.* in an  $n$ -component system,  $(n-1)^2$  diffusion coefficients are needed for the mass transport description. However, it is important to understand the concentration dependence of Fick diffusivities as they directly relate to the mea-

asurable quantities, *i.e.* concentrations, and thus can be accessed in experiments. In fact, all mutual diffusion experiments measure Fick diffusion coefficients.

For modeling multicomponent diffusion in liquids, the MS approach is often more convenient<sup>1;21;146</sup>. The key point of this approach is that the driving force for diffusion of component  $i$  (*i.e.* the chemical potential gradient  $\nabla\mu_i$ ) is balanced by a friction force, resulting in the following equation,

$$-\frac{1}{RT}\nabla\mu_i = \sum_{j=1, j \neq i}^n \frac{x_j(u_i - u_j)}{\mathcal{D}_{ij}}, \quad (6.3)$$

in which  $R$  and  $T$  are the gas constant and absolute temperature, respectively. The friction force between components  $i$  and  $j$  is proportional to the difference in average velocities of the components,  $(u_i - u_j)$ . The MS diffusivity  $\mathcal{D}_{ij}$  is an inverse friction coefficient describing the magnitude of the friction between components  $i$  and  $j$ . The MS diffusivities are symmetric,  $\mathcal{D}_{ij} = \mathcal{D}_{ji}$ . Compared to generalized Fick's law, the MS theory requires only  $n(n-1)/2$  diffusion coefficients for an  $n$ -component system and they are all positive<sup>21</sup>. Often, MS diffusivities depend less strongly on the concentration than Fick diffusivities<sup>21</sup>. It is impossible to obtain MS diffusivities directly from experiments as chemical potentials cannot be measured directly. Obtaining MS diffusivities from MD simulations is possible but requires large amounts of CPU time<sup>9;23;33-35;41-45;92;147</sup>.

As generalized Fick's law and the MS theory describe the same physical process, it is possible to relate the corresponding transport coefficients<sup>1;21;23</sup>. The corresponding equation to relate the coefficients in Eqs. (6.1) and (6.3) is

$$[D] = [B]^{-1}[\Gamma], \quad (6.4)$$

in which  $[D]$  is the  $(n-1) \times (n-1)$  matrix of Fick diffusivities. The elements of the matrix  $[B]$  are given by<sup>1;7;23</sup>

$$B_{ii} = \frac{x_i}{\mathcal{D}_{in}} + \sum_{j=1, j \neq i}^n \frac{x_j}{\mathcal{D}_{ij}} \quad \text{with } i = 1, \dots, (n-1) \quad (6.5)$$

$$B_{ij} = -x_i \left( \frac{1}{\mathcal{D}_{ij}} - \frac{1}{\mathcal{D}_{in}} \right) \quad \text{with } i, j = 1, \dots, (n-1) \text{ and } i \neq j. \quad (6.6)$$

The elements of the so-called matrix of thermodynamic factors  $[\Gamma]$  are defined by<sup>1,21</sup>

$$\Gamma_{ij} = \delta_{ij} + x_i \left( \frac{\partial \ln \gamma_i}{\partial x_j} \right)_{T,p,\Sigma}, \quad (6.7)$$

in which  $\delta_{ij}$  is the Kronecker delta, and  $\gamma_i$  is the activity coefficient of component  $i$ . The symbol  $\Sigma$  indicates that the partial differentiation of  $\ln \gamma_i$  with respect to mole fraction  $x_j$  is carried out at constant mole fraction of all other components except the  $n$ -th one, so that  $\sum_{i=1}^n x_i = 1$  during the differentiation. The constrained derivative of Eq. (6.7) can be written as a function of unconstrained derivatives as follows:

$$\left. \frac{\partial \ln \gamma_i}{\partial x_j} \right|_{T,p,\Sigma} = \left. \frac{\partial \ln \gamma_i}{\partial x_j} \right|_{T,p,j'} - \left. \frac{\partial \ln \gamma_i}{\partial x_n} \right|_{T,p,n'}. \quad (6.8)$$

Here, the primed symbols in the derivative evaluations indicate that the mole fractions of all other components are held constant. For any system in the limit of infinite dilution, the values of  $[\Gamma]$  are known, *i.e.*  $\Gamma_{ii}^{x_i \rightarrow 0} = 1$  and  $\Gamma_{ij,i \neq j}^{x_i \rightarrow 0} = 0$ . In binary mixtures, transport diffusion is described by a single MS and a single Fick diffusion coefficient. The following notation is used to relate these diffusivities

$$D = \Gamma \times \mathcal{D}_{12}, \quad (6.9)$$

in which  $D$  is the binary Fick diffusivity,  $\mathcal{D}_{12}$  is the MS diffusivity and  $\Gamma$  is the thermodynamic factor given by<sup>1</sup>

$$\Gamma = 1 + x_1 \left( \frac{\partial \ln \gamma_1}{\partial x_1} \right)_{T,p,\Sigma}. \quad (6.10)$$

Eq. (6.9) nicely visualizes the gap between experimental and molecular simulation approaches to mutual diffusion. In experiments, Fick diffusion coefficients are measured and molecular simulation usually provides MS diffusivities<sup>33;38;47;63;148</sup>. The two formalisms are related via the matrix of thermodynamic factor  $[\Gamma]$  but this is usually known only with relatively large uncertainties<sup>62;149</sup>. To obtain the matrix of thermodynamic factors, experimental vapor-liquid equilibrium data can be fitted using excess Gibbs energy models, *e.g.* Margules, van Laar, NRTL *etc.*<sup>2</sup>. Several models may provide estimates of  $\ln \gamma_i$  that give equally good fits to the vapor-liquid



equilibrium (VLE) data. However, the thermodynamic factor  $\Gamma_{ij}$  involves the first derivative of the activity coefficient  $\ln\gamma_i$  with respect to the composition. Errors of the size of 20% and larger are expected for this derivative<sup>80</sup>.

Currently used approaches for computing Fick diffusivities from molecular simulation suffer from inconsistencies or other problems:

- Direct calculation of Fick diffusivities using non-equilibrium MD (NEMD) requires very large concentration gradients<sup>30–32</sup>. This approach is usually not accurate and quite impractical as the concentration dependence of Fick diffusivities is not easily captured.
- Combining MS diffusivities obtained from equilibrium MD simulations with experimentally obtained equations of state or models for the excess Gibbs energy is inconsistent, as experiments and molecular models provide different values for the thermodynamic factor<sup>63;150;151</sup>.
- Currently used molecular simulation techniques to determine the thermodynamic factor of liquid mixtures are quite inefficient<sup>47;48</sup>. To the best of our knowledge, these techniques have only been applied to binary mixtures.

In this chapter, we introduce a consistent and efficient framework for the determination of Fick diffusivities in liquid mixtures directly from equilibrium MD simulations by calculating both the thermodynamic factor  $\Gamma$  and the MS diffusivity  $D_{12}$ . Up to now, approaches to compute Fick diffusivities from molecular simulation suffer from inconsistencies or other problems: (1) direct calculation of Fick diffusivities using NEMD requires significant efforts and very high concentration gradients<sup>30–32</sup>. This approach is usually not accurate and quite impractical as the concentration dependence of Fick diffusivities is not easily captured; (2) combining MS diffusivities obtained from equilibrium MD simulations with experimentally obtained equations of state or models for the excess Gibbs energy is inconsistent as experiments and molecular models in principle provide different values for the thermodynamic factor<sup>63;150;151</sup>; (3) presently used molecular simulation techniques to determine the thermodynamic factor of liquid mixtures are inefficient<sup>47;48</sup>. Recently, we developed an efficient method to obtain thermodynamic factor directly from equilibrium MD simulations<sup>48;49</sup>. This method is based on sampling concentration fluctuations inside small subvolumes inside the simulation box and correcting for finite-size effects.

We already validated this method for simple systems with only a single interaction site per molecule, *i.e.* mixtures in which the components interact using WCA or LJ interaction potentials. In this work, we implemented the method for more complex mixtures of acetone - methanol and acetone - tetrachloromethane ( $\text{CCl}_4$ ). Thereby, we can efficiently compute  $\Gamma$  such that in combination with computed MS diffusivities, we are able to compute Fick diffusion coefficients directly from equilibrium MD. Our MD results for  $\Gamma$ ,  $D_{12}$ , and  $D$  also agree very well quantitatively with the experiments suggesting that the tools for computing multicomponent Fick diffusivities efficiently from MD simulations are now available.

## 6.2 Diffusion coefficients and the thermodynamic factor

### 6.2.1 Obtaining diffusion coefficients from MD simulations

In equilibrium MD simulations, representative trajectories of a liquid mixture consisting of interacting molecules are obtained<sup>17;18;20</sup>. From the trajectory of the molecules, transport properties can be computed<sup>17</sup>. For more details on computing MS- and self diffusivities, we refer the reader to section 2.3 and appendix A.

### 6.2.2 Predictive models for diffusion

To obtain a better understanding of the concentration dependence of MS diffusivities, it is instructive to study the different contributions of the correlation function in Eq. (2.21), *i.e.* velocity auto- and cross-correlations. These contributions are defined as follows. Considering the Green-Kubo form of the Onsager coefficients (Eq. (2.21)), we can express  $\Lambda_{ii}$  as

$$\begin{aligned}
\Lambda_{ii} &= \frac{1}{3N} \int_0^\infty dt' \left\langle \sum_{l=1}^{N_i} v_{l,i}(t) \cdot \sum_{g=1}^{N_i} v_{g,i}(t+t') \right\rangle \\
&= \frac{1}{3N} \int_0^\infty dt' \left\langle \sum_{l=1}^{N_i} v_{l,i}(t) \cdot v_{l,i}(t+t') \right\rangle + \\
&\quad \frac{1}{3N} \int_0^\infty dt' \left\langle \sum_{l=1}^{N_i} \sum_{g=1, g \neq l}^{N_i} v_{l,i}(t) \cdot v_{g,i}(t+t') \right\rangle \\
&\approx x_i C_{ii} + x_i^2 N C_{ii}^* \\
&= x_i D_{i,\text{self}} + x_i^2 N C_{ii}^*, \tag{6.11}
\end{aligned}$$

in which  $C_{ii}$  and  $C_{ii}^*$  account for self- and cross-correlations of the velocities of molecules of component  $i$ , respectively. Here, we assumed that  $N_i^2 - N_i \approx N_i^2$ . For  $\Lambda_{ij}$  with  $i \neq j$ , *i.e.* the correlations between unlike molecules, we can write<sup>34</sup>

$$\begin{aligned}
\Lambda_{ij} &= \frac{1}{3N} \int_0^\infty dt' \left\langle \sum_{l=1}^{N_i} v_{l,i}(t) \cdot \sum_{k=1}^{N_j} v_{k,j}(t+t') \right\rangle \\
&\approx \frac{N_i N_j}{3N} \int_0^\infty dt' \langle v_{1,i}(t) \cdot v_{1,j}(t+t') \rangle \\
&= N x_i x_j C_{ij}. \tag{6.12}
\end{aligned}$$

For a binary system, combining Eqs. (2.19), (A.1), (6.11) and (6.12) leads to

$$\begin{aligned}
D_{12} &= x_2 C_{11} + x_1 C_{22} + x_1 x_2 N (C_{11}^* + C_{22}^* - 2C_{12}) \\
&= x_2 D_{1,\text{self}} + x_1 D_{2,\text{self}} + x_1 x_2 N (C_{11}^* + C_{22}^* - 2C_{12}). \tag{6.13}
\end{aligned}$$

In so-called ideal diffusing mixtures, the terms  $C_{ii}^*$  and  $C_{ij}$  are small compared to terms of the type  $C_{ii}$  resulting in the well-known binary Darken equation, see also appendix B and Refs.<sup>35;54;92</sup>:

$$D_{ij} = x_j D_{i,\text{self}} + x_i D_{j,\text{self}}. \tag{6.14}$$

A natural extension of Eq. (6.14) to multicomponent systems was presented in

chapter 4. It is important to note that the application of the Darken equation relies on the availability of self-diffusivities in the mixture. To parametrize the Darken equation, we proposed the following model to predict self-diffusivities in multicomponent systems from data at infinite dilution as discussed earlier in chapter 4:

$$\frac{1}{D_{i,\text{self}}} = \sum_{j=1}^n \frac{x_j}{D_{i,\text{self}}^{x_j \rightarrow 1}}. \quad (6.15)$$

We have shown in chapter 4 that Eq. (6.15) works well for WCA fluids and the ternary mixture n-hexane/toluene/cyclohexane.

### 6.2.3 Obtaining the thermodynamic factor from MD simulations

The elements of the matrix  $[\Gamma]$  can be expressed as average concentration fluctuations in the grand-canonical ensemble as derived by Kirkwood and Buff<sup>152;153</sup> in 1951. The natural method for obtaining these averages are grand-canonical Monte Carlo (GCMC) simulations. However, GCMC simulations of liquid mixtures at room temperature are very challenging as the insertion and deletion of molecules is very inefficient for dense liquids<sup>17</sup>. There is some recent improvement in this area<sup>154;155</sup> but these simulations remain quite inefficient. Kirkwood and Buff showed that in the thermodynamic limit the fluctuations in the grand-canonical ensemble can be related to the integrals of radial distribution functions over volume<sup>152;153</sup>, resulting in the following expression for the so-called Kirkwood-Buff (KB) coefficients:

$$G_{ij} = V \frac{\langle N_i N_j \rangle - \langle N_i \rangle \langle N_j \rangle}{\langle N_i \rangle \langle N_j \rangle} - \frac{\delta_{ij}}{c_i} \quad (6.16)$$

$$= 4\pi \int_0^\infty [g_{ij}(r) - 1] r^2 dr. \quad (6.17)$$

In these equations,  $V$  is the volume and  $c_i$  is the number density of component  $i$  defined by  $\langle N_i \rangle / V$ . The brackets  $\langle \dots \rangle$  denote an ensemble average in the grand-canonical ensemble.  $g_{ij}(r)$  is the radial distribution function for molecules of type  $i$  and  $j$  in the grand-canonical ensemble, and it is natural to define the distance  $r$  between two molecules as the distance between their centers of mass. As the choice of ensemble is irrelevant for large systems, in practice  $g_{ij}(r)$  is computed in the  $NpT$

or  $NVT$  ensemble. In binary mixtures, the thermodynamic factor  $\Gamma$  is related to the KB coefficients  $G_{ij}$  by<sup>152;153</sup>

$$\Gamma = 1 - x_i \frac{c_j (G_{ii} + G_{jj} - 2G_{ij})}{1 + c_j x_i (G_{ii} + G_{jj} - 2G_{ij})}. \quad (6.18)$$

For ternary systems, the values of the terms  $\Gamma_{ij}$  (Eq. (6.7)) follow in a similar way from the values of the KB coefficients  $G_{ij}$ , see Refs.<sup>93;156</sup> and also chapter 7.

It is important to consider the convergence of the integrals in Eq. (6.17). For infinitely large systems,  $g_{ij}(r) \rightarrow 1$  for  $r \rightarrow \infty$ . For finite systems with periodic boundary conditions,  $g_{ij}(r)$  does not converge to 1 for large  $r$  and therefore corrections have to be taken into account in practice<sup>48;49;157</sup>. This seriously hinders the direct estimation of KB coefficients from simulations.

Recently, we found that the average particle fluctuations in Eq. (6.16) can also be calculated by considering a large system in which smaller subvolumes are embedded. The subvolumes can exchange particles and energy with the large simulation box and therefore a subvolume can be considered as a system in the grand-canonical ensemble. However, corrections should be taken due to the finite size effect originating from the boundaries of the subvolumes<sup>48;49</sup>:

$$G_{ij}(L) = G_{ij}^{\infty} + \frac{(\text{constant})}{L}. \quad (6.19)$$

In this equation,  $L$  is the (linear) size of the subsystem in one dimension. The KB coefficient in the thermodynamic limit ( $G_{ij}^{\infty}$ ) can thus be obtained by simple extrapolation to  $L \rightarrow \infty$ . This approach was previously validated for molecules with a single interaction site only, *e.g.* systems in which the particle interact using a WCA or LJ potential<sup>48;49</sup>. In practice, the size of the simulation box needs to be at least 10 times the size of a typical molecule in the system<sup>48</sup>. For more details concerning this method, we refer the reader to Refs.<sup>48;49;158</sup>.

### 6.3 Simulation details

The binary systems acetone - methanol and acetone -  $\text{CCl}_4$  were studied. The OPLS force field was used for acetone and methanol<sup>159;160</sup> and a five-site model was used for  $\text{CCl}_4$ <sup>159</sup>. All components are treated as rigid bodies. The LJ potentials describe

**Table 6.1:** Force field and geometrical parameters for acetone, methanol and CCl<sub>4</sub>. Parameters for acetone and CCl<sub>4</sub> were taken from Ref<sup>159</sup>. Parameters for methanol were taken from Ref.<sup>160</sup>

Force field parameters				
site		$\sigma/\text{\AA}$	$(\epsilon/k_B)/\text{K}$	$q/e$
CH <sub>3</sub>	(acetone)	3.910	81.0866	0.0620
C	(acetone)	3.750	52.9463	0.3000
O	(acetone)	2.960	105.8997	-0.4240
C	(CCl <sub>4</sub> )	3.410	50.3972	-0.1616
Cl	(CCl <sub>4</sub> )	3.450	143.6321	0.0404
O	(methanol)	3.070	85.6753	-0.7000
H	(methanol)	-	-	0.4350
CH <sub>3</sub>	(methanol)	3.775	104.3223	0.2650

Standard geometrical parameters			
bond length/ $\text{\AA}$		bond angle/deg	
C-Cl	1.766	CH <sub>3</sub> -C-CH <sub>3</sub>	116.30
C=O	1.220	CH <sub>3</sub> -C=O	121.86
CH <sub>3</sub> -C	1.507	Cl-C-Cl	109.47
O-H	0.945	CH <sub>3</sub> -O-H	108.50
CH <sub>3</sub> -O	1.430		

the intermolecular non-bonded interactions which are truncated and shifted at 10 Å. The Lorentz-Berthelot mixing rules are applied to obtain the LJ parameters for the interaction of unlike atoms<sup>18</sup>. Electrostatic interactions are handled by Ewald summation using a relative precision<sup>85</sup> of  $10^{-5}$ . The force field parameters as well as the parameters defining the geometries of the molecules are listed in Table 6.1. Three dimensional periodic boundary conditions consistent with a cubic box were applied to obtain properties corresponding to bulk systems. The MD simulations were carried out at a temperature of 298 K and a pressure of 1 atm. All binary systems were first equilibrated in an  $NpT$  ensemble with a Nosé-Hoover thermostat and barostat using the time constants of 0.1 ps and 1 ps, respectively. The equations of motion were integrated using the leapfrog Verlet algorithm with a time step of 1 fs. The self- and MS diffusion coefficients are obtained from equilibrium MD simulations in the  $NVT$  ensemble using the Nosé-Hoover thermostat at a density corresponding to a pressure of 1 atm.<sup>17</sup> The box sizes were typically around  $(28 \text{ Å})^3$  resulting in a total number of molecules of the order of 300. The simulations for extracting diffusion coefficients were run for at least 100 ns to obtain MS diffusivities with an accuracy of around 5% and self-diffusivities with an accuracy of 2%. KB coefficients required for the calculation of thermodynamic factors were obtained from MD simulations in the  $NpT$  ensemble. Temperature and pressure were controlled using the Nosé-Hoover thermostat and barostat, respectively. In these simulations, the box size needs to be larger, see also section 6.2.3. The volume of the simulation box was typically fluctuating around  $(80 \text{ Å})^3$ . The maximum number of molecules used in these simulations was 8000. Simulation runs of at least 5 ns were needed to obtain accurate values of the thermodynamic correction factor.

## 6.4 Results and discussion

### 6.4.1 Model validation for pure component systems

In Table 6.2, we compare the computed densities and self-diffusivities of pure components to the experimental results. For all three components, MD simulations underestimate the densities of pure components by a maximal deviation of 3%. This directly results in an small overestimation of self-diffusivities in most cases, *i.e.* for pure methanol and pure  $\text{CCl}_4$ . The computed self-diffusivities of pure acetone, pure

**Table 6.2:** Densities and self-diffusivities of pure acetone, methanol and CCl<sub>4</sub> at 298 K, 1 atm.

Component	$\rho/(\text{g}\cdot\text{ml}^{-1})$		$D_{i,\text{self}}/(10^{-9}\text{m}^2\text{s}^{-1})$	
	This work (MD)	Experiment	This work (MD)	Experiment
acetone	0.76	0.78 <sup>a,b</sup> , 0.79 <sup>c</sup>	4.2	4.8 <sup>d</sup> , 4.4 <sup>e</sup>
methanol	0.75	0.79 <sup>a,b</sup>	2.5	2.3 <sup>f</sup> , 2.2 <sup>g</sup>
CCl <sub>4</sub>	1.54	1.58 <sup>c</sup>	1.8	1.5 <sup>d</sup>

<sup>a</sup> Experiments by Campbell *et al.*, Ref. <sup>161</sup>

<sup>b</sup> Experiments by Noda *et al.*, Ref. <sup>162</sup>

<sup>c</sup> Experiments reported in Ref. <sup>163</sup>

<sup>d</sup> Experiments by Hardt *et al.*, Ref. <sup>164</sup>

<sup>e</sup> Experiments by Toryanik *et al.*, Ref. <sup>165</sup>

<sup>f</sup> Experiments by Kamei *et al.*, Ref. <sup>166</sup>

<sup>g</sup> Experiments by Derlacki *et al.*, Ref. <sup>167</sup>

methanol and pure CCl<sub>4</sub> are 4.2, 2.5, and  $1.8 \cdot 10^{-9} \text{ m}^2\text{s}^{-1}$ , respectively. Several values for the experimental self-diffusivity of pure acetone are available ranging from 4.4 to  $4.8 \cdot 10^{-9} \text{ m}^2\text{s}^{-1}$  <sup>164;165</sup>. For pure methanol, experimental self-diffusivities reported in literature range from 2.2 to  $2.3 \cdot 10^{-9} \text{ m}^2\text{s}^{-1}$  <sup>166;167</sup>. The reported experimental self-diffusivity of pure CCl<sub>4</sub> is  $1.5 \cdot 10^{-9} \text{ m}^2\text{s}^{-1}$  <sup>164;166</sup>. The maximal deviation of computed self-diffusivities from experiments is thus 20%. We feel that this level of deviation between experiments and simulations is acceptable in our study. Noteworthy, the force fields used have not been fitted to transport properties. Thus, the presented results are predictive.

In this chapter, we studied diffusion in two binary systems, acetone - methanol and acetone - tetrachloromethane. The binary system methanol-tetrachloromethane was not studied in detail as this system shows a liquid-liquid separation <sup>168</sup>, which may introduce difficulties in the simulations.

## 6.4.2 Diffusion in acetone - methanol

Figure 6.1 compares the computed densities of acetone - methanol mixtures to the experimental data at 298 K, 1 atm. It is shown that the computed mixture densities from this work are consistent with the data obtained by Perera *et al.* using MD



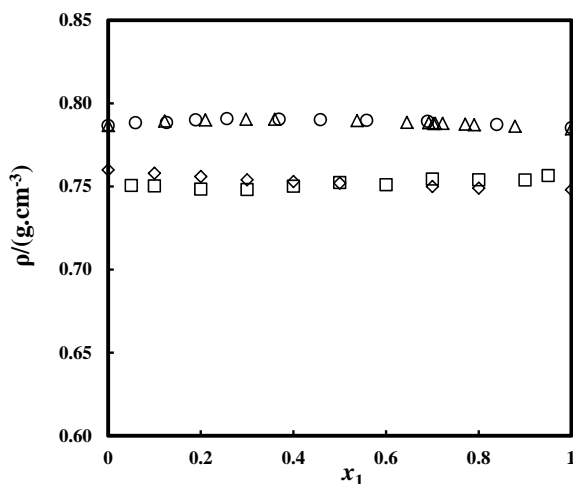


**Figure 6.1:** Densities of acetone (1) - methanol (2) mixtures at 298 K, 1 atm. Squares are the computed densities by this work using MD simulations. Diamonds are the computed densities by Perera *et al.* using MD simulations<sup>157</sup>. Circles are the experimental densities measured by Campbell *et al.*<sup>161</sup>. Triangles are the experimental densities measured by Noda *et al.*<sup>162</sup>.

simulations<sup>157</sup>. However, the results obtained from simulations are systematically somewhat lower than the experimental densities<sup>161;162</sup>. In acetone - methanol mixtures, both experiments and simulations show that densities are not sensitive to the composition.

Figure 6.2 shows how the thermodynamic factor varies with concentration. The computed  $\Gamma$  is less than unity suggesting a positive deviation from Raoult's law. That is, as the concentration of component 1 increasing, the activity coefficient of component 1 decreases suggesting that the attraction of acetone - acetone is stronger than that of acetone - methanol<sup>2</sup>. We observe that both the computed  $\Gamma$  in this work and the computations by Perera *et al.*<sup>157</sup> agree very well with experiments. Note that the data of Perera *et al.*<sup>157</sup> seems to have an inflection point around equimolar composition, which appears to be unphysical and due to limited accuracy in their simulations. The dependence of  $\Gamma$  on concentration is accurately described by our simulations. It is important to note that there are obvious differences between our simulations and those of Perera *et al.*. Perera *et al.*<sup>157</sup> obtained the KB coefficients by directly integrating the radial distribution functions over the volume (Eq. (6.17)), while we

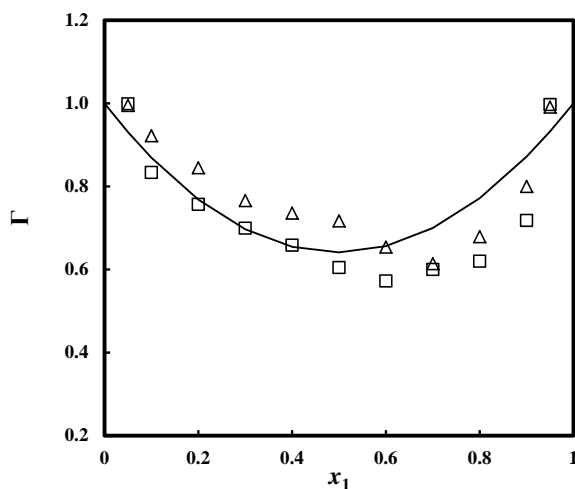
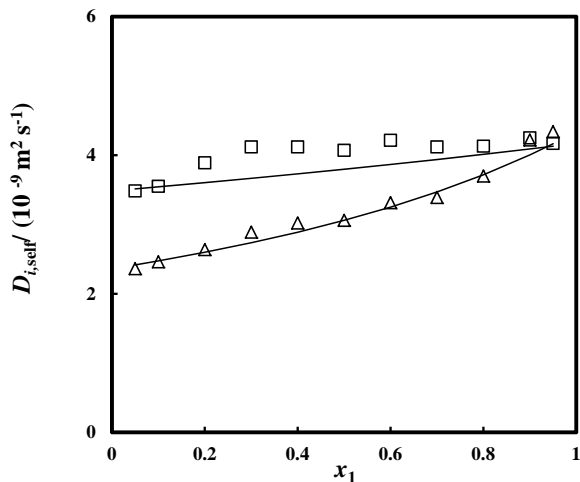


**Figure 6.2:** Thermodynamic factor  $\Gamma$  (Eq. (6.10)) in acetone (1) - methanol (2) mixtures at 298 K, 1 atm. Squares are the computed  $\Gamma$  by this work using MD simulations. Triangles are the computed  $\Gamma$  by Perera *et al.* using MD simulations<sup>157</sup>. The solid line represents  $\Gamma$  calculated from the NRTL model and fitted to experimental VLE data taken from Ref.<sup>168</sup>. Fitted parameters of the NRTL model are:  $\tau_{12} = 0.34$ ;  $\tau_{21} = 0.40$ ;  $\alpha = 0.15$ <sup>50</sup>.

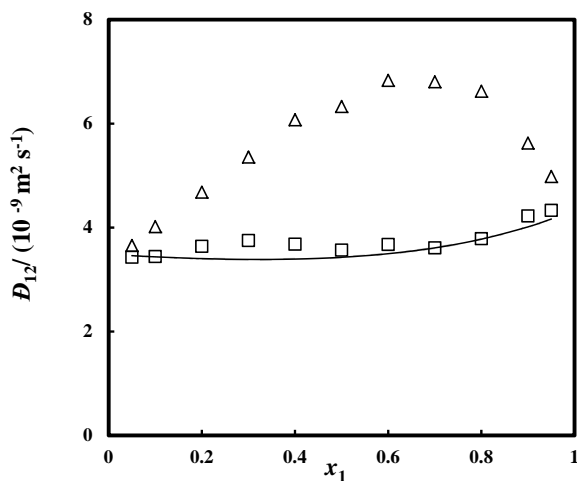
used the novel fluctuation method described in section 6.2.3. The agreement between the two methods clearly shows that macroscopic properties can be extrapolated from microscopic systems by applying finite-size corrections. The proposed fluctuation method is therefore not only valid in simple systems, *e.g.* WCA systems and homogeneous LJ systems. The presented results also show that it also works well for complicated molecular systems in which electrostatic interactions plays an important role.

Figure 6.3 shows self-diffusivities in acetone - methanol mixtures as a function of the composition. We are not aware of any experimental results for the self-diffusivities in acetone - methanol mixtures. To describe the dependence of self-diffusivities on concentration, Eq. (6.15) is used. The self-diffusivities at infinite dilution are required for this. Figure 6.3 clearly shows that Eq. (6.15) correctly captures the behavior of the self-diffusivities, *i.e.* as the concentration of acetone is increasing, the self-diffusivities of both components increase and the self-diffusivities of methanol show a stronger dependence on concentration.

Figure 6.4 compares the computed MS diffusivities using MD simulations (Eq.



**Figure 6.3:** Self-diffusivities in acetone (1) - methanol (2) mixtures at 298 K, 1 atm. Open symbols are the computed self-diffusivities by this work using MD simulations. Squares are the self-diffusivities of acetone (1). Triangles are the self-diffusivities of methanol (2). Solid lines are the predictions using Eq. (6.15).



**Figure 6.4:** MS diffusivities in acetone (1) - methanol (2) mixtures at 298 K, 1 atm. Triangles are the computed MS diffusivities by this work using MD simulations (Eq. (A.1)). Squares are the predictions using the Darken equation (Eq. (6.14)) with the self-diffusivities taken from MD simulations. The solid line represents the predictions using the Darken equation (Eq. (6.14)) with the self-diffusivities predicted using Eq. (6.15).

(A.1)) to the predictions using Darken equation (Eq. (6.14)). The self-diffusivities needed in the Darken equation are parametrized with both MD data and prediction using Eq. (6.15). As Eq. (6.15) accurately describes the dependence of self-diffusivities on concentration, the differences between both parametrization are small. There is, however, a significant difference between the computed MS diffusivities and the predicted MS diffusivities using the Darken equation. In MD simulations, MS diffusivities strongly depend on the concentration and this strong dependence is not captured by the Darken equation. It is important to consider the assumptions made in the derivation of the Darken equation, *i.e.* velocity cross-correlations are assumed to be much smaller than velocity auto-correlations. The deviations between MD simulations and predictions using the Darken equation suggest that this assumption does not hold in acetone - methanol mixtures. In Figure 6.5(a), we plot the intensive terms  $NC_{ii}^*$  and  $NC_{ij}$  (see Eqs. (6.11) and (6.12)) as a function of the concentration. We split the terms in Eq. (6.13) into a velocity auto-correlation part, *i.e.*  $(x_2C_{11} + x_1C_{22})$ , and a velocity cross-correlation part, *i.e.*  $x_1x_2N(C_{11}^* + C_{22}^* - 2C_{12})$ . The values of these two terms are plotted in Figure 6.5(b). When the concentration of one of the components is small, the terms involving velocity cross-correlations are much smaller than those for velocity auto-correlations. The prediction using the binary Darken equation is reasonable in this regime. In more concentrated systems, the terms describing velocity cross-correlations are comparable with those for velocity auto-correlations resulting in the failure of the binary Darken equation. This is mainly due to the strong correlations between distinct molecules of methanol (see the data for  $NC_{11}^*$  in Figure 6.5(a)).

Figure 6.6 shows the Fick diffusivities in acetone - methanol mixtures obtained from different approaches. Computed Fick diffusivities from MD simulations are in excellent agreement with experimental data. Combining the Darken equation with experimental values for the thermodynamic factor clearly results in significant deviations. Although both the thermodynamic factor and the MS diffusivity strongly depend on concentration, these effects cancel to a large degree for the Fick diffusivity.

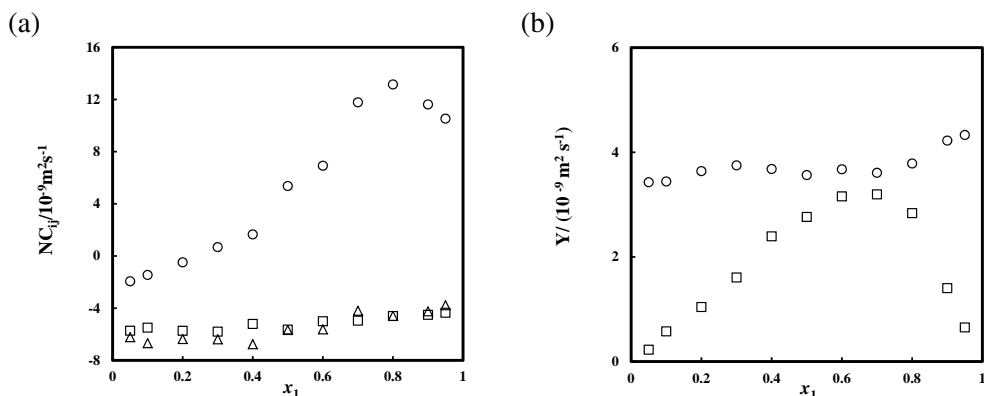


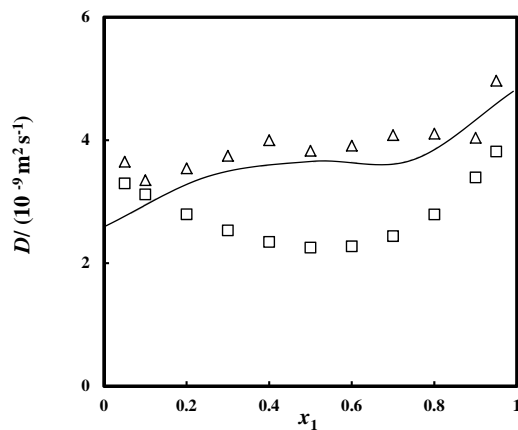
**Figure 6.5:** Velocity cross-correlations (see Eqs. (6.11), (6.12) and (6.13)) in acetone (1) - methanol (2) mixtures at 298 K, 1 atm. (a) Squares represent  $NC_{11}^*$ . Circles represent  $NC_{22}^*$ . Triangles represent  $NC_{12}$ . (b) Circles represent  $x_2 C_{11} + x_1 C_{22}$ . Squares represent  $x_1 x_2 N(C_{11}^* + C_{22}^* + C_{12})$ .

### 6.4.3 Diffusion in acetone - tetrachloromethane

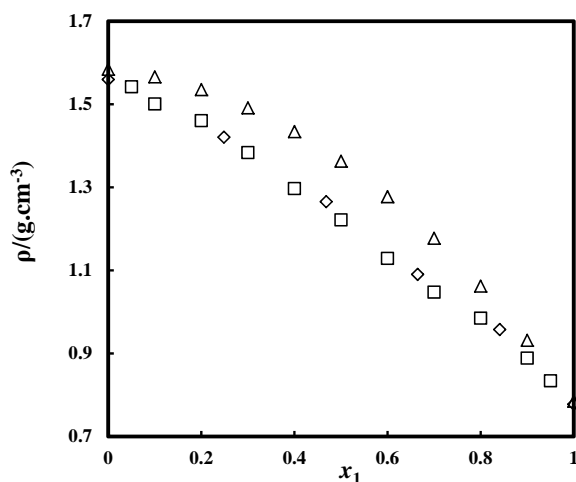
Figure 6.7 compares the densities of acetone -  $\text{CCl}_4$  mixtures at 1 atm. Ref.<sup>163</sup> reported experimental mixture densities at 298 K which are larger than the computed densities in this work. Kumar *et al.* also measured the densities of same mixtures at different temperatures<sup>170</sup>. Their results showed that the mixture densities are not very sensitive to the temperature. It is quite surprising to see such a big jump (ca. 10%) in density when temperature is raised from 298 to 303 K. It is unclear to us whether this effect is real or it is due to an error in the experiments.

Figure 6.8 shows the thermodynamic factor as a function of concentration. Again, an excellent agreement between simulations and experiments is obtained. The computed  $\Gamma$  shows a positive deviation from Raoult's law suggesting that the attraction of acetone - acetone is stronger than that of acetone -  $\text{CCl}_4$ <sup>2</sup>. The non-ideality is most pronounced at a mole fraction of acetone of 0.35. This is observed both in experiments and simulations.

Figure 6.9 compares the self-diffusivities obtained from different approaches. We observed that the computed self-diffusivities moderately increase with increasing concentration of acetone. In contrast, the experimental results show a stronger dependence of the self-diffusivities on concentration. The predictions using Eq. (6.15) agree well with the simulation results.



**Figure 6.6:** Fick diffusivities in acetone (1) - methanol (2) mixtures at 298 K, 1 atm. Triangles represent Fick diffusivities calculated using the computed  $\Gamma$  and MS diffusivities  $D_{12}$  by this work. Squares are the predictions of Fick diffusivities using  $\Gamma$  obtained from experiments<sup>168</sup> and MS diffusivities predicted using the Darken equation (Eq. (6.14)). Self-diffusivities appearing in Darken equation are estimated using Eq. (6.15). The solid line represents the experimental data taken from Ref.<sup>169</sup>.



**Figure 6.7:** Densities of acetone (1) -  $\text{CCl}_4$  (2) mixtures at 1 atm. Squares are the computed densities by this work using MD simulations at 298 K. Triangles are the experimental density taken from Ref.<sup>163</sup> at 298 K. Diamonds are the experimental density measured by Kumar *et al.* at 303 K<sup>170</sup>.

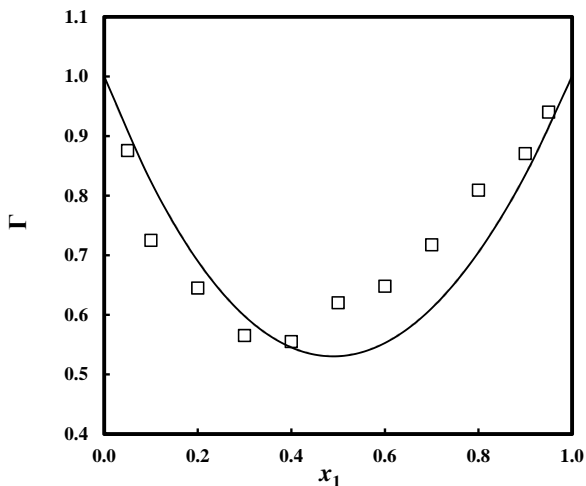


**Figure 6.8:** Thermodynamic factor  $\Gamma$  in acetone (1) -  $\text{CCl}_4$  (2) mixtures at 298 K, 1 atm. Squares are the computed  $\Gamma$  by this work using MD simulations. The solid line is  $\Gamma$  calculated from the NRTL model and fitted to experimental VLE data taken from Ref. <sup>168</sup>. Fitted parameters of the NRTL model are:  $\tau_{12} = 0.43$ ;  $\tau_{21} = 0.57$ ;  $\alpha = 0.21$  <sup>50</sup>.

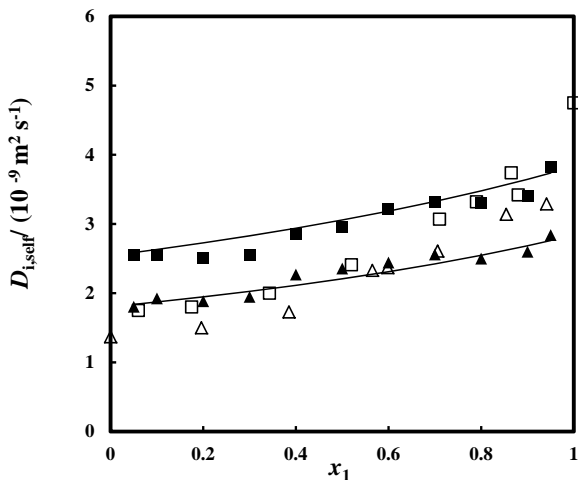


**Figure 6.9:** Self-diffusivities in acetone (1) -  $\text{CCl}_4$  (2) mixtures at 298 K, 1 atm. Filled symbols are the computed diffusivities by this work using MD simulations. Open symbols are the experimental results taken from Ref. <sup>164</sup>. Squares are the self-diffusivities of acetone (1). Triangles are the self-diffusivities of  $\text{CCl}_4$  (2). Solid lines are the predictions using Eq. (6.15).

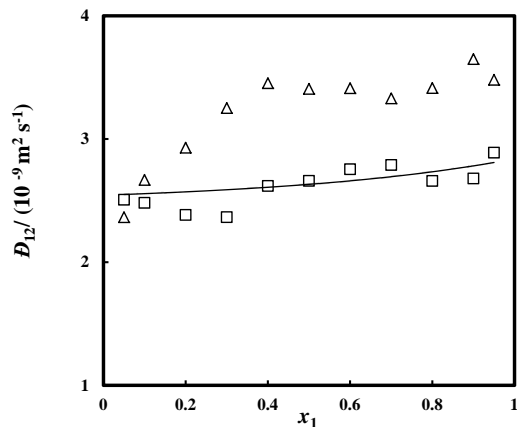


**Figure 6.10:** MS diffusivities in acetone (1) -  $\text{CCl}_4$  (2) mixtures at 298 K, 1 atm. Triangles are the computed MS diffusivities by this work using MD simulations (Eq. (A.1)). Squares are the predictions using the Darken equation with the self-diffusivities computed from MD simulations. The solid line represents the predictions using Darken equation (Eq. (6.14)) with the self-diffusivities estimated by Eq. (6.15).

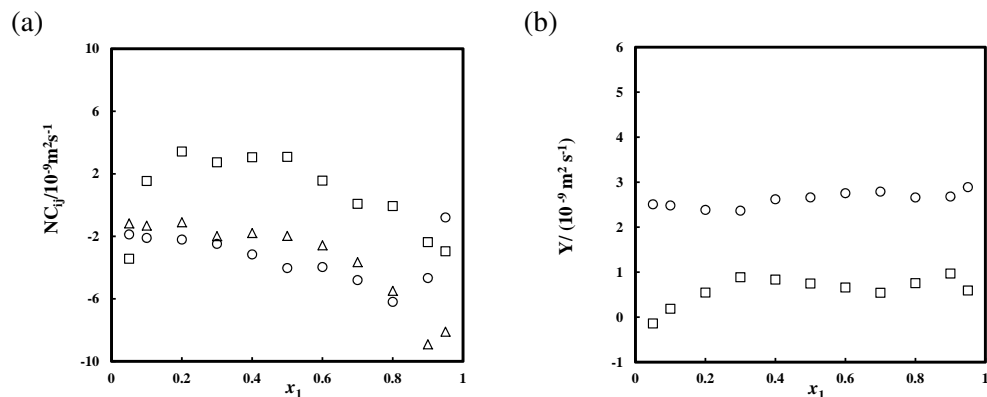


**Figure 6.11:** Velocity cross-correlations (see Eqs. (6.11), (6.12) and (6.13)) in acetone (1) -  $\text{CCl}_4$  (2) mixtures at 298 K, 1 atm. (a) Squares represent  $NC_{11}^*$ . Circles represent  $NC_{22}^*$ . Triangles represent  $NC_{12}$ . (b) Circles represent  $x_2C_{11} + x_1C_{22}$ . Squares represent  $x_1x_2N(C_{11}^* + C_{22}^* + C_{12})$ .



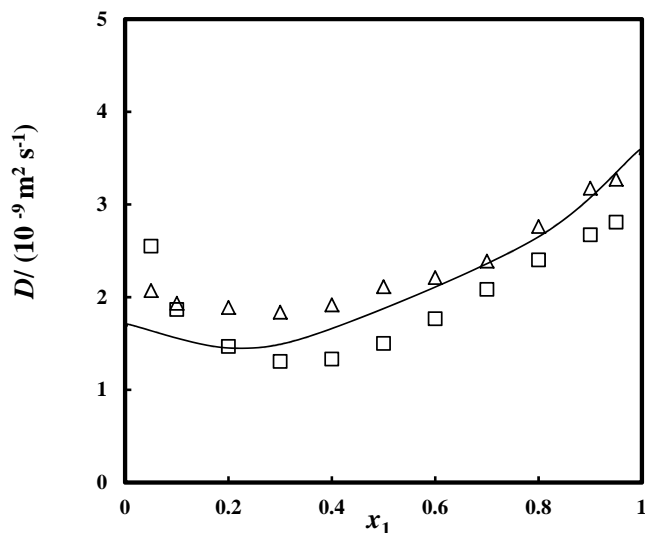


**Figure 6.12:** Fick diffusivities in acetone (1) -  $\text{CCl}_4$  (2) mixtures at 298 K, 1 atm. Triangles represent Fick diffusivities calculated using the computed  $\Gamma$  and MS diffusivities  $\mathcal{D}_{12}$  in this work. Squares are the predictions of Fick diffusivities using  $\Gamma$  obtained from experiments<sup>168</sup> and MS diffusivities predicted using the Darken equation (Eq. (6.14)). Self-diffusivities appearing in the Darken equation are estimated using Eq. (6.15). Solid line represents the experimental data taken from Ref.<sup>171</sup>.

Figure 6.10 shows the computed and predicted MS diffusivities. The Darken equation suggests an almost linear relation between MS diffusivities and mole fraction while the computed MS diffusivities do not show this behavior. In Figure 6.11, we plot the values of the velocity cross-correlations and velocity auto-correlations as a function of the concentration, (see Eqs. (6.11), (6.12) and (6.13)). The contributions of velocity cross-correlations in acetone -  $\text{CCl}_4$  mixtures are smaller than those in acetone - methanol mixtures. This may suggest that Darken equation works better in acetone -  $\text{CCl}_4$  mixtures, see Figures 6.4 and 6.10. Figure 6.11(a) also shows that the terms  $C_{11}^*$ ,  $C_{22}^*$  and  $C_{12}$  are all of the same order of magnitude.

Using the thermodynamic factor  $\Gamma$  and MS diffusivities  $\mathcal{D}_{ij}$  shown in Figures 6.8 and 6.10, we calculated Fick diffusivities as a function of concentration, see Figure 6.12. Again, an excellent agreement between the computed Fick diffusivities from equilibrium MD simulations and the ones reported by experimental work is obtained. The comparison of Fick diffusivities in Figure 6.12 clearly shows that from equilibrium MD simulation we can quantitatively predict Fick diffusivities in a consistent way. As velocity cross-correlations are relatively small for this system, the predicted Fick diffusivities using the Darken equation and Eqs. (6.9) and (6.15) are in reasonable agreement with the experimental results. However, this agreement cannot be expected in general as the level of agreement strongly depends on the quality of the predictive model for MS diffusivities (here: the binary Darken equation). Indeed, predictive models may not work well (or even significantly fail) in systems in which molecules are highly associated<sup>34,91</sup>.

## 6.5 Conclusions

We presented a method to compute Fick diffusivities from MD simulations. The key ingredient of this approach is the application of a novel method to extract the thermodynamic factor from MD. The described approach was tested for two binary systems, acetone - methanol and acetone -  $\text{CCl}_4$ . Excellent agreement between molecular simulation and experimental results were found for Fick- and MS diffusivities, as well as the thermodynamic factor. The binary Darken equation is not applicable to these systems as velocity cross-correlations have a large effect on the computed Onsager coefficients. Our approach is in principle directly applicable to obtain Fick diffusivities from simulations for multicomponent systems ( $n \geq 3$ ).

# 7

---

## Fick Diffusion Coefficients in Ternary Liquid Systems from Equilibrium Molecular Dynamics Simulation

---

This chapter is for a large part based on:

X. Liu, A. Martín-Calvo, E. McGarrity, S.K. Schnell, S. Calero, J-M, Simon, D. Bedeaux, S. Kjelstrup, A. Bardow and T.J.H. Vlugt, *Fick diffusion coefficients in ternary liquid systems from equilibrium Molecular Dynamics simulations*, *Industrial & Engineering Chemistry Research*, **2012**, 51, 10247-10258.

## 7.1 Introduction

In chapter 6, we developed a consistent methodology to calculate binary Fick diffusivities using MS diffusivities  $\mathcal{D}_{ij}$  and thermodynamic factors  $[\Gamma]$  from equilibrium MD simulations<sup>172;173</sup>. Thermodynamic factors can be computed by studying density fluctuations in small subvolumes inside a larger simulation box and correcting for finite-size effects<sup>48;49</sup>. This approach was validated for the binary systems acetone - methanol and acetone - tetrachloromethane in chapter 6<sup>172;173</sup>. In these simulations, all molecules were treated as rigid bodies interacting through LJ and electrostatic interactions. Our MD results for these systems quantitatively agree with the experimental data for binary Fick diffusion coefficients  $D$  as well for the thermodynamic factor  $\Gamma$ <sup>172;173</sup>. Our approach thus bridges the gap between experiments and molecular simulations. Here, this approach is extended and validated for the ternary system chloroform - acetone - methanol. Our MD results show good agreement with experiments. Even with simple molecular models taken from standard classical force fields, *i.e.* excluding polarization effects, we shall see that it is possible to predict Fick diffusivities with reasonable accuracy. This may suggest that the use of more realistic/complex force fields is not needed for predicting transport diffusivities of typical small molecules.

This chapter is organized as follows. In section 7.2, we explain how to obtain the MS diffusivities and thermodynamic factors from equilibrium MD simulations. The details of the simulations are addressed in section 7.3. In section 7.4, we validate the methodology for computing Fick diffusivities for the ternary system chloroform - acetone - methanol. Our findings are summarized in section 7.5.

## 7.2 Computation of diffusion coefficients and thermodynamic factors

### 7.2.1 Obtaining diffusion coefficients from MD simulations

In equilibrium MD simulations, representative trajectories of a system consisting of interacting molecules are obtained<sup>17;18;20</sup>. From these trajectories, transport properties can be computed<sup>17</sup>. For details on the computation of self- and MS diffusivities, we refer the readers to section 2.3.

## 7.2.2 Obtaining thermodynamic factors from MD simulations

In section 6.2.3, we showed that the elements of  $[\Gamma]$  follow from the so-called KB coefficients and we explained how these can be computed from simulations. In ternary systems, the elements of thermodynamic factor  $[\Gamma]$  are related to the KB coefficients  $G_{ij}$  by<sup>93;153;156</sup>

$$\Gamma_{11} = -\frac{1}{\eta} [-c_2c_3G_{22} - c_2 + 2c_2c_3G_{23} - c_2c_3G_{33} - c_3 + c_1(c_2G_{12} - c_2G_{22} - 1 + c_2G_{23} - c_2G_{13})], \quad (7.1)$$

$$\Gamma_{12} = -\frac{c_1}{\eta} (c_2G_{12} + c_3G_{12} - c_2G_{13} - c_3G_{13} - c_2G_{22} + c_2G_{23} - c_3G_{23} + c_3G_{33}), \quad (7.2)$$

$$\Gamma_{21} = \frac{c_2}{\eta} (c_1G_{11} - c_1G_{12} - c_3G_{12} - c_1G_{13} + c_3G_{13} + c_1G_{23} + c_3G_{23} - c_3G_{33}), \quad (7.3)$$

$$\Gamma_{22} = \frac{1}{\eta} (c_1c_3G_{11} + c_1 - 2c_1c_3G_{13} + c_1c_3G_{33} + c_3 + c_2(c_1G_{11} - c_1G_{12} - c_1G_{13} + 1 + c_1G_{23})), \quad (7.4)$$

in which

$$\eta = c_1 + c_2 + c_3 + c_1c_2\Omega_{12} + c_2c_3\Omega_{23} + c_1c_3\Omega_{13} - \frac{1}{4}c_1c_2c_3(\Omega_{12}^2 + \Omega_{23}^2 + \Omega_{13}^2 - 2\Omega_{13}\Omega_{23} - 2\Omega_{12}\Omega_{13} - 2\Omega_{12}\Omega_{23}), \quad (7.5)$$

and

$$\Omega_{ij} = G_{ii} + G_{jj} - 2G_{ij}. \quad (7.6)$$

The KB coefficients allow the computation of the thermodynamic factor from MD simulations and thus avoid the insertion and deletion of particles as needed in simulations in the grand-canonical ensemble. It is important to consider the convergence of the integrals in Eq. (6.17). For infinitely large systems,  $g_{ij}(r) \rightarrow 1$  for  $r \rightarrow \infty$ . For finite systems with periodic boundary conditions, however,  $g_{ij}(r)$  does not converge to 1 for large  $r$  resulting in a divergence of  $G_{ij}$ <sup>153</sup>. To improve the convergence of

$G_{ij}$ , a natural choice is to make the system larger and to use longer simulations. However, this is computationally inefficient and seriously hinders the direct estimation of KB coefficients from simulations. Recently, some effort has been made in computing the KB coefficients using different methods. Wedberg *et al.* accounted for finite size effects in simulations by introducing tail corrections to the correlation functions based on integral equation theory<sup>174</sup>. These corrections are based on the hypernetted chain closure which is accurate at high densities. This method requires the optimization of two parameters, the joining radius and the tail approximation. Nichols *et al.* discussed the effects of truncation of the KB integrals are discussed<sup>175</sup>. In addition, a method for estimating the KB integrals using the Fourier transformed atomic positions is described. This method is shown to account for the corners of the simulation box and is less sensitive to cutoff effects than the traditional method of Eq. (6.17). An empirical method for extrapolating the partial volume, compressibility and activity coefficients for binary mixtures through the use of seven parameters was also presented. Mukherji *et al.* obtained the KB coefficients by coupling a small all-atom region to a very large coarse-grained reservoir. Exchanging molecules between the small system and the reservoir is allowed via a hybrid region. The difficulties of this approach are that the system should be very large and the thermodynamic force which ensures the thermodynamic equilibrium over the whole system should be calculated for each concentration<sup>176</sup>. The simplest and in the most past frequently used approach is to simply use a switching function to force the radial distribution function  $g(r)$  to converge to 1 for large distance  $r$ . However, it turns out that the final result depends on the choice of the switching function<sup>157;176</sup>.

Recently, we found that the average particle fluctuations in Eq. (6.16) can also be calculated by considering a large system in which smaller subvolumes are embedded. These subvolumes can exchange particles and energy with the simulation box and therefore a subvolume can be considered as a system in the grand-canonical ensemble. However, corrections should be taken due to the finite size effect originating from the boundaries of the subvolumes<sup>48;49;158</sup>. We refer the reader to section 6.2.3 and appendix A for more details.

### 7.2.3 Obtaining thermodynamic factors from COSMO-SAC

An alternative method to compute the thermodynamic factors for a mixture is through a model for the activity coefficients  $\gamma_i$ <sup>177</sup>. The COSMO-SAC theory is a quantum-mechanically based predictive model for the activity coefficients<sup>178;179</sup>. In brief, the molecules are represented by a set of screening charge densities known as their  $\sigma$ -profiles. These profiles are generated by placing each molecule in a conducting or dielectric cavity and compute a charge distribution using density functional theory (DFT) which completely screens the molecular charge distribution from the outside. The resulting  $\sigma$ -profiles represent “fingerprints” of each molecule which can be used to model a solution by mixing them in their appropriate mole fractions. Since COSMO-SAC is an activity coefficient model, the dispersion is assumed to cancel in the reference fluid. The outcome of this modeling are the activity coefficients for all species as a function of their concentration. The thermodynamic factors  $\Gamma_{ij}$  then follow from numerical differentiation using Eqs. (6.7) and (6.8). This predictive excess Gibbs energy model is used as a benchmark and reference in this work.

## 7.3 Simulations details

In the ternary mixture chloroform - acetone - methanol, the OPLS force field is used for acetone and methanol<sup>159;160</sup>. A five-site model for chloroform is used<sup>180</sup>. All components are treated as rigid molecules. The LJ potentials describe the intermolecular non-bonded interactions which are truncated and shifted at 10 Å. The Lorentz-Berthelot mixing rules are applied to obtain the LJ interaction between unlike atoms<sup>18</sup>. Electrostatic interactions are handled by Ewald summation using a relative precision<sup>85</sup> of  $10^{-5}$ . The force field parameters as well as the parameters defining the geometries of the molecules can be found in Table 7.1. Three dimensional periodic boundary conditions consistent with a cubic box are applied to obtain properties corresponding to bulk systems. MD simulations were carried out at a temperature of 298 K and a pressure of 1 atm. Systems were first equilibrated in an  $NpT$  ensemble with a Nosé-Hoover thermostat and barostat using the time constants of 0.1 ps and 1 ps, respectively. The equations of motion were integrated using the leapfrog Verlet algorithm with a time step of 1 fs. The MS diffusion coefficients are obtained from equilibrium MD simulations in the  $NVT$  ensemble using the Nosé-Hoover ther-

**Table 7.1:** Force field and geometrical parameters for acetone, methanol and chloroform. Parameters for acetone were taken from Ref<sup>159</sup>. Parameters for chloroform were taken from Ref<sup>180</sup>. Parameters for methanol were taken from Ref.<sup>160</sup>

Force field parameters				
site		$\sigma/\text{\AA}$	$(\epsilon/k_B)/\text{K}$	$q/e$
CH <sub>3</sub>	(acetone)	3.910	81.0866	0.0620
C	(acetone)	3.750	52.9463	0.3000
O	(acetone)	2.960	105.8997	-0.4240
C	(CHCl <sub>3</sub> )	3.800	37.7726	-0.0500
H	(CHCl <sub>3</sub> )	-	-	0.1850
Cl	(CHCl <sub>3</sub> )	3.470	15.1067	-0.0450
O	(methanol)	3.070	85.6753	-0.7000
H	(methanol)	-	-	0.4350
CH <sub>3</sub>	(methanol)	3.775	104.3223	0.2650

Standard geometrical parameters			
bond length/\AA		bond angle/deg	
C-Cl	1.771	CH <sub>3</sub> -C-CH <sub>3</sub>	116.30
C-H	1.094	CH <sub>3</sub> -C=O	121.86
C=O	1.220	CH <sub>3</sub> -O-H	108.50
CH <sub>3</sub> -C	1.507	Cl-C-Cl	110.60
O-H	0.945	H-C-Cl	108.31
CH <sub>3</sub> -O	1.430		



mostat at a density corresponding to a pressure of 1 atm.<sup>17</sup>. The box volume was typically around  $(28 \text{ \AA})^3$  resulting in a total number of molecules of the order of 200. The simulations for extracting diffusion coefficients were run for at least 100 ns to obtain MS diffusivities with an accuracy of around 5%. KB coefficients required for the calculation of thermodynamic factors were obtained from MD simulations in the  $NpT$  ensemble. Temperature and pressure were controlled using the Nosé-Hoover thermostat and barostat, respectively. In these simulations, the box size needs to be larger, see also section 7.2.2. The box volume was typically fluctuating around  $(85 \text{ \AA})^3$ . The maximum number of molecules used in these simulations was typically 7000. Simulation runs of at least 5 ns were needed to obtain accurate values of the thermodynamic factors. The error bars of the computed thermodynamic factors are less than 3%.

The COSMO-SAC computations were performed with the 2011.03 release ADF Theoretical Chemistry software<sup>181</sup>. The COSMO surfaces were calculated using BP functionals and the TZP bases<sup>181</sup>. The standard values of the parameters for the model were used in all calculations<sup>179</sup>. To obtain accurate numerical derivatives, calculations for the logarithmic activities of each mixture were performed at mole fraction intervals of at most 0.05 in each component. The unconstrained derivatives from Eq. (6.8) were then calculated in MATLAB directly from these activities using a central differencing scheme. In the case of the ternary system, the derivatives were computed using a barycentric coordinate system. The constrained derivatives were then computed using Eq. (6.7).

## 7.4 Results and discussion

As ternary experimental data of diffusion coefficients are lacking for the ternary system chloroform - methanol - acetone, we validated our method in the relevant binary mixtures and predicted the ternary diffusion coefficients assuming that the quality of our method in ternary mixtures is similar to that of binary systems. The binary system acetone - methanol has been studied in our previous work<sup>172;173</sup>. The computed Fick diffusivity  $D$  and thermodynamic factor  $\Gamma$  quantitatively agree with the experiments<sup>172;173</sup>.

**Table 7.2:** Densities of pure chloroform, acetone and methanol at 298 K, 1 atm.

Component	$\rho/(\text{g}\cdot\text{ml}^{-1})$	
	This work (MD)	Experiments
acetone	0.76	0.78 <sup>a,b</sup> , 0.79 <sup>c</sup>
methanol	0.75	0.79 <sup>a,b</sup>
CHCl <sub>3</sub>	1.48	1.47 <sup>d</sup>

<sup>a</sup> Experiments by Campbell *et al.*, Ref. <sup>161</sup>

<sup>b</sup> Experiments by Noda *et al.*, Ref. <sup>162</sup>

<sup>c</sup> Experiments reported in Ref. <sup>163</sup>

<sup>d</sup> Experiments reported in Ref. <sup>182</sup>

### 7.4.1 Chloroform - acetone

Karr *et al.* measured the densities of chloroform - acetone mixtures at 298 K, 1 atm<sup>182</sup>. In Figure 7.1, the computed densities using MD simulations are compared to the experiments as a function of the composition. The computed mixture densities show a slightly stronger dependence on mixture composition suggesting a lower density of pure acetone and a higher density of pure chloroform. This is also shown in Table 7.2 in which computed pure-component densities are compared to the experimental ones.

Figure 7.2 shows the thermodynamic factor  $\Gamma$  obtained from experiment and MD simulation in the binary mixture chloroform - acetone for various compositions. The computed  $\Gamma$  is larger than unity suggesting a negative deviation from Raoult's law. The activity coefficient  $\gamma_1$  increases with increasing  $x_1$ , that is, the repulsion between chloroform - chloroform is stronger than that of chloroform - acetone<sup>2</sup>. In Ref<sup>168</sup>, the VLE data are provided from which the activity coefficients  $\gamma_i$  can be calculated. By fitting these activity coefficients  $\gamma_i$  using the NRTL model, the thermodynamic factor  $\Gamma$  was obtained. Compared to the experiment,  $\Gamma$  obtained from COSMO-SAC shows good agreement.

Using the computed MS diffusivity  $D_{12}$  and thermodynamic factor  $\Gamma$  from MD, we calculate the Fick diffusivity  $D$  as a function of composition, see Figure 7.3. A good agreement of Fick diffusivity  $D$  between experiments and MD simulations is seen. The very good agreement is partially due to error cancellation: the computed

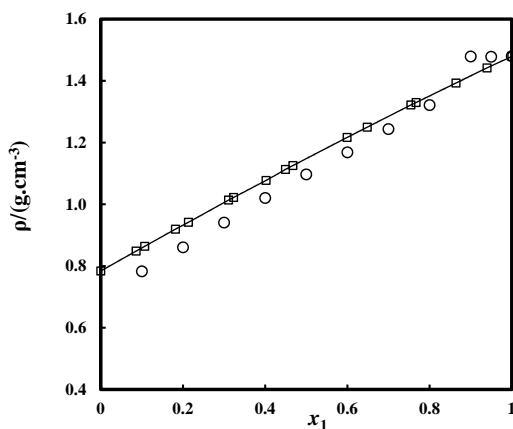


**Figure 7.1:** Densities of chloroform (1) - acetone (2) mixtures at 298 K, 1 atm. Circles are the computed densities by this work using MD simulations. Squares are the experimental densities measured by Karr *et al.*<sup>182</sup>.

value of  $\Gamma$  is lower than in experiments implying larger values of the computed MS diffusivity  $\mathcal{D}_{12}$ . This is reasonable since the computed mixture densities are lower than in the experiments and larger values of diffusion coefficients are thus expected.

#### 7.4.2 Chloroform - methanol

In the binary mixture chloroform - methanol, the computed mixture densities agree very well with the experiments<sup>183</sup>, see Figure 7.4. Figure 7.5 shows thermodynamic factor  $\Gamma$  as a function of composition for the same binary mixture. COSMO-SAC accurately predicts  $\Gamma$  when the concentration of chloroform is low. As the concentration of chloroform increases,  $\Gamma$  computed using MD simulations is closer to the experimental data<sup>168</sup>. Figure 7.6 shows the computed MS diffusivity  $\mathcal{D}_{12}$  and Fick diffusivity  $D$  from MD simulations. The Fick diffusivity  $D$  is calculated using the computed MS diffusivity  $\mathcal{D}_{12}$  and the thermodynamic factor  $\Gamma$ . We observe that the MS diffusivity  $\mathcal{D}_{12}$  increases as the concentration of chloroform increases. However, the increasing chloroform concentration drives the mixture away from ideal mixing behavior resulting in a reduced concentration dependence of Fick diffusivity  $D$ . The Fick diffusivity  $D$  has a minimum value around a concentration of  $x_1 = 0.7$ , while the MS diffusivity  $\mathcal{D}_{12}$  displays a maximum in the same concentration range. The MS diffusivity  $\mathcal{D}_{12}$  ranges from 3 to  $6 \cdot 10^{-9} \text{ m}^2 \cdot \text{s}^{-1}$  and the Fick diffusivity  $D$  ranges

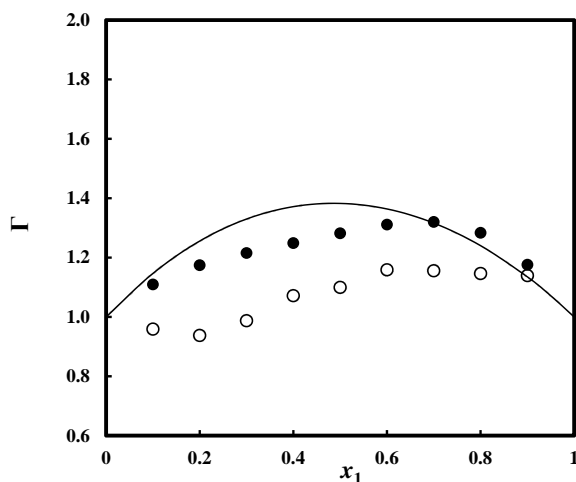


**Figure 7.2:** Thermodynamic factor  $\Gamma$  in the binary system chloroform (1) - acetone (2) at 298 K, 1 atm. Open symbols are the computed  $\Gamma$  in this work using MD simulations. Filled symbols are the computed  $\Gamma$  using COSMO-SAC. The solid line represents  $\Gamma$  calculated from the NRTL model and fitted to experimental VLE data taken from Ref. <sup>168</sup>. Fitted parameters of the NRTL model are:  $\tau_{12} = -0.40$ ,  $\tau_{21} = -0.32$ ;  $\alpha = 0.42$ <sup>50</sup>.

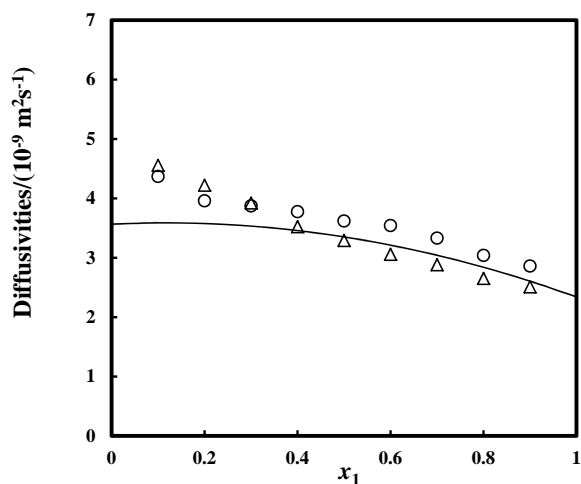


**Figure 7.3:** Computed MS diffusivities  $\mathcal{D}_{12}$  (triangles) and Fick diffusivities  $D$  (circles) in the binary system chloroform (1) - acetone (2) at 298 K, 1 atm. Fick diffusivities are calculated using the computed thermodynamic factor  $\Gamma$  and MS diffusivities  $\mathcal{D}_{12}$  from MD simulations. The error bars of computed diffusivities are smaller than the symbol size. Solid line represent the experimental Fick diffusivities.

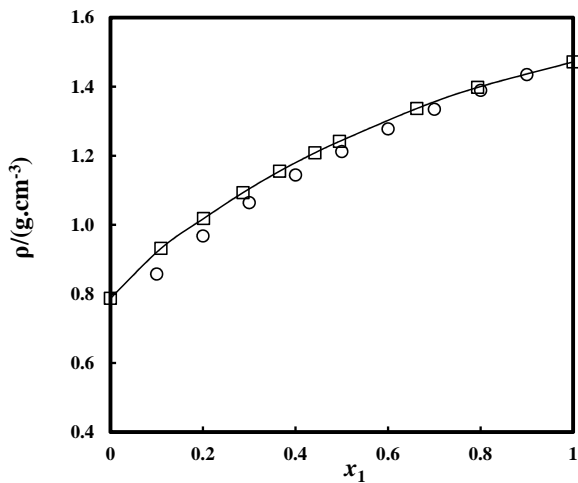


**Figure 7.4:** Densities of chloroform (1) - methanol (2) mixtures at 298 K, 1 atm. Circles are the computed densities from this work using MD simulations. Squares are the experimental density taken from Ref. <sup>183</sup>.

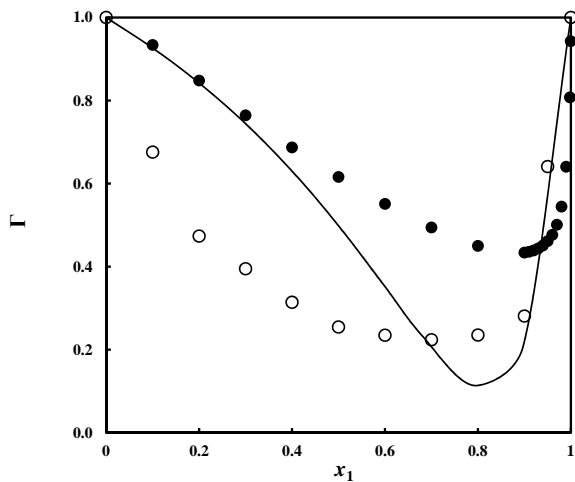


**Figure 7.5:** Thermodynamic factor  $\Gamma$  in the binary system chloroform (1) - methanol (2) at 298 K, 1 atm. Open symbols are the computed  $\Gamma$  by this work using MD simulations. Filled symbols represent  $\Gamma$  computed using COSMO-SAC. The solid line represents  $\Gamma$  calculated from the NRTL model and fitted to experimental VLE data taken from Ref. <sup>168</sup>. Fitted parameters of the NRTL model are:  $\tau_{12} = 0.51$ ;  $\tau_{21} = 0.05$ ;  $\alpha = 0.47$  <sup>50</sup>.

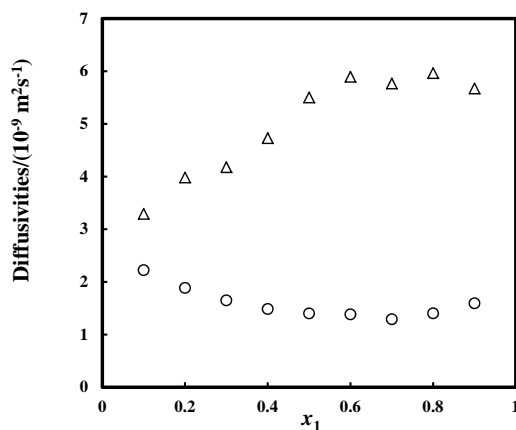


**Figure 7.6:** Computed MS diffusivity  $\mathcal{D}_{12}$  and Fick diffusivities  $D$  in the binary system chloroform (1) - methanol (2) at 298 K, 1 atm. Fick diffusivities (circles) calculated using the computed thermodynamic factor  $\Gamma$  and MS diffusivities  $\mathcal{D}_{12}$  (triangles) from MD simulations. The error bars of computed diffusivities are smaller than the symbol size.

from  $1.5$  to  $2.5 \cdot 10^{-9} \text{ m}^2 \cdot \text{s}^{-1}$ .

### 7.4.3 Chloroform - acetone - methanol

Figure 7.7 shows the densities in chloroform - acetone - methanol mixtures at 298 K, 1 atm. We observe a linear relation between mixture densities and composition. Figures 7.8, 7.9 and 7.10 show the thermodynamic factors  $\Gamma_{ij}$  in the ternary mixtures as a function of the composition. Data are reported for  $\Gamma_{ij}$  as a function of  $x_i$  while keeping  $x_j = x_k$  (with  $i \neq j \neq k$ ). Oracz *et al.* measured the vapor-liquid equilibrium for this ternary mixtures at 303 K<sup>184</sup>. These VLE data were converted to the matrix of thermodynamic factors  $\Gamma_{ij}$  using the NRTL model<sup>1;62</sup>. The ternary VLE data are very well described by the NRTL model. The computed  $\Gamma_{ij}$  using MD simulation show quantitative agreement with the experimental data and the results from COSMO-SAC deviate from experiments. We feel that the agreement is very good considering the fact that simple molecular interaction models were used in the MD simulations, *i.e.* polarization effects are not accounted for.

MS diffusivities  $\mathcal{D}_{ij}$  can not be measured directly in experiments. However, it is possible to predict MS diffusivities  $\mathcal{D}_{ij}$  using easily obtained self-diffusivities  $D_{i,\text{self}}$ . For this purpose, we have recently proposed a multicomponent Darken model as

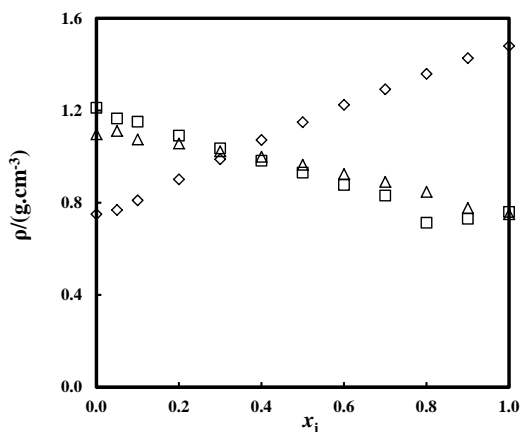


**Figure 7.7:** Densities of chloroform (1) - acetone (2) - methanol (3) mixtures at 298 K, 1 atm. The densities are plotted as a function of the mole fraction of one of the components, while keeping the mole fractions of the other components equal to each other. Diamonds represent  $i = 1, x_2 = x_3$ . Squares represent  $i = 2, x_1 = x_3$ . Triangles represent  $i = 3, x_1 = x_2$ .

**Table 7.3:** Computed self-diffusivities  $D_{i,\text{self}}/10^{-9} \text{ m}^2 \cdot \text{s}^{-1}$  in the ternary system chloroform (1) - acetone (2) - methanol (3) using MD simulations. The simulations were carried out at 298 K, 1 atm. The mole fraction of component  $i$  ( $x_i$ ) is varied while keeping mole fraction of components  $j$  and  $k$  equal ( $x_j = x_k, i \neq j \neq k$ ).

$x_1$	$D_{1,\text{self}}$	$D_{2,\text{self}}$	$D_{3,\text{self}}$	$x_2$	$D_{1,\text{self}}$	$D_{2,\text{self}}$	$D_{3,\text{self}}$	$x_3$	$D_{1,\text{self}}$	$D_{2,\text{self}}$	$D_{3,\text{self}}$
0.1	3.96	4.58	3.38	0.1	2.74	2.91	2.02	0.1	3.19	3.61	3.26
0.2	3.65	4.18	3.02	0.2	2.94	3.22	2.33	0.2	3.15	3.51	2.78
0.3	3.28	3.73	2.78	0.3	3.12	3.51	2.55	0.3	3.24	3.67	2.77
0.4	3.07	3.38	2.57	0.4	3.35	3.83	2.92	0.4	3.19	3.57	2.64
0.5	2.89	3.17	2.39	0.5	3.61	4.18	3.28	0.5	3.24	3.59	2.59
0.6	2.71	2.86	2.23	0.6	3.94	4.61	3.77	0.6	3.28	3.79	2.69
0.7	2.62	2.74	2.17	0.7	4.18	4.92	4.32	0.7	3.19	3.73	2.50
0.8	2.50	2.54	2.13	0.8	4.49	5.28	5.00	0.8	3.17	3.67	2.41

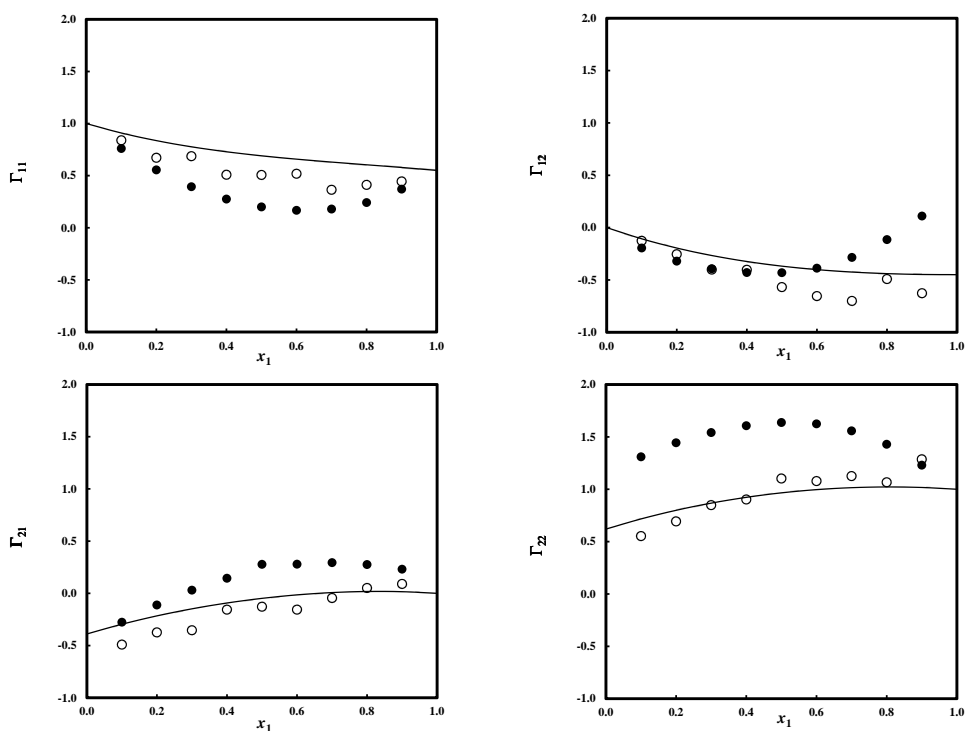


**Figure 7.8:** Thermodynamic factor  $\Gamma_{ij}$  in the ternary system chloroform (1) - acetone (2) - methanol (3) at 1 atm. Open circles are the computed values of  $\Gamma_{ij}$  using MD simulations at 298 K. Filled circles are the computed values of  $\Gamma_{ij}$  using COSMO-SAC at 298 K. Solid lines represent  $\Gamma_{ij}$  calculated from the NRTL model and fitted to experimental VLE data taken from Ref.<sup>184</sup> at 303 K. Fitted parameters of the NRTL model are:  $\tau_{12} = 0.0$ ;  $\tau_{13} = 14.49$ ;  $\tau_{21} = 0.0$ ;  $\tau_{23} = 0.0$ ;  $\tau_{31} = 0.79$ ;  $\tau_{32} = 0.76$ ;  $\alpha_{12} = 0.0$ ;  $\alpha_{13} = 0.25$ ;  $\alpha_{23} = 0.010$ <sup>50</sup>.  $x_1$  is varied while keeping  $x_2 = x_3$ .



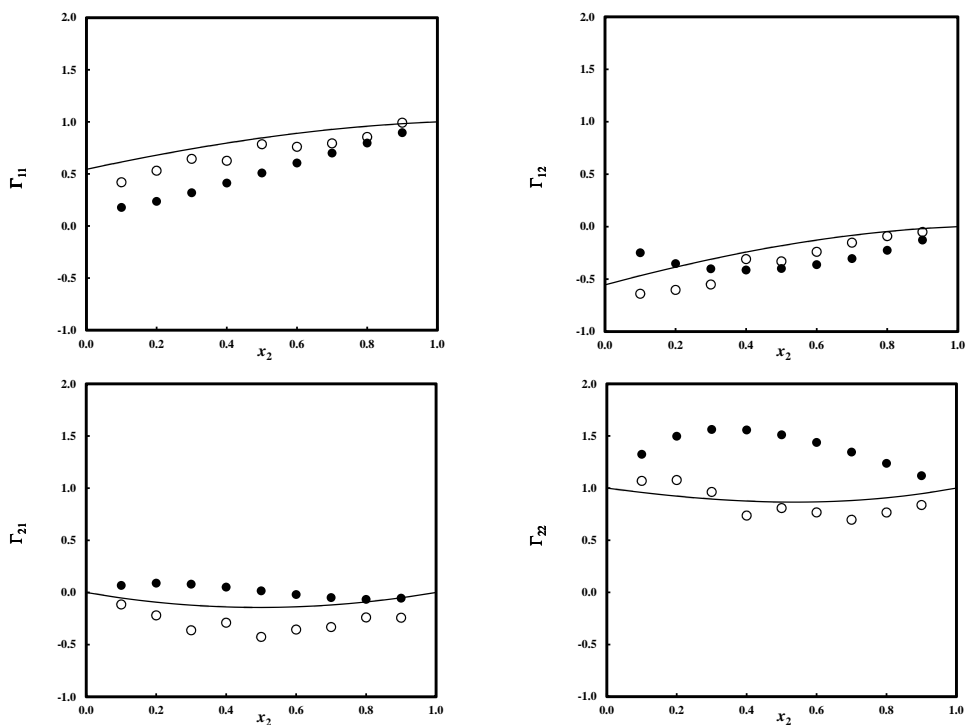


**Figure 7.9:** Thermodynamic factor  $\Gamma_{ij}$  in the ternary system chloroform (1) - acetone (2) - methanol (3) at 1 atm. Open circles are the computed values of  $\Gamma_{ij}$  using MD simulations at 298 K. Filled circles are the computed values of  $\Gamma_{ij}$  using COSMO-SAC at 298 K. Solid lines represent  $\Gamma_{ij}$  calculated from the NRTL model and fitted to experimental VLE data taken from Ref. <sup>184</sup> at 303 K. (*see the caption of Figure 7.8*).  $x_2$  is varied while keeping  $x_1 = x_3$ .

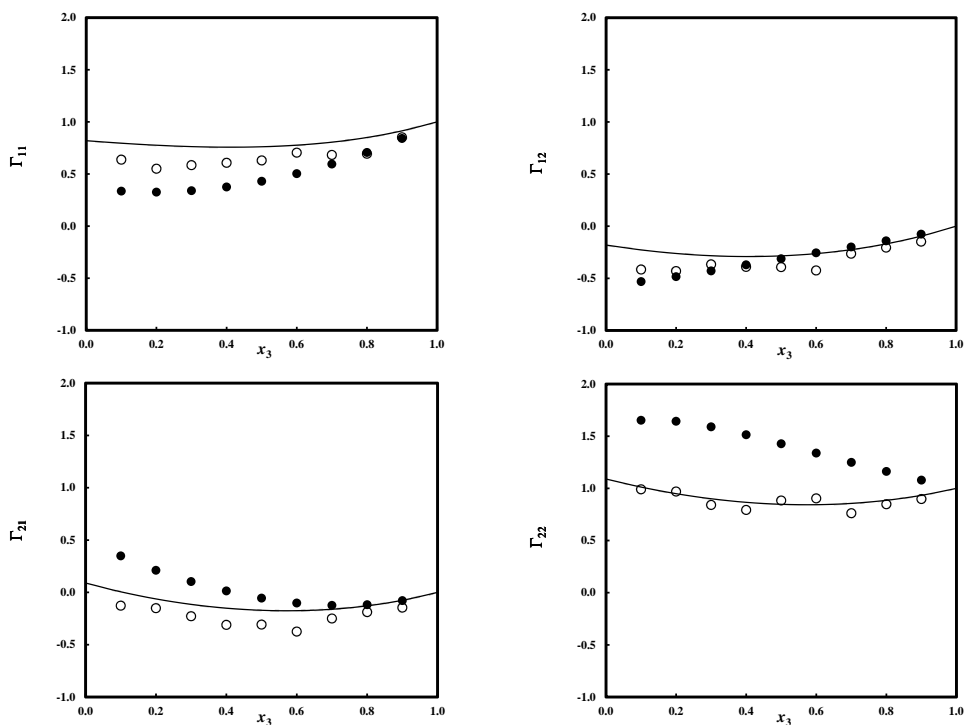


**Figure 7.10:** Thermodynamic factor  $\Gamma_{ij}$  in the ternary system chloroform (1) - acetone (2) - methanol (3) at 1 atm. Open circles are the computed values of  $\Gamma_{ij}$  using MD simulations at 298 K. Filled circles are the computed values of  $\Gamma_{ij}$  using COSMO-SAC at 298 K. Solid lines represent  $\Gamma_{ij}$  calculated from the NRTL model and fitted to experimental VLE data taken from Ref. <sup>184</sup> at 303 K. (see the caption of Figure 7.8)  $x_3$  is varied while keeping  $x_1 = x_2$ .

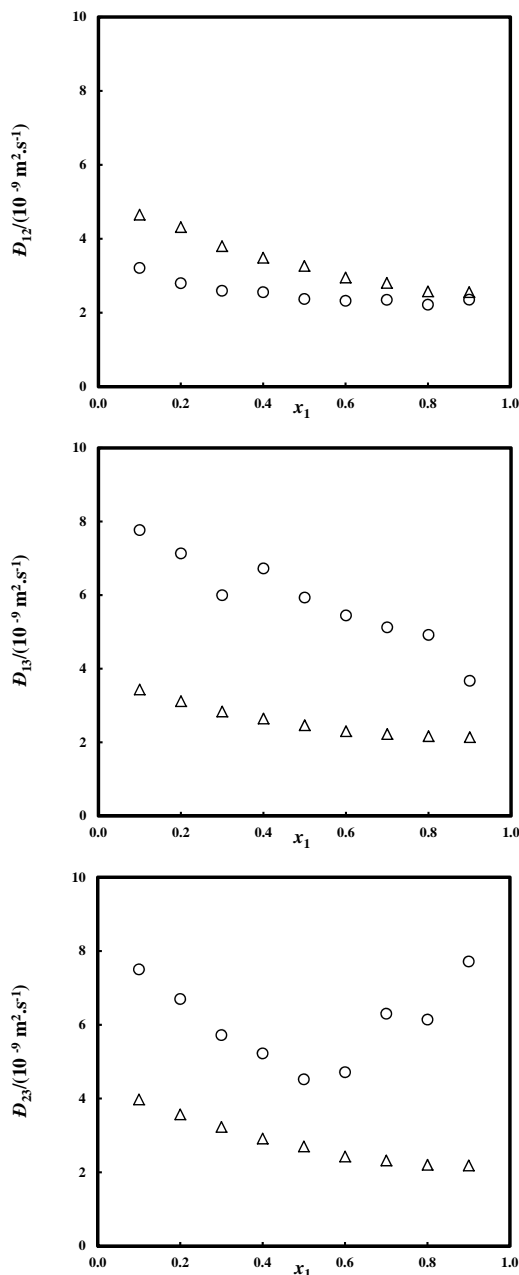


**Figure 7.11:** Comparison of the computed MS diffusivities  $D_{ij}$  and the predicted MS diffusivities  $\hat{D}_{ij}$  in the ternary system chloroform (1) - acetone (2) - methanol (3) at 298 K, 1 atm.  $x_1$  varies while keeping  $x_2 = x_3$ . Circles are the computed  $D_{ij}$  using MD simulations. Triangles are the predicted  $\hat{D}_{ij}$  using multicomponent Darken equation (Eq. (7.7)). The computed self-diffusivities from MD simulations are used to parametrize Eq. (7.7) and listed in Table 7.3.

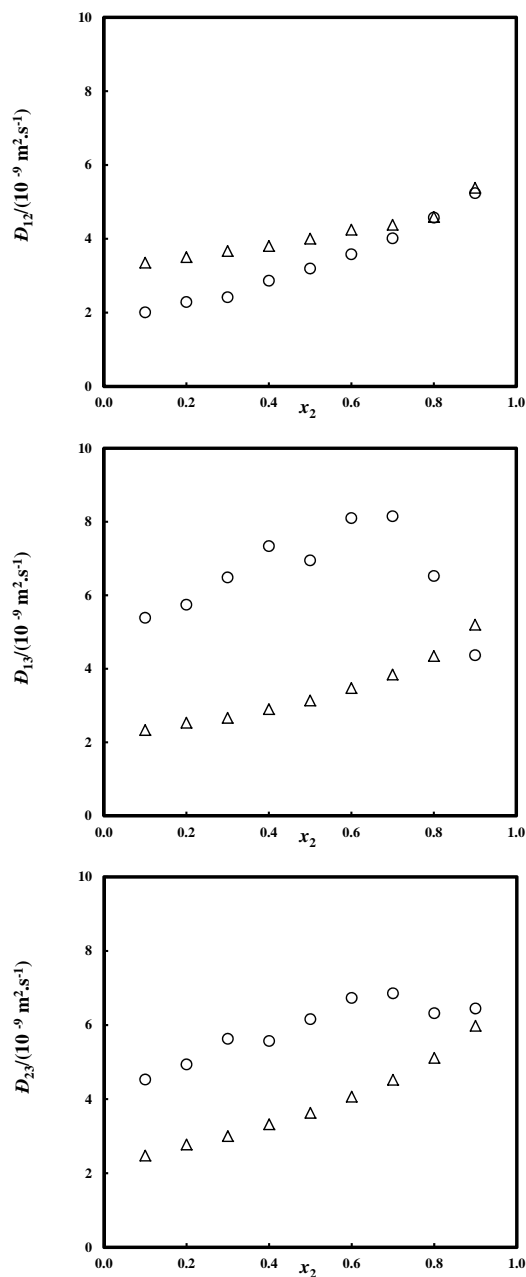


**Figure 7.12:** Comparison of the computed MS diffusivities  $D_{ij}$  and the predicted MS diffusivities  $\hat{D}_{ij}$  in the ternary system chloroform (1) - acetone (2) - methanol (3) at 298 K, 1 atm.  $x_2$  varies while keeping  $x_1 = x_3$ . Circles are the computed  $D_{ij}$  using MD simulations. Triangles are the predicted  $\hat{D}_{ij}$  using multicomponent Darken equation (Eq. (7.7)). The computed self-diffusivities from MD simulations are used to parametrize Eq. (7.7) and listed in Table 7.3.

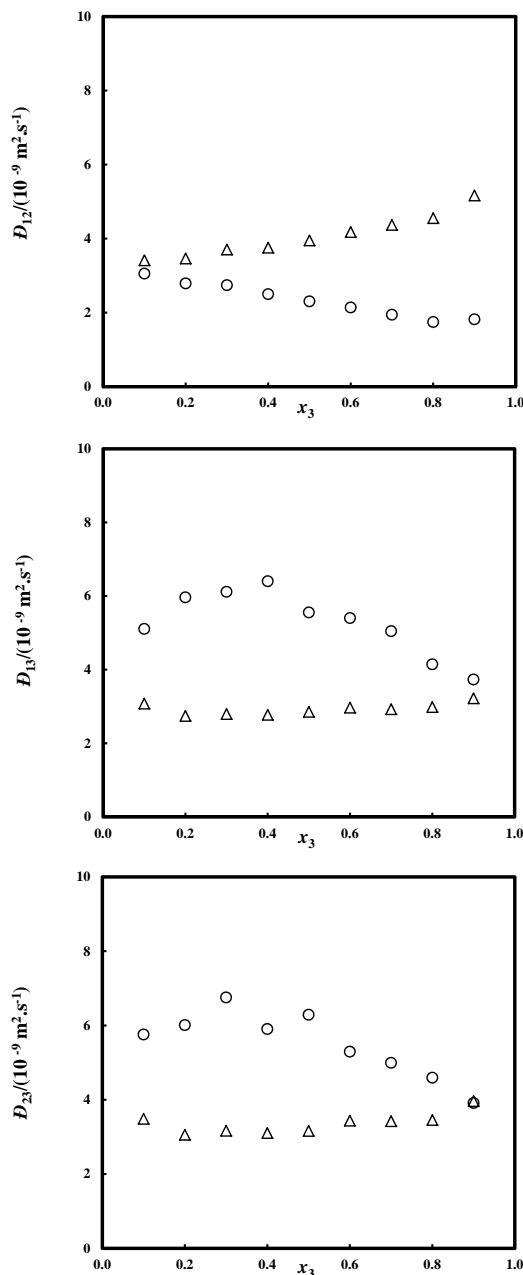


**Figure 7.13:** Comparison of the computed MS diffusivities  $\mathcal{D}_{ij}$  and the predicted MS diffusivities  $\hat{\mathcal{D}}_{ij}$  in the ternary system chloroform (1) - acetone (2) - methanol (3) at 298 K, 1 atm.  $x_3$  varies while keeping  $x_1 = x_2$ . Circles are the computed  $\mathcal{D}_{ij}$  using MD simulations. Triangles are the predicted  $\hat{\mathcal{D}}_{ij}$  using multicomponent Darken equation Eq. (7.7). The computed self-diffusivities from MD simulations are used to parametrize (Eq. (7.7)) and listed in Table 7.3.

shown in chapter 4. In this model, we neglect the velocity cross-correlations between unlike molecules<sup>35</sup>. The resulting multicomponent Darken equation is

$$\mathcal{D}_{ij} = D_{i,\text{self}} \cdot D_{j,\text{self}} \sum_{i=1}^n \frac{x_i}{D_{i,\text{self}}}, \quad (7.7)$$

in which  $D_{i,\text{self}}$  is the self-diffusivity of component  $i$  in the mixture. The computed self-diffusivities  $D_{i,\text{self}}$  in the ternary system chloroform - acetone - methanol can be found in appendix F. The multicomponent Darken equation has been shown to allow for the most robust and accurate prediction of diffusion coefficients in ideal diffusing mixtures where the neglect of velocity cross-correlations is justified<sup>34;35</sup>. Figures 7.11, 7.12 and 7.13 show the computed MS diffusivities  $\mathcal{D}_{ij}$  and the predicted MS diffusivities  $\mathcal{D}_{ij}$ . From these figures, it can be seen that the concentration dependence of MS diffusivities  $\mathcal{D}_{ij}$  is not well captured by the multicomponent Darken equation. The MS diffusivities are either underestimated or overestimated by the multicomponent Darken equation suggesting that the correlations of different molecules are important in the chloroform - acetone - methanol system. The deviation of the predicted  $\mathcal{D}_{ij}$  using the multicomponent Darken equation from the computed  $\mathcal{D}_{ij}$  was already observed for the binary mixtures acetone - methanol and acetone - tetrachloromethane<sup>172;173</sup>. The comparison to the multicomponent Darken equation demonstrates the potential of molecular simulations for the prediction of multicomponent Fick diffusion coefficients as the molecular models also allow the prediction of non-ideal systems.

Figure 7.14 shows the computed Fick diffusivities  $D_{ij}$  using the computed MS diffusivities  $\mathcal{D}_{ij}$  and thermodynamic factors  $\Gamma_{ij}$ . It can be observed that: (1) the diagonal Fick diffusivities are always positive and the off-diagonal Fick diffusivities are may be negative; (2) the diagonal Fick diffusivities are about one order of magnitude larger than the off-diagonal Fick diffusivities suggesting the diffusion flux of component  $i$  mainly depends on its own concentration gradient while the concentration gradient of other components plays a minor role. This behavior is in accordance with the bound placed on off-diagonal coefficients by the entropy production for ternary diffusion<sup>12</sup>. It is important to note that the values of the elements of the matrices  $[\Gamma]$  and  $[D]$  depend on the labeling of the components (this follows directly from Eqs. (6.1) and (6.7)). This problem does not apply for MS diffusivities. The com-

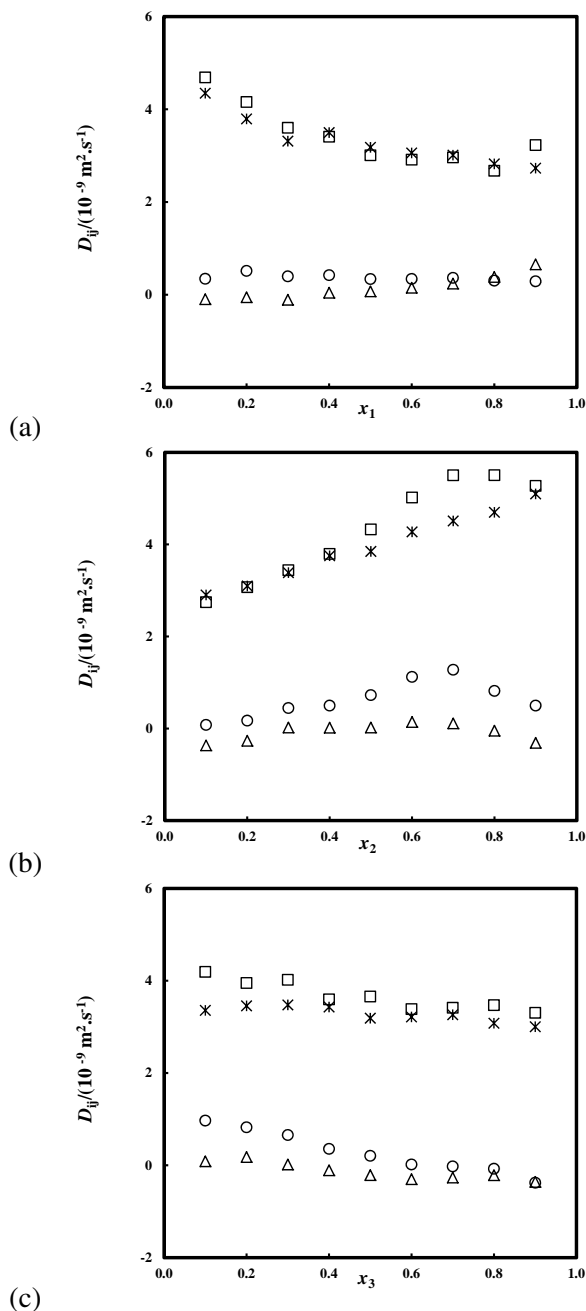


**Figure 7.14:** Fick diffusivities  $D_{ij}$  in the ternary system chloroform (1) - acetone (2) - methanol (3) at 298 K, 1 atm. Fick diffusivities  $D_{ij}$  are calculated using the computed MS diffusivities  $\mathcal{D}_{ij}$  and thermodynamic factors  $\Gamma_{ij}$ . Stars- $D_{11}$ ; Circles- $D_{12}$ ; Triangles- $D_{21}$ ; Squares- $D_{22}$ . (a)  $x_1$  varies while keeping  $x_2 = x_3$ ; (b)  $x_2$  varies while keeping  $x_1 = x_3$ ; (c)  $x_3$  varies while keeping  $x_1 = x_2$ .

puted ternary Fick diffusivities can be considered as true predictions as they directly originate from the force field.

## 7.5 Conclusions

In this chapter, we present a consistent method for computing ternary Fick diffusivities from equilibrium MD simulations. For this purpose, MS diffusivities and thermodynamic factors are computed to calculate the matrix of Fick diffusivities. Our approach is applied to a ternary mixture chloroform - acetone - methanol. Even though a simple molecular model is used, the computed thermodynamic factors  $[\Gamma]$  are in close agreement with experiments. This findings suggests that the method outlined in section 6.2.3 (Eq. (6.18)) is well suited for computing thermodynamic properties of mixtures in general since the framework relies on the KB coefficients which become now accessible in practical computations. Validation data for diffusion is only available for two binary sub-systems. Here, MD results and experiments do agree well. Therefore, we expect that the computed Fick diffusivities should also be comparable with experiments. The presented approach allows for an efficient and consistent prediction of multicomponent Fick diffusion coefficients from molecular models.



**A**

---

**Obtaining Maxwell-Stefan Diffusivities  
from Molecular Dynamics  
Trajectories**

---

In this section, we provide the exact expressions for MS diffusivities in binary, ternary and quaternary systems as a function of the Onsager coefficients  $\Lambda_{ij}$  (Eqs. (2.20) and (2.21)). We also refer the reader to Refs. <sup>35;38</sup>.

## A.1 Binary systems

In binary systems, the MS diffusivity  $\mathcal{D}_{12}$  is related to the Onsager coefficients by<sup>23</sup>

$$\mathcal{D}_{12} = \frac{x_2}{x_1} \Lambda_{11} + \frac{x_1}{x_2} \Lambda_{22} - 2\Lambda_{12}, \quad (\text{A.1})$$

in which the Onsager coefficients  $\Lambda_{ij}$  are defined as

$$\Lambda_{ij} = \frac{1}{3N} \int_0^\infty dt' \left\langle \sum_{l=1}^{N_i} v_{l,i}(t) \cdot \sum_{k=1}^{N_j} v_{k,j}(t+t') \right\rangle. \quad (\text{A.2})$$

In this equation,  $N$  is the total number of molecules in the simulation,  $N_i$  is the number of molecules of component  $i$ ,  $v_{l,i}(t)$  is the center of mass velocity of the  $l^{\text{th}}$  molecule of component  $i$  at time  $t$ . An alternative expression for  $\Lambda_{ij}$  in terms of particle positions is given by Eq. (2.20).

## A.2 Ternary systems

In ternary systems, a matrix  $[\Delta]$  is defined with elements following from the Onsager coefficients  $\Lambda_{ij}$ .<sup>23</sup>

$$\Delta_{11} = (1 - x_1) \left( \frac{\Lambda_{11}}{x_1} - \frac{\Lambda_{13}}{x_3} \right) - x_1 \left( \frac{\Lambda_{21}}{x_1} - \frac{\Lambda_{23}}{x_3} + \frac{\Lambda_{31}}{x_1} - \frac{\Lambda_{33}}{x_3} \right), \quad (\text{A.3})$$

$$\Delta_{12} = (1 - x_1) \left( \frac{\Lambda_{12}}{x_2} - \frac{\Lambda_{13}}{x_3} \right) - x_1 \left( \frac{\Lambda_{22}}{x_2} - \frac{\Lambda_{23}}{x_3} + \frac{\Lambda_{32}}{x_2} - \frac{\Lambda_{33}}{x_3} \right), \quad (\text{A.4})$$

$$\Delta_{21} = (1 - x_2) \left( \frac{\Lambda_{21}}{x_1} - \frac{\Lambda_{23}}{x_3} \right) - x_2 \left( \frac{\Lambda_{11}}{x_1} - \frac{\Lambda_{13}}{x_3} + \frac{\Lambda_{31}}{x_1} - \frac{\Lambda_{33}}{x_3} \right), \quad (\text{A.5})$$

$$\Delta_{22} = (1 - x_2) \left( \frac{\Lambda_{22}}{x_2} - \frac{\Lambda_{23}}{x_3} \right) - x_2 \left( \frac{\Lambda_{12}}{x_2} - \frac{\Lambda_{13}}{x_3} + \frac{\Lambda_{32}}{x_2} - \frac{\Lambda_{33}}{x_3} \right). \quad (\text{A.6})$$

The matrix  $[\Delta]$  can be inverted to obtain the matrix  $[B]$

$$[B] = [\Delta]^{-1}. \quad (\text{A.7})$$

The MS diffusivities follow directly from the elements of matrix  $[B]$ <sup>23</sup>

$$\mathcal{D}_{13} = \frac{1}{B_{11} + (x_2/x_1)B_{12}}, \quad (\text{A.8})$$

$$\mathcal{D}_{12} = \frac{1}{B_{11} - ((x_1 + x_3)/x_1)B_{12}}, \quad (\text{A.9})$$

$$\mathcal{D}_{23} = \frac{1}{B_{22} + (x_1/x_2)B_{21}}. \quad (\text{A.10})$$

The final expression for the MS diffusivity  $\mathcal{D}_{12}$  is

$$\mathcal{D}_{12} = \frac{A + (x_1 + x_3)B/C}{x_1D}, \quad (\text{A.11})$$

in which  $x_i$  is the mole fraction of component  $i$  and the terms  $A$ ,  $B$ ,  $C$  and  $D$  are given by

$$\begin{aligned} A &= -\Lambda_{11}\Lambda_{23}x_2 - \Lambda_{12}x_3\Lambda_{21} + \Lambda_{11}x_3\Lambda_{22} - \Lambda_{11}x_3x_2\Lambda_{22} + \Lambda_{11}\Lambda_{23}x_2^2 - \Lambda_{11}x_3x_2\Lambda_{32} \\ &\quad + \Lambda_{11}\Lambda_{33}x_2^2 - \Lambda_{13}x_1\Lambda_{22} - x_1x_3\Lambda_{11}\Lambda_{22} + \Lambda_{13}\Lambda_{22}x_1^2 - x_1\Lambda_{31}x_3\Lambda_{22} + \Lambda_{33}x_1^2\Lambda_{22} \\ &\quad + \Lambda_{12}\Lambda_{23}x_1 + \Lambda_{12}x_3x_2\Lambda_{21} + \Lambda_{13}x_1x_2\Lambda_{22} + \Lambda_{12}x_3\Lambda_{31}x_2 + \Lambda_{13}x_2\Lambda_{21} - \Lambda_{13}x_2^2\Lambda_{21} \\ &\quad - \Lambda_{13}x_2^2\Lambda_{31} + x_1\Lambda_{12}x_3\Lambda_{21} - x_1^2\Lambda_{12}\Lambda_{23} + x_1\Lambda_{32}x_3\Lambda_{21} - x_1^2\Lambda_{32}\Lambda_{23} + \Lambda_{13}x_1x_2\Lambda_{32} \\ &\quad + x_1\Lambda_{11}\Lambda_{23}x_2 + x_1\Lambda_{31}\Lambda_{23}x_2 - \Lambda_{12}x_1\Lambda_{23}x_2 - \Lambda_{12}x_1\Lambda_{33}x_2 - x_1\Lambda_{13}x_2\Lambda_{21} \\ &\quad - x_1\Lambda_{33}x_2\Lambda_{21}, \\ B &= \Lambda_{12}x_3 - \Lambda_{13}x_2 - x_1x_3\Lambda_{12} + x_1x_2\Lambda_{23} - x_1x_3\Lambda_{32} + x_1x_2\Lambda_{33}, \end{aligned} \quad (\text{A.12})$$

$$\begin{aligned}
C &= -\Lambda_{11}\Lambda_{23}x_2 - \Lambda_{12}\Lambda_{21}x_3 + x_3\Lambda_{11}\Lambda_{22} - x_2x_3\Lambda_{11}\Lambda_{22} + \Lambda_{11}\Lambda_{23}x_2^2 - x_2x_3\Lambda_{11}\Lambda_{32} \\
&+ \Lambda_{11}\Lambda_{33}x_2^2 - \Lambda_{13}\Lambda_{22}x_1 - x_1x_3\Lambda_{11}\Lambda_{22} + x_1^2\Lambda_{13}\Lambda_{22} - x_1x_3\Lambda_{31}\Lambda_{22} + x_1^2\Lambda_{22}\Lambda_{33} \\
&+ x_1\Lambda_{12}\Lambda_{23} + x_2x_3\Lambda_{12}\Lambda_{21} + x_1x_2\Lambda_{13}\Lambda_{22} + x_2x_3\Lambda_{12}\Lambda_{31} + x_2\Lambda_{13}\Lambda_{21} - x_2^2\Lambda_{13}\Lambda_{21} \\
&- x_2^2\Lambda_{13}\Lambda_{31} + x_1x_3\Lambda_{12}\Lambda_{21} - x_1^2\Lambda_{12}\Lambda_{23} + x_1x_3\Lambda_{32}\Lambda_{21} - x_1^2\Lambda_{32}\Lambda_{23} + x_1x_2\Lambda_{13}\Lambda_{32} \\
&+ x_1x_2\Lambda_{11}\Lambda_{23} + x_1x_2\Lambda_{31}\Lambda_{23} - x_1x_2\Lambda_{12}\Lambda_{23} - x_1x_2\Lambda_{12}\Lambda_{33} - x_1x_2\Lambda_{13}\Lambda_{21} \\
&- x_1x_2\Lambda_{33}\Lambda_{21}, \\
D &= \Lambda_{22}x_3 - \Lambda_{23}x_2 - \Lambda_{22}x_3x_2 + \Lambda_{23}x_2^3 - x_2\Lambda_{12}x_3 + \Lambda_{13}x_2^2 - x_2\Lambda_{32}x_3 + \Lambda_{33}x_2^2.
\end{aligned}$$

The expression for  $\mathcal{D}_{13}$  and  $\mathcal{D}_{23}$  follow directly from a permutation of the component labels and can be found in the Supporting Information of Ref.<sup>34</sup>.

### A.3 Quaternary systems

In quaternary systems, a matrix  $[\Delta]$  is defined with elements following from the Onsager coefficients  $\Lambda_{ij}$ .<sup>23</sup>

$$\Delta_{11} = (1 - x_1) \left( \frac{\Lambda_{11}}{x_1} - \frac{\Lambda_{14}}{x_4} \right) - x_1 \left( \frac{\Lambda_{21}}{x_1} - \frac{\Lambda_{24}}{x_4} + \frac{\Lambda_{31}}{x_1} - \frac{\Lambda_{34}}{x_4} + \frac{\Lambda_{41}}{x_1} - \frac{\Lambda_{44}}{x_4} \right), \quad (\text{A.13})$$

$$\Delta_{12} = (1 - x_1) \left( \frac{\Lambda_{12}}{x_2} - \frac{\Lambda_{14}}{x_4} \right) - x_1 \left( \frac{\Lambda_{22}}{x_2} - \frac{\Lambda_{24}}{x_4} + \frac{\Lambda_{32}}{x_2} - \frac{\Lambda_{34}}{x_4} + \frac{\Lambda_{42}}{x_2} - \frac{\Lambda_{44}}{x_4} \right), \quad (\text{A.14})$$

$$\Delta_{13} = (1 - x_1) \left( \frac{\Lambda_{13}}{x_3} - \frac{\Lambda_{14}}{x_4} \right) - x_1 \left( \frac{\Lambda_{23}}{x_3} - \frac{\Lambda_{24}}{x_4} + \frac{\Lambda_{33}}{x_3} - \frac{\Lambda_{34}}{x_4} + \frac{\Lambda_{43}}{x_3} - \frac{\Lambda_{44}}{x_4} \right), \quad (\text{A.15})$$

$$\Delta_{21} = (1 - x_2) \left( \frac{\Lambda_{21}}{x_1} - \frac{\Lambda_{24}}{x_4} \right) - x_2 \left( \frac{\Lambda_{11}}{x_1} - \frac{\Lambda_{14}}{x_4} + \frac{\Lambda_{31}}{x_1} - \frac{\Lambda_{34}}{x_4} + \frac{\Lambda_{41}}{x_1} - \frac{\Lambda_{44}}{x_4} \right), \quad (\text{A.16})$$

$$\Delta_{22} = (1 - x_2) \left( \frac{\Lambda_{22}}{x_2} - \frac{\Lambda_{24}}{x_4} \right) - x_2 \left( \frac{\Lambda_{12}}{x_2} - \frac{\Lambda_{14}}{x_4} + \frac{\Lambda_{32}}{x_2} - \frac{\Lambda_{34}}{x_4} + \frac{\Lambda_{42}}{x_2} - \frac{\Lambda_{44}}{x_4} \right), \quad (\text{A.17})$$

$$\Delta_{23} = (1 - x_2) \left( \frac{\Lambda_{23}}{x_3} - \frac{\Lambda_{24}}{x_4} \right) - x_2 \left( \frac{\Lambda_{13}}{x_3} - \frac{\Lambda_{14}}{x_4} + \frac{\Lambda_{33}}{x_3} - \frac{\Lambda_{34}}{x_4} + \frac{\Lambda_{43}}{x_3} - \frac{\Lambda_{44}}{x_4} \right), \quad (\text{A.18})$$

$$\Delta_{31} = (1 - x_3) \left( \frac{\Lambda_{31}}{x_1} - \frac{\Lambda_{34}}{x_4} \right) - x_3 \left( \frac{\Lambda_{11}}{x_1} - \frac{\Lambda_{14}}{x_4} + \frac{\Lambda_{21}}{x_1} - \frac{\Lambda_{24}}{x_4} + \frac{\Lambda_{41}}{x_1} - \frac{\Lambda_{44}}{x_4} \right), \quad (\text{A.19})$$

$$\Delta_{32} = (1 - x_3) \left( \frac{\Lambda_{32}}{x_2} - \frac{\Lambda_{34}}{x_4} \right) - x_3 \left( \frac{\Lambda_{12}}{x_2} - \frac{\Lambda_{14}}{x_4} + \frac{\Lambda_{22}}{x_2} - \frac{\Lambda_{24}}{x_4} + \frac{\Lambda_{42}}{x_2} - \frac{\Lambda_{44}}{x_4} \right), \quad (\text{A.20})$$

$$\Delta_{33} = (1 - x_3) \left( \frac{\Lambda_{33}}{x_3} - \frac{\Lambda_{34}}{x_4} \right) - x_3 \left( \frac{\Lambda_{13}}{x_3} - \frac{\Lambda_{14}}{x_4} + \frac{\Lambda_{23}}{x_3} - \frac{\Lambda_{24}}{x_4} + \frac{\Lambda_{43}}{x_3} - \frac{\Lambda_{44}}{x_4} \right). \quad (\text{A.21})$$

By inverting  $[\Delta]$ , we obtain the matrix  $[B]$

$$[B] = [\Delta]^{-1}. \quad (\text{A.22})$$

The MS diffusivities follow from the elements of matrix  $[B]$ <sup>23</sup>

$$\mathcal{D}_{14} = \frac{1}{B_{11} + (x_2/x_1)B_{12} + (x_3/x_1)B_{13}}, \quad (\text{A.23})$$

$$\mathcal{D}_{24} = \frac{1}{B_{22} + (x_1/x_2)B_{21} + (x_3/x_2)B_{23}}, \quad (\text{A.24})$$

$$\mathcal{D}_{34} = \frac{1}{B_{33} + (x_1/x_3)B_{31} + (x_2/x_3)B_{32}}, \quad (\text{A.25})$$

$$\mathcal{D}_{12} = \frac{1}{1/\mathcal{D}_{24} - B_{21}/x_2}, \quad (\text{A.26})$$

$$\mathcal{D}_{13} = \frac{1}{1/\mathcal{D}_{14} - B_{13}/x_1}, \quad (\text{A.27})$$

$$\mathcal{D}_{23} = \frac{1}{1/\mathcal{D}_{24} - B_{23}/x_2}. \quad (\text{A.28})$$



# **B**

---

## **Obtaining a Darken Equation for Multicomponent Systems**

---

MD simulations can be used to directly compute MS diffusivities  $D_{ij}$  from local fluctuations using linear response theory<sup>17;18;20</sup>. First, the so-called Onsager coefficients  $\Lambda_{ij}$  can be obtained from MD trajectories, see section 2.3 and appendix A. We express  $\Lambda_{ii}$  as<sup>34</sup>

$$\begin{aligned}\Lambda_{ii} &= \frac{1}{3N} \int_0^\infty dt' \left\langle \sum_{l=1}^{N_i} v_{l,i}(t) \cdot \sum_{g=1}^{N_i} v_{g,i}(t+t') \right\rangle \\ &= \frac{1}{3N} \int_0^\infty dt' \left\langle \sum_{l=1}^{N_i} v_{l,i}(t) \cdot v_{l,i}(t+t') \right\rangle +\end{aligned}\quad (\text{B.1})$$

$$\begin{aligned}&\frac{1}{3N} \int_0^\infty dt' \left\langle \sum_{l=1}^{N_i} \sum_{g=1, g \neq l}^{N_i} v_{l,i}(t) \cdot v_{g,i}(t+t') \right\rangle \\ &\approx x_i C_{ii} + x_i^2 N C_{ii}^*,\end{aligned}\quad (\text{B.2})$$

in which  $x_i = N_i/N$  and  $C_{ii}$  and  $C_{ii}^*$  account for self- and cross correlations of the velocities of molecules of type  $i$ , respectively. For  $\Lambda_{ij}$  with  $i \neq j$ , *i.e.* correlations between unlike molecules, we can write<sup>34</sup>

$$\begin{aligned}\Lambda_{ij} &= \frac{1}{3N} \int_0^\infty dt' \left\langle \sum_{l=1}^{N_i} v_{l,i}(t) \cdot \sum_{k=1}^{N_j} v_{k,j}(t+t') \right\rangle \\ &\approx \frac{N_i N_j}{3N} \int_0^\infty dt' \langle v_{1,i}(t) \cdot v_{1,j}(t+t') \rangle \\ &= N x_i x_j C_{ij}.\end{aligned}\quad (\text{B.3})$$

It is important to note that all elements of the matrix  $[\Lambda]$  are intensive so  $C_{ij, i \neq j}$  and  $C_{ii}^*$  scale with  $1/N^2$ . As is shown in section 4.2,  $C_{ii}$  follows from the self-diffusivity of component  $i$ :

$$C_{ii} = D_{i,\text{self}}. \quad (\text{B.4})$$

## B.1 Binary systems

In binary systems, the MS diffusivity equals<sup>23</sup>



$$\mathcal{D}_{12} = \frac{x_2}{x_1}\Lambda_{11} + \frac{x_1}{x_2}\Lambda_{22} - 2\Lambda_{12}. \quad (\text{B.5})$$

Inserting Eqs. (B.2) and (B.3) into Eq. (B.5) we obtain

$$\mathcal{D}_{12} = x_2C_{11} + x_1C_{22} + x_1x_2N(C_{11}^* + C_{22}^* - 2C_{12}). \quad (\text{B.6})$$

Following Schoen and Hoheisel<sup>92</sup>, we assume that cross-correlations are much smaller than self-correlations<sup>34</sup>, *i.e.*

$$x_1x_2N(C_{11}^* + C_{22}^* - 2C_{12}) \ll x_2C_{11} + x_1C_{22}. \quad (\text{B.7})$$

This directly results in the well-known Darken equation for binary systems<sup>54</sup>

$$\mathcal{D}_{12} = x_2C_{11} + x_1C_{22} = x_2D_{1,\text{self}} + x_1D_{2,\text{self}}. \quad (\text{B.8})$$

## B.2 Ternary systems

In ternary systems, the MS diffusivity  $\mathcal{D}_{12}$  is given by Eq. (A.11). Inserting Eqs. (B.2) and (B.3) into Eq. (A.11), we obtain

$$\mathcal{D}_{12} = \frac{BD}{AD - CB}, \quad (\text{B.9})$$

with the terms  $A, B, C, D$  defined as

$$\begin{aligned}
A &= -C_{22} - x_2 NC_{22}^* + Nx_2 C_{23} + x_2 C_{22} + x_2^2 NC_{22}^* - x_2^2 NC_{23} + Nx_1 x_2 C_{12} \\
&\quad - Nx_1 x_2 C_{13} + Nx_2 x_3 C_{23} - x_2 C_{33} - x_2 x_3 NC_{33}^*, \\
B &= -C_{11} C_{22} + x_2 C_{11} C_{22} - x_2 C_{11} C_{33} + x_1 C_{11} C_{22} - x_1 C_{22} C_{33} + x_1 x_2 NC_{11}^* C_{22} \\
&\quad - x_1 NC_{11}^* C_{22} - x_1 x_2^2 N^2 C_{12}^2 + x_1 x_2 N^2 C_{12} - x_1 x_2 NC_{11}^* C_{33} + x_1^2 NC_{11}^* C_{22} \\
&\quad + 2x_1 x_2 NC_{12} C_{33} - x_1^2 x_2 N^2 C_{12}^2 - x_2^2 NC_{11} C_{23} - x_1 x_2^2 N^2 C_{11}^* C_{23} + x_1^2 x_2 N^2 C_{11}^* C_{22}^* \\
&\quad - x_1 x_2 NC_{13} C_{22} + x_1 x_2^2 N^2 C_{12} C_{23} + x_1 x_2^2 N^2 C_{12} C_{13} - x_2 NC_{11} C_{22}^* - x_1 x_2 N^2 C_{12} C_{23} \\
&\quad + x_2 NC_{11} C_{23} + x_2^2 NC_{11} C_{22}^* - x_1 x_2 N^2 C_{11}^* C_{22}^* + x_1 x_2 N^2 C_{11}^* C_{23} + x_1 x_2^2 N^2 C_{11}^* C_{22}^* \\
&\quad + x_1 x_2 x_3 N^2 C_{11}^* C_{23} - x_1 x_2 x_3 N^2 C_{11}^* C_{33}^* + x_1 x_2 N^2 C_{13} C_{22}^* - x_1 x_2^2 N^2 C_{13} C_{22}^* \\
&\quad + x_1^2 x_2 N^2 C_{12} C_{13} + 2x_1 x_2 x_3 N^2 C_{13} C_{23} + x_1 x_2 NC_{11} C_{22}^* - x_1 x_2 NC_{11} C_{23} \\
&\quad - x_1^2 x_2 N^2 C_{11}^* C_{23} - x_1^2 x_2 N^2 C_{13} C_{22}^* + x_1 x_2 x_3 N^2 C_{13} C_{22}^* - x_1 x_2 C_{22}^* C_{33} \\
&\quad - x_1 x_2 x_3 N^2 C_{22}^* C_{33}^* + x_1 NC_{13} C_{22} - x_1^2 NC_{13} C_{22} + x_2 x_3 NC_{11} C_{23} - x_2 x_3 NC_{11} C_{33}^* \\
&\quad + x_1 x_3 NC_{13} C_{22} - x_1 x_3 NC_{22} C_{33}^* + x_1 x_2 x_3 N^2 C_{13}^2 - x_1 x_2 N^2 C_{12} C_{23} - x_1 x_2 N^2 C_{12} C_{13} \\
&\quad + x_1 x_2 x_3 N^2 C_{23}^2 - x_1 x_2 x_3 N^2 C_{12} C_{13} + 2x_1 x_2 x_3 N^2 C_{12} C_{33}^* + x_1^2 x_2 N^2 C_{12} C_{23}, \\
C &= (x_1 + x_3)(-NC_{12} + NC_{13} + x_1 NC_{12} - x_1 NC_{13} + C_{22} + x_2 C_{22}^* - C_{33} - x_3 NC_{33}^*), \\
D &= -C_{11} C_{22} + x_2 C_{11} C_{22} - x_2 C_{11} C_{33} + x_1 C_{11} C_{22} - x_1 C_{22} C_{33} + x_1 x_2 NC_{11}^* C_{22} \\
&\quad - x_1 NC_{11}^* C_{22} - x_1 x_2^2 N^2 C_{12}^2 + x_1 x_2 N^2 C_{12}^2 - x_1 x_2 NC_{11}^* C_{33} + x_1^2 NC_{11}^* C_{22} \\
&\quad + 2x_1 x_2 NC_{12} C_{33} - x_1^2 x_2 N^2 C_{12}^2 - x_2^2 NC_{11} C_{23} - x_1 x_2^2 N^2 C_{11}^* C_{23} - x_1 x_2 NC_{13} C_{22} \\
&\quad + x_1 x_2^2 N^2 C_{12} C_{23} + x_1 x_2^2 N^2 C_{12} C_{13} - x_2 NC_{11} C_{22}^* - x_2 C_{11} C_{22}^* + x_2 NC_{11} C_{23} \\
&\quad + x_2^2 NC_{11} C_{22}^* - x_1 x_2 N^2 C_{11}^* C_{22}^* + x_1 x_2 N^2 C_{11}^* C_{23} + x_1 x_2^2 N^2 C_{11}^* C_{22}^* + x_1 x_2 x_3 N^2 C_{11}^* C_{23} \\
&\quad - x_1 x_2 x_3 N^2 C_{11}^* C_{33}^* + x_1 x_2 N^2 C_{22}^* C_{13} - x_1 x_2^2 N^2 C_{13} C_{22}^* + x_1^2 x_2 N^2 C_{13} C_{12} \\
&\quad - 2x_1 x_2 x_3 N^2 C_{13} C_{23} + x_1 x_2 NC_{11} C_{22}^* - x_1 x_2 NC_{11} C_{23} + x_1^2 x_2 N^2 C_{11}^* C_{22}^* - x_1^2 x_2 N^2 C_{11}^* C_{23} \\
&\quad - x_1^2 x_2 N^2 C_{13} C_{22}^* + x_1 x_2 x_3 N^2 C_{13} C_{22}^* - x_1 x_2 NC_{22}^* C_{33} - x_1 x_2 x_3 N^2 C_{22}^* C_{33}^* + x_1 NC_{13} C_{22} \\
&\quad - x_1^2 NC_{13} C_{22} + x_2 x_3 NC_{11} C_{23} - x_2 x_3 NC_{11} C_{33}^* + x_1 x_3 NC_{13} C_{22} - x_1 x_3 NC_{22} C_{33}^* \\
&\quad + x_1 x_2 x_3 N^2 C_{13}^2 - x_1 x_2 N^2 C_{12} C_{23} - x_1 x_2 N^2 C_{12} C_{13} + x_1 x_2 x_3 N^2 C_{23}^2 - x_1 x_2 x_3 N^2 C_{12} C_{13} \\
&\quad + 2x_1 x_2 x_3 N^2 C_{12} C_{33}^* + x_1^2 x_2 N^2 C_{12} C_{23} - x_1 x_2 x_3 N^2 C_{12} C_{23}.
\end{aligned}$$

By assuming that the leading terms in these equations are of the type  $C_{ii}$ <sup>34</sup>, we finally

obtain

$$\begin{aligned}
 \mathcal{D}_{12} &= \frac{x_1 C_{22} C_{33} + x_2 C_{11} C_{33} + x_3 C_{11} C_{22}}{C_{33}}, \\
 &= C_{11} C_{22} \left( \frac{x_1}{C_{11}} + \frac{x_2}{C_{22}} + \frac{x_3}{C_{33}} \right), \\
 &= D_{1,\text{self}} D_{2,\text{self}} \left( \frac{x_1}{D_{1,\text{self}}} + \frac{x_2}{D_{2,\text{self}}} + \frac{x_3}{D_{3,\text{self}}} \right). \tag{B.10}
 \end{aligned}$$

### B.3 Quaternary systems

MS diffusivities in quaternary systems follow from the Onsager coefficients according to Eqs. (A.13)-(A.28). Using these equations, it is possible to obtain an expression for  $\mathcal{D}_{12}$  in terms of  $C_{ii}$ ,  $C_{ii}^*$  and  $C_{ij,j \neq i}$  in which  $i, j = 1, 2, 3, 4$ . By assuming that the leading terms in these equations are of the type  $C_{ii}$ <sup>34</sup>, we finally obtain

$$\begin{aligned}
 \mathcal{D}_{12} &= C_{11} C_{22} \left( \frac{x_1}{C_{11}} + \frac{x_2}{C_{22}} + \frac{x_3}{C_{33}} + \frac{x_4}{C_{44}} \right), \\
 &= D_{1,\text{self}} D_{2,\text{self}} \left( \frac{x_1}{D_{1,\text{self}}} + \frac{x_2}{D_{2,\text{self}}} + \frac{x_3}{D_{3,\text{self}}} + \frac{x_4}{D_{4,\text{self}}} \right). \tag{B.11}
 \end{aligned}$$



**C**

---

**Additional Data for Chapter 3**

---

**Table C.1:** Computed values of self- and MS diffusivities in ternary mixtures in which particles interact with a WCA potential. We consider the case that components 1 and 2 are diluted in component 3. All reported values are in reduced units. In all cases, the total number of molecules is 400. The statistical errors in the computed diffusivities are less than 3%.

		Self-diffusivity			MS Diffusivity		
		$D_{1,\text{self}}$	$D_{2,\text{self}}$	$D_{3,\text{self}}$	$\mathcal{D}_{13}$	$\mathcal{D}_{23}$	$\mathcal{D}_{12}$
Number Density <sup>a</sup>	0.1	2.375	1.980	1.108	2.315	2.010	3.294
	0.2	1.042	0.896	0.648	1.009	0.876	1.411
	0.5	0.256	0.245	0.199	0.251	0.244	0.318
	0.7	0.133	0.116	0.103	0.122	0.111	0.144
	0.8	0.085	0.083	0.072	0.086	0.081	0.094
Mass of Species 3 <sup>b</sup>	5	1.042	0.896	0.648	1.009	0.876	1.411
	50	0.793	0.677	0.210	0.761	0.666	2.692
	100	0.758	0.645	0.148	0.738	0.623	3.348
	500	0.738	0.595	0.066	0.713	0.585	6.238
	2500	0.795	0.661	0.028	0.734	0.637	17.609
$\rho = 0.2$	5000	0.958	0.809	0.018	0.898	0.766	41.794
	5	0.256	0.245	0.199	0.251	0.244	0.318
	10	0.208	0.187	0.142	0.203	0.182	0.270
	50	0.125	0.117	0.065	0.133	0.124	0.218
	100	0.086	0.085	0.046	0.086	0.084	0.172
Mass of Species 3 <sup>c</sup>	1/3	0.255	0.246	0.198	0.251	0.242	0.318
	1	0.256	0.245	0.199	0.251	0.244	0.318
	3	0.256	0.246	0.199	0.252	0.246	0.318
Ratio of $x_1/x_2$ <sup>d</sup> with $x_3 = 0.95$	1/3	0.256	0.246	0.199	0.252	0.244	0.318
	1	0.254	0.246	0.198	0.251	0.244	0.318
	3	0.254	0.244	0.199	0.251	0.242	0.319
Ratio of $x_1/x_2$ <sup>e</sup> with $x_3 = 0.97$	1/3	0.256	0.246	0.199	0.252	0.244	0.318
	1	0.254	0.246	0.198	0.251	0.244	0.318
	3	0.254	0.244	0.199	0.251	0.242	0.319

<sup>a</sup>  $M_1 = 1; M_2 = 1.5; M_3 = 5; x_1/x_2 = 1; x_3 = 0.95; T = 2$

<sup>b</sup>  $\rho = 0.2; M_1 = 1; M_2 = 1.5; x_1/x_2 = 1; x_3 = 0.95; T = 2$

<sup>c</sup>  $\rho = 0.5; M_1 = 1; M_2 = 1.5; x_1/x_2 = 1; x_3 = 0.95; T = 2$

<sup>d</sup>  $\rho = 0.5; M_1 = 1; M_2 = 1.5; M_3 = 5; x_3 = 0.95; T = 2$

<sup>e</sup>  $\rho = 0.5; M_1 = 1; M_2 = 1.5; M_3 = 5; x_3 = 0.97; T = 2$

**Table C.2:** Computed values for  $C_{ij}$  for a system with WCA interactions, see Eqs. (3.3) to (3.8). We consider the case that components 1 and 2 are diluted in component 3. All reported values are in reduced units. In all cases, the total number of molecules is 400. The statistical errors in the computed values of  $C_{ij}$  are less than 3%.

		$C_{11}$ / $10^{-1}$	$C_{22}$ / $10^{-1}$	$C_{33}$ / $10^{-1}$	$C_{12}$ / $10^{-4}$	$C_{13}$ / $10^{-4}$	$C_{23}$ / $10^{-4}$	$C_{33}^*$ / $10^{-3}$	$C_x$ / $10^{-2}$
Number Density <sup>a</sup>	0.1	23.7	20.5	14.1	9.7	-11.4	-16.6	-3.7	3.2
	0.2	10.0	8.9	6.5	2.7	-5.4	-7.9	-1.7	-3.6
	0.5	2.5	2.5	2.0	2.1	-1.0	-2.0	-0.5	-0.8
	0.7	1.2	1.1	1.0	0.9	-0.8	-0.8	-0.3	-1.2
	0.8	0.9	0.8	0.7	0.1	-0.4	-0.6	-0.2	0.2
Mass of Species 3 <sup>b</sup>	5	10.0	8.9	6.5	2.7	-5.4	-7.9	-1.7	-3.6
	50	7.9	6.9	2.1	4.2	-0.4	-0.5	-0.6	-1.5
	100	7.7	6.5	1.5	3.3	-0.2	-0.2	-0.4	-0.6
	500	7.5	6.1	0.7	1.7	0.0	0.0	-0.2	0.4
Mass of Species 3 <sup>c</sup>	5	2.5	2.5	2.0	2.1	-1.0	-2.0	-0.5	-0.8
	10	2.1	1.9	1.4	2.4	-0.6	-0.6	-0.4	-0.4
	50	1.4	1.3	0.7	1.8	-0.1	-0.1	-0.2	1.3
	100	0.9	0.9	0.5	1.1	0.0	0.0	-0.1	-0.3
Ratio of $x_1/x_2$ <sup>d</sup>	1/3	2.5	2.4	2.0	1.3	-1.7	-1.9	-0.5	-1.2
	1	2.5	2.5	2.0	2.1	-1.0	-2.0	-0.5	-0.8
	with $x_3 = 0.95$	3	2.5	2.4	2.0	1.6	-1.6	-1.6	-0.5
Ratio of $x_1/x_2$ <sup>e</sup>	1/3	2.5	2.4	2.0	1.3	-1.7	-1.9	-0.5	-1.2
	1	2.5	2.5	2.0	1.8	-1.3	-1.9	-0.5	-1.1
	with $x_3 = 0.97$	3	2.5	2.4	2.0	1.8	-1.3	-1.9	-0.5

<sup>a</sup>  $M_1 = 1; M_2 = 1.5; M_3 = 5; x_1/x_2 = 1; x_3 = 0.95; T = 2$

<sup>b</sup>  $\rho = 0.2; M_1 = 1; M_2 = 1.5; x_1/x_2 = 1; x_3 = 0.95; T = 2$

<sup>c</sup>  $\rho = 0.5; M_1 = 1; M_2 = 1.5; x_1/x_2 = 1; x_3 = 0.95; T = 2$

<sup>d</sup>  $\rho = 0.5; M_1 = 1; M_2 = 1.5; M_3 = 5; x_3 = 0.95; T = 2$

<sup>e</sup>  $\rho = 0.5; M_1 = 1; M_2 = 1.5; M_3 = 5; x_3 = 0.97; T = 2$

**Table C.3:** Computed self- and MS diffusivities for binary mixtures in which the particles interact with a WCA potential. We consider the case that component  $i$  is diluted in component  $j$  (10 molecules of  $i$ , 390 molecules of  $j$ ). All reported values are in reduced units. The statistical errors in the computed diffusivities are less than 3%.

$i - j^a$	$D_{i,\text{self}}$	$D_{j,\text{self}}$	$\mathcal{D}_{ij}$
1 - 2	1.279	1.158	1.279
2 - 1	1.314	1.414	1.314
1 - 3	1.032	0.638	1.032
2 - 3	0.879	0.640	0.879
$i - j^b$	$D_{i,\text{self}}$	$D_{j,\text{self}}$	$\mathcal{D}_{ij}$
1 - 2	0.365	0.355	0.365
2 - 1	0.414	0.431	0.414
1 - 3	0.255	0.196	0.255
2 - 3	0.241	0.201	0.241
$i - j^c$	$D_{i,\text{self}}$	$D_{j,\text{self}}$	$\mathcal{D}_{ij}$
1 - 2	1.279	1.158	1.279
2 - 1	1.314	1.414	1.314
1 - 3	0.725	0.145	0.725
2 - 3	0.641	0.145	0.641
$i - j^d$	$D_{i,\text{self}}$	$D_{j,\text{self}}$	$\mathcal{D}_{ij}$
1 - 2	0.365	0.355	0.365
2 - 1	0.414	0.431	0.414
1 - 3	0.086	0.045	0.101
2 - 3	0.085	0.044	0.100

<sup>a</sup>  $\rho = 0.2$ ;  $M_1 = 1$ ;  $M_2 = 1.5$ ;  $M_3 = 5$ ;  $T = 2$

<sup>b</sup>  $\rho = 0.5$ ;  $M_1 = 1$ ;  $M_2 = 1.5$ ;  $M_3 = 5$ ;  $T = 2$

<sup>c</sup>  $\rho = 0.2$ ;  $M_1 = 1$ ;  $M_2 = 1.5$ ;  $M_3 = 100$ ;  $T = 2$

<sup>d</sup>  $\rho = 0.5$ ;  $M_1 = 1$ ;  $M_2 = 1.5$ ;  $M_3 = 100$ ;  $T = 2$



**Table C.4:** Computed self- and MS diffusivities in ternary mixtures of n-hexane(1)-cyclohexane(2)-toluene(3) at 298 K, 1 atm. The statistical errors in the computed diffusivities are less than 5%.

	Self-diffusivity/( $10^{-9} \text{ m}^2\text{s}^{-1}$ )			MS diffusivity/( $10^{-9} \text{ m}^2\text{s}^{-1}$ )		
$x_1 \rightarrow 1^a$	$D_{1,\text{self}}$ 5.50	$D_{2,\text{self}}$ 4.30	$D_{3,\text{self}}$ 4.84	$\bar{D}_{12}$ 4.19	$\bar{D}_{13}$ 4.42	$\bar{D}_{23}$ 4.07
$x_2 \rightarrow 1^b$	$D_{1,\text{self}}$ 2.63	$D_{2,\text{self}}$ 2.05	$D_{3,\text{self}}$ 2.10	$\bar{D}_{12}$ 2.56	$\bar{D}_{23}$ 2.10	$\bar{D}_{13}$ 2.19
$x_3 \rightarrow 1^c$	$D_{1,\text{self}}$ 2.98	$D_{2,\text{self}}$ 2.73	$D_{3,\text{self}}$ 2.89	$\bar{D}_{13}$ 2.89	$\bar{D}_{23}$ 2.68	$\bar{D}_{12}$ 2.99

<sup>a</sup> 598 n-hexane molecules; 1 cyclohexane molecule; 1 toluene molecule

<sup>b</sup> 1 n-hexane molecule; 598 cyclohexane molecules; 1 toluene molecule

<sup>c</sup> 1 n-hexane molecule; 1 cyclohexane molecule; 598 toluene molecules

**Table C.5:** Computed values for  $C_{ij}/(\text{m}^2\text{s}^{-1})$  for the system n-hexane(1)-cyclohexane(2)-toluene(3) system at 298 K and 1 atm., see Eqs. (3.3) to (3.8). The statistical errors in the computed diffusivities are less than 5%.

$x_1 \rightarrow 1^a$	$C_{11}$ / $10^{-9}$ 5.50	$C_{22}$ / $10^{-9}$ 4.28	$C_{33}$ / $10^{-9}$ 4.84	$C_{12}$ / $10^{-11}$ -0.45	$C_{13}$ / $10^{-11}$ -0.51	$C_{23}$ / $10^{-11}$ 3.96	$C_{11}^*$ / $10^{-11}$ -5.40	$C_x$ / $10^{-10}$ -4.76
$x_2 \rightarrow 1^b$	$C_{11}$ / $10^{-9}$ 2.56	$C_{22}$ / $10^{-9}$ 2.10	$C_{33}$ / $10^{-9}$ 2.10	$C_{12}$ / $10^{-11}$ -0.02	$C_{13}$ / $10^{-11}$ 0.38	$C_{23}$ / $10^{-11}$ 0.0	$C_{22}^*$ / $10^{-11}$ -0.35	$C_x$ / $10^{-10}$ 3.33
$x_3 \rightarrow 1^c$	$C_{11}$ / $10^{-9}$ 2.92	$C_{22}$ / $10^{-9}$ 2.68	$C_{33}$ / $10^{-9}$ 2.89	$C_{12}$ / $10^{-11}$ 0.05	$C_{13}$ / $10^{-11}$ -0.02	$C_{23}$ / $10^{-11}$ -0.38	$C_{33}^*$ / $10^{-11}$ -0.48	$C_x$ / $10^{-10}$ -2.20

<sup>a</sup> 598 n-hexane molecules; 1 cyclohexane molecule; 1 toluene molecule

<sup>b</sup> 1 n-hexane molecule; 598 cyclohexane molecules; 1 toluene molecule

<sup>c</sup> 1 n-hexane molecule; 1 cyclohexane molecule; 598 toluene molecules

**Table C.6:** Computed MS diffusivities in ternary mixtures of methanol(1)-ethanol(2)-water(3) at 298 K, 1 atm. The statistical errors in computed diffusivities are less than 5%.

	Self-diffusivity/( $10^{-9} \text{ m}^2\text{s}^{-1}$ )			MS diffusivity/( $10^{-9} \text{ m}^2\text{s}^{-1}$ )		
$x_1 \rightarrow 1^a$	$D_{1,\text{self}}$ 1.01	$D_{2,\text{self}}$ 1.73	$D_{3,\text{self}}$ 0.91	$\bar{D}_{12}$ 1.71	$\bar{D}_{13}$ 0.91	$\bar{D}_{23}$ 2.68
$x_2 \rightarrow 1^b$	$D_{1,\text{self}}$ 1.84	$D_{2,\text{self}}$ 2.03	$D_{3,\text{self}}$ 2.29	$\bar{D}_{12}$ 1.84	$\bar{D}_{23}$ 2.31	$\bar{D}_{13}$ 3.24
$x_3 \rightarrow 1^c$	$D_{1,\text{self}}$ 1.55	$D_{2,\text{self}}$ 1.89	$D_{3,\text{self}}$ 2.78	$\bar{D}_{13}$ 1.54	$\bar{D}_{23}$ 1.90	$\bar{D}_{12}$ 4.76

<sup>a</sup> 168 ethanol molecules; 1 methanol molecule; 1 water molecule

<sup>b</sup> 1 ethanol molecule; 248 methanol molecules; 1 water molecule

<sup>c</sup> 1 ethanol molecule; 1 methanol molecule; 598 water molecules

**Table C.7:** Computed values for  $C_{ij}/(\text{m}^2\text{s}^{-1})$  for the system ethanol(1)-methanol(2)-water(3) at 298 K, 1 atm., see Eqs. (3.3) to (3.8). The statistical errors in the computed values are less than 5%.

$x_1 \rightarrow 1^a$	$C_{11}$ / $10^{-9}$ 1.01	$C_{22}$ / $10^{-9}$ 1.72	$C_{33}$ / $10^{-9}$ 0.92	$C_{12}$ / $10^{-11}$ 0.00	$C_{13}$ / $10^{-11}$ 0.00	$C_{23}$ / $10^{-11}$ 0.33	$C_{11}^*$ / $10^{-12}$ -5.96	$C_x$ / $10^{-10}$ -4.17
$x_2 \rightarrow 1^b$	$C_{11}$ / $10^{-9}$ 1.83	$C_{22}$ / $10^{-9}$ 2.03	$C_{33}$ / $10^{-9}$ 2.32	$C_{12}$ / $10^{-11}$ -1.25	$C_{13}$ / $10^{-11}$ -1.09	$C_{23}$ / $10^{-11}$ -0.36	$C_{22}^*$ / $10^{-12}$ -8.04	$C_x$ / $10^{-10}$ -6.95
$x_3 \rightarrow 1^c$	$C_{11}$ / $10^{-9}$ 1.53	$C_{22}$ / $10^{-9}$ 1.89	$C_{33}$ / $10^{-9}$ 2.78	$C_{12}$ / $10^{-11}$ -1.20	$C_{13}$ / $10^{-11}$ -0.71	$C_{23}$ / $10^{-11}$ -0.58	$C_{33}^*$ / $10^{-12}$ -4.58	$C_x$ / $10^{-9}$ -2.20

<sup>a</sup> 168 ethanol molecules; 1 methanol molecule; 1 water molecule

<sup>b</sup> 1 ethanol molecule; 248 methanol molecules; 1 water molecule

<sup>c</sup> 1 ethanol molecule; 1 methanol molecule; 598 water molecules

**Table C.8:** Computed self-diffusivities (in units of  $10^{-9} \text{ m}^2\text{s}^{-1}$ ) for binary mixtures containing ethanol, methanol and/or water. Component  $i$  is diluted in component  $j$ , so  $\mathcal{D}_{ij} = D_{i,\text{self}}$ . Here, “1”: ethanol; “2”: methanol; “3”: water. The statistical errors in the computed diffusivities are less than 5%.

$i - j$	$D_{i,\text{self}}$	$D_{j,\text{self}}$	$\mathcal{D}_{ij}$
1 - 2 <sup>a</sup>	1.83	2.00	1.83
2 - 1 <sup>b</sup>	1.73	1.01	1.73
1 - 3 <sup>c</sup>	1.57	2.79	1.57
3 - 1 <sup>d</sup>	0.91	1.02	0.91
2 - 3 <sup>e</sup>	1.88	2.78	1.88
3 - 2 <sup>f</sup>	2.28	2.02	2.28

<sup>a</sup> 1 ethanol molecule; 249 methanol molecules

<sup>b</sup> 169 ethanol molecules; 1 methanol molecule

<sup>c</sup> 1 ethanol molecule; 599 water molecules

<sup>d</sup> 169 ethanol molecules; 1 water molecule

<sup>e</sup> 1 methanol molecule; 599 water molecules

<sup>f</sup> 249 methanol molecules; 1 water molecule



**D**

---

**Additional Data for Chapter 4**

---

**Table D.1:** Computed and predicted MS diffusivities in ternary mixtures in which particles interact with a WCA potential. All reported quantities are in reduced units. Simulation details:  $\rho = 0.2$ ;  $M_1 = 1$ ;  $M_2 = 5$ ;  $M_3 = 10$ ;  $T = 2$ ;  $N = 400$ . The statistic errors of computed diffusivities are less than 5%.

$x_1$	$x_2$	$D_{ij}$	MD	Multicomp. Darken		Darken-LBV		Vignes-LBV		Generalized Darken	
				Eq. (4.12) <sup>a</sup>	AD <sup>b</sup>	Eq. (4.12) <sup>c</sup>	AD	Eq. (4.4)	AD	Eq. (4.6) <sup>d</sup>	AD
0.2	0.32	$D_{12}$	1.01	1.01	0%	1.01	0%	1.06	5%	0.80	21%
		$D_{13}$	0.93	0.88	5%	0.87	6%	0.93	0%	0.81	13%
		$D_{23}$	0.55	0.55	0%	0.55	0%	0.61	11%	0.55	0%
0.2	0.48	$D_{12}$	1.03	1.00	3%	1.00	3%	1.05	2%	0.85	17%
		$D_{13}$	0.97	0.88	9%	0.87	10%	0.92	5%	0.79	19%
		$D_{23}$	0.57	0.56	2%	0.56	2%	0.61	7%	0.55	4%
0.4	0.36	$D_{12}$	1.04	0.98	6%	0.99	5%	1.08	4%	0.80	23%
		$D_{13}$	1.00	0.88	12%	0.87	13%	0.96	4%	0.71	29%
		$D_{23}$	0.58	0.59	2%	0.59	2%	0.67	16%	0.58	0%
0.4	0.48	$D_{12}$	1.09	0.98	10%	0.99	9%	1.07	2%	0.85	22%
		$D_{13}$	1.04	0.90	13%	0.87	16%	0.96	8%	0.68	35%
		$D_{23}$	0.59	0.61	3%	0.60	2%	0.68	15%	0.60	2%
0.6	0.08	$D_{12}$	1.07	0.99	7%	1.00	7%	1.12	5%	0.68	36%
		$D_{13}$	1.05	0.90	14%	1.01	4%	0.70	33%	0.70	33%
		$D_{23}$	0.58	0.62	7%	0.74	28%	0.62	7%	0.62	7%
0.6	0.24	$D_{12}$	1.14	1.00	12%	1.00	12%	1.11	3%	0.78	32%
		$D_{13}$	1.10	0.92	16%	0.89	19%	1.01	8%	0.69	37%
		$D_{23}$	0.59	0.65	10%	0.64	8%	0.75	27%	0.64	8%
0.8	0.04	$D_{12}$	1.13	1.07	5%	1.04	8%	1.15	2%	0.76	33%
		$D_{13}$	1.11	1.01	9%	0.94	15%	1.06	5%	0.73	34%
		$D_{23}$	0.60	0.77	28%	0.71	18%	0.83	38%	0.72	20%
0.8	0.16	$D_{12}$	1.16	1.06	9%	1.06	9%	1.14	2%	0.88	24%
		$D_{13}$	1.12	1.01	10%	0.97	13%	1.05	6%	0.77	31%
		$D_{23}$	0.61	0.77	26%	0.74	21%	0.83	36%	0.77	26%
AAD <sup>e</sup>				9%		9%		10%		21%	
MaxD <sup>f</sup>				28%		28%		38%		37%	

<sup>a</sup> Eq. (4.12) is parametrized with computed self-diffusivities from MD

<sup>b</sup> Absolute difference normalized with corresponding value from MD simulations

<sup>c</sup> Darken-LBV, all self-diffusivities in Eq. (4.12) are parametrized using Eq. (4.14).

<sup>d</sup> Eq. (4.6) is parametrized with predicted self-diffusivities using Eq. (4.7)

<sup>e</sup> Averaged absolute difference

<sup>f</sup> Maximum deviation

**Table D.2:** Computed and predicted MS diffusivities in ternary mixtures in which particles interact with a WCA potential. All reported quantities are in reduced units. Simulation details:  $\rho = 0.5$ ;  $M_1 = 1$ ;  $M_2 = 5$ ;  $M_3 = 10$ ;  $T = 2$ ;  $N = 400$ . The statistic errors of computed diffusivities are less than 5%.

$x_1$	$x_2$	$D_{ij}$	MD	Multicomp. Darken		Darken-LBV		Vignes-LBV		Generalized Darken	
				Eq. (4.12) <sup>a</sup>	AD <sup>b</sup>	Eq. (4.12) <sup>c</sup>	AD	Eq. (4.4)	AD	Eq. (4.6) <sup>d</sup>	AD
0.2	0.16	$D_{12}$	0.25	0.24	4%	0.25	0%	0.26	4%	0.19	24%
		$D_{13}$	0.23	0.22	4%	0.21	9%	0.23	0%	0.20	13%
		$D_{23}$	0.17	0.17	0%	0.18	6%	0.19	12%	0.17	0%
0.2	0.32	$D_{12}$	0.26	0.25	4%	0.25	4%	0.26	0%	0.24	8%
		$D_{13}$	0.24	0.23	4%	0.21	13%	0.23	4%	0.20	17%
		$D_{23}$	0.17	0.17	0%	0.18	6%	0.19	12%	0.17	0%
0.4	0.24	$D_{12}$	0.30	0.27	10%	0.26	13%	0.29	3%	0.28	7%
		$D_{13}$	0.29	0.25	14%	0.23	21%	0.25	14%	0.19	34%
		$D_{23}$	0.19	0.19	0%	0.19	0%	0.22	16%	0.18	5%
0.4	0.36	$D_{12}$	0.32	0.27	16%	0.26	19%	0.29	9%	0.28	13%
		$D_{13}$	0.27	0.25	7%	0.23	15%	0.25	7%	0.19	30%
		$D_{23}$	0.20	0.20	0%	0.20	0%	0.22	10%	0.18	10%
0.4	0.48	$D_{12}$	0.29	0.28	3%	0.26	10%	0.28	3%	0.29	0%
		$D_{13}$	0.28	0.26	7%	0.23	18%	0.25	11%	0.19	32%
		$D_{23}$	0.21	0.20	5%	0.20	5%	0.22	5%	0.18	14%
0.6	0.08	$D_{12}$	0.32	0.29	9%	0.29	9%	0.32	0%	0.31	3%
		$D_{13}$	0.32	0.27	16%	0.25	22%	0.29	9%	0.20	38%
		$D_{23}$	0.19	0.21	11%	0.21	11%	0.25	32%	0.19	0%
0.6	0.16	$D_{12}$	0.32	0.29	9%	0.29	9%	0.32	0%	0.31	3%
		$D_{13}$	0.31	0.27	13%	0.25	19%	0.29	6%	0.20	35%
		$D_{23}$	0.20	0.22	10%	0.22	10%	0.25	25%	0.20	0%
0.6	0.24	$D_{12}$	0.32	0.30	6%	0.29	9%	0.32	0%	0.32	0%
		$D_{13}$	0.31	0.28	10%	0.26	16%	0.29	6%	0.20	35%
		$D_{23}$	0.20	0.22	10%	0.22	10%	0.25	25%	0.20	0%
AAD <sup>e</sup>				7%		11%		9%		13%	
MaxD <sup>f</sup>				16%		22%		32%		38%	

<sup>a</sup> Eq. (4.12) is parametrized with computed self-diffusivities from MD

<sup>b</sup> Absolute difference normalized with corresponding value from MD simulations

<sup>c</sup> Darken-LBV, all self-diffusivities in Eq. (4.12) are parametrized using Eq. (4.14).

<sup>d</sup> Eq. (4.6) is parametrized with predicted self-diffusivities using Eq. (4.7)

<sup>e</sup> Averaged absolute difference

<sup>f</sup> Maximum deviation

**Table D.3:** Computed and predicted self-diffusivities in ternary mixtures in which particles interact with a WCA potential. All reported quantities are in reduced units. Simulation details:  $\rho = 0.2$  (top) and  $0.5$  (bottom);  $M_1 = 1$ ;  $M_2 = 5$ ;  $M_3 = 10$ ;  $T = 2$ ;  $N = 400$ . The statistical errors of computed diffusivities are less than 2%.

$x_1$	$x_2$	$D_{1,\text{self}}^a$	$D_{2,\text{self}}^a$	$D_{3,\text{self}}^a$	$D_{1,\text{self}}^b$	$D_{2,\text{self}}^b$	$D_{3,\text{self}}^b$	$D_{1,\text{self}}^c$	$D_{2,\text{self}}^c$	$D_{3,\text{self}}^c$
0.2	0.32	1.01	0.63	0.55	1.00	0.64	0.55	0.94	0.58	0.50
0.2	0.48	1.03	0.66	0.58	1.02	0.66	0.57	0.96	0.60	0.52
0.4	0.36	1.10	0.74	0.66	1.09	0.74	0.65	0.98	0.63	0.55
0.4	0.48	1.11	0.76	0.69	1.11	0.76	0.67	1.01	0.66	0.58
0.6	0.08	1.17	0.81	0.73	1.16	0.81	0.72	0.98	0.64	0.55
0.6	0.24	1.19	0.84	0.78	1.18	0.84	0.75	1.02	0.69	0.60
0.8	0.04	1.30	1.00	0.94	1.27	0.96	0.81	1.06	0.74	0.66
0.8	0.16	1.31	1.00	0.94	1.29	0.99	0.91	1.14	0.83	0.75
AAD <sup>d</sup>		-			2%			16%		
0.2	0.16	0.24	0.18	0.17	0.23	0.19	0.16	0.21	0.18	0.15
0.2	0.32	0.25	0.19	0.17	0.23	0.20	0.17	0.21	0.18	0.15
0.4	0.24	0.29	0.22	0.20	0.27	0.23	0.19	0.23	0.19	0.16
0.4	0.36	0.29	0.23	0.21	0.27	0.23	0.20	0.23	0.20	0.17
0.4	0.48	0.30	0.24	0.22	0.27	0.24	0.21	0.24	0.20	0.18
0.6	0.08	0.32	0.25	0.24	0.30	0.26	0.22	0.24	0.20	0.17
0.6	0.16	0.33	0.26	0.24	0.31	0.26	0.23	0.24	0.21	0.18
0.6	0.24	0.33	0.27	0.25	0.31	0.27	0.24	0.24	0.21	0.19
AAD <sup>d</sup>		-			5%			18%		

<sup>a</sup> Computed self-diffusivities using MD

<sup>b</sup> Predicted self-diffusivities using Eq. (4.14)

<sup>c</sup> Predicted self-diffusivities using Eq. (4.6)

<sup>d</sup> Averaged absolute difference normalized with MD results



**Table D.4:** Computed self- and MS diffusivities in binary mixtures in which particles interact with a WCA potential. We consider the case that component  $i$  is diluted in component  $j$ , so here  $\mathcal{D}_{ij} = D_{i,\text{self}}$ . Note that  $D_{j,\text{self}}^{x_j \rightarrow 1}$  is the self-diffusivity of the pure component  $j$ . All reported quantities are in reduced units. The statistical errors in the computed diffusivities are less than 2%. Simulation details:  $\rho = 0.2$  (top) and 0.5 (bottom);  $M_1 = 1$ ;  $M_2 = 5$ ;  $M_3 = 10$ ;  $M_4 = 20$ ;  $T = 2$ ;  $N = 400$ .

$i - j$	$D_{i,\text{self}}^{x_j \rightarrow 1}$	$D_{j,\text{self}}^{x_j \rightarrow 1}$	$\mathcal{D}_{ij}^{x_j \rightarrow 1}$
2 - 1	1.17	1.41	1.17
3 - 1	1.10	1.41	1.10
4 - 1	1.06	1.41	1.06
1 - 2	0.99	0.64	0.99
3 - 2	0.56	0.64	0.56
4 - 2	0.51	0.64	0.51
1 - 3	0.90	0.45	0.90
2 - 3	0.54	0.45	0.54
4 - 3	0.38	0.45	0.38
1 - 4	0.82	0.32	0.82
2 - 4	0.47	0.32	0.47
3 - 4	0.37	0.32	0.37
<hr/>			
2 - 1	0.39	0.44	0.39
3 - 1	0.36	0.44	0.36
4 - 1	0.35	0.44	0.35
1 - 2	0.23	0.19	0.23
3 - 2	0.17	0.19	0.17
4 - 2	0.16	0.19	0.16
1 - 3	0.20	0.14	0.20
2 - 3	0.17	0.14	0.17
4 - 3	0.13	0.14	0.13
1 - 4	0.15	0.10	0.15
2 - 4	0.13	0.10	0.13
3 - 4	0.11	0.10	0.11

**Table D.5:** Computed and predicted MS diffusivities in ternary mixtures in which particles interact with a WCA potential. All reported quantities are in reduced units. Simulation details:  $\rho = 0.2$ ;  $M_1 = 1$ ;  $M_2 = 5$ ;  $M_3 = 10$ ;  $T = 2$ ;  $N = 400$ . The statistical errors of computed diffusivities are less than 5%.

$x_1$	$x_2$	$\mathcal{D}_{ij}$	MD	Generalized Darken	
				Eq. (4.6) <sup>a</sup>	AD
0.2	0.32	$\mathcal{D}_{12}$	1.01	0.87	14%
		$\mathcal{D}_{13}$	0.93	0.88	5%
		$\mathcal{D}_{23}$	0.55	0.60	9%
0.2	0.48	$\mathcal{D}_{12}$	1.03	0.92	11%
		$\mathcal{D}_{13}$	0.97	0.86	11%
		$\mathcal{D}_{23}$	0.57	0.60	5%
0.4	0.36	$\mathcal{D}_{12}$	1.04	0.91	13%
		$\mathcal{D}_{13}$	1.00	0.83	17%
		$\mathcal{D}_{23}$	0.58	0.69	19%
0.4	0.48	$\mathcal{D}_{12}$	1.09	0.95	13%
		$\mathcal{D}_{13}$	1.04	0.79	24%
		$\mathcal{D}_{23}$	0.59	0.70	19%
0.6	0.08	$\mathcal{D}_{12}$	1.07	0.85	21%
		$\mathcal{D}_{13}$	1.05	0.89	15%
		$\mathcal{D}_{23}$	0.58	0.79	36%
0.6	0.24	$\mathcal{D}_{12}$	1.14	0.94	18%
		$\mathcal{D}_{13}$	1.10	0.86	22%
		$\mathcal{D}_{23}$	0.59	0.80	36%
0.8	0.04	$\mathcal{D}_{12}$	1.13	1.01	11%
		$\mathcal{D}_{13}$	1.11	1.00	10%
		$\mathcal{D}_{23}$	0.60	0.99	65%
0.8	0.16	$\mathcal{D}_{12}$	1.16	1.05	9%
		$\mathcal{D}_{13}$	1.12	0.96	14%
		$\mathcal{D}_{23}$	0.61	0.96	57%
AAD <sup>b</sup>					20%

<sup>a</sup> Eq. (4.6) is parametrized with the computed self-diffusivities from MD

<sup>b</sup> Averaged absolute difference

**Table D.6:** Computed and predicted MS diffusivities in ternary mixtures in which particles interact with a WCA potential. All reported quantities are in reduced units. Simulation details:  $\rho = 0.5$ ;  $M_1 = 1$ ;  $M_2 = 5$ ;  $M_3 = 10$ ;  $T = 2$ ;  $N = 400$ . The statistical errors of computed diffusivities are less than 5%.

$x_1$	$x_2$	$\mathcal{D}_{ij}$	MD	Generalized Darken	
				Eq. (4.6) <sup>a</sup>	AD
0.2	0.32	$\mathcal{D}_{12}$	0.25	0.21	16%
		$\mathcal{D}_{13}$	0.23	0.22	4%
		$\mathcal{D}_{23}$	0.17	0.18	6%
0.2	0.48	$\mathcal{D}_{12}$	0.26	0.23	12%
		$\mathcal{D}_{13}$	0.24	0.23	4%
		$\mathcal{D}_{23}$	0.17	0.18	6%
0.4	0.36	$\mathcal{D}_{12}$	0.30	0.25	17%
		$\mathcal{D}_{13}$	0.29	0.24	17%
		$\mathcal{D}_{23}$	0.19	0.22	16%
0.4	0.48	$\mathcal{D}_{12}$	0.32	0.26	19%
		$\mathcal{D}_{13}$	0.27	0.24	11%
		$\mathcal{D}_{23}$	0.20	0.22	10%
0.6	0.08	$\mathcal{D}_{12}$	0.29	0.27	7%
		$\mathcal{D}_{13}$	0.28	0.24	14%
		$\mathcal{D}_{23}$	0.21	0.22	5%
0.6	0.24	$\mathcal{D}_{12}$	0.32	0.26	19%
		$\mathcal{D}_{13}$	0.32	0.27	16%
		$\mathcal{D}_{23}$	0.19	0.25	32%
0.8	0.04	$\mathcal{D}_{12}$	0.32	0.27	16%
		$\mathcal{D}_{13}$	0.31	0.27	13%
		$\mathcal{D}_{23}$	0.20	0.25	25%
0.8	0.16	$\mathcal{D}_{12}$	0.32	0.28	13%
		$\mathcal{D}_{13}$	0.31	0.27	13%
		$\mathcal{D}_{23}$	0.20	0.26	30%
AAD <sup>b</sup>					14%

<sup>a</sup> Eq. (4.6) is parametrized with the computed self-diffusivities from MD

<sup>b</sup> Averaged absolute difference

**Table D.7:** Computed and predicted self-diffusivities in quaternary mixtures in which particles interact with a WCA potential. All reported quantities are in reduced units. Simulation details:  $\rho = 0.2$  (top) and  $0.5$  (bottom);  $M_1 = 1$ ;  $M_2 = 5$ ;  $M_3 = 10$ ;  $M_4 = 20$ ;  $T = 2$ ;  $N = 400$ . The statistical errors of computed diffusivities are less than 2%.

$x_1$	$x_2$	$x_3$	$D_{1,\text{self}}^a$	$D_{2,\text{self}}^a$	$D_{3,\text{self}}^a$	$D_{4,\text{self}}^a$	$D_{1,\text{self}}^b$	$D_{2,\text{self}}^b$	$D_{3,\text{self}}^b$	$D_{4,\text{self}}^b$	$D_{1,\text{self}}^c$	$D_{2,\text{self}}^c$	$D_{3,\text{self}}^c$	$D_{4,\text{self}}^c$
0.1	0.2	0.14	0.90	0.53	0.45	0.39	0.90	0.54	0.44	0.38	0.84	0.49	0.40	0.34
0.1	0.2	0.56	0.94	0.57	0.49	0.44	0.94	0.57	0.48	0.42	0.89	0.53	0.45	0.38
0.1	0.6	0.24	0.99	0.62	0.55	0.50	0.99	0.63	0.54	0.48	0.93	0.58	0.49	0.44
0.2	0.4	0.16	0.99	0.62	0.54	0.48	0.98	0.62	0.53	0.47	0.89	0.54	0.45	0.39
0.2	0.4	0.32	1.00	0.63	0.55	0.51	1.00	0.64	0.55	0.48	0.92	0.57	0.48	0.42
0.3	0.2	0.20	1.02	0.63	0.54	0.48	1.00	0.63	0.53	0.47	0.87	0.52	0.43	0.38
0.3	0.2	0.30	1.02	0.64	0.56	0.50	1.01	0.64	0.54	0.48	0.89	0.54	0.45	0.39
0.3	0.2	0.40	1.03	0.65	0.57	0.52	1.02	0.65	0.56	0.49	0.91	0.56	0.47	0.41
AAD <sup>d</sup>			-				2%				13%			
0.1	0.2	0.14	0.20	0.15	0.13	0.12	0.18	0.15	0.13	0.12	0.16	0.14	0.12	0.11
0.1	0.2	0.56	0.22	0.17	0.15	0.14	0.21	0.17	0.15	0.14	0.19	0.16	0.14	0.13
0.1	0.6	0.24	0.24	0.19	0.17	0.16	0.22	0.19	0.17	0.16	0.21	0.17	0.15	0.14
0.2	0.4	0.24	0.25	0.19	0.17	0.16	0.22	0.19	0.17	0.15	0.19	0.16	0.14	0.13
0.2	0.4	0.32	0.25	0.19	0.18	0.16	0.23	0.19	0.17	0.16	0.20	0.17	0.15	0.14
0.3	0.2	0.20	0.25	0.19	0.17	0.16	0.22	0.19	0.16	0.15	0.18	0.15	0.13	0.12
0.3	0.2	0.30	0.25	0.19	0.17	0.16	0.23	0.19	0.17	0.16	0.19	0.16	0.14	0.13
0.3	0.2	0.40	0.26	0.20	0.18	0.17	0.24	0.20	0.17	0.16	0.20	0.17	0.14	0.14
AAD <sup>d</sup>			-				3%				16%			

<sup>a</sup> Computed self-diffusivities using MD

<sup>b</sup> Predicted self-diffusivities using Eq. (4.14)

<sup>c</sup> Predicted self-diffusivities using Eq. (4.7)

<sup>d</sup> Averaged absolute difference normalized with MD results

**Table D.8:** Computed and predicted MS diffusivities in quaternary mixtures in which particles interact with a WCA potential. All reported quantities are in reduced units. Simulation details:  $\rho = 0.2$ ;  $M_1 = 1$ ;  $M_2 = 5$ ;  $M_3 = 10$ ;  $M_4 = 40$ ;  $T = 2$ ;  $N = 400$ . The statistic errors of computed diffusivities are less than 5%.

$x_1$	$x_2$	$x_3$	$D_{ij}$	MD	Multicomp. Darken		Darken-LBV		Vignes-LBV		Generalized Darken	
					Eq. (4.12) <sup>a</sup>	AD <sup>b</sup>	Eq. (4.12) <sup>c</sup>	AD	Eq. (4.4)	AD	Eq. (4.6) <sup>d</sup>	AD
0.1	0.2	0.14	$D_{12}$	1.50	1.07	29%	1.10	27%	1.13	25%	0.73	51%
			$D_{13}$	1.03	0.90	13%	0.89	14%	0.94	9%	0.66	36%
			$D_{14}$	0.79	0.79	0%	0.79	0%	0.82	4%	0.77	3%
			$D_{23}$	0.50	0.53	6%	0.54	8%	0.57	14%	0.44	12%
			$D_{24}$	0.49	0.46	6%	0.47	4%	0.50	2%	0.45	8%
			$D_{34}$	0.41	0.39	5%	0.38	7%	0.42	2%	0.39	5%
0.1	0.2	0.56	$D_{12}$	1.17	1.03	12%	1.05	10%	1.08	8%	0.77	34%
			$D_{13}$	0.83	0.88	6%	0.88	6%	0.92	11%	0.82	1%
			$D_{14}$	0.78	0.79	1%	0.76	3%	0.80	3%	0.68	13%
			$D_{23}$	0.53	0.53	0%	0.54	2%	0.57	8%	0.51	4%
			$D_{24}$	0.48	0.48	0%	0.47	2%	0.50	4%	0.45	6%
			$D_{34}$	0.42	0.41	2%	0.39	7%	0.42	0%	0.40	5%
0.1	0.6	0.24	$D_{12}$	1.33	1.00	25%	1.01	24%	1.04	22%	0.88	34%
			$D_{13}$	0.90	0.88	2%	0.86	4%	0.90	0%	0.81	10%
			$D_{14}$	0.82	0.81	1%	0.77	6%	0.81	1%	0.62	24%
			$D_{23}$	0.56	0.55	2%	0.55	2%	0.58	4%	0.52	7%
			$D_{24}$	0.54	0.51	6%	0.49	9%	0.52	4%	0.45	17%
			$D_{34}$	0.43	0.45	5%	0.42	2%	0.45	5%	0.45	5%
0.2	0.4	0.16	$D_{12}$	0.99	1.01	2%	1.02	3%	1.09	10%	0.77	22%
			$D_{13}$	0.96	0.87	9%	0.86	10%	0.93	3%	0.64	33%
			$D_{14}$	0.95	0.79	17%	0.76	20%	0.84	12%	0.66	31%
			$D_{23}$	0.53	0.54	2%	0.54	2%	0.61	15%	0.47	11%
			$D_{24}$	0.53	0.49	8%	0.48	9%	0.55	4%	0.45	15%
			$D_{34}$	0.42	0.43	2%	0.41	2%	0.47	12%	0.42	0%

<sup>a</sup> Eq. (4.12) is parametrized with computed self-diffusivities from MD

<sup>b</sup> Absolute difference normalized with corresponding value from MD simulations

<sup>c</sup> Darken-LBV, all self-diffusivities in Eq. (4.12) are parametrized using Eq. (4.14)

<sup>d</sup> Eq. (4.6) is parametrized with predicted self-diffusivities using Eq. (4.7)

<sup>e</sup> Averaged absolute difference

<sup>f</sup> Maximum deviation

Table D.8 (continued):

$x_1$	$x_2$	$x_3$	$D_{ij}$	MD	Multicomp. Darken		Darken-LBV		Vignes-LBV		Generalized Darken	
					Eq. (4.12) <sup>a</sup>	AD <sup>b</sup>	Eq. (4.12) <sup>c</sup>	AD	Eq. (4.4)	AD	Eq. (4.6) <sup>d</sup>	AD
0.2	0.4	0.32	$D_{12}$	1.04	1.00	4%	1.01	3%	1.07	3%	0.80	22%
			$D_{13}$	0.95	0.87	8%	0.86	9%	0.93	2%	0.75	21%
			$D_{14}$	0.87	0.80	8%	0.76	13%	0.83	5%	0.57	34%
			$D_{23}$	0.56	0.55	2%	0.55	2%	0.61	9%	0.52	7%
			$D_{24}$	0.55	0.51	7%	0.49	11%	0.54	2%	0.45	18%
			$D_{34}$	0.41	0.44	7%	0.42	2%	0.47	15%	0.43	5%
0.3	0.2	0.20	$D_{12}$	1.06	1.02	4%	1.03	3%	1.12	6%	0.66	38%
			$D_{13}$	0.99	0.88	11%	0.87	12%	0.96	3%	0.61	38%
			$D_{14}$	0.94	0.79	16%	0.76	19%	0.87	7%	0.62	34%
			$D_{23}$	0.53	0.55	4%	0.55	4%	0.64	21%	0.48	9%
			$D_{24}$	0.54	0.49	9%	0.48	11%	0.57	6%	0.46	15%
			$D_{34}$	0.40	0.42	5%	0.41	2%	0.49	23%	0.41	2%
0.3	0.2	0.30	$D_{12}$	1.05	1.01	4%	1.02	3%	1.11	6%	0.68	35%
			$D_{13}$	0.97	0.88	9%	0.87	10%	0.96	1%	0.67	31%
			$D_{14}$	0.96	0.79	18%	0.76	21%	0.86	10%	0.59	39%
			$D_{23}$	0.52	0.55	6%	0.55	6%	0.64	23%	0.50	4%
			$D_{24}$	0.56	0.50	11%	0.49	13%	0.57	2%	0.46	18%
			$D_{34}$	0.42	0.43	2%	0.41	2%	0.49	17%	0.41	2%
0.3	0.2	0.40	$D_{12}$	1.08	1.00	7%	1.01	6%	1.10	2%	0.70	35%
			$D_{13}$	1.00	0.87	13%	0.87	13%	0.95	5%	0.72	28%
			$D_{14}$	0.95	0.80	16%	0.76	20%	0.85	11%	0.54	43%
			$D_{23}$	0.57	0.55	4%	0.56	2%	0.64	12%	0.53	7%
			$D_{24}$	0.50	0.50	0%	0.49	2%	0.57	14%	0.46	8%
			$D_{34}$	0.42	0.44	5%	0.42	0%	0.49	17%	0.42	0%
AAD <sup>e</sup>					7%		8%		8%		18%	
MaxD <sup>f</sup>					29%		27%		25%		51%	

<sup>a</sup> Eq. (4.12) is parametrized with computed self-diffusivities from MD

<sup>b</sup> Absolute difference normalized with corresponding value from MD simulations

<sup>c</sup> Darken-LBV, all self-diffusivities in Eq. (4.12) are parametrized using Eq. (4.14)

<sup>d</sup> Eq. (4.6) is parametrized with predicted self-diffusivities using Eq. (4.7)

<sup>e</sup> Averaged absolute difference

<sup>f</sup> Maximum deviation

**Table D.9:** Computed and predicted MS diffusivities in quaternary mixtures in which particles interact with a WCA potential. All reported quantities are in reduced units. Simulation details:  $\rho = 0.5$ ;  $M_1 = 1$ ;  $M_2 = 5$ ;  $M_3 = 10$ ;  $M_4 = 20$ ;  $T = 2$ ;  $N = 400$ . The statistic errors of computed diffusivities are less than 5%.

$x_1$	$x_2$	$x_3$	$D_{ij}$	MD	Multicomp. Darken		Darken-LBV		Vignes-LBV		Generalized Darken	
					Eq. (4.12) <sup>a</sup>	AD <sup>b</sup>	Eq. (4.12) <sup>c</sup>	AD	Eq. (4.4)	AD	Eq. (4.6) <sup>d</sup>	AD
0.1	0.2	0.14	$D_{12}$	0.21	0.22	5%	0.21	0%	0.22	5%	0.15	29%
			$D_{13}$	0.19	0.20	5%	0.18	5%	0.19	0%	0.14	26%
			$D_{14}$	0.19	0.18	5%	0.16	16%	0.18	5%	0.15	21%
			$D_{23}$	0.15	0.15	0%	0.16	7%	0.17	13%	0.13	13%
			$D_{24}$	0.15	0.14	7%	0.14	7%	0.15	0%	0.13	13%
			$D_{34}$	0.13	0.12	8%	0.12	8%	0.13	0%	0.12	8%
0.1	0.2	0.56	$D_{12}$	0.25	0.23	8%	0.23	8%	0.24	4%	0.18	28%
			$D_{13}$	0.19	0.21	11%	0.20	5%	0.21	11%	0.18	5%
			$D_{14}$	0.19	0.19	0%	0.18	5%	0.20	5%	0.16	16%
			$D_{23}$	0.16	0.16	0%	0.17	6%	0.18	13%	0.15	6%
			$D_{24}$	0.18	0.15	17%	0.16	11%	0.17	6%	0.14	22%
			$D_{34}$	0.13	0.13	0%	0.13	0%	0.14	8%	0.13	0%
0.1	0.6	0.24	$D_{12}$	0.28	0.24	14%	0.23	18%	0.24	14%	0.20	29%
			$D_{13}$	0.25	0.22	12%	0.20	20%	0.21	16%	0.19	24%
			$D_{14}$	0.18	0.21	17%	0.19	6%	0.20	11%	0.17	6%
			$D_{23}$	0.18	0.17	6%	0.17	6%	0.18	0%	0.16	11%
			$D_{24}$	0.16	0.16	0%	0.16	0%	0.17	6%	0.15	6%
			$D_{34}$	0.14	0.15	7%	0.14	0%	0.15	7%	0.15	7%
0.2	0.4	0.24	$D_{12}$	0.31	0.25	19%	0.23	26%	0.25	19%	0.18	42%
			$D_{13}$	0.26	0.23	12%	0.20	23%	0.22	15%	0.17	35%
			$D_{14}$	0.23	0.21	9%	0.19	17%	0.21	9%	0.16	30%
			$D_{23}$	0.17	0.17	0%	0.17	0%	0.19	12%	0.15	12%
			$D_{24}$	0.17	0.16	6%	0.16	6%	0.18	6%	0.14	18%
			$D_{34}$	0.14	0.15	7%	0.14	0%	0.16	14%	0.14	0%

<sup>a</sup> Eq. (4.12) is parametrized with computed self-diffusivities from MD

<sup>b</sup> Absolute difference normalized with corresponding value from MD simulations

<sup>c</sup> Darken-LBV, all self-diffusivities in Eq. (4.12) are parametrized using Eq. (4.14)

<sup>d</sup> Eq. (4.6) is parametrized with predicted self-diffusivities using Eq. (4.7)

<sup>e</sup> Averaged absolute difference

<sup>f</sup> Maximum deviation

**Table D.9 (continued):**

$x_1$	$x_2$	$x_3$	$D_{ij}$	MD	Multicomp. Darken		Darken-LBV		Vignes-LBV		Generalized Darken	
					Eq. (4.12) <sup>a</sup>	AD <sup>b</sup>	Eq. (4.12) <sup>c</sup>	AD	Eq. (4.4)	AD	Eq. (4.6) <sup>d</sup>	AD
0.2	0.4	0.32	$D_{12}$	0.26	0.25	4%	0.24	8%	0.25	4%	0.19	27%
			$D_{13}$	0.26	0.23	12%	0.21	19%	0.22	15%	0.18	31%
			$D_{14}$	0.21	0.21	0%	0.20	5%	0.21	0%	0.16	24%
			$D_{23}$	0.17	0.18	6%	0.17	0%	0.19	12%	0.16	6%
			$D_{24}$	0.18	0.16	11%	0.17	6%	0.18	0%	0.14	22%
			$D_{34}$	0.14	0.15	7%	0.14	0%	0.16	14%	0.14	0%
0.3	0.2	0.20	$D_{12}$	0.25	0.25	0%	0.23	8%	0.26	4%	0.16	36%
			$D_{13}$	0.24	0.23	4%	0.20	17%	0.23	4%	0.15	38%
			$D_{14}$	0.24	0.21	13%	0.19	21%	0.21	13%	0.15	38%
			$D_{23}$	0.18	0.17	6%	0.17	6%	0.20	11%	0.14	22%
			$D_{24}$	0.16	0.16	0%	0.16	0%	0.18	13%	0.14	13%
			$D_{34}$	0.14	0.14	0%	0.14	0%	0.16	14%	0.13	7%
0.3	0.2	0.30	$D_{12}$	0.27	0.25	7%	0.24	11%	0.26	4%	0.17	37%
			$D_{13}$	0.25	0.23	8%	0.21	16%	0.23	8%	0.16	36%
			$D_{14}$	0.25	0.21	16%	0.19	24%	0.22	12%	0.15	40%
			$D_{23}$	0.17	0.17	0%	0.18	6%	0.20	18%	0.15	12%
			$D_{24}$	0.17	0.16	6%	0.16	6%	0.19	12%	0.14	18%
			$D_{34}$	0.14	0.15	7%	0.14	0%	0.17	21%	0.13	7%
0.3	0.2	0.40	$D_{12}$	0.28	0.25	11%	0.25	11%	0.27	4%	0.18	36%
			$D_{13}$	0.23	0.23	0%	0.21	9%	0.24	4%	0.18	22%
			$D_{14}$	0.21	0.21	0%	0.20	5%	0.22	5%	0.15	29%
			$D_{23}$	0.18	0.18	0%	0.18	0%	0.20	11%	0.16	11%
			$D_{24}$	0.17	0.16	6%	0.17	0%	0.19	12%	0.15	12%
			$D_{34}$	0.14	0.15	7%	0.15	7%	0.17	21%	0.14	0%
AAD <sup>e</sup>					6%		8%		9%		19%	
MaxD <sup>f</sup>					19%		26%		21%		42%	

<sup>a</sup> Eq. (4.12) is parametrized with computed self-diffusivities from MD

<sup>b</sup> Absolute difference normalized with corresponding value from MD simulations

<sup>c</sup> Darken-LBV, all self-diffusivities in Eq. (4.12) are parametrized using Eq. (4.14)

<sup>d</sup> Eq. (4.6) is parametrized with predicted self-diffusivities using Eq. (4.7)

<sup>e</sup> Averaged absolute difference

<sup>f</sup> Maximum deviation



**Table D.10:** Computed and predicted self-diffusivities/( $10^{-8} \text{ m}^2 \text{ s}^{-1}$ ) in ternary mixtures of n-hexane(1)-cyclohexane(2)-toluene(3) at 298 K, 1 atm. The statistic errors of computed diffusivities are less than 5%.

$x_1$	$x_2$	$D_{1,\text{self}}^a$	$D_{2,\text{self}}^a$	$D_{3,\text{self}}^a$	$D_{1,\text{self}}^b$	$D_{2,\text{self}}^b$	$D_{3,\text{self}}^b$	$D_{1,\text{self}}^c$	$D_{2,\text{self}}^c$	$D_{3,\text{self}}^c$
0.2	0.40	0.273	0.241	0.255	0.310	0.258	0.270	0.334	0.278	0.297
0.2	0.20	0.277	0.244	0.265	0.319	0.275	0.291	0.340	0.290	0.312
0.2	0.60	0.260	0.226	0.238	0.302	0.242	0.252	0.328	0.265	0.282
0.4	0.30	0.342	0.298	0.325	0.345	0.286	0.304	0.387	0.315	0.343
0.4	0.15	0.343	0.319	0.331	0.356	0.302	0.323	0.391	0.324	0.354
0.6	0.10	0.352	0.294	0.340	0.404	0.335	0.363	0.443	0.359	0.396
AAD <sup>d</sup>		-			8%			16%		

<sup>a</sup> Computed self-diffusivities using MD

<sup>b</sup> Predicted self-diffusivities using Eq. (4.14)

<sup>c</sup> Predicted self-diffusivities using Eq. (4.7)

<sup>d</sup> Averaged absolute difference normalized with MD results

**Table D.11:** Computed and predicted MS diffusivities/( $10^{-8} \text{ m}^2 \text{ s}^{-1}$ ) in ternary mixtures of n-hexane(1)-cyclohexane(2)-toluene(3) at 298 K, 1 atm. The statistic errors of computed diffusivities are less than 5%.

$x_1$	$x_2$	$D_{ij}$	MD	Multicomp. Darken		Darken-LBV		Vignes-LBV		Generalized Darken	
				Eq. (4.12) <sup>a</sup>	AD <sup>b</sup>	Eq. (4.12) <sup>c</sup>	AD	Eq. (4.4)	AD	Eq. (4.6) <sup>d</sup>	AD
0.2	0.40	$D_{12}$	0.284	0.261	8%	0.294	4%	0.303	7%	0.315	11%
		$D_{13}$	0.310	0.276	11%	0.308	1%	0.290	6%	0.322	4%
		$D_{23}$	0.264	0.244	8%	0.256	3%	0.260	1%	0.287	9%
0.2	0.20	$D_{12}$	0.255	0.257	1%	0.300	18%	0.310	22%	0.315	24%
		$D_{13}$	0.284	0.279	2%	0.317	12%	0.309	9%	0.333	17%
		$D_{23}$	0.206	0.246	9%	0.273	21%	0.280	24%	0.296	30%
0.2	0.60	$D_{12}$	0.266	0.250	6%	0.287	8%	0.297	12%	0.312	17%
		$D_{13}$	0.320	0.264	18%	0.299	7%	0.273	15%	0.305	5%
		$D_{23}$	0.227	0.229	1%	0.240	6%	0.253	11%	0.277	22%
0.4	0.30	$D_{12}$	0.284	0.316	11%	0.317	12%	0.331	17%	0.346	22%
		$D_{13}$	0.363	0.344	5%	0.337	7%	0.330	9%	0.362	0%
		$D_{23}$	0.277	0.300	8%	0.277	0%	0.296	7%	0.329	19%
0.4	0.15	$D_{12}$	0.355	0.327	8%	0.324	9%	0.337	5%	0.343	3%
		$D_{13}$	0.360	0.340	6%	0.346	4%	0.345	4%	0.375	4%
		$D_{23}$	0.299	0.316	6%	0.294	2%	0.308	3%	0.333	11%
0.6	0.10	$D_{12}$	0.317	0.303	4%	0.353	11%	0.365	15%	0.371	17%
		$D_{13}$	0.336	0.351	9%	0.383	14%	0.387	15%	0.412	23%
		$D_{23}$	0.269	0.293	9%	0.318	18%	0.337	25%	0.368	37%
AAD <sup>e</sup>				7%		9%		11%		15%	
MaxD <sup>f</sup>				18%		21%		25%		37%	

<sup>a</sup> Eq. (4.12) is parametrized with computed self-diffusivities from MD

<sup>b</sup> Absolute difference normalized with corresponding value from MD simulations

<sup>c</sup> Darken-LBV, all self-diffusivities in Eq. (4.12) are parametrized using Eq. (4.14)

<sup>d</sup> Eq. (4.6) is parametrized with predicted self-diffusivities using Eq. (4.7)

<sup>e</sup> Averaged absolute difference

<sup>f</sup> Maximum deviation

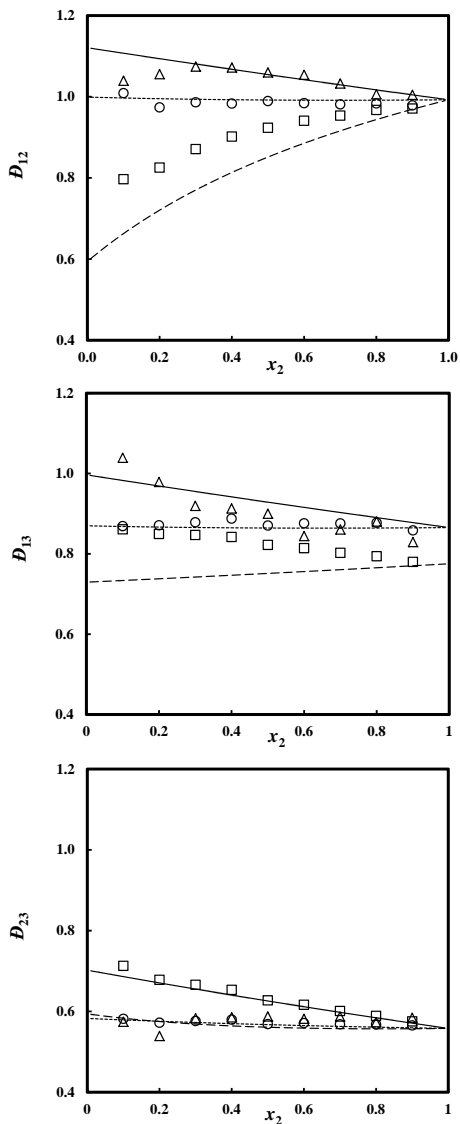


**Figure D.1:** Computed and predicted MS diffusivities in ternary systems in which particles interact with a WCA potential. Triangles represent computed MS diffusivities using MD. Solid lines represent predictions using the Vignes-LBV equation (Eq. (4.4)). Dashed lines represent predictions using the generalized Darken equation (Eqs. (4.6) and (4.7)). Squares represent predictions using the generalized Darken equation with the self-diffusivities obtained from MD simulation (Eq. (4.6)+MD). Dotted lines represent predictions using the Darken-LBV equation (Eqs. (4.12) and (4.14)). Circles represent predictions using the multicomponent Darken equation with the self-diffusivities obtained from MD simulation (Eq. (4.12)+MD). Simulation details:  $\rho = 0.2$ ;  $M_1 = 1$ ;  $M_2 = 5$ ;  $M_3 = 10$ ;  $T = 2$ ;  $N = 400$ ,  $x_1/x_3 = 1$ .

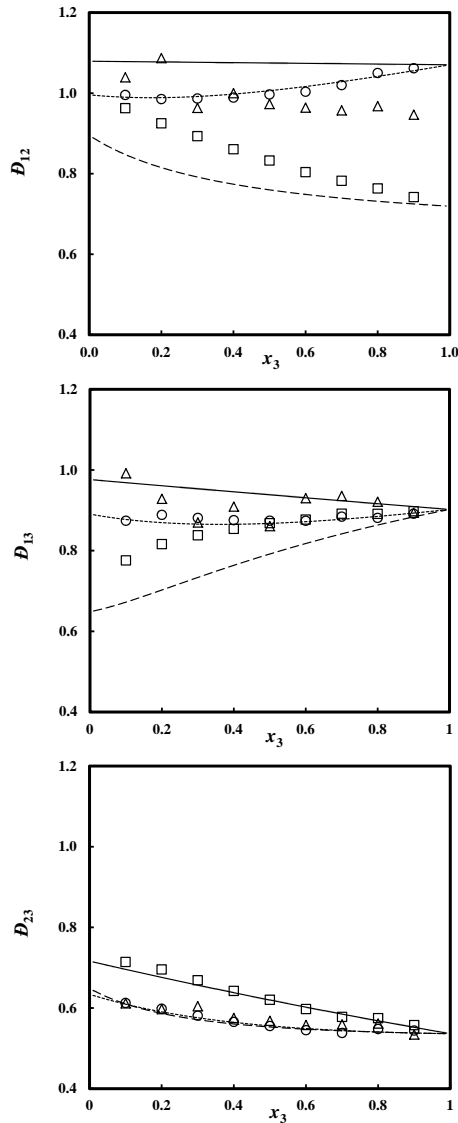


**Figure D.2:** Computed and predicted MS diffusivities in ternary systems in which particles interact with a WCA potential. Triangles represent computed MS diffusivities using MD. Solid lines represent predictions using the Vignes-LBV equation (Eq. (4.4)). Dashed lines represent predictions using the generalized Darken equation (Eqs. (4.6) and (4.7)). Squares represent predictions using the generalized Darken equation with the self-diffusivities obtained from MD simulation (Eq. (4.6)+MD). Dotted lines represent predictions using the Darken-LBV equation (Eqs. (4.12) and (4.14)). Circles represent predictions using the multicomponent Darken equation with the self-diffusivities obtained from MD simulation (Eq. (4.12)+MD). Simulation details:  $\rho = 0.2$ ;  $M_1 = 1$ ;  $M_2 = 5$ ;  $M_3 = 10$ ;  $T = 2$ ;  $N = 400$ ,  $x_1/x_2 = 1$ .

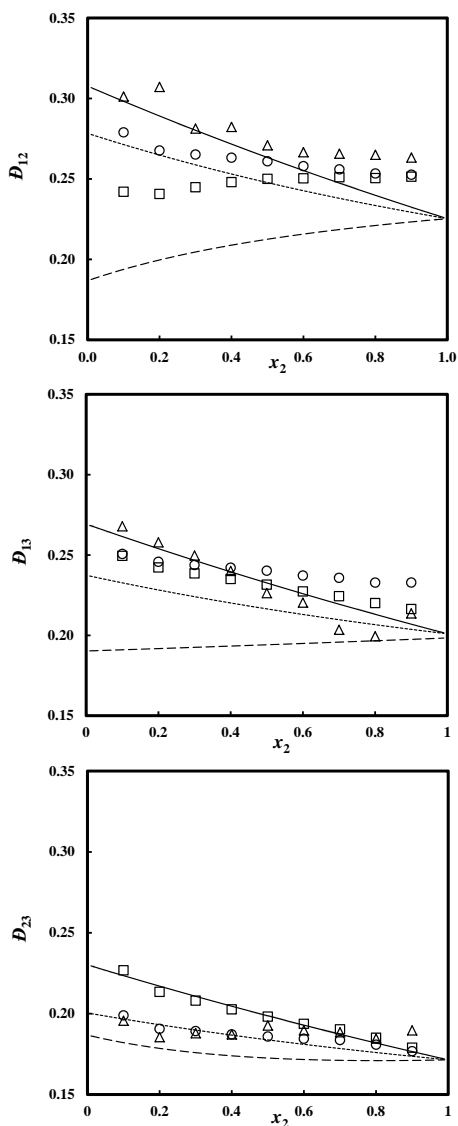


**Figure D.3:** Computed and predicted MS diffusivities in ternary systems in which particles interact with a WCA potential. Triangles represent computed MS diffusivities using MD. Solid lines represent predictions using the Vignes-LBV equation (Eq. (4.4)). Dashed lines represent predictions using the generalized Darken equation (Eqs. (4.6) and (4.7)). Squares represent predictions using the generalized Darken equation with the self-diffusivities obtained from MD simulation (Eq. (4.6)+MD). Dotted lines represent predictions using the Darken-LBV equation (Eqs. (4.12) and (4.14)). Circles represent predictions using the multicomponent Darken equation with the self-diffusivities obtained from MD simulation (Eq. (4.12)+MD). Simulation details:  $\rho = 0.5$ ;  $M_1 = 1$ ;  $M_2 = 5$ ;  $M_3 = 10$ ;  $T = 2$ ;  $N = 400$ ,  $x_1/x_3 = 1$ .

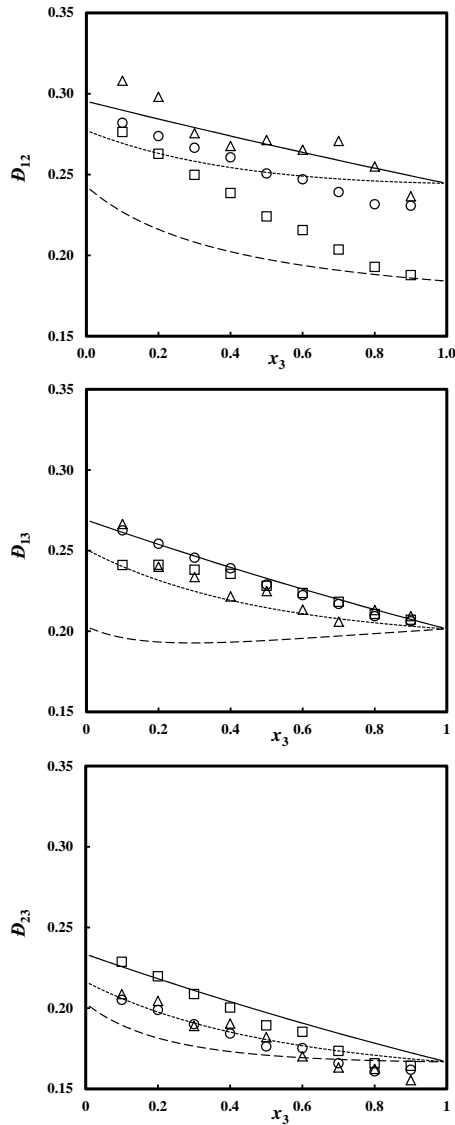


**Figure D.4:** Computed and predicted MS diffusivities in ternary systems in which particles interact with a WCA potential. Triangles represent computed MS diffusivities using MD. Solid lines represent predictions using the Vignes-LBV equation (Eq. (4.4)). Dashed lines represent predictions using the generalized Darken equation (Eqs. (4.6) and (4.7)). Squares represent predictions using the generalized Darken equation with the self-diffusivities obtained from MD simulation (Eq. (4.6)+MD). Dotted lines represent predictions using the Darken-LBV equation (Eqs. (4.12) and (4.14)). Circles represent predictions using the multicomponent Darken equation with the self-diffusivities obtained from MD simulation (Eq. (4.12)+MD). Simulation details:  $\rho = 0.5$ ;  $M_1 = 1$ ;  $M_2 = 5$ ;  $M_3 = 10$ ;  $T = 2$ ;  $N = 400$ ,  $x_1/x_2 = 1$ .

**E**

---

**Additional Data for Chapter 5**

---

**Table E.1:** LJ parameters and partial charges used for  $C_n\text{mimCl}$  (see Ref. <sup>110</sup>). The LJ interactions between unlike pseudo-atoms are calculated using the Lorentz-Berthelot mixing rules<sup>18</sup>. The LJ interactions are truncated and shifted at 12 Å. Electrostatic interactions are handled by Ewald summation using a relative precision<sup>85</sup> of  $10^{-5}$ .

Atom	LJ Parameters		$q/e$	
	$\sigma/\text{Å}$	$\epsilon/k_B$ [K]	$C_1\text{mimCl}$	$C_n\text{mimCl}$ ( $n \geq 2$ )
NA <sup>a</sup>	3.250	85.68	0.0276	0.015
CR	3.500	43.34	0.0050	0.00
CW	3.400	43.34	-0.1734	-0.16
H5	1.247	15.12	0.1544	0.15
H4	1.604	15.12	0.2118	0.20
CN3	3.813	95.75	0.2543	0.26
CN2	3.822	71.56	0.2543	0.23
CT2	3.947	67.03	-	0.05 <sup>b</sup>
CT3	3.902	93.23	-	0.00
Cl	3.742	75.60	-0.80	-0.80

<sup>a</sup> The notation is explained in Fig. 5.1

<sup>b</sup> The reported value is for CT2 connected to CN2. For other CT2 groups, the charge is zero, see Ref. <sup>110</sup>.

**Table E.2:** The LJ parameters and partial charges used for DMSO and water<sup>87;119</sup>. The LJ interactions between unlike pseudo-atoms are calculated using the Lorentz-Berthelot mixing rules<sup>18</sup>. The LJ interactions are truncated and shifted at 12 Å. Electrostatic interactions are handled by Ewald summation using a relative precision<sup>85</sup> of  $10^{-5}$ .

pseudo-atom	$\sigma/[\text{Å}]$	$\epsilon/k_B$ [K]	$q/e$
O (in DMSO)	2.92	185	-0.459
S (in DMSO)	3.60	139	0.139
CH3 (in DMSO)	3.80	98.95	0.160
O (in H <sub>2</sub> O)	3.16	90.48	-0.820
H (in H <sub>2</sub> O)	-	-	0.410



**Table E.3:** Computed self-diffusivities  $D_{i,\text{self}}/(10^{-9} \text{ m}^2 \cdot \text{s}^{-1})$  and MS diffusivities  $\bar{D}_{ij}/(10^{-9} \text{ m}^2 \cdot \text{s}^{-1})$  in  $C_n\text{mimCl-H}_2\text{O}$  mixtures at 1 atm.  $\bar{D}_{\text{IL}}$  is the MS diffusivity of IL molecules defined by Eq. (5.9). The total number of molecules ranges from 100 (IL rich) to 600 (water rich).

C <sub>1</sub> mimCl (1) + H <sub>2</sub> O (2) at 298 K							
$x_1$	$D_{+,\text{self}}$	$D_{-,\text{self}}$	$D_{\text{H}_2\text{O},\text{self}}$	$\bar{D}_{+-}$	$\bar{D}_{+\text{H}_2\text{O}}$	$\bar{D}_{-\text{H}_2\text{O}}$	$\bar{D}_{\text{IL}}$
0.1	0.30	0.43	0.68	0.39	0.35	0.37	0.36
0.2	0.08	0.10	0.16	0.10	0.12	0.10	0.11
0.3	0.03	0.04	0.06	0.02	0.04	0.04	0.04
C <sub>2</sub> mimCl (1) + H <sub>2</sub> O (2) at 368 K							
$x_1$	$D_{+,\text{self}}$	$D_{-,\text{self}}$	$D_{\text{H}_2\text{O},\text{self}}$	$\bar{D}_{+-}$	$\bar{D}_{+\text{H}_2\text{O}}$	$\bar{D}_{-\text{H}_2\text{O}}$	$\bar{D}_{\text{IL}}$
0.1	1.15	1.68	2.95	0.85	1.68	1.80	1.74
0.2	0.54	0.69	1.17	0.51	0.95	0.66	0.78
0.3	0.31	0.37	0.62	0.28	0.71	0.27	0.39
0.4	0.26	0.30	0.51	0.23	0.78	0.21	0.33
0.5	0.16	0.16	0.29	0.16	0.65	0.14	0.23
0.6	0.15	0.14	0.24	0.15	0.97	0.13	0.22
0.7	0.14	0.12	0.21	0.12	1.07	0.12	0.21
0.8	0.12	0.11	0.17	0.13	0.66	0.12	0.21
0.9	0.11	0.09	0.13	0.09	0.89	0.09	0.17
C <sub>4</sub> mimCl (1) + H <sub>2</sub> O (2) at 368 K							
$x_1$	$D_{+,\text{self}}$	$D_{-,\text{self}}$	$D_{\text{H}_2\text{O},\text{self}}$	$\bar{D}_{+-}$	$\bar{D}_{+\text{H}_2\text{O}}$	$\bar{D}_{-\text{H}_2\text{O}}$	$\bar{D}_{\text{IL}}$
0.1	0.87	1.47	2.57	0.73	1.29	1.39	1.34
0.2	0.35	0.58	1.04	0.24	0.77	0.62	0.68
0.3	0.17	0.26	0.52	0.15	0.51	0.25	0.33
0.4	0.11	0.18	0.39	0.10	0.64	0.17	0.27
0.5	0.06	0.10	0.20	0.05	0.52	0.09	0.16
0.6	0.05	0.06	0.12	0.04	0.52	0.09	0.15
0.7	0.04	0.05	0.12	0.04	0.55	0.09	0.16
0.8	0.04	0.04	0.10	0.03	0.41	0.10	0.16
0.9	0.03	0.03	0.08	0.03	0.42	0.07	0.13
C <sub>8</sub> mimCl (1) + H <sub>2</sub> O (2) at 368 K							
$x_1$	$D_{+,\text{self}}$	$D_{-,\text{self}}$	$D_{\text{H}_2\text{O},\text{self}}$	$\bar{D}_{+-}$	$\bar{D}_{+\text{H}_2\text{O}}$	$\bar{D}_{-\text{H}_2\text{O}}$	$\bar{D}_{\text{IL}}$
0.1	0.30	1.29	2.23	0.44	1.53	1.61	1.57
0.2	0.11	0.46	0.88	0.23	0.81	0.47	0.60
0.3	0.06	0.16	0.39	0.07	0.63	0.22	0.33
0.4	0.03	0.09	0.23	0.05	0.36	0.13	0.19
0.5	0.03	0.06	0.16	0.04	0.32	0.11	0.16
0.6	0.02	0.03	0.10	0.03	0.29	0.08	0.13
0.7	0.02	0.03	0.07	0.03	0.25	0.06	0.09
0.8	0.01	0.02	0.06	0.02	0.31	0.04	0.07
0.9	0.01	0.01	0.05	0.02	0.28	0.03	0.06

**Table E.4:** Computed self-diffusivities  $D_{i,\text{self}}/(10^{-9} \text{ m}^2 \cdot \text{s}^{-1})$  and MS diffusivities  $\bar{D}_{ij}/(10^{-9} \text{ m}^2 \cdot \text{s}^{-1})$  in  $\text{C}_n\text{mimCl}$ -DMSO mixtures at 1 atm.  $\bar{D}_{\text{IL}}$  is the MS diffusivity of IL molecules defined by Eq. (5.9). The total number of molecules ranges from 100 (IL rich) to 600 (water rich).

$\text{C}_1\text{mimCl (1) + DMSO (2) at 298K}$							
$x_1$	$D_{+,\text{self}}$	$D_{-,\text{self}}$	$D_{\text{DMSO},\text{self}}$	$\bar{D}_{+-}$	$\bar{D}_{+\text{DMSO}}$	$\bar{D}_{-\text{DMSO}}$	$\bar{D}_{\text{IL}}$
0.1	0.25	0.23	0.60	0.03	0.47	1.42	0.71
0.2	0.12	0.12	0.39	0.02	0.40	1.11	0.59
$\text{C}_2\text{mimCl (1) + DMSO (2) at 368K}$							
$x_1$	$D_{+,\text{self}}$	$D_{-,\text{self}}$	$D_{\text{DMSO},\text{self}}$	$\bar{D}_{+-}$	$\bar{D}_{+\text{DMSO}}$	$\bar{D}_{-\text{DMSO}}$	$\bar{D}_{\text{IL}}$
0.1	0.82	0.95	1.75	0.10	2.08	3.52	2.61
0.2	0.62	0.70	1.42	0.13	1.34	2.69	1.79
0.3	0.49	0.49	1.02	0.14	1.49	2.31	1.81
0.4	0.31	0.33	0.81	0.13	1.00	1.50	1.20
0.5	0.22	0.22	0.59	0.12	0.59	1.39	0.83
0.6	0.21	0.19	0.41	0.16	0.52	0.86	0.65
0.7	0.19	0.16	0.40	0.13	0.37	0.65	0.47
0.8	0.13	0.12	0.25	0.11	0.28	0.51	0.36
0.9	0.10	0.09	0.21	0.10	0.24	0.32	0.27
$\text{C}_4\text{mimCl (1) + DMSO (2) at 368K}$							
$x_1$	$D_{+,\text{self}}$	$D_{-,\text{self}}$	$D_{\text{DMSO},\text{self}}$	$\bar{D}_{+-}$	$\bar{D}_{+\text{DMSO}}$	$\bar{D}_{-\text{DMSO}}$	$\bar{D}_{\text{IL}}$
0.1	0.67	0.86	1.75	0.09	1.32	2.82	1.80
0.2	0.43	0.52	1.23	0.09	0.83	2.46	1.24
0.3	0.30	0.35	0.92	0.09	0.78	2.20	1.13
0.4	0.22	0.26	0.70	0.09	0.78	2.20	0.81
0.5	0.17	0.17	0.50	0.08	0.43	1.17	0.62
0.6	0.10	0.12	0.41	0.07	0.38	0.75	0.50
0.7	0.07	0.07	0.26	0.06	0.26	0.41	0.32
0.8	0.06	0.06	0.20	0.05	0.17	0.35	0.23
0.9	0.04	0.04	0.14	0.04	0.16	0.30	0.21

**Table E.5:** Computed self-diffusivities  $D_{i,\text{self}}/(10^{-9} \text{ m}^2 \cdot \text{s}^{-1})$  and MS diffusivities  $\mathcal{D}_{ij}/(10^{-9} \text{ m}^2 \cdot \text{s}^{-1})$  at infinite dilution. The simulations were carried out at 368 K, 1 atm. Here, we consider a case which component  $i$  is diluted in component  $j$ .

$i - j$	$D_{+,\text{self}}$	$D_{-,\text{self}}$	$D_{\text{H}_2\text{O},\text{self}}$	$\mathcal{D}_{+-}$	$\mathcal{D}_{+j}$	$\mathcal{D}_{-j}$
$\text{C}_2\text{mimCl-H}_2\text{O}^a$	3.52	5.39	8.27	1.08	3.52	5.39
$\text{C}_4\text{mimCl-H}_2\text{O}^b$	3.10	5.45	8.27	0.84	3.10	5.45
$\text{C}_8\text{mimCl-H}_2\text{O}^c$	2.40	5.34	8.27	0.56	2.40	5.34
$\text{C}_2\text{mimCl-DMSO}^d$	1.62	3.62	2.38	0.11	1.62	3.62
$\text{C}_4\text{mimCl-DMSO}^e$	1.14	2.26	2.38	0.07	1.14	2.26
$i - j$	$D_{+,\text{self}}$	$D_{-,\text{self}}$	$D_{\text{H}_2\text{O},\text{self}}$	$\mathcal{D}_{+-}$	$\mathcal{D}_{+i}$	$\mathcal{D}_{-i}$
$\text{H}_2\text{O-C}_2\text{mimCl}^f$	0.109	0.074	0.13	0.07	0.80	0.08
$\text{H}_2\text{O-C}_4\text{mimCl}^g$	0.027	0.026	0.04	0.02	0.42	0.07
$\text{H}_2\text{O-C}_8\text{mimCl}^h$	0.007	0.008	0.02	0.01	0.25	0.03
$\text{DMSO-C}_2\text{mimCl}^i$	0.109	0.074	0.19	0.10	0.24	0.32
$\text{DMSO-C}_4\text{mimCl}^j$	0.027	0.026	0.15	0.03	0.07	0.28

<sup>a</sup> 1 molecule of  $\text{C}_2\text{mimCl}$ ; 599 water molecules

<sup>b</sup> 1 molecule of  $\text{C}_4\text{mimCl}$ ; 599 water molecules

<sup>c</sup> 1 molecule of  $\text{C}_8\text{mimCl}$ ; 599 water molecules

<sup>d</sup> 1 molecule of  $\text{C}_2\text{mimCl}$ ; 199 DMSO molecules

<sup>e</sup> 1 molecule of  $\text{C}_4\text{mimCl}$ ; 199 DMSO molecules

<sup>f</sup> 99 molecules of  $\text{C}_2\text{mimCl}$ ; 1 water molecule

<sup>g</sup> 99 molecules of  $\text{C}_4\text{mimCl}$ ; 1 water molecule

<sup>h</sup> 99 molecules of  $\text{C}_8\text{mimCl}$ ; 1 water molecule

<sup>i</sup> 99 molecules of  $\text{C}_2\text{mimCl}$ ; 1 DMSO molecule

<sup>j</sup> 99 molecules of  $\text{C}_4\text{mimCl}$ ; 1 DMSO molecule

**Table E.6:** Computed values for  $D_{k,\text{self}}/(10^{-9}\text{m}^2\text{s}^{-1})$  and  $C_x/(10^{-9}\text{m}^2\text{s}^{-1})$  for the system  $\text{C}_n\text{mimCl}$ -water and  $\text{C}_n\text{mimCl}$ -DMSO mixtures at 368K, 1atm. See Eq. (5.6).

$i - k$	$D_{k,\text{self}}$	$C_x$	$C_x/D_{k,\text{self}}$
$\text{C}_2\text{mimCl-H}_2\text{O}$ <sup>a</sup>	8.27	9.36	1
$\text{C}_4\text{mimCl-H}_2\text{O}$ <sup>b</sup>	8.27	8.63	1
$\text{C}_8\text{mimCl-H}_2\text{O}$ <sup>c</sup>	8.27	14.5	2
$\text{C}_2\text{mimCl-DMSO}$ <sup>d</sup>	2.38	52.1	22
$\text{C}_4\text{mimCl-DMSO}$ <sup>e</sup>	2.38	34.1	14

<sup>a</sup> 1 molecule of  $\text{C}_2\text{mimCl}$ ; 599 water molecules

<sup>b</sup> 1 molecule of  $\text{C}_4\text{mimCl}$ ; 599 water molecules

<sup>c</sup> 1 molecule of  $\text{C}_8\text{mimCl}$ ; 599 water molecules

<sup>d</sup> 1 molecule of  $\text{C}_2\text{mimCl}$ ; 199 DMSO molecules

<sup>e</sup> 1 molecule of  $\text{C}_4\text{mimCl}$ ; 199 DMSO molecules

# F

---

## Kirkwood-Buff Coefficients from Sampling Fluctuations in Subvolumes

---

In MD simulations, we obtained the KB coefficients  $G_{ij}$  by computing density fluctuations in subvolumes of the simulation box, see section 6.2.3. Figure F.1 shows typical results for the scaling of  $G_{ij}$  with  $1/L$  using this method ( $L$  being the linear length of subvolumes). Only the linear part of  $1/L$  can be used to obtain  $G_{ij}^\infty$  as: (1) for  $1/L \rightarrow 1 \text{ \AA}^{-1}$ , number of molecules within subvolumes is too small to sample accurately; (2) for  $1/L \rightarrow 0$ , the large simulation box is not sufficiently large to act as a grand-canonical reservoir leading to corrections for Eq. (6.18)<sup>158</sup>. The fitting range for obtaining  $G_{ij}^\infty$  is determined by calculating the squared correlation coefficient  $R^2$  defined as

$$R^2 = 1 - \frac{\sum_i (G_{ij} - G_{ij}^p)^2}{\sum_i (G_{ij} - \bar{G}_{ij})^2}, \quad (\text{F.1})$$

$G_{ij}^p$  is the predicted value and  $\bar{G}_{ij}$  is the average value of  $G_{ij}$  over the selected range.  $R^2 \rightarrow 1$  indicates that the linear model fits well to the simulations within the selected range. The range of  $1/L$  where the squared correlation coefficient  $R^2$  is larger than 0.9 for the corresponding  $G_{ij}$  is selected to obtain  $G_{ij}^\infty$ . Figure F.1 shows the computed KB coefficients  $G_{ij}$  in an acetone - methanol mixture at equimolar composition using both cubic and spherical subvolumes<sup>158</sup>. In case of cubic subvolumes,  $L$  is the length of subvolume in one dimension. In case of spherical subvolumes,  $L$  is the diameter of the subvolume. We observed that the linear regime of  $G_{ij}$  is a bit more difficult

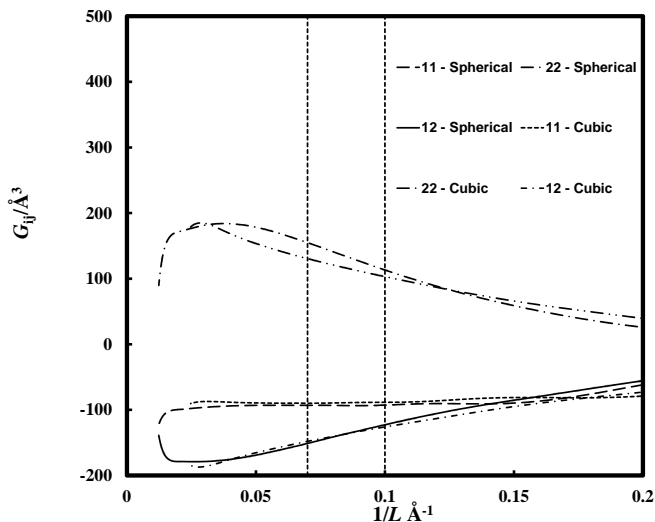


**Figure F.1:** Kirkwood-Buff coefficients  $G_{ij}$  in the binary equimolar system acetone (1) - methanol (2) at 298 K, 1 atm.  $G_{ij}$  is computed by the fluctuation method (Eq.(6.17)). Solid lines represent the data for spherical subvolumes. Dashed lines represent the data for the cubic subvolumes. Data between vertical dotted lines are used for extrapolating the KB coefficients in the thermodynamic limit.

to identify when cubic subvolumes are used. Using spherical subvolumes, the linear regime of computed  $G_{ij}$  is much wider. In our previous work<sup>172</sup>, we used cubic subvolumes for computing the KB coefficients  $G_{ij}$ . Here, we used spherical subvolumes for computing the KB coefficients  $G_{ij}$ . In the studied systems, the linear regime of  $G_{ij}$  occurs between  $1/L = 0.07 \text{ \AA}^{-1}$  and  $1/L = 0.10 \text{ \AA}^{-1}$ .

Figure F.2 shows the thermodynamic factor  $\Gamma$  in the binary systems acetone - methanol and acetone - tetrachloromethane. The MD results with cubic subvolumes are taken from our previous work<sup>172</sup>. Compared to the experimental data,  $\Gamma$  obtained from MD simulations using the fluctuation method agrees very well with the result obtained from COSMO-SAC. The concentration dependence of  $\Gamma$  is correctly captured and the local minimum is reproduced. Although the linear regime is easier to identify using spherical subvolumes, our results computed using the cubic subvolumes do not significantly deviate from the ones with spherical subvolumes.

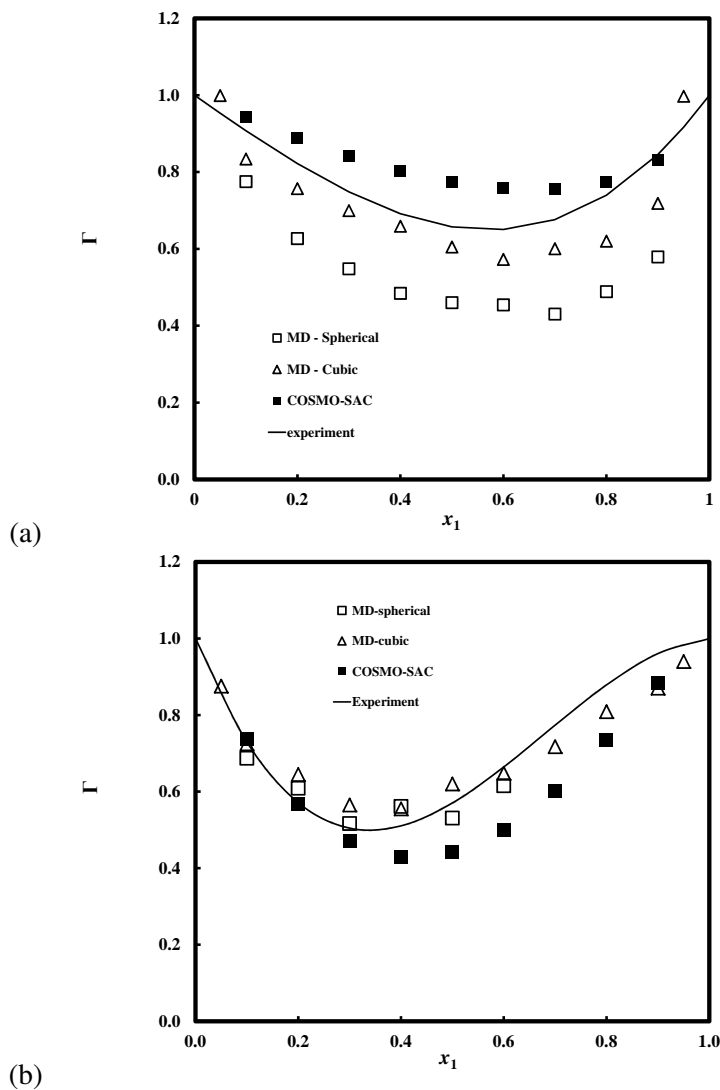


**Figure F.2:** The thermodynamic factor  $\Gamma$  for the binary mixtures (a) acetone (1) - methanol (2) and (b) acetone (1) - tetrachloromethane (2) at 298K, 1 atm. Solid lines represents  $\Gamma$  calculated from experimental VLE data taken from Ref. <sup>168</sup>. Filled symbols represent  $\Gamma$  computed by this work using COSMO-SAC. Open symbols represent the computed  $\Gamma$  using MD simulations. Triangles represent the cubic subvolumes were used in MD simulations. Squares represent the spherical subvolumes were used in MD simulations. The MD data with cubic subvolumes are taken from our previous work <sup>172</sup>.





## Bibliography

- [1] R. Taylor and R. Krishna, *Multicomponent mass transfer*, Wiley, New York, NY, 1st edition, 1993.
- [2] B. Poling, J. Prausnitz, and J. O'Connell, *The properties of gases and liquids*, McGraw-Hill, New York, 5th edition, 2004.
- [3] E. L. Cussler, *Diffusion, mass transfer in fluid systems*, Cambridge University Press, New York, 3rd edition, 2005.
- [4] J. D. Seader and E. J. Henley, *Separation process principles*, Wiley, New York, 3rd edition, 2006.
- [5] C. Geankoplis, *Transport processes and separation process principles*, Prentice Hall Press, NJ, USA, 4th edition, 2003.
- [6] R. B. Bird, W. E. Stewart, and E. N. Lightfoot, *Transport Phenomena*, John Wiley & Sons, Inc., New York, 2nd edition, 2007.
- [7] A. Bardow, E. Kriesten, M. A. Voda, F. Casanova, B. Blümich, and W. Marquardt, *Prediction of multicomponent mutual diffusion in liquids: model discrimination using NMR data*, *Fluid Phase Equilibria* **278**, 27 (2009).
- [8] A. Bardow, V. Göke, H. J. Koß, and W. Marquardt, *Ternary diffusivities by model-based analysis of Raman spectroscopy measurements*, *AIChE* **52**, 4004 (2006).
- [9] I. M. J. J. van de Ven-Lucassen, T. J. H. Vlugt, A. J. J. van der Zanden, and P. J. A. M. Kerkhof, *Using Molecular Dynamics to obtain Maxwell-Stefan diffusion coefficients in liquid systems*, *Mol. Phys.* **94**, 495 (1998).

- [10] I. M. J. J. van de Ven-Lucassen, F. G. Kieviet, and P. J. A. M. Kerkhof, *Fast and convenient implementation of the Taylor dispersion method*, J. Chem. Eng. Data **40**, 407 (1995).
- [11] I. M. J. J. van de Ven-Lucassen, M. F. Kemmere, and P. J. A. M. Kerkhof, *Complications in the use of the Taylor dispersion method for ternary diffusion measurements: methanol+acetone+water mixtures*, J. Solution Chem. **26**, 1145 (1997).
- [12] S. Kjelstrup and D. Bedeaux, *Non-equilibrium thermodynamics of heterogeneous systems*, World Science, Singapore, 1st edition, 2008.
- [13] C. F. Curtiss, *Symmetric gaseous diffusion coefficients*, J. Chem. Phys. **49**, 2917 (1968).
- [14] D. W. Condiff, *On symmetric multicomponent diffusion coefficients*, J. Chem. Phys. **51**, 4209 (1969).
- [15] H. J. Merk, *The macroscopic equations for simultaneous heat and mass transfer in isotropic, continuous and closed systems*, Appl. Sci. Res. **A8**, 73 (1959).
- [16] J. A. Wesselingh, P. Vonk, and G. Kraaijeveld, *Exploring the Maxwell-Stefan description of ion exchange*, Chem. Eng. J. **57**, 75 (1995).
- [17] D. Frenkel and B. Smit, *Understanding molecular simulation: from algorithms to applications*, Academic Press, San Diego, 2nd edition, 2002.
- [18] M. P. Allen and D. J. Tildesley, *Computer simulation of liquids*, Oxford University Press, New York, 1st edition, 1987.
- [19] M. E. Tuckerman, *Statistical mechanics: theory and molecular simulation*, Oxford University Press, Great Britain, 2nd edition, 2010.
- [20] D. Rapaport, *The art of Molecular Dynamics simulation*, Cambridge University Press, Cambridge, 2nd edition, 2004.
- [21] R. Krishna and J. A. Wesselingh, *The Maxwell-Stefan approach to mass transfer*, Chem. Eng. Sci. **52**, 861 (1997).

- 
- [22] S. Kjelstrup, D. Bedeaux, E. Johannessen, and J. Gross, *Non-equilibrium thermodynamics for engineers*, World Science Publishing Co. Pte. Ltd., Singapore, 1st edition, 2010.
- [23] R. Krishna and J. M. van Baten, *The Darken relation for multicomponent diffusion in liquid mixtures of linear alkanes: an investigation using Molecular Dynamics (MD) simulations*, *Ind. Eng. Chem. Res.* **44**, 6939 (2005).
- [24] J. A. Wesselingh and R. Krishna, *Elements of mass transfer*, Ellis Hoewood, Chichester, 1st edition, 1990.
- [25] R. Krishna and J. M. van Baten, *Validating the Darken relation for diffusion in fluid mixtures of varying densities by use of MD simulations*, *Chem. Eng. Technol.* **29**, 761 (2006).
- [26] R. Krishna and J. M. van Baten, *MD simulations of diffusivities in methanol-hexane mixtures near the liquid-liquid phase splitting region*, *Chem. Eng. Technol.* **29**, 516 (2006).
- [27] R. Krishna and J. M. van Baten, *Unified Maxwell-Stefan description of binary mixture diffusion in micro- and meso-porous materials*, *Chem. Eng. Sci.* **64**, 3159 (2009).
- [28] R. Krishna and J. M. van Baten, *Highlighting pitfalls in the Maxwell-Stefan modeling of water-alcohol mixture permeation across pervaporation membranes*, *J. Membrane Sci.* **360**, 476 (2010).
- [29] R. Krishna and J. M. van Baten, *Hydrogen bonding effects in adsorption of water-alcohol mixtures in zeolites and the consequences for the characteristics of the Maxwell-Stefan diffusivities*, *Langmuir* **26**, 10854 (2010).
- [30] E. J. Maginn, A. T. Bell, and D. N. Theodorou, *Transport diffusivity of methane in silicalite from equilibrium and nonequilibrium simulations*, *J. Phys. Chem.* **97**, 4173 (1993).
- [31] M. Tsige and G. S. Grest, *Molecular Dynamics simulation of solvent polymer interdiffusion: Fickian diffusion*, *J. Chem. Phys.* **120**, 2989 (2004).

- [32] M. Tsige and G. S. Grest, *Interdiffusion of solvent into glassy polymer films: a Molecular Dynamics study*, J. Chem. Phys. **121**, 7513 (2004).
- [33] X. Liu, T. J. H. Vlugt, and A. Bardow, *Maxwell-Stefan diffusivities in liquid mixtures: using Molecular Dynamics for testing model predictions*, Fluid Phase Equilibria **301**, 110 (2011).
- [34] X. Liu, A. Bardow, and T. J. H. Vlugt, *Multicomponent Maxwell-Stefan diffusivities at infinite dilution*, Ind. Eng. Chem. Res. **50**, 4776 (2011).
- [35] X. Liu, T. J. H. Vlugt, and A. Bardow, *Predictive Darken equation for Maxwell-Stefan diffusivities in multicomponent systems*, Ind. Eng. Chem. Res. **50**, 10350 (2011).
- [36] J. MacElroy, *Nonequilibrium Molecular Dynamics simulation of diffusion and flow in thin microporous membranes*, J. Chem. Phys. **101**, 5274 (1994).
- [37] G. S. Heffelfinger and D. M. Ford, *Massively parallel dual control grand canonical Molecular Dynamics with LADERT: 2 gradient driven diffusion through polymers*, Mol. Phys. **94**, 659 (1998).
- [38] D. R. Wheeler and J. Newman, *Molecular Dynamics simulations of multicomponent diffusion. 2. nonequilibrium method*, J. Phys. Chem. B **108**, 18362 (2004).
- [39] D. J. Evans and G. P. Morriss, *Statistical mechanics of nonequilibrium liquids*, Academic Press, London, 2nd edition, 1990.
- [40] D. MacGowan and D. J. Evans, *Heat and matter transport in binary liquid mixtures*, Phys. Rev. A **34**, 2133 (1986).
- [41] G. Guevara-Carrion, J. Vrabec, and H. Hasse, *Prediction of transport properties of liquid ammonia and its mixture with methanol by molecular simulation*, Int. J. Thermophys. **33**, 449 (2012).
- [42] G. Guevara-Carrion, J. Vrabec, and H. Hasse, *On the prediction of transport properties of monomethylamine, dimethylether and hydrogen chloride by molecular simulation*, Fluid Phase Equilibria **316**, 46 (2012).

- 
- [43] G. Guevara-Carrion, J. Vrabec, and H. Hasse, *Prediction of self-diffusion coefficient and shear viscosity of water and its binary mixtures with methanol and ethanol by molecular simulations*, J. Chem. Phys. **134**, 074508 (2011).
- [44] G. A. Fernandez, J. Vrabec, and H. Hasse, *Self-Diffusion and binary Maxwell-Stefan diffusion coefficients of quadrupolar real fluids from molecular simulation*, Int. J. Thermophys. **26**, 1389 (2005).
- [45] G. A. Fernandez, J. Vrabec, and H. Hasse, *Self-diffusion and binary Maxwell-Stefan diffusion in simple fluids with the Green-Kubo method*, Int. J. Thermophys. **25**, 175 (2004).
- [46] G. Guevara-Carrion, C. Nieto-Draghi, J. Vrabec, and H. Hasse, *Prediction of transport properties by molecular simulation: methanol and ethanol and their mixture*, J. Phys. Chem. B **112**, 16664 (2008).
- [47] D. J. Keffer and A. Adhangale, *The composition dependence of self and transport diffusivities from Molecular Dynamics simulations*, Chem. Eng. J. **100**, 51 (2004).
- [48] S. K. Schnell, X. Liu, J. M. Simon, A. Bardow, D. Bedeaux, T. J. H. Vlugt, and S. Kjelstrup, *Calculating thermodynamic properties from fluctuations at small scales*, J. Phys. Chem. B **115**, 10911 (2011).
- [49] S. K. Schnell, T. J. H. Vlugt, J. M. Simon, D. Bedeaux, and S. Kjelstrup, *Thermodynamics of a small system in a  $\mu T$  reservoir*, Chem. Phys. Lett. **504**, 199 (2011).
- [50] H. A. Kooijman and R. Taylor, *Estimation of diffusion coefficients in multi-component liquid systems*, Ind. Eng. Chem. Res. **30**, 1217 (1991).
- [51] S. Rehfeldt and J. Stichlmair, *Measurement and calculation of multicomponent diffusion coefficients in liquids*, Fluid Phase Equilibria **256**, 99 (2007).
- [52] A. Vignes, *Diffusion in binary solutions. variation of diffusion coefficient with composition*, Ind. Eng. Chem. Fundamen. **5**, 189 (1966).
- [53] C. R. Wilke and P. Chang, *Correlation of diffusion coefficients in dilute solutions*, AIChE J. **1**, 264 (1955).

- [54] L. S. Darken, *Diffusion, mobility and their interrelation through free energy in binary metallic systems*, Transactions of the American Institute of Mining and Metallurgical Engineers **175**, 184 (1948).
- [55] F. A. L. Dullien, *Statistical test of Vignes correlation of liquid-phase diffusion coefficients*, Ind. Eng. Chem. Fund. **10**, 41 (1971).
- [56] R. Car and M. Parrinello, *Unified approach for Molecular Dynamics and density functional theory*, Phys. Rev. Lett. **55**, 2471 (1985).
- [57] J. van den Bergh, S. Ban, T. J. H. Vlugt, and F. Kapteijn, *Modeling the loading dependency of diffusion in zeolites: the relevant site model extended to mixtures in DDR-type zeolite*, J. Phys. Chem. C **113**, 21856 (2009).
- [58] A. Bardow, W. Marquardt, V. Göke, H. J. Koß, and K. Lucas, *Model-based measurement of diffusion using Raman spectroscopy*, AIChE **49**, 323 (2003).
- [59] Y. D. Hsu and Y. P. Chen, *A group contribution correlation of the mutual diffusion coefficients of binary liquid mixtures*, Fluid Phase Equilibria **173**, 1 (2000).
- [60] C. He, *Prediction of the concentration dependence of mutual diffusion coefficients in binary liquid mixtures*, Ind. Eng. Chem. Res. **34**, 2148 (1995).
- [61] S. R. P. da Rocha and J. V. de Oliveira, *An evaluation of density corrections for estimating diffusivities in liquids and liquid mixtures*, Chem. Eng. Sci. **52**, 1097 (1997).
- [62] R. Taylor and H. A. Kooijman, *Composition derivatives of activity coefficient models for the estimation of thermodynamic factors in diffusion*, Chem. Eng. Commun. **102**, 87 (1991).
- [63] D. J. Keffer, B. J. Edwards, and P. Adhangale, *Determination of statistically reliable transport diffusivities from Molecular Dynamics simulation*, J. Non-Newtonian Fluid Mech. **120**, 41 (2004).
- [64] A. Leahy-Dios and A. Firoozabadi, *Unified model for nonideal multicomponent molecular diffusion coefficients*, AIChE **53**, 2932 (2007).

- 
- [65] D. Bosse and H. Bart, *Prediction of diffusion coefficients in liquid systems*, Ind. Eng. Chem. Res. **45**, 1822 (2006).
- [66] J. A. Wesselingh and A. M. Bollen, *Multicomponent diffusion from the free volume theory*, Chem. Eng. Res. Des. **75**, 590 (1997).
- [67] S. Rehfeldt and J. Stichlmair, *Measurement and prediction of multicomponent diffusion coefficients in four ternary liquid systems*, Fluid Phase Equilibria **290**, 1 (2010).
- [68] C. D. Wick, M. G. Martin, and J. I. Siepmann, *Transferable potentials for phase equilibria. 4.united-atom description of linear and branched alkenes and alkylbenzenes*, J. Phys. Chem. B **104**, 8008 (2000).
- [69] D. Dubbeldam, S. Calero, T. J. H. Vlugt, R. Krishna, T. L. M. Maesen, and B. Smit, *United atom force field for alkanes in nanoporous materials*, J. Phys. Chem. B **108**, 12301 (2004).
- [70] S. A. Beg, N. M. Tukur, D. K. Al-Harbi, and E. Z. Hamad, *Saturated liquid densities of benzene, cyclohexane, and hexane from 298.15 to 473.15 K*, J. Chem. Eng. Data **38**, 461 (1993).
- [71] J. L. E. Chevalier, P. J. Petrino, and Y. H. Gaston-Bonhomme, *Viscosity and density of some aliphatic, cyclic, and aromatic hydrocarbons binary liquid mixtures*, J. Chem. Eng. Data **35**, 206 (1990).
- [72] S. S. Joshi, T. M. Aminabhavi, and R. H. Balundgi, *Densities and viscosities of binary liquid mixtures of nitrobenzene with cyclohexane and n,n-dimethylformamide*, J. Chem. Eng. Data **35**, 185 (1990).
- [73] A. A. Asfour, M. H. Siddique, and T. D. Vavanellos, *Density-composition data for eight binary systems containing toluene or ethylbenzene and CB-C,6 n-alkanes at 293.15, 298.15, 308.15, and 313.15 K*, J. Chem. Eng. Data **35**, 192 (1990).
- [74] M. Frenkel, *TRC thermodynamic tables, hydrocarbons, supplement No. 92; thermodynamics research center*, Texas A&M University, College Station, TX, 1st edition, 1986.

- [75] D. Dubbeldam, D. C. Ford, D. E. Ellis, and R. Q. Snurr, *A new perspective on the order- $n$  algorithm for computing correlation functions*, *Mol. Sim.* **35**, 1084 (2009).
- [76] D. Dubbeldam, E. Beerdsen, T. J. H. Vlugt, and B. Smit, *Molecular simulation of loading-dependent diffusion in nanoporous materials using extended dynamically corrected transition state theory*, *J. Chem. Phys.* **122**, 224712 (2005).
- [77] H. Iloukhani, M. Rezaei-Sameti, and H. A. Zarei, *Volumetric and viscometric studies of molecular interaction of the ternary system toluene-cyclohexane-hexane at 298.15K*, *Thermochimica Acta* **438**, 9 (2005).
- [78] T. Merzliak, I. Bartussek, S. Stapf, M. A. Voda, B. Blümich, and A. Pfennig, *Description of intra-diffusion in liquid mixtures*, *Fluid Phase Equilibria* **245**, 158 (2006).
- [79] K. Aoyagi and J. G. Albright, *Tracer diffusion and viscosity study at 25°C in binary and ternary liquid systems*, *J. Phys. Chem.* **76**, 2572 (1972).
- [80] O. O. Medvedev and A. A. Shapiro, *Verifying reciprocal relations for experimental diffusion coefficients in multicomponent mixtures*, *Fluid Phase Equilibria* **208**, 291 (2003).
- [81] J. D. Weeks, D. Chandler, and H. C. Andersen, *Role of repulsive forces in determining the equilibrium structure of simple liquids*, *J. Chem. Phys.* **54**, 5237 (1971).
- [82] X. Liu, A. Bardow, and T. J. H. Vlugt, *Maxwell-Stefan diffusivities and velocity cross-correlations in dilute ternary systems*, *Diffusion-fundamentals.org* **16**, 81 (2011).
- [83] W. Marbach, H. G. Hertz, and H. Weingärtner, *Self- and mutual diffusion coefficients of some binary liquid  $n$ -alkane mixtures - a velocity correlation study*, *Zeitschrift für Physikalische Chemie* **189**, 63 (1995).
- [84] J. P. Ryckaert, G. Ciccotti, and H. J. C. Berendsen, *Numerical integration of the Cartesian equations of motion of a system with constraints: Molecular Dynamics of  $n$ -alkanes*, *J. Comp. Phys.* **23**, 237 (1977).



- 
- [85] W. Smith, T. R. Forester, I. T. Todorov, and M. Leslie, *The DLPOLY2 user manual*, (2006), <ftp://ftp.dl.ac.uk>.
- [86] B. Chen, J. J. Potoff, and J. I. Siepmann, *Monte Carlo calculation for alcohols and their mixtures with alkanes*, *J. Phys. Chem. B* **105**, 3093 (2001).
- [87] Y. Wu, H. L. Tepper, and G. A. Voth, *Flexible simple point charge water model with improved liquid state properties*, *J. Chem. Phys.* **124**, 24503 (2006).
- [88] R. Krishna and J. M. van Baten, *An investigation of the characteristics of Maxwell-Stefan diffusivities of binary mixtures in silica nanopores*, *Chem. Eng. Sci.* **64**, 870 (2009).
- [89] C. R. Wilke and P. Chang, *Correlation of diffusion coefficients in dilute solutions*, *AIChE* **1**, 264 (1955).
- [90] Z. A. Makrodimitri, D. J. M. Unruh, and I. G. Economou, *Molecular simulation of diffusion of hydrogen, carbon monoxide and water in heavy n-alkanes*, *J. Phys. Chem. B* **115**, 1429 (2011).
- [91] H. J. V. Tyrell and K. R. Harris, *Diffusion in Liquids*, Butterworths, London, 2nd edition, 1984.
- [92] M. Schoen and C. Hoheisel, *Static and dynamic cross correlation in thermodynamically stable and unstable mixtures*, *Mol. Phys.* **53**, 1367 (1984).
- [93] Y. H. Zhou and G. H. Miller, *Green-Kubo formulas for mutual diffusion coefficients in multicomponent systems*, *J. Phys. Chem.* **100**, 5516 (1996).
- [94] M. A. Granato, M. Jorge, T. J. H. Vlugt, and A. E. Rodrigues, *Diffusion of propane, propylene and isobutane in 13X zeolite by molecular dynamics*, *Chem. Eng. Sci.* **65**, 2656 (2010).
- [95] A. R. Cooper, *Model for multi-component diffusion*, *Phys. Chem. Glasses* **6**, 55 (1965).
- [96] R. C. Remsing, R. P. Swatloski, R. D. Rogers, and G. Moyna, *Mechanism of cellulose dissolution in the ionic liquid 1-n-butyl-3-methylimidazolium chloride: a  $^{13}\text{C}$  and  $^{35/37}\text{Cl}$  NMR relaxation study on model systems*, *Chem. Comm.* **12**, 1271 (2006).

- [97] P. Wasserscheid and T. Welton, *Ionic Liquids in Synthesis*, WILEY-VCH, Verlag GmbH, Co. KGaA, Weinheim, 1st edition, 2008.
- [98] Y. Zhang, C. Z. Sun, J. Liang, and Z. C. Shang, *Catalysis by l-lysine: a green method for the condensation of aromatic aldehydes with acidic methylene compounds in water at room temperature*, *Chinese Journal of Chemistry* **28**, 2255 (2010).
- [99] M. S. and M. Dinari, *Environmentally friendly methodology for preparation of amino acid containing polyamides*, *Journal of Polymers and the Environment* **18**, 705 (2010).
- [100] A. Jeihanipour, K. Karimi, C. Niklasson, and M. J. Taherzadeh, *A novel process for ethanol or biogas production from cellulose in blended-fibers waste textiles*, *Waste Manag.* **30**, 2504 (2010).
- [101] M. Ramdin, T. W. de Loos, and T. J. H. Vlucht, *State-of-the-art of CO<sub>2</sub> capture with ionic liquids*, *Ind. Eng. Chem. Res.* **51**, 8149 (2012).
- [102] J. G. Huddleston, H. D. Willauer, R. P. Swatloski, A. E. Visser, and R. D. Rogers, *Room temperature ionic liquids as novel media for clean liquid-liquid extraction*, *Chem. Comm.* **16**, 1765 (1998).
- [103] R. P. Swatloski, S. K. Spear, J. D. Holbrey, and R. D. Rogers, *Dissolution of cellulose with ionic liquids*, *J. Am. Chem. Soc.* **124**, 4974 (2002).
- [104] T. G. A. Youngs, C. Hardacre, and J. D. Holbrey, *Glucose solvation by the ionic liquid 1,3-dimethylimidazolium chloride: a simulation study*, *J. Phys. Chem.* **111**, 13765 (2007).
- [105] A. R. Porter, S. Y. Liem, and P. L. A. Popelier, *Room temperature ionic liquids containing low water concentrations - a Molecular Dynamics study*, *Phys. Chem. Chem. Phys.* **10**, 4240 (2008).
- [106] C. S. Lovell, A. Walker, R. A. Damion, A. Radhi, S. F. Tanner, T. Budtova, and M. E. Ries, *Influence of cellulose on ion diffusivity in 1-ethyl-3-methylimidazolium acetate cellulose solutions*, *Biomacromolecules* **11**, 2927 (2010).

- 
- [107] C. Iacob, J. R. Sangoro, P. Papadopoulos, T. Schubert, S. Naumov, R. Valiullin, J. Karger, and F. Kremer, *Charge transport and diffusion of ionic liquids in nanoporous silica membranes*, *Phys. Chem. Chem. Phys.* **12**, 13798 (2010).
- [108] J. E. Bara, T. K. Carlisle, C. J. Gabriel, D. Camper, A. Finotello, D. L. Gin, and R. D. Noble, *Guide to CO<sub>2</sub> separations in imidazolium-based room-temperature ionic liquids*, *Ind. Eng. Chem. Res.* **48**, 2793 (2009).
- [109] O. Borodin and D. Smith, *Structure and dynamics of n-methyl-n-propylpyrrolidinium bis(trifluoromethanesulfonyl)imide ionic liquid from Molecular Dynamics simulations*, *J. Phys. Chem. B* **110**, 11481 (2006).
- [110] Z. P. Liu, T. Chen, A. Bell, and B. Smit, *Improved united-atom force field for 1-alkyl-3-methylimidazolium chloride*, *J. Phys. Chem. B* **114**, 4572 (2010).
- [111] T. Méndez-Morales, J. Carrete, O. Cabeza, L. Gallego, and L. Varela, *Molecular Dynamics simulation of the structure and dynamics of water-Alkyl-3-methylimidazolium ionic liquid mixtures*, *J. Phys. Chem. B* **115**, 6995 (2011).
- [112] W. C. Su, C. H. Chou, D. S. H. Wong, and M. H. Li, *Diffusion coefficients and conductivities of alkylimidazolium tetrafluoroborates and hexafluorophosphates*, *Journal of Solution Chemistry* **252**, 74 (2007).
- [113] C. L. Wong, A. N. Soriano, and M. H. Li, *Diffusion coefficients and molar conductivities in aqueous solutions of 1-ethyl-3-methylimidazolium-based ionic liquids*, *Fluid Phase Equilibria* **271**, 43 (2008).
- [114] A. Heintz, J. Lehmann, E. Schmidt, and A. Wandschneider, *Diffusion coefficients of imidazolium based ionic liquids in aqueous solutions*, *Journal of Solution Chemistry* **38**, 1079 (2009).
- [115] S. Sarraute, M. F. Costa Gomes, and A. A. H. Padua, *Diffusion coefficients of 1-alkyl-3-methylimidazolium ionic liquids in water, methanol, and acetonitrile at infinite dilution*, *J. Chem. Eng. Data* **54**, 2389 (2009).
- [116] C. A. Nieto de Castro, E. Langa, A. L. Morais, M. L. Matos Lopes, M. J. V. Lourenco, F. J. V. Santos, M. S. C. S. Santos, J. N. Canongia Lopes, H. I. M.

- Veiga, M. Macatrao, J. M. S. S. Esperanca, C. S. Marques, L. P. N. Rebelo, and C. A. M. Afonso, *Studies on the density, heat capacity, surface tension and infinite dilution diffusion with the ionic liquids [C<sub>4</sub>mim][NTf<sub>2</sub>], [C<sub>4</sub>mim][dca], [C<sub>2</sub>mim][EtOSO<sub>3</sub>] and [Aliquat][dca]*, *Fluid Phase Equilibria* **294**, 157 (2010).
- [117] A. Heintz, R. Ludwig, and E. Schmidt, *Limiting diffusion coefficients of ionic liquids in water and methanol: a combined experimental and Molecular Dynamics study*, *Phys. Chem. Chem. Phys.* **13**, 3268 (2011).
- [118] J. Richter, A. Leuchter, and N. Grosser, *Digital image holography for diffusion measurements in molten salts and ionic liquids - method and first results*, *J. Mol. Liq.* **103**, 359 (2003).
- [119] M. Chalaris, S. Marinakis, and D. Dellis, *Temperature effects on the structure and dynamics of liquid dimethyl sulfoxide: A Molecular Dynamics study*, *Fluid Phase Equilibria* **267**, 47 (2008).
- [120] T. Chen, M. Chidambaram, Z. P. Liu, B. Smit, and A. T. Bell, *Viscosities of the mixtures of 1-ethyl-3-methylimidazolium chloride with water, acetonitrile and glucose: A Molecular Dynamics simulation and experimental study*, *J. Phys. Chem. B* **114**, 5790 (2010).
- [121] P. S. Nikam, M. C. Jadhav, and M. Hasan, *Density and viscosity of mixtures of dimethyl sulfoxide methanol, ethanol, propan-1-ol, propan-2-ol, butan-1-ol, 2-methylpropan-1-ol, 2-methylpropan-2-ol at 298,15 K and 313.15 K*, *J. Chem. Eng. Data* **41**, 1028 (1996).
- [122] H. N. Bordallo, K. W. Herwig, B. M. Luther, and N. E. Levinger, *Quasi-elastic neutron scattering study of dimethyl-sulfoxide-water mixtures: probing molecular mobility in a nonideal solution*, *J. Chem. Phys.* **121**, 12457 (2004).
- [123] M. Holz, S. Heil, and A. Sacco, *Temperature dependent self-diffusion coefficients of water and six selected molecular liquids for calibration in accurate <sup>1</sup>H NMR PFG measurements*, *Phys. Chem. Chem. Phys.* **2**, 4740 (2000).
- [124] G. S. Kell, *Precise representation of volume properties of water at one atmosphere*, *J. Chem. Phys.* **121**, 12457 (2004).

- 
- [125] G. S. Kell, *Density, thermal expansivity and compressibility of liquid water from 0° to 150° C*, J. Chem. Eng. Data **20**, 97 (1975).
- [126] H. R. Pruppacher, *Self diffusion coefficient of supercooled water*, J. Chem. Phys. **56**, 101 (1972).
- [127] J. S. Newman, *Electrochemical system*, Prentice-hall, Inc, United State of America, 1st edition, 1991.
- [128] F. A. A., D. A. Floreani, L. A. King, J. S. Landers, B. J. Piersma, D. J. Stch, R. L. Vaughn, J. S. Wilkes, and J. L. Williams, *Properties of 1,3-dialkylimidazolium chloride - aluminum chloride ionic liquids*, J. Phys. Chem. **88**, 2614 (1984).
- [129] L. Dong, D. X. Zheng, Z. Wei, and X. H. Wu, *Synthesis of 1,3-dimethylimidazolium chloride and volumetric property investigations of its aqueous solution*, Int. J. Thermophys. **30**, 1480 (2009).
- [130] M. Shukla, N. Srivastava, and S. Saha, *Theoretical and spectroscopic studies of 1-butyl-3-methylimidazolium iodide room temperature ionic liquid: its differences with chloride and bromide derivatives*, Journal of Molecular Structure **975**, 349 (2010).
- [131] U. Domanska, E. Bogel-Lukasik, and R. Bogel-Lukasik, *1-octanol/water partition coefficients of 1-alkyl-3-methylimidazolium chloride*, Chem. Eur. J. **9**, 3033 (2003).
- [132] S. L. Feng and G. A. Voth, *Molecular Dynamics simulations of imidazolium-based ionic liquid/water mixtures*, Fluid Phase Equilibria **294**, 148 (2010).
- [133] C. Nieto-Draghi, J. B. Avalos, and B. Rousseau, *Transport properties of dimethyl sulfoxide aqueous solutions*, J. Chem. Phys. **119**, 4782 (2003).
- [134] A. K. Soper and A. Luzar, *Orientation of water molecules around small polar and non-polar groups in solution: a neutron diffraction and computer simulation study*, J. Phys. Chem. **100**, 1357 (1996).

- [135] S. Miyanaga, K. Tamura, and S. Murakami, *Excess enthalpies and excess heat capacities of the binary mixtures of acetonitrile, dimethylformamide, and benzene at 298.15K*, J. Therm. Anal. **38**, 1767 (1992).
- [136] A. K. Soper and A. Luzar, *A neutron diffraction study of dimethyl sulfoxide*, J. Chem. Phys. **97**, 1320 (1992).
- [137] A. Luzar and D. Chandler, *Structure and hydrogen bond dynamics of water-dimethyl sulfoxide mixtures by computer simulations*, J. Chem. Phys. **98**, 8160 (1993).
- [138] I. I. Vaisman and M. L. Berkowitz, *Local structure order and molecular associations in water-DMSO mixtures*, J. Am. Chem. Soc. **114**, 7889 (1992).
- [139] R. C. Remsing, Z. W. Liu, I. Sergeyev, and G. Moyna, *Solvation and aggregation of *n,n*-dialkylimidazolium ionic liquids: a multinuclear NMR spectroscopy and Molecular Dynamics simulation study*, J. Phys. Chem. B **112**, 7363 (2008).
- [140] W. Zhao, F. Leroy, B. Heggen, S. Zahn, B. Kirchner, S. Balasubramanian, and F. Müller-Plathe, *Are there stable ion pairs in room-temperature ionic liquids? Molecular Dynamics simulations of 1-*n*-butyl-3-methylimidazolium hexafluorophosphate*, J. Am. Chem. Soc. **131**, 15825 (2009).
- [141] Y. T. Zhang, X. H. Du, H B. Qian, and E. Y. X. Chem, *Ionic liquid-water mixtures: Enhanced  $K_w$  for efficient cellulose biomass conversion*, J. Am. Chem. Soc. **114**, 7889 (1992).
- [142] H. Shekaari and S. S. Mousavi, *Osmotic coefficients and refractive indices of aqueous solutions of ionic liquids containing 1-butyl-3-methylimidazolium halide at  $T = 298.15$  to  $328.15K$* , J. Chem. Eng. Data **54**, 823 (2009).
- [143] C. P. Fredlake, J. M. Crosthwaite, D. G. Hert, S. N. V. J. Aki, and J. F. Brennecke, *Thermophysical properties of imidazolium-based ionic liquids*, J. Chem. Eng. Data **49**, 954 (2004).
- [144] Q. Gan, D. Rooney, M. L. Xue, G. Thompson, and Y. R. Zou, *An experimental study of gas transport and separation properties of ionic liquids supported on nanofiltration membranes*, J. Membrane Sci. **280**, 948 (2006).

- 
- [145] E. Hendriks, G. M. Kontogeorgis, R. Dohrn, J. C. de Hemptinne, I. G. Economou, L. F. Zilnik, and V. Vesovic, *Industrial requirements for thermodynamics and transport properties*, Ind. Eng. Chem. Res. **49**, 11131 (2010).
- [146] G. D. C. Kuiken, *Thermodynamics of irreversible processes: applications to diffusion and rheology*, Wiley, 1st edition, 1994.
- [147] X. Liu, T. J. H. Vlugt, and A. Bardow, *Maxwell-Stefan diffusivities in binary mixtures of ionic liquids with DMSO and H<sub>2</sub>O*, J. Phys. Chem. B **115**, 8506 (2011).
- [148] D. R. Wheeler and J. Newman, *Molecular Dynamics simulations of multicomponent diffusion. 1. equilibrium method*, J. Phys. Chem. B **108**, 18353 (2004).
- [149] O. O. Medvedev and A. A. Shapiro, *Modeling diffusion coefficients in binary mixtures*, Fluid Phase Equilibria **225**, 13 (2004).
- [150] D. J. Keffer, C. Y. Gap, and B. J. Edwards, *On the relationship between Fickian diffusivities at the continuum and molecular levels*, J. Phys. Chem. B **109**, 5279 (2005).
- [151] D. Zabala, C. Nieto-Draghi, J. C. de Hemptinne, and A. L. López de Ramos, *Diffusion coefficients in CO<sub>2</sub>/n-alkane binary liquid mixtures by molecular simulation*, J. Phys. Chem. B **112**, 16610 (2008).
- [152] J. G. Kirkwood and F. P. Buff, *The statistical mechanical theory of solution*, J. Chem. Phys. **19**, 774 (1951).
- [153] A. Ben-Naim, *Molecular theory of solutions*, Oxford university press, Oxford, 2nd edition, 2006.
- [154] W. Shi and E. J. Maginn, *Continuous fractional component Monte Carlo: an adaptive biasing method for open system atomistic Simulations*, J. Chem. Theory Comput. **3**, 1451 (2007).
- [155] W. Shi and E. J. Maginn, *Improvement in molecule exchange efficiency in Gibbs ensemble Monte Carlo: development and implementation of the continuous fractional component move*, J. Comp. Chem. **29**, 2520 (2008).

- [156] E. Ruckenstein and I. Shulgin, *Entrainer effect in supercritical mixtures*, Fluid Phase Equilibria **180**, 345 (2001).
- [157] A. Perera, L. Zoranic, F. Sokolic, and R. Mazighi, *A comparative Molecular Dynamics study of water-methanol and acetone-methanol mixtures*, J. Mol. Liq. **159**, 52 (2011).
- [158] S. K. Schnell, T. J. H. Vlugt, J. M. Simon, D. Bedeaux, and S. Kjelstrup, *Thermodynamics of small systems embedded in a reservoir: a detailed analysis of finite size effects*, Mol. Phys. **110**, 1069 (2012).
- [159] N. R. Tummala and A. Striolo, *Hydrogen-bond dynamics for water confined in carbon tetrachloride-acetone mixtures*, J. Phys. Chem. B **112**, 10675 (2008).
- [160] W. L. Jorgensen, *Optimized intermolecular potential functions for liquid alcohols*, J. Phys. Chem. **90**, 1276 (1986).
- [161] A. N. Campbell and E. M. Kartzmark, *Thermodynamic and other properties of methanol + acetone, carbon disulphide + acetone, carbon disulphide + methanol, and carbon disulphide + methanol + acetone*, J. Chem. Thermodyn. **5**, 163 (1973).
- [162] K. Noda, M. Ohashi, and K. Ishida, *Viscosities and densities at 298.15K for mixtures of methanol, acetone and water*, J. Chem. Eng. Data **27**, 326 (1982).
- [163] J. Timmermans, *The physico-chemical constants of binary systems in concentrated solutions*, Interscience Publishers, New York, 1st edition, 1959.
- [164] A. P. Hardt, D. K. Anderson, R. Rathbun, B. W. Mar, and A. L. Babb, *Self diffusion in liquids*, J. Phys. Chem. **63**, 2059 (1959).
- [165] A. I. Toryanik and V. N. Taranenko, *Molecular mobility and structure in water-acetone mixtures*, J. Struct. Chem. **28**, 714 (1988).
- [166] Y. O. Kamei and H. Sumie, *Relation between self-diffusion coefficients and interdiffusion coefficients in methanol-carbon tetrachloride and ethanol-carbon tetrachloride systems*, J. Chem. Phys. **61**, 2227 (1974).



- 
- [167] Z. J. Derlacki, A. J. Easteal, A. V. J. Edge, L. A. Woolf, and Z. Roksandic, *Diffusion coefficients of methanol and water and mutual diffusion coefficient in methanol-water solutions at 278 and 298K*, J. Phys. Chem. **89**, 5318 (1985).
- [168] J. Gmehling and U. Onken, *Vapor-liquid equilibrium data collection*, DECHEMA, Germany, 1st edition, (2005).
- [169] A. Alimadadian and C. P. Colver, *A new technique for the measurement of ternary molecular diffusion coefficients in liquid systems*, Can. J. Chem. Eng. **54**, 208 (1976).
- [170] R. Kumar, S. Jayakumar, and V. Kannappan, *Study of molecular interactions in binary liquid mixtures*, Indian J. Pure. Ap. Mat. **46**, 169 (2008).
- [171] D. K. Anderson, J. R. Hall, and A. L. Babb, *Mutual diffusion in non-ideal binary liquid mixtures*, J. Phys. Chem. **62**, 404 (1958).
- [172] X. Liu, S. K. Schnell, J. M. Simon, D. Bedeaux, S. Kjelstrup, A. Bardow, and T. J. H. Vlucht, *Fick diffusion coefficients of liquid mixtures directly obtained from equilibrium Molecular Dynamics*, J. Phys. Chem. B **115**, 12921 (2011).
- [173] X. Liu, S. K. Schnell, J. M. Simon, D. Bedeaux, S. Kjelstrup, A. Bardow, and T. J. H. Vlucht, *Correction to: Fick diffusion coefficients of liquid mixtures directly obtained from equilibrium Molecular Dynamics*, J. Phys. Chem. B **116**, 6070 (2012).
- [174] R. Wedberg, J. P. O. Connell, G. H. Peters, and J. Abildskov, *Pair correction function integrals: computation and use*, J. Chem. Phys. **135**, 084113 (2011).
- [175] J. W. Nichols, S. G. Moore, and D. R. Wheeler, *Improved implementation of Kirkwood-Buff solution theory in periodic molecular simulations*, Phys. Rev. E **80**, 051203 (2009).
- [176] D. Mukherji, N. F. A. van der Vegt, K. Kremer, and L. D. Site, *Kirkwood-Buff analysis of liquid mixtures in an open boundary simulation*, J. Chem. Theory Comput. **8**, 375 (2012).

- [177] R. Taylor and H. A. Kooijman, *Composition derivative of activity coefficient models for the estimation of thermodynamic factors in diffusion*, Chem. Eng. Commun. **102**, 87 (1991).
- [178] S. T. Lin and S. I. Sandler, *A prior phase equilibrium prediction from a segment contribution solvation model*, Industrial & Engineering Chemistry Research **41**, 899 (2002).
- [179] C. M. Hsieh, S. I. Sandler, and S. T. Lin, *Improvements of COSMO-SAC for vapor-liquid and liquid-liquid equilibrium predictions*, Fluid Phase Equilibria **297**, 90 (2010).
- [180] R. Gupta and A. Chandra, *Structural, single-particle and pair dynamical properties of acetone-chloroform mixtures with dissolved solutes*, Chem. Phys. **383**, 41 (2011).
- [181] *ADF, SCM*, Theoretical Chemistry, Vrije Universiteit, Amsterdam, The Netherlands, <http://www.scm.com>.
- [182] A. E. Karr, W. M. Bowes, and E. G. Scheibel, *Analysis of binary and ternary mixtures*, Anal. Chem. **23**, 459 (1951).
- [183] I. C. Wei and R. L. Rowley, *Binary liquid mixture viscosities and densities*, J. Chem. Eng. Data **29**, 332 (1984).
- [184] P. Oracz and S. Warycha, *Vapour-liquid equilibria. The ternary system methanol-chloroform-acetone at 303.15K*, Fluid Phase Equilibria **137**, 149 (1997).

## Summary

The aim of this thesis is to study multicomponent diffusion in liquids using Molecular Dynamics (MD) simulations. Diffusion plays an important role in mass transport processes. In binary systems, mass transfer processes have been studied extensively using both experiments and molecular simulations. From a practical point of view, systems consisting more than two components are more interesting. However, experimental and simulation data on transport diffusion for such systems are scarce. Therefore, a more detailed knowledge on mass transfer in multicomponent systems is required. The presence of multiple components in a system introduces difficulties in studying diffusion in experiments. Investigating the concentration dependence of diffusion coefficients seriously increases the required experimental effort. In this thesis, we will use MD simulation based on classical force fields to study multicomponent diffusion in liquids. Diffusion can be described using both Fick and Maxwell-Stefan (MS) diffusion coefficients. Experiments provide Fick diffusion coefficients while simulations usually provide MS diffusion coefficients. Fick and MS diffusivities are related via the matrix of thermodynamic factors. A brief survey on methods for studying liquid diffusion and their limitations is presented in chapter 1

In chapter 2, we study the diffusion in the ternary system n-hexane-cyclohexane-toluene. The existing models for predicting MS diffusivities at finite concentrations (*i.e.* the Vignes equation) as well as the predictions at infinite dilution (*i.e.* predictions of  $\mathcal{D}_{ij}^{x_k \rightarrow 1}$  using the so-called WK, KT, VKB, DKB and RS models) are tested using MD simulations. We find that (1) the Vignes equation only results in reasonable predictions for MS diffusivities yielding differences of 13% compared to the actual diffusion coefficients; (2) the best predictive model (the KT model) for calculating MS diffusivities at infinite dilution results in differences of 8% compared to the actual diffusion coefficients. It is important to note that the differences of 8% can be a coincidence since KT model is empirical and does not have a theoretical basis. This

limitation makes KT model unreliable for other systems.

To overcome the difficulties in predicting ternary MS diffusivities at infinite dilution (*i.e.*  $D_{ij}^{x_k \rightarrow 1}$ ), we derive the so-called LBV model based on the Onsager relations. MS diffusivities at infinite dilution can be expressed in terms of binary and pure component self-diffusivities and integrals over velocity cross-correlation functions. By neglecting the latter terms, we obtain the LBV model. In chapter 3, the LBV model is validated for WCA fluids and the ternary systems n-hexane-cyclohexane-toluene and methanol-ethanol-water. We find that: (1) for ideal mixtures *i.e.* the WCA system, as well as the n-hexane-cyclohexane-toluene system, the LBV model is accurate and superior compared to the existing models for predicting ternary MS diffusivities at infinite dilution (*i.e.* the WK, KT, VKB, DKB and RS models); (2) in mixtures containing associating components, *i.e.* the ethanol-methanol-water system, the LBV model indicates that in this system the integrals over velocity cross-correlation functions are important and cannot be neglected. Moreover, the LBV model provides an explanation why the MS diffusivity describing the friction between adsorbed components in a porous material is usually very large.

In chapter 4, we focus on describing the values of MS diffusivities at finite concentration. A multicomponent Darken model for describing the concentration dependence of MS diffusivities is derived from linear response theory and the Onsager relations. In addition, a predictive model for the required self-diffusivities in the mixture is proposed leading to the so-called predictive Darken-LBV model. We compare our novel models to the existing generalized Vignes equation and the generalized Darken equation. Two systems are considered: (1) ternary and quaternary WCA systems; (2) the ternary system n-hexane-cyclohexane-toluene. Our results show that in all studied systems, our predictive Darken-LBV equation describes the concentration dependence better than the existing models. The physically-based Darken-LBV model provides a sound and robust framework for prediction of MS diffusion coefficients in multicomponent mixtures.

In chapter 5, diffusion in more complex ionic liquid (IL) systems are investigated. Previous research reported in literature has largely focused on self-diffusion in ILs. For practical applications, mutual (transport) diffusion is by far more important than self-diffusion. We compute the MS diffusivities in binary systems containing 1-alkyl-3-methylimidazolium chloride ( $C_n\text{mimCl}$ ), water and/or dimethyl sulfoxide (DMSO). The dependence of MS diffusivities on mixture composition are

investigated. Our results show that: (1) For solutions of ILs in water and DMSO, self-diffusivities decrease strongly with increasing IL concentration. For the system DMSO-IL, an exponential decay is observed for this; (2) For both water-IL and DMSO-IL, MS diffusivities vary by a factor of 10 within the concentration range which is still significantly smaller than the variation of the self diffusivities; (3) The MS diffusivities of the investigated IL are almost independent of the alkyl chain length; (4) ILs stay in a form of isolated ions in  $C_n\text{mimCl-H}_2\text{O}$  mixtures, however, dissociation into ions is much less observed in  $C_n\text{mimCl-DMSO}$  systems. This has a large effect on the concentration dependence of MS diffusivities; (5) The LBV model for predicting the MS diffusivity at infinite dilution described in chapter 3 suggests that velocity cross-correlation functions in ionic liquids cannot be neglected and that the dissociation of ILs into ion pairs has a very strong influence on diffusion.

In experiments, Fick diffusion coefficients are measured and molecular simulation usually provides MS diffusivities. These approaches are related via the matrix of thermodynamic factors which is usually known only with large uncertainties. This leaves a gap between theory and application. In chapter 6, we introduce a consistent and efficient framework for the determination of Fick diffusivities in liquid mixtures directly from equilibrium MD simulations by calculating both the thermodynamic factor and the MS diffusivity. This provides the missing step to extract Fick diffusion coefficients directly from equilibrium MD simulations. The computed Fick diffusivities of acetone-methanol and acetone-tetrachloromethane mixtures are in excellent agreement with experimental values. The suggested framework thus provides an efficient route to model diffusion in liquids based on a consistent molecular picture.

In chapter 7, we validate our method for computing Fick diffusivities using equilibrium MD simulations for the ternary system chloroform - acetone - methanol. Even though a simple molecular model is used (*i.e.* rigid molecules that interact by Lennard-Jones and electrostatic interactions), the computed thermodynamic factors are in close agreement with experiments. Validation data for diffusion coefficients is only available for two binary sub-systems. In these binary systems, MD results and experiments do agree well. For the ternary system, the computed thermodynamic factors using Molecular Dynamics simulation are in excellent agreement with experimental data and better than the ones obtained from COSMO-SAC calculations. Therefore, we expect that the computed Fick diffusivities should also be comparable with experiments. Our results suggest that the presented approach allows for an ef-

ficient and consistent prediction of multicomponent Fick diffusion coefficients from MD simulations. Now, a tool for guiding experiments and interpreting multicomponent mass transfer is available.

# Samenvatting

Het doel van dit proefschrift is het bestuderen van diffusie in ternaire vloeistoffen met behulp van Moleculaire Dynamica (MD) simulaties. Diffusie speelt een belangrijke rol bij de beschrijving van massatransport. In binaire systemen is massatransport door diffusie uitvoerig bestudeerd door zowel experimenten als door moleculaire simulaties. Vanuit een praktisch oogpunt zijn systemen bestaande uit meer dan twee componenten interessanter dan binaire systemen. Nauwkeurige gegevens uit experimenten en simulaties zijn vaak niet beschikbaar voor deze systemen. Derhalve is meer gedetailleerde kennis op het gebied van diffusie in systemen bestaande uit minimaal drie componenten noodzakelijk. De aanwezigheid van meerdere componenten in een systeem leidt tot complicaties bij diffusie experimenten. Het onderzoeken van de concentratie afhankelijkheid van diffusiecoëfficiënten door middel van experimenten vergt aanzienlijk meer inspanning. In dit proefschrift worden MD simulaties gebaseerd op klassieke “force fields” gebruikt om diffusie in binaire en ternaire vloeistoffen te bestuderen. Diffusie kan worden beschreven door Fick en Maxwell-Stefan (MS) diffusiecoëfficiënten. Experimenten resulteren in Fick diffusie coëfficiënten, terwijl simulaties doorgaans MS diffusiecoëfficiënten opleveren. Fick and MS diffusiecoëfficiënten zijn aan elkaar gekoppeld via de zogenaamde matrix van thermodynamische factoren. Een kort overzicht van methoden om diffusie in vloeistoffen te bestuderen en de bijbehorende beperkingen hiervan wordt beschreven in hoofdstuk 1.

In hoofdstuk 2 wordt diffusie in het ternaire systeem n-hexane-cyclohexane-toluene bestudeerd. De bestaande modellen voor het voorspellen van MS diffusiecoëfficiënten bij eindige concentraties (d.w.z. de Vignes vergelijking) en bij oneindig verdunde oplossingen (d.w.z. voorspellingen van  $D_{ij}^{x_k \rightarrow 1}$  op basis van de zogenaamde WK, KT, VKB, DKB en RS modellen) zijn onderzocht met behulp van MD simulaties. Hieruit kunnen we concluderen dat: (1) De voorspellingen met de Vignes vergelijking zijn

redelijk en leveren een verschil op van gemiddeld 13% vergeleken met de berekende diffusiecoëfficiënten uit MD; (2) Het best voorspellende model (het KT model) voor het bepalen van MS diffusiecoëfficiënten bij oneindige verdunning resulteert in verschillen van 8% vergeleken met de berekende diffusiecoëfficiënten. Hierbij dient te worden opgemerkt dat de verschillen van 8% toeval kunnen zijn, aangezien het KT model geen theoretische basis heeft en dus empirisch is. Deze beperking maakt het KT model onbetrouwbaar voor andere systemen.

Om ternaire MS diffusiecoëfficiënten bij oneindige verdunning  $D_{ij}^{x_k \rightarrow 1}$  te kunnen voorspellen hebben wij het zogenaamde LBV model afgeleid. Dit model is gebaseerd op de Onsager relaties. MS diffusiecoëfficiënten bij oneindige verdunning kunnen worden uitgedrukt in termen van zelf-diffusiecoëfficiënten van de corresponderende zuivere stoffen en binaire systemen, alsmede uit de integralen van snelheid “cross correlation” functies. Bij het verwaarlozen van de laatste genoemde termen wordt het LBV model verkregen. In hoofdstuk 3 wordt het LBV model gevalideerd voor WCA vloeistoffen en de ternaire systemen n-hexaan-cyclohexaan-tolueen en methanol-ethanol-water. Uit de simulaties kan geconcludeerd worden dat: (1) Voor ideale mengsels (d.w.z. het WCA systeem en het n-hexaan-cyclohexaan-tolueen systeem) is het LBV model accuraat en superieur aan de bestaande modellen voor het voorspellen van ternaire diffusiecoëfficiënten bij oneindige verdunning (d.w.z. de WK, KT, VKB, DKW en RS modellen); (2) In mengsels die associërende componenten bevatten (b.v. methanol-ethanol-water) zijn de integralen van de snelheid “cross-correlation” functies belangrijk en kunnen niet worden verwaarloosd. Bovendien geeft het LBV model een verklaring waarom de MS diffusiecoëfficiënt die de frictie tussen geadsorbeerde componenten in een poreuze media beschrijft, vrijwel altijd erg groot is.

In hoofdstuk 4 richten we ons op het beschrijven en voorspellen van MS diffusiecoëfficiënten bij eindige concentraties. Een Darken model voor het beschrijven van de concentratie afhankelijkheid van MS diffusiecoëfficiënten in systemen bestaande uit drie of meer componenten is afgeleid met behulp van lineaire respons theorie en de Onsager relaties. Daarnaast wordt voor deze mengsels een voorspellende model voor de benodigde zelf- diffusiecoëfficiënten voorgesteld, hetgeen uiteindelijk leidt tot het voorspellende Darken-LBV model. We vergelijken onze nieuwe modellen met de bestaande Vignes vergelijking voor ternaire systemen en de zogenaamde “generalized Darken” vergelijking. Twee systemen worden bestudeerd: (1) ternaire en



quaternaire WCA systemen; (2) het ternaire systeem n-hexane-cyclohexane-toluene. Onze resultaten wijzen uit dat in alle bestudeerde systemen de voorspellende Darken-LBV vergelijking de concentratie afhankelijkheid beter omschrijft dan de bestaande modellen. Het fysisch gebaseerde Darken-LBV model geeft een solide en robuust kader voor het voorspellen van de MS diffusiecoëfficiënten in systemen bestaande uit meer dan 2 componenten.

In hoofdstuk 5 wordt diffusie (meer complexe) ionische vloeistoffen (Ionic Liquids, ILs) onderzocht. Reeds bestaand onderzoek was voornamelijk gericht op zelf-diffusie in ILs. Voor praktische toepassingen is transport diffusie veel belangrijker dan zelf-diffusie. We hebben de MS diffusiecoëfficiënten berekend voor de binaire systemen 1-alkyl-3-methylimidazolium chloride ( $C_n\text{mimCl}$ ) met water of dimethylsulfoxide (DMSO). De afhankelijkheid van MS diffusiecoëfficiënten voor de samenstelling van het mengsel is onderzocht. Onze resultaten laten zien dat: (1) Voor oplossingen van ILs in water en DMSO nemen de zelf-diffusiecoëfficiënten sterk af bij verhoogde IL concentraties. Voor het systeem DMSO- $C_n\text{mimCl}$  is een exponentiële afname hiervoor zichtbaar; (2) Zowel bij water- $C_n\text{mimCl}$  als bij DMSO- $C_n\text{mimCl}$  variëren de MS diffusiecoëfficiënten met een factor 10 binnen het concentratiebereik. Dit is kleiner is dan de verandering van zelf-diffusiecoëfficiënten; (3) MS diffusiecoëfficiënten van de onderzochte ILs zijn vrijwel onafhankelijk van de lengte van de alkylketen; (4) ILs blijven in een vorm van geïsoleerde ionen in  $C_n\text{mimCl-H}_2\text{O}$  mengsels, maar deze dissociatie is veel minder voor  $C_n\text{mimCl-DMSO}$  systemen. Dit heeft een groot effect op de concentratieafhankelijkheid van MS diffusiecoëfficiënten; (5) Het LBV model voor het voorspellen van MS diffusiecoëfficiënten bij oneindige verdunning zoals beschreven in hoofdstuk 3 suggereert dat snelheid “cross-correlation” functies in ILs niet kunnen worden verwaarloosd en dat de dissociatie van ILs tot ion paren een sterke invloed heeft op diffusie.

In experimenten worden Fick diffusiecoëfficiënten gemeten, terwijl MD simulaties MS diffusiecoëfficiënten opleveren. Deze verschillende beschrijvingen kunnen in elkaar worden omgerekend door middel van de matrix van thermodynamische factoren, welke meestal een hoge onnauwkeurigheid bevat. Hierdoor is het lastig om simulaties en theorie met elkaar te vergelijken. In hoofdstuk 6 introduceren wij een consistente en efficiënte methode voor het bepalen van Fick diffusiecoëfficiënten in vloeistof mengsels uit MD simulaties. Dit kan door het direct berekenen van de matrix van thermodynamische factoren en de MS diffusiecoëfficiënten. Dit

is de ontbrekende stap om Fick diffusiecoëfficiënten direct te berekenen uit MD simulaties. De berekende Fick diffusiecoëfficiënten van aceton-methanol en aceton-tetrachloromethaan mengsels komen uitstekend overeen met experimentele waarden. De methode resulteert in een efficiënte route om diffusie in vloeistoffen te bestuderen, gebaseerd op consistente moleculaire voorstellingen.

In hoofdstuk 7 valideren wij de methode uit hoofdstuk 6 voor het ternaire systeem chloroform-aceton-methanol. Ondanks het gebruik van een simpel moleculair model (d.w.z. rigide moleculen met een Lennard-Jones en elektrostatisch interacties) komen de berekende thermodynamische factoren uitstekend overeen met de experimentele waarden. Experimentele gegevens voor de diffusiecoëfficiënten is alleen beschikbaar voor de twee binaire subsystemen. In deze binaire systemen zijn MD resultaten en experimenten in overeenstemming. Voor het ternaire systeem zijn de uit MD simulaties berekende thermodynamische factoren in overeenstemming met de experimentele waarden. Bovendien blijken onze MD berekeningen een betere voorspelling te geven dan zogenaamde COSMO-SAC berekeningen. Derhalve verwachten we dat de berekende Fick diffusiecoëfficiënten voor het ternaire systeem eveneens overeenkomen met experimenten. Onze resultaten laten zien dat de gebruikte methode resulteert in een efficiënte en consistente voorspelling van Fick diffusiecoëfficiënten uit MD simulaties.

## **Curriculum Vitae**

Xin Liu was born on August 8, 1983 in Daqing, P.R. China. She received her bachelor of science degree in Henan University of Technology in food science (June 2006). She came to Netherlands in September 2006 and started her master in biochemical engineering at Delft University of Technology. After obtaining her master degree (October 2008), she worked on her PhD project with Prof. A. Bardow (Lehrstuhl für Technische Thermodynamik of RWTH Aachen University, Germany) and Prof. T.J.H Vlugt (Engineering Thermodynamics of Delft University of Technology, Delft, The Netherlands.)

## Published Work

- X. Liu, A. Martin-Calvo, E. McGarrity, S.K. Schnell, S. Calero, J.M. Simon, D. Bedeaux, S. Kjelstrup, A. Bardow, T.J.H. Vlugt, Fick diffusion coefficients in ternary liquid systems from equilibrium Molecular Dynamics simulations, *Ind. Eng. Chem. Res.*, 2012, 51, 10247
- X. Liu, A. Bardow, T.J.H. Vlugt, Maxwell-Stefan diffusivities and velocity cross-correlations in dilute ternary systems, *Diffusion-fundamentals.org*, 2011, 16, 81.
- X. Liu, S.K. Schnell, J-M Simon, D. Bedeaux, S. Kjelstrup, A. Bardow, T.J.H. Vlugt, Fick diffusion coefficients of liquid mixtures directly obtained from equilibrium Molecular Dynamics, *J. Phys. Chem. B*, 2011, 115, 12921-12929. Erratum: doi: 10.1021/jp3039835
- S.K. Schnell, X. Liu, J-M Simon, A. Bardow, D. Bedeaux, T.J.H. Vlugt, S. Kjelstrup, Calculating thermodynamic properties from fluctuations at small scales, *J. Phys. Chem. B*, 2011, 115, 10911-10918.
- X. Liu, T.J.H. Vlugt, A. Bardow, Predictive Darken equation for Maxwell-Stefan diffusivities in multicomponent mixtures, *Ind. Eng. Chem. Res.*, 2011, 50, 10350-10358.
- X. Liu, T.J.H. Vlugt, A. Bardow, Maxwell-Stefan diffusivities in binary mixtures of ionic liquids with DMSO and H<sub>2</sub>O, *J. Phys. Chem. B*, 2011, 115, 8506-8517.
- X. Liu, A. Bardow, T.J.H. Vlugt, Multicomponent Maxwell-Stefan diffusivities at infinite dilution, *Ind. Eng. Chem. Res.*, 2011, 50, 4776-4782.

- X. Liu, T.J.H. Vlugt, A. Bardow, Maxwell-Stefan diffusivities in liquid mixtures: using molecular dynamics for testing model predictions, *Fluid Phase Equilibria*, 2011, 301, 110-117.
- X. Liu, D. Newsome, M-O. Coppens, Dynamic Monte Carlo simulations of binary self-diffusion in ZSM-5, *Microporous Mesoporous Mater.*, 2009, 125, 149-159.
- J.J. Gutiérrez-Sevillano, D. Dubbeldam, X. Liu, T.J.H. Vlugt, S. Calero, Exploiting the features of Cu-BTC for ethanol-water separation, submitted
- X. Liu, S.K. Schnell, J.M. Simon, P. Krüger, D. Bedeaux, S. Kjelstrup, A. Bardow, T.J.H. Vlugt, Application of equilibrium Molecular Dynamics simulation to obtain mutual diffusion coefficient, submitted.

# Acknowledgments

- First, I would like to thank my supervisors Prof. T.J.H. Vlugt and Prof. A. Bardow. I really like working in your groups. both from a professional and a personal point of view.
- Second, I would like to thank all my colleagues both in Delft and in Aachen. I have learned a lot from you.
- Finally, I would like to thank my family and friends that are not related to my research. You have been very supportive during the last few years.